Universidade Estadual de Londrina

ANGEL ESTEBAN LABRADOR RIVAS

FAULT DETECTION, RELIABILITY, EFFICIENCY AND RANDOM ACCESS IN SMART GRID SYSTEMS

Londrina
2022

ANGEL ESTEBAN LABRADOR RIVAS

FAULT DETECTION, RELIABILITY, EFFICIENCY AND RANDOM ACCESS IN SMART GRID SYSTEMS

A Thesis submitted to the Electrical Engineering Graduate Program at the State University of Londrina in Partial Fulfillment of the Requirements for the Degree of Doctor of Philosophy in Electrical Engineering. Area: Signal Processing & Telecommunications Systems

Orientador: Taufik Abrão

Londrina
2022

Labrador Rivas, Angel Esteban

Fault Detection, Reliability, Efficiency and Random Access in Smart Grid Systems. Londrina, 2022. 193 p.

Supervisor: Taufik Abrão

Thesis (Doctor of Philosophy) – Department of Electrical Engineering – State University of Londrina

1. Smart Grid, 2. Power Energy System, 3. Fault Condition, 4. Renewable Energy, 5. Harmonics 6. Communications, 7. Random Access Protocols, 8. ALOHA, 9. IRSA, 10. Massive MTC, 11. QoS. 12. RIS, 13. Multiple Access, 14. IoT, 15. Manifolds, 16. PSO.

ANGEL ESTEBAN LABRADOR RIVAS

FAULT DETECTION, RELIABILITY, EFFICIENCY AND RANDOM ACCESS IN SMART GRID SYSTEMS

A Thesis submitted to the Electrical Engineering Graduate Program at the State University of Londrina in Partial Fulfillment of the Requirements for the Degree of Doctor of Philosophy in Electrical Engineering. Area: Signal Processing & Telecommunications Systems.

EXAMINATION BOARD

Orientador: Prof. Dr. Taufik Abrão
Department of Electrical Engineering - UEL

Prof. Dr. Helder Roberto de Oliveira Rocha
Department of Electrical Engineering – UFES

Prof. Dr. Cristiano Magalhães Panazio
Department of Telecommunication and Control (PTC) – EPUSP

Prof. Dr. José Carlos Marinello
Academic Department of Electrical Engineering – UTFPR

Prof. Dr. Silvio Giuseppe Di Santo
Department of Power Engineering and Automation (PEA) EPUSP

Londrina, March 11, 2022.

To God, my strength and consolation.

To Juan Esteban, my greatest motivation.

To Angela, for her infinite love and understanding.

To my mother and grandmother, for all I am.

To my father, who supports us from Heaven.

Acknowledgements

Thanks to the State University of Londrina for allowing me to obtain a Ph.D. in Electrical Engineering. This work would not have been possible without the financial support of Capes, CNPq, and PROPPG/UEL.

As my supervisor and guide to Professor Ph.D. Taufik Abrão, thanks for trusting me and always supporting me. Even in tough times when motivation fades up, he helped me out to see beyond. Prof. Taufik never puts constraints on what you can achieve. At UEL, advisors or supervisors are commonly (and unofficially) called "*Pai*" (Portuguese for "dad"). In society, a parent has the role of educating a child to ensure healthy development; In this path, an advisor is undoubtedly beyond the academic. Thankful for his collaboration, guidance, and contribution during the realization of this work.

Thanks to Professor Ekram Hossain, who gave me his support and welcomed me to Canada. The final stage of my research would not have been possible without the research group at UofM.

Grateful to all those who gave their spontaneous and disinterested collaboration in realizing this work. To all my friends and colleagues in the signal processing and communication laboratory for all shared moments.

To my family, for their unconditional love. To my friends and colleagues during this journey. Brazil and UEL left me with deeper bounds beyond the academic. At least, I have to write down the names of those who have been part of it; special mention to (Non-exhaustive list <funny laugh>): Gersson Sandoval, Ricardo Kobayashi, Augusto Kamizake, Lucas Silva, Luis Pareja, Rosangela Santos, Marc Jean Baptiste, Camila Galo, Karina Yamashita, Daniela Campos, Edgar Candales, Angelo Vera.

Obrigado por tudo!.

"The Lord is my strength and my defense;
he has become my salvation.
Shouts of joy and victory resound in the tents of the righteous:
"The Lord's right hand has done mighty things!
The Lord's right hand is lifted high;
the Lord's right hand has done mighty things!"
(Psalm 118:14-16 Holy Bible (NIV))

Abstract

Smart Grid (SG) is a multidisciplinary concept that implies real-time information with specific communication requirements. System reliability relies on the best capabilities for monitoring and controlling the grid, and communication technologies are fundamental. Considering fault detection and classification a pivotal factor to SG reliability, the first part of this work presents a survey on SG fault detection and classification infrastructure, including SG communication support and relevant state-of-the-art papers from the most significant research databases. Hence, an adaptive technique to reliable monitoring harmonic distortion in the power network has been proposed. A performance-complexity tradeoff analysis demonstrated each filtering method's (dis)advantages. The second part of this thesis highlights the significance of existing and future random access (RA) protocols for massive smart grid communication (m-SGC) devices and system performance. We propose a new, improved irregular repetition slotted ALOHA (RapIRSA) RA protocol to better respond to critical high-reliability QoS requirements under a 5G communications perspective, summarizing the potential challenges in implementing the proposed RA protocol. From the communication perspective, we investigate a distributed precoding design for energy efficiency (EE) maximization in a reflecting intelligence surfaces (RIS)-aided multi-user (MU) MIMO uplink (UL) network with multi-antenna at the base station (BS) and multi-antenna at user terminals (UTs). We deploy a Manifold PSO-based optimization technique to solve the non-convex EE maximization. We show that the proposed framework significantly increases system EE values compared with non-optimized precoding schemes such as random schemes. Finally, We present the conclusions and prospective future works.

Keywords: 1. Smart Grid, 2. Power Energy System, 3. Fault Condition, 4. Renewable Energy, 5. Harmonics 6. Communications, 7. Random Access Protocols, 8. ALOHA, 9. IRSA, 10. Massive MTC, 11. QoS. 12. RIS, 13. Multiple Access, 14. IoT, 15. Manifolds, 16. PSO.

Resumo

Smart Grid (SG) é um conceito multidisciplinar que implica informação em tempo real com requisitos específicos de comunicação. A confiabilidade do sistema depende das melhores capacidades de monitoramento e controle da rede, e nesse quesito as tecnologias de comunicação são fundamentais. Considerando a detecção e classificação de falhas um fator crucial para a confiabilidade do SG, a primeira parte deste trabalho apresenta uma revisão sistemática sobre a infraestrutura de detecção e classificação de falhas em SG, incluindo suporte à comunicação SG, bem como a classificação dos trabalhos relevantes de última geração encontrados nos bancos de dados de pesquisa mais significativos. Assim, foi proposta uma técnica adaptativa para o monitoramento confiável de distorções harmônicas na rede elétrica. Conclusivamente, uma análise de compensação de complexidade de desempenho demonstrou as (des)vantagens de cada método de filtragem. A segunda parte desta tese destaca a importância dos protocolos de acesso aleatório (RA) existentes e futuros para dispositivos de comunicação massiva de *micro Smart Grid* (m-SGC) e desempenho do sistema. Propõe-se um novo e aprimorado protocolo RA ALOHA (RapIRSA) com repetição irregular aprimorado para responder melhor aos requisitos críticos de QoS de alta confiabilidade sob uma perspectiva de comunicações 5G, abordando possíveis desafios na implementação do protocolo RA proposto. Ainda sob a perspectiva da comunicação, investiga-se o problema da pré-codificação distribuída para a maximização da eficiência energética (EE) em uma rede MIMO *uplink* (UL) multiusuário auxiliada por superfícies refletoras inteligentes (RIS) assumindo estações radio-base (BS) com múltiplas antenas e terminais de usuário (UTs) também com múltiplas antena. Implementamos uma técnica de otimização baseada em *Manifold Particle swarm optimization* PSO para resolver a maximização de EE não-convexa. Mostra-se que a estrutura proposta aumenta significativamente os valores de EE do sistema em comparação com esquemas de pré-codificação não otimizados, pré-definidos. Por fim, apresenta-se as conclusões e trabalhos futuros prospectivos.

Palavras-chave: 1. Rede Inteligente, 2. Sistema de Energia Elétrica, 3. Condição de Falha, 4. Energia Renovável, 5. Harmônicos 6. Comunicações, 7. Protocolos de Acesso Aleatório, 8. ALOHA, 9. IRSA, 10. MTC Massivo, 11. QoS . 12. RIS, 13. Acesso Múltiplo, 14. IoT, 15. Manifolds, 16. PSO.

List of abbreviations and acronyms

μSG micro-Smart-Grid.
μG micro-Grid.
1PPS One pulse-per-second.
3GPP 3rd Generation Partnership Project.
3P three-phase.
5G fifth generation technology standard for cellular networks.
AC alternating current.
ACR application complying rate.
ADC Analog-to-Digital conversion.
ADR automated demand response.
AI Artificial Intelligence.
AMI Advanced Metering Infrastructure.
ANN Artificial Neural Networks.
ANSI American National Standards Institute.
ARQ automatic repeat request.
ATM Asynchronous Transfer Mode.
AWGN additive white Gaussian noise.
BEC binary erasure channel.
BLER Block Error Rate.
BS base station.
CB Circuit Breaker.
CBG Code Block Group.
CDMA Code Division Multiple Access.
CES Conventional Energy Systems.
CIS Consumer Information System.
CPT conservative power theory.
CPU Central Processing Unit.
CRDSA contention resolution diversity slotted ALOHA.
CSMA Carrier-sense Multiple Access.
CT Current Transformer.
DA Distribution Automation.
DC direct current.
DCU Data Collector Unit.
DER Distributed Energy Resources.
DFR Digital Fault Recording.
DFT Discrete Fourier Transform.
DG Distributed Generation.
DLR Dynamic Line Rating.
DM Distribution Management System.
DMS Distribution Management System.
DOCSIS Data Over Cable Service Interface Specification.
DoS Denial of Service.
DR Demand Response.
DS distributed storage.
DSL Digital Subscriber Line.
DSM Demand Side Management.
DSO Distribution System Operator.
DSP Digital Signal Processor.
DWT Discrete Wavelet Transform.
E2E End-to-End.
EDGE Enhanced Data rates for GSM Evolution.
EE energy efficiency.
EMS Energy Management System.
eMTC enhanced Machine-Type Communication.
EV Electrical Vehicle.
FAN Field Area Network.
FD/L-SG fault Detection and/or Location in SG Systems.
FEC forward error correction.
FFT Fast Fourier transform.
FLOP floating point operation.
GB *grant-based*.
GF *grant-free*.
GPRS General Packet Radio Service.

GPS Global Positioning System.
GSM Global System for Mobile Communications.
H2H Human-to-Human.
HAN Home Area Network.
HD Hard Delay.
HE harmonics estimation.
HMI Human Machine Interface.
HV High Voltage.
HVDC High-voltage DC.
IAB Integrated Access Backhaul.
IC interference canceller.
ICT Information and Communication Technology.
IEC International Electrotechnical Commission.
IED Intelligent Electronic Device.
IEEE Institute of Electrical and Electronics Engineers.
IGBT Insulated-Gate Bipolar Transistor.
IIR Infinite Impulse Response.
IoE Internet-of-Energy.
IoT Internet-of-Things.
IoTG Internet-of-Things-Grid.
IP Internet Protocol.
IRIG-B Inter-Range Instrumentation Group-B.
IRSA irregular repetition slotted ALOHA.
ISP Internet Service Provider.
IT Information Technology.
KF Kalman filter.
LAN Local Area Network.
LDPC low-density parity-check.
LF likelihood function.
LLF Log-likelihood function.
LMS least mean square.
LoS Line-of-Sight.
LPWAN low-power wide-area network.
LR-WPAN Low-Rate Wireless Personal Area Network.
LS least square.
LTE Long Term Evolution.
LV Low Voltage.
m-SGC massive Smart Grid communication.
M2M Machine-to-Machine.
MA Moving Average.
MCS Monte Carlo Simulation.
MDMS Meter Data Management System.
MIMO Multiple-Input Multiple-Output.
ML Machine Learning.
MLE Maximum Likelihood estimation.
mMTC massive Machine-Type Communication.
MPckR multipacket reception.
MPR multipath-relaying.
MPU Main Processing Unit.
MR message rate.
MSE mean squared error.
MTC Machine-Type Communication.
MTT Measurement Transfer Time.
MTU Master Terminal Unit.
MU multi-user.
MU Merging Unit.
MV Medium Voltage.
NAN Neighborhood Area Network.
NB-IoT Narrowband Internet-of-Things.
NMSE normalized mean squared error.
NN Neural Network.
NR New Radio.
NSP Network Service Providers.
NTP Network Time Protocol.
OF optical fiber.
OPC Open Platform Communications.
P2G Phase to Ground.
P2P Phase to Phase.
P2P Single-Phase to Phase.
PCC point of common coupling.

PDC Phasor Data Concentrator.
PDCP Packet Data Convergence Protocol.
PDF probability density function.
PDR Packet Delivery Rate.
PEM Proton Exchange Membrane.
PLC Programmable Logic Controller.
PLC Power Line Communication.
PLR Packet Loss Rate.
PME proton exchange membrane.
PMU Phasor Measurement Unit.
PP2G Two-Phase to Ground.
PPP Three-Phase.
PPP Point-to-Point Protocol.
PPP2G Three-Phase to Ground.
PQ power quality.
PQA Power Quality Analyzer.
PS power system.
PSFB Phase-Shifted Full-Bridge.
PSO particle swarm optimization.
PT potential transformer.
PTP Precision Time Protocol.
PV photovoltaic.
PWM Pulse Width Modulation.
QoS Quality of Service.
RA Random Access.
RACH Random Access Channel.
RAF Random Access Frame.
RAN Radio Access Network.
RapC Raptor codes-structured.
RapIRSA Combining Raptor Codes and IRSA.
RF Radio frequency.
RFFT reduced fast Fourier transform.
RIAPS Resilient Information Architecture Platform for Smart Grid.
RIS reflecting intelligence surfaces.
RTU Remote Terminal Units.
S-ALOHA slotted-ALOHA.
SA Service and System Aspects.
SCADA Supervisory Control and Data Acquisition.
ScS Subcarrier-Spacing.
SD Soft Delay.
SDH/SONET Synchronous Digital Hierarchy/Synchronous Optical Network.
SDOs Standards Development Organizations.
SE spectral efficiency.
SG Smart Grid.
SGC smart grid communication.
SGSC Smart Grid Security Classification.
SIC successive interference cancellation.
SM smart meter.
SMPS Synchronized Phasor Measurement System.
SN slot number.
SNR Signal-to-noise ratio.
SP-IRSA Service Priority-based Irregular Repetition Slotted ALOHA.
SPM Synchro-Phasor Measurement.
SS Smart Sensor.
ST Smart Transformer.
STFT short-time Fourier transform.
SUN Smart Utility Network.
SV Sampled Values.
SVC Static var compensator.
SVD singular value decomposition.
SVM Support Vector Machine.
SyG Synchronous Generator.
TCP Transmission Control Protocol.
TDD total demand distortion.
THD total harmonic distortion.
TL Transmission Line.
TSC Time-Sensitive Communications.
TSN Time-Sensitive Network.
TW time window.
UDP User Datagram Protocol .
UL Uplink.

UMTS Universal Mobile Telecommunications System.

URLLC Ultra-Reliable Low-Latency Communication.

UT user terminals.

VoIP Voice over IP.

VSC Voltage-Sourced Converter.

VT Voltage Transformer.

VVWC Voltage, Var, and Watt Control.

WAMS Wide Area Measurement System.

WAN Wide Area Network.

WASA Wide-Area Situational Awareness.

WCDMA Wideband Code Division Multiple Access.

WGT wind turbine.

WiMAX Worldwide Interoperability for Microwave Access.

WindT wind turbine.

WLAN Wireless Local Area Network.

WNAN Wireless Neighborhood Area Network.

WSN wireless sensor network.

WT wavelet transform.

ZF Zero-forcing.

List of Symbols Ch. 3

I_L maximum fundamental load current.
I_{SC} short circuit current.
K total number of sinusoids.
L Window's size.
P_N Poisson random process.
$P_{iN}(n)$ train of pulses occurring at random and independent times.
TDD total demand distortion.
$THD_{\mathbf{i}}$ total current harmonic distortion.
$THD_{\mathbf{v}}$ total voltage harmonic distortion.
$\alpha_k - \beta_k$ parameters to estimate or the vector $\boldsymbol{\theta}(n)$.
$\boldsymbol{\theta}$ vector for the amplitudes to estimate of dimension K.
λ average number of impulses per time unit.
$\mathcal{N}$ additive white Gaussian noise.
ω_k harmonic (or interharmonic) frequency in radius.
ϕ_k initial harmonic phase angle.
σ^2 $\mathcal{N}$ variance.
$\mathbf{tdd}[\tau]$ true TDD at instant τ.
$\tilde{\vec{s}}$ error in the estimated and the measured values.
$\vec{A}$ state transition matrix.
$\vec{C}$ relation between the state vector $\vec{x}(n)$ and the measurement $\vec{z}(n)$.
$\vec{H}$ system structure matrix of dimension KxL.
$\vec{K}$ Kalman gain matrix.
$\vec{N}$ discrete-time vector finite length.
$\vec{P}$ Kalman covariance matrix.
$\vec{Q}_w$ $\vec{w}$ noise correlation matrix.
$\vec{Q}_\eta$ $\vec{\eta}$ noise correlation matrix.
$\vec{\eta}$ $\mathcal{N}$ mean.
$\vec{\eta}$ zero-mean white noise process.
$\vec{i}_r$ input for the estimation algorithm to obtain the individual harmonic current estimation.
$\vec{i}_{MS}$ Current Signal from Matlab-Simulink.
$\vec{s}$ signal vector.
$\vec{w}$ zero-mean white noise process.
$\vec{x}$ vector of state variables.
$\vec{z}$ discrete-time vector measured signal.
a_k harmonic amplitude magnitude.
f_k harmonic (or interharmonic) frequency.
i total current.
i_a Active current.
i_f amplitude of the fundamental harmonics of the measured current.
i_g Load-generated current harmonics.
i_k amplitude of the nth harmonics of the measured current.
i_r Reactive current.
i_v Void current.
i_{sa} Scattered active current terms.
i_{sr} Scattered reactive current terms.
n discrete-time index.
n instant of time.
s_k kth harmonic component.
$s_{k,i}$ imaginary component of s_k.
$s_{k,r}$ real component of $s_k(n)$.
z Kalman current observation.

List of Symbols Ch. 4

A service area.
$BW_{\mathbf{req}}$ required network bandwith.
$B_{\mathbf{off}}$ S-Aloha Back-off limit.
F frame.
G channel traffic or load.
L latency.
M number of nodes.
M_v r.v. of the active users.
PDR packet delivery ratio.
PLR packet loss ratio.
P_{R_i} number of packets received by user i.
$P_{\mathbf{G}_i}$ number of packets generated by user i.
$P_{\mathbf{G}}$ number of packets generated.
$P_{\mathbf{R}}$ number of packets received.
S throughput.
SF sub-frame.
T electrical utility cycle.
$T_{\mathbf{Ac}}$ accumulation time.
$T_{\mathbf{A}}$ activation time.
$T_{\mathbf{RAF}}$ duration of an IRSA frame RAF.
$T_{\mathbf{F}}$ duration of a frame F.
$T_{\mathbf{SF}}$ duration of a sub-frame SF.
$T_{\mathbf{S}}$ duration of a slot.
$T_{\mathbf{W}}$ waiting time.
U_i^k active users i who succeed in sending a packet in each k slot within the latency requirement τ_{req_i}.
U_m number of total active users during N slots.
$\Delta_{\mathbf{C}}$ critical Latency Response.
$\Delta_{\mathbf{N}}$ network latency.
$\Delta_{\mathbf{X}}$ network changing state latency.
$\Lambda(x)$ user degree distribution.
η target throughput coefficient.
λ parameter of the Poisson distribution.
$\mathcal{G}_{\mathbf{BS}}$ SN of Graph as seen in BS.
$\mathcal{R}$ reliability.
$\mathcal{R}_{\mathbf{ACR}}$ ACR reliability.
τ delay factor.
$\tau_{\mathbf{req}}$ delay requirement.
$\tau_{HD_{req}}$ HD delay requirement.
$c\mathcal{N}$ connecting nodes.
d repetition rate.
d_m maximum number of replicas.
f utility frequency.
m active users in at any time t/frame.
n slot.
n_q SN of SN of $c\mathcal{N}$s.
$n_{\mathbf{RapC}}$ SN in the frame.
$n_{\mathbf{raf}}$ slots of an IRSA frame RAF.
$pk_{\mathbf{s}}$ application packet size.
q number of $c\mathcal{N}$.

List of Symbols Ch. 5

B Number of Antennas at BS.

BW Transmission Bandwidth.

L Number of maximum iterations.

M Number of UT's.

N_R Number of RIS elements.

N_m Number of Antennas per UT.

P_m m-th link power consumption.

$P_{\max}$ Max power per UT.

$P_{\mathbf{tot}}$ total power consumption.

$P_{c,m}$ Power circuitry per UT.

$P_{c,m}$ circuit power consumption at UT m.

$P_{\mathbf{bs}}$ Power at BS.

$P_{\mathbf{ris}}$ Power of each RIS element.

$\kappa_{\mathbf{dB}}$ Rician κ factor.

ρ_m efficiency of the transmit power amplifiers.

ee system ergodic EE.

se system ergodic SE.

$\vec{H}_{\mathbf{B}}$ channel matrix between RIS-to-B.

$\vec{H}_{\mathbf{A},m}$ channel matrix from the M UT-to-RIS.

$\vec{Q}_m$ covariance matrix.

$\vec{V}_m$ SVD precoding matrix for the m-th user.

$\vec{W}_{\mathbf{ZF}_m}$ ZF precoding matrix for the m-th user.

$\vec{W}_m$ precoding matrix for the m-th user.

$\vec{\Phi}$ RIS phase shift matrix.

$\vec{n}$ thermal noise.

$\vec{r}$ received signal.

$\vec{s}_m$ m-th transmitted signal.

ξ_m inefficiency of the transmit power amplifiers.

ξ_m Inefficiency of UT power amplif..

List of Figures

List of Tables

Contents

1 Introduction

The SG importance relies on adopting renewable energy resources, increasing the efficiency of grid operations by reducing losses, and improving system reliability and security (GRID; DESIGNS, 2012). The design framework of the SG requires optimizing all power system elements as comprehensively as possible (YE, 2018).

Power systems evolution to SG implies improving the network of transmission lines, equipment, controls, and new technologies to integrate information and communications technology. This evolution considers every aspect of electricity generation, transmission, delivery, and consumption to minimize environmental impact, enhance markets, improve reliability and service, reduce costs and improve efficiency.

SG describes the integrated action from all connected end-users into the power grid. Bidirectional communications between end-users and the grid operator are critical to extending the power grid accessibility. Thus, consumers connected to the Information and Communication Technology (ICT) infrastructures of Distribution System Operators (DSOs) through smart meters (SMs) via a Wide Area Network (WAN) (MATTIOLI; MOULINOS, 2016). SMs set the separation point between the DSO-ICT infrastructure and the Customer Premises Network.

SG demands real-time state estimation utilizing synchronized Phasor Measurement Unit (PMU) at high sampling rates (COSOVIC et al., 2017). Wide Area Measurement System (WAMS) explores those PMU data requiring a novel communication infrastructure support. WAMS aims to identify and neutralize power grid disturbances in real-time applications, consequently requiring a communication infrastructure capable of integrating a high number of PMU devices with exceptional reliability and ultra-low latency and provide backward compatibility to legacy measurements from Supervisory Control and Data Acquisition (SCADA) systems (SALEEM et al., 2019).

SGs include upgrade technology versions of Energy Management System (EMS), Distribution Management System (DMS), and SCADA. Telecommunication operators or Internet Service Provider (ISP) offer communication infrastructure support, mainly for WAN communications. Thus these shared-communication infrastructures represent cybersecurity risks for the grid. Communication networks entitle todays' grid "smart" concept as real-time grid awareness allows instant actions and updated consumption information. Those assets bring multiple cybersecurity concerns and the possible effects of an attack to the grid.

The arrival of fifth generation technology standard for cellular networks (5G) communication networks will considerably promote the requirement of the distributed data acquisition and processing services for WAMS systems (BOCKELMANN et al., 2018). Also, the awakening of Massive Machine-Type Communication (mMTC) services will

provide support for a large-scale deployment Advanced Metering Infrastructure (AMI) (SALEEM et al., 2019). This work also explores aspects related to the communication networks and the inter-connectivity compliance in SGs, identifying vulnerabilities, risks, and threat agents. Table A.1 summarizes the relevant published research inside the scope of SG systems, illustrating trending topics for the development of this work.

Smart transmission and distribution grids need data sensing to monitor substations, transformers, and power lines. Smart features demand adaptive communication networks admitting open-standardized communication protocols to operate on a unique platform. The micro-Grid (μG) concept couples the micro source Distributed Generation (DG), loads, control, and storage components, performing together in islanded or grid-connected mode. The μG involves advanced technologies, control, sensors, and reliable data transmission systems. It implies a large number of data sources introducing the big data concept in the next-generation power grid systems (RANA et al., 2018; MOHARM, 2019). Real-time control based on fast and reliable information exchange in different platforms will enhance the system resilience by the enhancement of system reliability and security and optimization of the grid assets utilization (MOMOH, 2012).

Defining communication technology depends on SG applications based on throughput, latency, and reliability requirements. For example, among technologies uses are but not limited to satellite communication, Data Over Cable Service Interface Specification (DOCSIS), optical fiber (OF), unlicensed Radio frequency (RF) mesh, Long Term Evolution (LTE), Worldwide Interoperability for Microwave Access (WiMAX), Global System for Mobile Communications (GSM), Enhanced Data rates for GSM Evolution (EDGE), Universal Mobile Telecommunications System (UMTS), General Packet Radio Service (GPRS), Wideband Code Division Multiple Access (WCDMA), Code Division Multiple Access (CDMA), and proprietary microwave links (EMMANUEL; RAYUDU, 2016). Communication and sensor data collection in transmission lines uses individual sensors to communicate with a central storage and processing location using radiofrequency satellite or cell phone networks (INSTITUTE, 2009); yet Power Line Communication (PLC) represents an important role.

A monitoring network for the transmission lines in the SG entails upgrading the existing monitoring equipment to obtain precise and timely status information (YE et al., 2018). Indeed, smart sensors offer suitable characteristics for such upgrading. A smart sensor is a system that includes, at least, a primary sensor, integrated signal conditioning, and processing capabilities, and communication (MARTINEZ-FIGUEROA et al., 2017). The state measurement modules based on PMU are more efficient than the current state estimation methods since synchronized phasor signals provide state variables, particularly voltage angles. Besides, data collected is synchronized, disregarding topology checking and improving data detection (LI et al., 2010). In some cases in which exist a limited number of synchronized PMUs, the harmonic state estimation methodology for power distribution

networks is usually based on optimization models (MELO et al., 2019). During system upgrading, the future grid will use current metering or protection devices connected to the sending and receiving ends of the transmission line to monitor system conditions. (STANOJEVIC et al., 2018; RODRIGUEZ-CALVO et al., 2018; ABU-SIADA; MIR, 2019).

The estimation of amplitude and phase of fundamental, harmonic, and inter-harmonic signals, including stochastic noise, is a particularly challenging task to evaluate the QoS characteristics in SG (IRFAN et al., 2017; REZKALLAH et al., 2019). Discrete Fourier Transform (DFT) or Fast Fourier transform (FFT) are well-known techniques for harmonic estimation; however, these techniques have disadvantages (i.e. aliasing, leakage, and picket-fence effect) (GARANAYAK et al., 2015). The Goertzel algorithm (DFT based estimation) for power quality measurements on SG systems is deployed in (KOZIY et al., 2013; SRIDHARAN et al., 2015).

On the other hand, real-time applications require fast convergence techniques in different sampling conditions. The work in (GIRGIS et al., 1991) introduces a scheme for tracking the harmonics in power systems based on Kalman filtering theory for the optimal estimation of the system parameters operating under time-varying harmonics content. (KENNEDY et al., 1996) applies a Fourier linear combiner that uses a linear adaptive neural network called Adaline, while (BETTAYEB; QIDWAI, 1998) presents the estimation of harmonics in a distorted voltage or current waveform; the distortion of the signal considers the case of different noise levels using different least square (LS) based algorithms. A variable step-size least mean square (LMS) approach for power harmonics estimation is presented in (PANDA et al., 2013); this method is an adaptation of a LS algorithm. LS is also implemented in (LIN; HUANG, 2011; GARANAYAK et al., 2015) remarking that many situations in the power system imply dynamical changes in loading, changes in topologies from various outgrowths in the system, as well as faults occurrence, which demand adaptive estimation methods (AFTAB et al., 2020).

In general, a fault is a condition of something reporting that it is not working correctly. In an electric power system, a fault is usually associated with an abnormal electric current; specifically, a short circuit is a fault in which current exceeds normal operating conditions.

Recently, (KATIC; STANISAVLJEVIC, 2018) implemented nonparametric methods for harmonic estimation in real-time for voltage dips detection using voltage harmonic footprints. Four Fourier-based algorithms, FFT, short-time Fourier transform (STFT), reduced fast Fourier transform (RFFT), and wavelet transform (WT) based estimation methods have been compared. Such comparison has been done in terms of speed, cost-effectiveness, and precision, inferring potential applications for power quality conditioning. Furthermore, (BELTRAN-CARBAJAL et al., 2022; KHAZAEI et al., 2016) propose a harmonic estimation approach and power system oscillation identification using the Prony algorithm.

A block orthogonal matching pursuit algorithm estimating principal pollution sources based on harmonic presence has been proposed recently in (CARTA et al., 2019). It requires upgrading the distributed monitoring system and several significant harmonic sources lower than the number of loads connected to the grid. Besides, (HU; GHARAVI, 2019) brings a two-stage processing approach that consists of a subspace-based estimation method to detect and identify harmonic components, followed by an algorithm to monitor frequency variations of voltage and current signals in real-time, under the assumption that the signal is stationary. (HU; GHARAVI, 2019) takes into consideration a fixed window that compromises adaptive performance to reduce complexity.

Beyond 5G technology includes reflecting intelligence surfaces (RIS) are likely to be used (e.g., in buildings and vehicles) for maintaining reliability in scenarios where there exist physical obstacles between the transmitter and the receiver (IMOIZE et al., 2021). RIS represents an important add-on in remote sensing networks for SG (ZHOU et al., 2020b) presents a structure for RIS-aided transmission in Multiple-Input Multiple-Output (MIMO) systems. Distributed precoding design for massive MIMO reduces CSI exchange among the user terminals (UT) and the base station (BS) (GOUDA et al., 2020). (WU; ZHANG, 2019a) and (XIE et al., 2020a) consider active and passive beamforming subject to users' average transmit power limitations. Besides, (XIE et al., 2020a) focuses on optimizing Uplink (UL) beamforming at the BS and passive beamforming at the RIS, employing a low-complexity max-min strategy. Joint beamforming optimization design for a multi-cell system aiming to maximize spectral efficiency (SE) and minimize the mean squared error (MSE) of the users' received symbols is developed in (REHMAN et al., 2021a). The above works do not consider UT side beamforming for multi-antenna devices. We consider a scenario where mobile wireless users maintain quasi-stationary positions to benefit from distributed precoding and they establish connections to the BS aided by an outdoor or indoor RIS.

1.1 Smart Grid: a multidisciplinary problem

This section introduces a discussion within the interconnection among topics studied/developed on SG systems. This multidisciplinary work presents as key for understanding the next-generation power grid. Also, this thesis explore and highlights a few trends to develop the wireless communication applications into SG.

The Internet-of-Energy (IoE) for smart cities includes various heterogeneous technologies such as the Internet-of-Things (IoT) and wireless sensor network (WSN). However, to reach these important objectives, efficient networking and communication protocols are needed to provide the necessary coordination and control of the various system components. The mMTC and Ultra-Reliable Low-Latency Communication (URLLC) modes are an essential implementation for critical IoT devices which require ultra stable, reliable secure,

and real-time capable communication. Therefore these networks are today dedicated optical wireline networks.

Up to this point, we provide a systematic review (Chapter 2) as a survey to bring state-of-the-art research to identify good topics. Furthermore, in Chapter 3 we have been working on real-time applications for the smart grid scenario. This part of the thesis includes real-time state estimation under fault conditions. In this sense, highlighting some signal processing techniques capable of retrieving the faults information to achieve QoS. Next, Chapter 4 introduces the significance of existing and future random access protocols for massive Smart Grid communication (m-SGC) devices and system performance. In summary, we evaluate the potential challenges in implementing the proposed Random Access (RA) protocol for SG critical applications considering a massive number of Smart Sensor (SS). Finally, Chapter 5 provides an understanding of Energy Efficiency concepts in reflecting intelligent surfaces network analyses with a distributed precoding design.

Smart-grid applications demand distributed communication to improve robustness, assessing frameworks capable of monitoring and controlling actions in real-time. Future communication networks need to include the city infrastructure and utilization of resources. Smart Cities introduce a benefit from digitizing various ecosystems at a city level. Recent advances in the design of reconfigurable intelligent surfaces reinforce the idea of a smart environment by taking advantage of the infrastructure to boost wireless networks performance. RIS offers flexibility in creating a more innovative communication system, including applications in smart cities and the grid. Computing, networks, and even global energy consumption in 6G networks front up considerable openness to innovation and radical approaches to hardware design. RIS novel designs convey power, performance, size, and space augmentation.

1.2 Objectives

- The main objective of this Thesis is to develop a study on the SG approaches to interconnect power grid, signal processing, and communication system perspective, including state-of-the-art trends in the smart world concept.

In order to reach the main objective, the above specific objectives are defined:

- Develop a systematic review of SG faults from the most significant research databases and state-of-the-art research papers to analyze and indicate relevant topics for future developments related to fault detection and classification in SG systems.
- Compare estimation techniques for harmonic detection in SG and micro-Smart-Grid (μSG) systems considering non-stationary scenarios and critical elements in the SG scenarios.

- Evaluate the communication network's importance on reliable monitoring power lines SG and μSG system applications.
- Explore the main SG critical application while characterizing the QoS requirements in smart grid communication (SGC) systems to propose an improved random access protocol.
- Propose and comprehensively characterize modifications to suit RA protocols, depending on existing applications and the number of devices in SG applications.
- Evaluate the implementation of RIS to improve the overall system Energy Efficiency under smart cities 5BG networks perspective.
- Describe a smart city scenario to maximize EE using distributed precoding in a RIS-aided scenario.

1.3 Outlines of the Work

The thesis is organized as follows:

Chapter 1: ***Introduction***. This chapter provides the purpose, statement of the problem, objectives, and research methodology of this thesis.

Chapter 2: ***Faults according to Smart Grid systems***. This chapter gives a State-of-the-Art resume with a systematic review and summarizes the monitoring infrastructure. This chapter aggregates concepts and procedures associated with the SG faults detection and location.

Chapter 3: ***Harmonics in Power System***. Chapter 3 presents an introduction of power systems harmonics. This chapter implements different harmonics estimation methods, following up with the discussion.

Chapter 4: ***Quality of Services and random access protocols.*** This chapter highlights the significance of existing and future random access protocols for m-SGC devices and system performance. This chapter shows RA protocols' influence in achieving QoS m-SGC requirements and introduces an improved RA protocol for critical SG applications.

Chapter 5: ***Energy Efficiency Optimization in Reflecting Intelligent Surfaces-Aided Systems***. This chapter analyzes a distributed precoding design for energy efficiency (EE) maximization in a RIS-aided multi-user (MU) MIMO UL network with a set of

multi-antenna BS and multi-antenna UT.

Chapter 6: ***Conclusions and Final Remarks***. The conclusions are based on research discussions. The main objective is to present a study of fault conditions on SG systems from a signal processing perspective.

1.4 Submissions and Publications

This section enumerates the works developed throughout the doctorate work, which are divided into published and submitted papers.

1.4.1 Published Papers

[P1] Angel Esteban Labrador Rivas, Newton da Silva, Taufik Abrão. "Adaptive Current Harmonic Estimation Under Fault Conditions for Smart Grid Systems", *Electric Power System Research*. ISSN: 0378-7796, Volume 183, June 2020, pp. 106276. Elsevier journal (A2-Qualis, IF: 3.414). DOI: 10.1016/j.epsr.2020.106276

[P2] Angel Esteban Labrador Rivas, Taufik Abrão. "Faults in smart grid systems: Monitoring, detection and classification", *Electric Power System Research*. ISSN: 0378-7796 Volume 189, December 2020, pp. 106602. Elsevier journal (A2-Qualis, IF: 3.414). DOI: 10.1016/j.epsr.2020.106602

1.4.2 Submitted (Under review) Papers

[P3] Angel Esteban Labrador Rivas, Taufik Abrão. "Raptor-IRSA Grant-free Random Access Protocol for Smart Grids Applications", (Submitted on May 2021 to *Sustainable Energy, Grids and Networks (A2-Qualis, IF: 3.899)*).

[P4] Angel Esteban Labrador Rivas, Taufik Abrão, Ekram Hossain. "Energy Efficiency Optimization in RIS-Aided Uplink Multi-User MIMO With Distributed Precoding", (Submitted on Jan 2022 to *IEEE Wireless Communications Letters (A1-Qualis, IF: 4.348)*).

2 Faults according to Smart Grid systems

This chapter provides a comparative framework for classifying a vast number of components of SG systems, aiming at gaining understanding on monitoring, locating, detecting, and classifying faults in SG systems. We discuss common faults occurring in electric power systems and how such concepts differ depending on the faulted section. Besides, a brief comparison of different power failure categories is offered. Furthermore, this chapter brings a discussion on AMI under the perspective of power faults in SG systems. Nevertheless, evaluating communication network importance on fault detection. Moreover, this chapter provides a systematic review on SG faults from the most significant research databases and state-of-the-art research papers to create a comprehensive classification framework on the relevant requirements.

The main published surveys and tutorials on Fault Detection and/or Location in SG Systems (FD/L-SG) are compiled and compared in this subsection in terms of the range of application, covered topics, and trending research.

Existing surveys: Table 2.1 lists the existing surveys related to fault detection and/or location in the SG systems context. Most of the published surveys do not contain a wide range of applications. The currently published surveys either focus on particular components of the SG system or do not cover monitoring components or prominent communication technologies to achieve QoS requirements and constraints in SG systems.

Table 2.1 – A list of surveys in fault detection and/or location for the SG systems context

Year	Ref.	Description
2017	(BAHMANYAR et al., 2017)	A review of fault location and outage area location methods for distribution systems
2016	(FERREIRA et al., 2016)	A survey on intelligent system application to fault diagnosis in electric power system transmission lines
2017	(MADETI; SINGH, 2017a)	A comprehensive study on different types of faults and detection techniques for solar PV
2018	(ANDRESEN et al., 2018)	Fault detection and prediction in smart grid systems
2018	(BABAEI et al., 2018)	A survey on fault detection, isolation, and reconfiguration methods in electric ship power systems
2018	(FARUGHIAN et al., 2018)	A review of the principles of fault location and indication techniques and their application considerations

To fill this gap, in this work, we investigate in-depth the role of sensing and

monitoring within FD/L-SG scenarios. We have covered the latest surveys on FD/L-SG and related papers until Q2 2020. Note that detection/location depends on many system components and different system-level applications; therefore, covering the entire spectrum of applications to evaluate future research directions is out of the scope of this review.

We focus on future topics related to monitoring and communication techniques for SG systems.

Summary of the contributions: This chapter covers different aspects of fault detection in SG systems. The goal is to indicate relevant topics for future development to bridge the gap between legacy and future fault detection techniques. The main contributions of this work can be summarized as follows:

1. We provide a systematic review of Gls SG faults from major research databases and cutting-edge scientific articles to create a comprehensive structure for classifying the relevant requirements.

2. We conduct in-depth and comprehensive research on the role of several components of the legacy power system and SG systems.

3. We discuss in detail the classification of different fault scenarios in a comprehensive framework including system-level of application, *e.g.*, transmission, distribution, commercial, DG, and Electrical Vehicle (EV).

4. We analyze and indicate relevant topics for future developments related to the monitoring and fault detection and classification in SG systems.

We outline future research opportunities and directions. The graphic illustration of the scope of this chapter is shown in Fig. 2.1. Finally, based on the handled reports regarding faults in SG systems, considering monitoring, detection, and classification, we identify the existing challenges and future research directions.

2.1 Failure in SG Systems Components

The demand for electric power is growing with the arrival and establishment of smart cities and Industry 4.0. Fault analysis is essential to enhance performance and minimize interruptions in the smart power system. It is fundamental to detect, locate, and apparent faults at any power system level to keep the system operating in average condition. This task requires intelligent control to perform quickly and efficiently (TOKEL et al., 2018).

Next, we describe the concepts in a physical framework approach, avoiding evaluation of the software framework (sometimes called Resilient Information Architecture

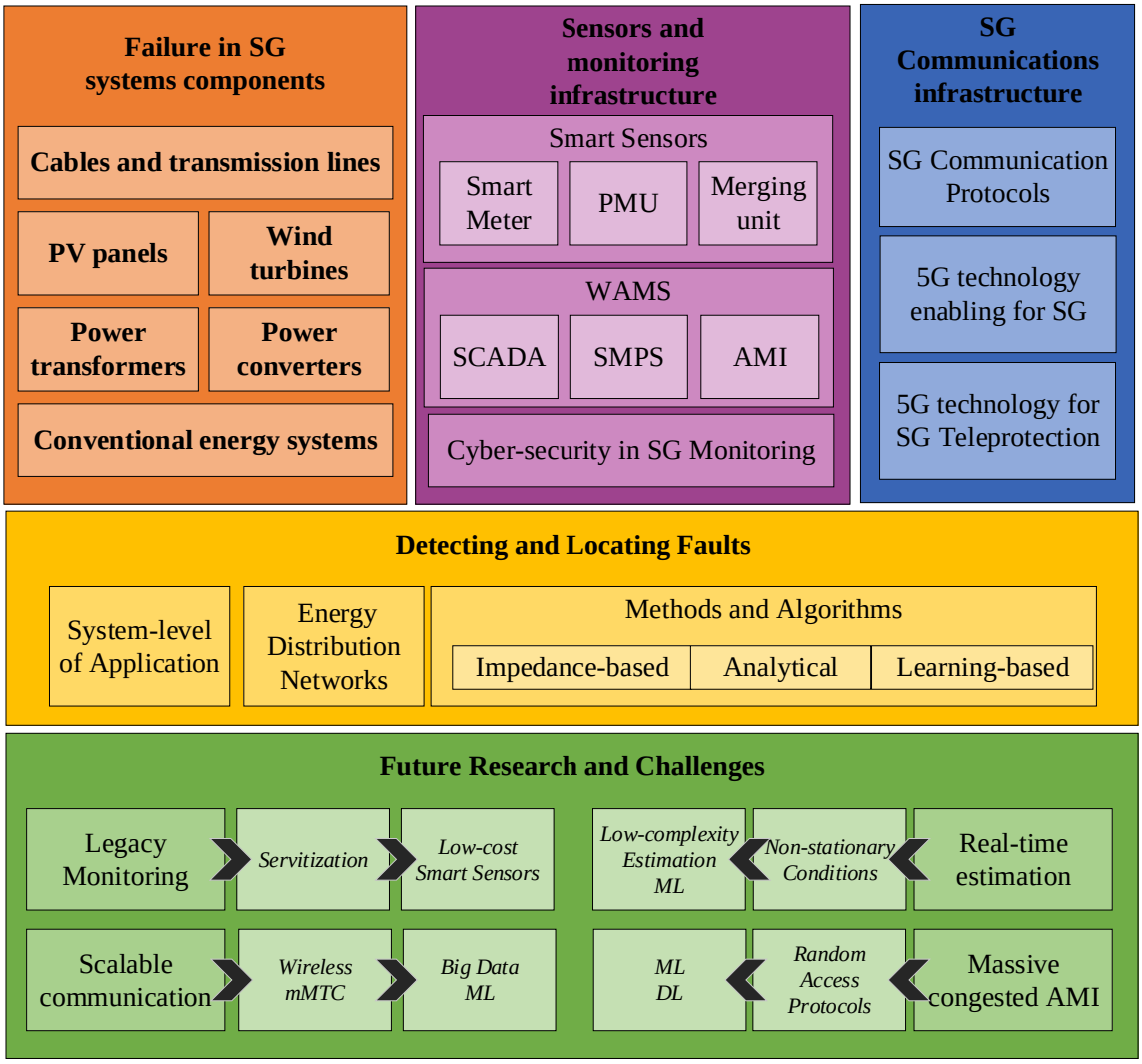

Figure 2.1 – Composition and SG topics discussed in this chapter.

Platform for Smart Grid (RIAPS)), which includes architectures for a highly resilient, hierarchical fault management scheme. The problem of reliability and resilience in decentralized, real-time, embedded systems concerning fault detection and mitigation per the physical layer is remarkable, deserving massive researches in the future.

Faults that can arise at different layers of the system can be categorized as follows:

1. **Physical devices/components fault:** These faults occur when a physical element does not function properly.

2. **Communication fault:** These faults occur in communication devices/channels. Related to faults in the physical links, or failure establishing communications in a critical time period.

3. **Software/Hardware-level fault:** These faults occur when a component of the control center fail command and/or operation.

On a physical level, the grid itself conforms to the $N-1$ power system rules, which means any physical component, *e.g.*, circuit breakers, transformers, transmission lines, etc., can fail, but the power system is still operating (GHOSH et al., 2020). This principle carries over to the sensors and actuators, *i.e.,* there is sufficient redundancy in the system.

The fault management technology mainly relies on the communication network of the SG system. Additionally, fault management is critical to reducing synchronization issues and improving incoming systems. However, most fault management techniques require a data processing center to monitor and diagnose the operation of the system in real time, as well as fault indicators, local automation and communication equipment. In addition, it is critical to detect and locate faults fast enough to avoid overall system collapse.

Faults in the electrical infrastructure of the SG include various components of the μG and also the causes and effects of the faults, Fig. 2.2. The following subsections provide details of these failure modes for various physical systems and components inside the SG architecture.

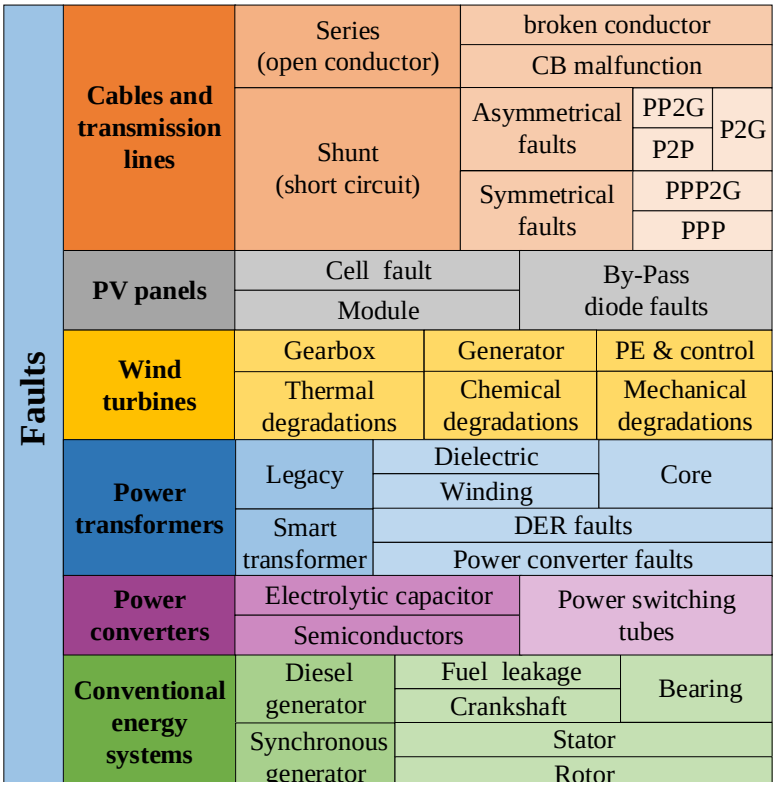

Figure 2.2 – Types of faults in the SG infrastructure

2.1.1 Cables and Transmission Lines

Power cables constitute the critical links between the generation sources and loads, including transmission and distribution-level lines. They usually carry low voltage, step down from the transmission grid, or are generated by distributed generation systems.

Power cables are usually installed underground, while transmission lines are laid overhead (HARE et al., 2016; DILEEP, 2020). Underground cables are subject to mechanical failure, thermal runaway due to compacted soil as an insulator, and typical wear and tear. In contrast, overhead lines are susceptible to natural causes that may fail due to lightning strikes, icing, breakage caused by animal or tree obstructions, short circuits, overloading, aging, human actions, or lack of maintenance.

Faults may be classified into two types, i.e. series (open conductor) faults and shunt (short circuit) faults. Differences among the impedances of three phases indicate a series type fault, which is usually caused by the interruption of one or two phases. Series faults in transmission/distribution lines may occur due to a broken conductor or a Circuit Breaker (CB) malfunction in one or more phases. Short circuit faults are divided into two types, i.e. asymmetrical faults, and symmetrical faults. The asymmetrical or balanced fault affects each of the three phases equally. An asymmetric or unbalanced fault does not equally affect each of the three phases. Asymmetrical faults Phase to Ground (P2G), Single-Phase to Phase (P2P), and Two-Phase to Ground (PP2G), and symmetrical faults are Phase to Phase (P2P) and Three-Phase to Ground (PPP2G) faults (TLEIS, 2008).

2.1.2 Photovoltaic (PV) Panels

Photovoltaic (PV) panels use solar radiation to generate electricity for μG. Their structure consists of glass, metal, polymer, and semiconductors. Common failures in the PV panel include:

1. *Cell faults:* These faults can also be divided into three main faults: (i) battery open/short, (ii) hot spot faults, and (iii) degradation faults. An open/shorted battery is induced when a battery is disconnected or shorted, an open/shorted battery is induced, resulting in battery loss. A hotspot fault is indicated when the panel is partially shaded or damaged, reducing battery current. Degradation failures are affected when cell series resistance is elevated due to overexposure; cell shunt resistance is reduced due to crystal damage/impurities in cross junctions, garbage buildup on surfaces, cell mismatch, and overheating.

2. *Module faults:* These failures typically include open or short circuits, glass breakage, and delamination. In most cases, these failures occur due to manufacturing defects, mechanical loads (such as snow accumulation), corrosion, natural phenomena, and degradation of the battery's anti-reflective coating.

3. *By-Pass diode faults:* These faults occur due to short or open circuits. In an open-circuit failure, the battery can develop a hot spot, while a short-circuit failure reduces power generation efficiency. These usually happen due to overheating of the diode.

The failure modes described above corresponding to the PV panels result in decreased output power leading to reduced voltage and current signals in the μG.

2.1.3 Wind Turbines

Wind turbines represent another renewable energy source that uses wind energy to generate electricity. Turbines experience various failures in the following subsystems:

1. *Gearbox:* Gearbox failures are typically bearing failures which are a significant concern of wind turbine failures as they occur in many subsystems. Bearing defects usually fall into two categories: inner/outer race defects or ball defects, which result from abrasive wear, corrosion, lack of lubrication, and build-up of debris.

2. *Generator:* generators can fail due to bearing, stator and rotor defects. The above-described disadvantages of the bearings are similar. Stator and rotor failures are mainly open / shorted circuits, bad connections in the windings, broken rotor rod, air eccentricity, and demagnetization. Stator failures occur due to insulation degradation causing short circuits, while rotor failures occur with broken or shorted windings. Generator failures result in unbalanced voltages and currents, reduced average torque, overheating and poor generation efficiency.

3. *Power electronics and electric control:* The faults here mainly occur in semiconductor devices and include short or open oxygen reactions. Their structure consists of membrane, electrocatalyst, catalyst, and gas diffusion layers, which degrade over time. The following degradations occur in these layers:

    - *Mechanical degradations:* Fractures can produce these due to incorrect MEA structure and humidity cycling.
    - *Thermal degradations:* These are usually caused by changes in hydration in Proton Exchange Membrane (PEM), whether due to flooding or dehydration. This usually occurs when the fuel cell is operating outside the recommended operating range.
    - *Chemical degradations:* These occur due to the combustion of hydrogen and oxygen. When they burn, foreign cations may form, causing the coating to degrade.

    PEM fuel cells also contain three other components that suffer from degradation: the bipolar plate, a sealing gasket, and a compressor motor

2.1.4 Power Converters

The power electronics converters are widely used in the fields of energy conversion, in which the Phase-Shifted Full-Bridge (PSFB) DC-DC converters play a crucial role in multiple cases such as aeronautics, astronautics, hybrid EV applications, among others. Power switching tubes are one of the most vulnerable components in power electronic converters because of over-voltage, over-heating, or erroneous signal (KOU et al., 2020).

The most critical elements of power converters are electrolytic capacitors and semiconductors. Due to their cost, size, and performance, capacitors are the usual choice for smoothing the output voltage in DC-DC power converters. Nevertheless, according to (SILVEIRA; ARAÚJO, 2020), electrolytic capacitors frequently determine the lifetime of Pulse Width Modulation (PWM) converters and are responsible for more than 50% of their failures. The fault of the power semiconductor comprehends a short-circuit fault and open-circuit fault. Short-circuit faults, usually protected by the standard protection circuit, are considered as the most dangerous, and the Insulated-Gate Bipolar Transistor (IGBT) will shut off instantly once short-circuit fault is detected. On the contrary, the open-circuit faults ordinarily last for some time and may cause subsequent damage to other equipment.

2.1.5 Power Transformer

Power transformers are fundamental components of power systems, and damage to or failure of transformers causes significant economic and social injuries. Consequently, performing efficient and reasonable transformer fault diagnosis is essential for power systems' safe and secure operation. An in-service transformer handles numerous harmful operating conditions that can break down the insulating materials and release gaseous decomposition products dissolved in the oil (ZHAO et al., 2019).

2.1.5.1 Smart Transformer (ST)

The Smart Transformer (ST) is a device for active Medium Voltage (MV) to Low Voltage (LV) substations replacing the classical electromagnetic transformer with an AC/DC/AC power conversion frame with a high-frequency transformer. This framework makes ST sensible to those failures present on power converters. Those STs support loads during a partial disconnection in an High Voltage (HV)/MV power system. For a system fault, the storage unit placed in the ST and the Distributed Energy Resources (DER) located downstream from STs provide active power to other MV feeders (COUTO et al., 2019).

2.1.6 Conventional Energy Systems (CES)

Conventional Energy Systems (CES) include power plants using fossil fuels (natural gas, diesel, coal, etc.). In SG architecture CES, commonly Diesel generators, back-up renewable power generation. Diesel engines have the following faults (HARE et al., 2016):

- *Fuel Leak:* this is caused by the growth of small holes in the system and causes air pollution. This results in a reduction in gas pressure, which further reduces combustion efficiency.
- *Bearing faults:* these faults are the same as those described for outer ring and ball faults, which are caused by increased mechanical load, wear and corrosion.
- *Crankshaft failure:* the main failure of the crankshaft is the generation and propagation of cracks. This is caused by corrosion or poor assembly and can result in a reduced ability to generate rotational energy as the crack grows; the impact of the failure increases until the shaft snaps in half.

The faults associated with diesel generators cause a decrease in their performance, causing current and voltage drops.

2.1.6.1 Synchronous Generators (SyG)

Power systems are mainly fed by the synchronous generators of large thermal power plants. The fault behavior of these Synchronous Generator (SyG) is well defined: when a fault occurs a SyG responds as an ideal voltage source behind an impedance and inject fault currents up to 5–10 PU (BAECKELAND et al., 2020).SyGs are one of the most critical elements of power systems. Unlike other power system components, SyGs need protection from several different types of faults and abnormal operating conditions, such as stator winding faults, overload, unbalanced operation, loss-of-excitation, loss-of-synchronism, and motoring. Modern digital signal processing techniques and advanced model-based analytical methods improve generator protection (MORAIS et al., 2018), especially from a potential stator fault. This type of fault may cause severe damage to the generator.

The most common type of fault that SyGs are subject to is ground faults in stator windings. When SyGs are grounded with high impedance, it is difficult for differential protection to detect faults on stator winding since small fault currents are generated. The faults for these components are single/multiple phase short circuits, inter-turn short circuits, saturation, grounded windings, rotor bending/cracking, air eccentricity, and permanent magnet degradations (KOSMADAKIS et al., 2013). Such failures occur due to insulation damage/degradation, reduced lubrication, overheating, and manufacturing defects, resulting in voltage and current harmonic imbalances, reduced power generation efficiency, and current phase shifts.

The various failure modes of the different μG components described in this section illustrate the scope of failure in the SG architecture. We know that these are limited categories in the syllabus of the vast power system.

2.2 Sensors, Actuators, and Monitoring Infrastructure

Sensors play a critical role in real-time monitoring and controlling power transmission and distribution systems. Besides, sensors are fundamental for maintaining grid health and stability. Sensors measure several physical parameters at different system-level of application, including power generation, transmission lines, substations, distribution lines, energy storage, consumption, and customer profile. Among those sensors, Current Transformers (CTs) and Voltage Transformers (VTs) keep large partitions between legacy and smart power system installations. Recently, the number of measuring devices and sensors in the power grid has increased quickly, within PMUs and SMs, also named AMI, as most extended devices demanding attention for future research (ANDRESEN et al., 2018). We present a non-exhaustive list of sensor devices commonly used in power systems. (SONG et al., 2017):

- Merging Units (MUs)
- temperature sensors
- humidity sensors
- accelerometers
- rain gauges
- internet protocol (IP) network cameras
- pyranometers and pyrheliometers (solar irradiance)
- weather stations
- sonic anemometers
- partial discharge sensors
- gas sensors
- ultrasound and ultra-high frequency sensors
- torque sensors
- discharge rate sensors
- load-leveling sensors
- occupancy sensors

- Power Quality Analyzers (PQAs);

Fig. 2.3 depicts an SG overview that includes crucial monitoring devices (PMUs and SMs), whether communications and power links exist among all-important connections.

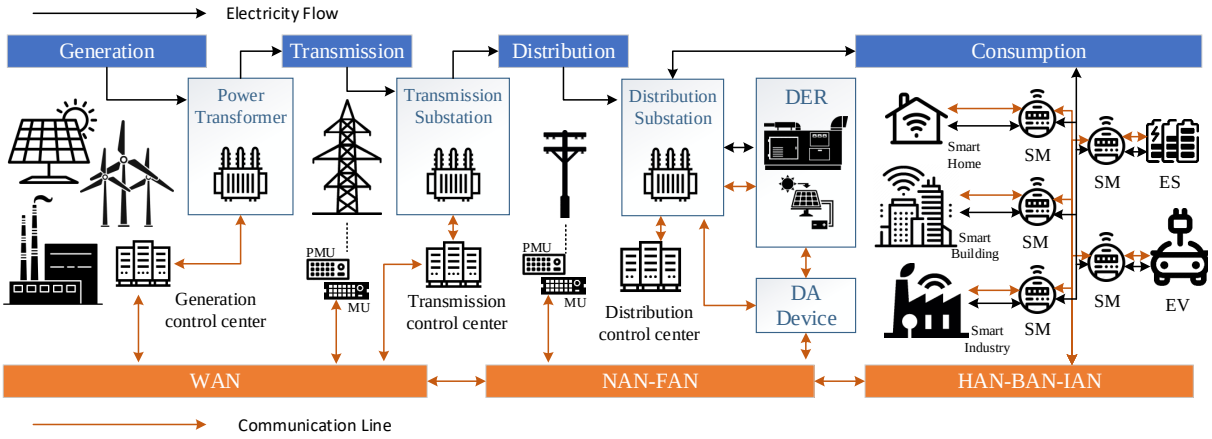

Figure 2.3 – Smart Grid infra-structure overview, including monitoring key devices.

With the broader deployment of PQA and PMU devices, the SG enables real-time monitoring through an effective communication network. This allows the continuous evaluation of the current state of the grid, indicating congestions, frequency oscillations, and overall load distribution (ARTALE et al., 2017). They empower the real-time application of estimation algorithms for fault diagnostic to reduce fault recurrence.

SG continually produce data such as voltage, current, phase angle, power (kW, kVA, kVAR), temperature, type of grid connectivity, and statistics on supply and demand. In their primary form, such raw data signals are noisy, verbose, and require large amounts of memory to store. Therefore, these data signals require conversion into informative features for meaningful and timely analysis (PHAN; CHEN, 2017).

Assembling the power grid smart relies on recognizing the unprecedented penetration of sensing data to draw insights into the system's behavior and automate the available controls. With these volumes of data collected increased, new architectures, concepts, algorithms, and procedures will be necessary to obtain a more intelligent system. The risen volume of measurement data from the power grid, in combination with tending methods within machine learning (IBRAHIM et al., 2020), gives innovative possibilities in terms of fault detection and mitigation (MUNSHI; MOHAMED, 2017). Table 2.2 summarizes the data sources characterization, which contributes to assessing the SG trending behavior qualitatively. Legacy sources still represent an essential portion of the data origins. Moreover, the tendency of incorporating data generated from the new AMI and PMU devices for fault detection/location is another critical direction to be considered. Reliability Improvement represents a challenging task whether a massive number of devices arises in SG systems.

Table 2.2 – Data source for fault detection/location in SG systems

Source	Reference
Miscellaneous data (Historical, operation)	(MESKINA et al., 2014; BANGALORE; TJERNBERG, 2015; CHEN et al., 2016a; SUN et al., 2016)
AMI	(SANTIS et al., 2018; CHAKRABORTY; DAS, 2018; KOZIY et al., 2013; MANANDHAR et al., 2014; PASDAR et al., 2013; SHAO et al., 2017; KUO et al., 2017; WISCHKAEMPER et al., 2015; MARTINEZ-FIGUEROA et al., 2017; MOGHADDASS; WANG, 2018; YEN et al., 2019; ZHANG et al., 2013a; DEVI et al., 2018; DHEND; CHILE, 2017)
Legacy Sources (CT, VT, DFR)	(MISHRA et al., 2016; ZHANG; MU, 2018; TOKEL et al., 2018; MILIOUDIS et al., 2015; MESKINA et al., 2014; ALHELOU et al., 2018; HE; BLUM, 2011; KATIC; STANISAVLJEVIC, 2018; MAHFOUZ; EL-SAYED, 2016; RAWAT et al., 2016; DAS et al., 2017; DHAR et al., 2018; LI et al., 2018; SALEH et al., 2017b; YU et al., 2017; HARROU et al., 2018; CHAITANYA; YADAV, 2018; CHEN et al., 2016a; CHEN et al., 2016b; DARYALAL; SARLAK, 2017; MADETI; SINGH, 2017b; QI et al., 2017; SALEH et al., 2017a; WANG et al., 2018; XI et al., 2017; YANG et al., 2016; YI; ETEMADI, 2017; ZHANG; MU, 2018; HUANG et al., 2016; CHEN et al., 2015; MISHRA et al., 2014; ROBSON et al., 2014)
PMU	(HE; ZHANG, 2011; RAHMAN et al., 2015; JIANG et al., 2018b; JIANG et al., 2014; GHARAVI; HU, 2018; HE; ZHANG, 2010; JIANG et al., 2016; DOBAKHSHARI; RANJBAR, 2015; GOPAKUMAR et al., 2018; AFFIJULLA; TRIPATHY, 2018; HASHEMI et al., 2017; NAGANANDA et al., 2015; KUMAR; BHOWMIK, 2018; SEYEDI et al., 2017b; ACHLERKAR et al., 2018)
Other (GOOSE, TWITTER, SCADA)	(PARIKH et al., 2013; SUN et al., 2016; ZHANG et al., 2013a)

The figure of merit reliability- *vs*-costs measures the impacts of a monitoring system. In SG system failures rise severely for smart monitoring if the availability of this system decreases progressively (HONARMAND et al., 2019). The utility expenses limitations create an optimization framework requirement to evaluate the annual cost saving with a minimal, intelligent monitoring infrastructure.

WAMS is an advanced measurement technology consisting of advanced information tools and operational infrastructure that facilitates the operation of complex networks by collecting data. It provides complete monitoring, control, and protection. This section will explain the main components of a wide area system. PMU is the facilitator of WAMS which prevents any blackouts in the electricity network. The SCADA, PMU, and AMI are explained in the sequel. Important WAMS applications include a) detection of loss in synchronism; b) temperature identification; c) power system restoration; d) phase angle monitoring; e) voltage stability monitoring; f) line thermal monitoring; g) power oscillation monitoring; h) power damping monitoring (PHADKE et al., 2016; PISANI; GIANNUZZI, 2016).

μGs are self-governing electricity environments that operate within a more extensive electrical system. They can respond to a crisis or recommend the best operation response inside the necessary time frame to manage local problems when required. Centralized power-sharing, dispatching, and frequency/voltage restoration depend on the μG's reliable and optimal monitoring operation. The presence or absence of DG units affects fault currents that flow through the feeders (SEYEDI et al., 2017a). Therefore, Intelligent Electronic Devices (IEDs) protect the grid by adapting protection settings to overcome new fault characteristics in the μG.

2.2.1 Smart Sensors (SSs)

SSs are sensors with built-in intelligence deployed in the grid, including temperature sensors, pressure sensors, humidity sensors, weather stations, current sensors, and voltage sensors. SS is a sensing device with digitization capabilities and digital information processing capabilities. SSs may communicate using standardized communication protocols, such as the IEEE 1451 family of Smart Transducer Interface Standards (IEEE. . . , 2004), IEEE 1815 Standard for Electric Power Systems Communications - DNP3 (IEEE. . . , 2012), IEEE C37.238 PTP Power Profile (IEEE. . . , 2017), IEC 61850 and others.

Figure 2.4 represents a general model of SSs to achieve requirements for SGs. A SS contains a set of sensors, the Main Processing Unit (MPU) with an internal clock linked with an optional external time reference, and a network communication module. Four modules can define the main basic skills of a smart sensor:

1. sensing through sensors;

2. processing module composed by: analog signal conditioning, Analog-to-Digital conversion (ADC), and sensor data processing;

3. timing and synchronization by an internal clock with optional external time reference;

4. network communication module for communicating with the outside world

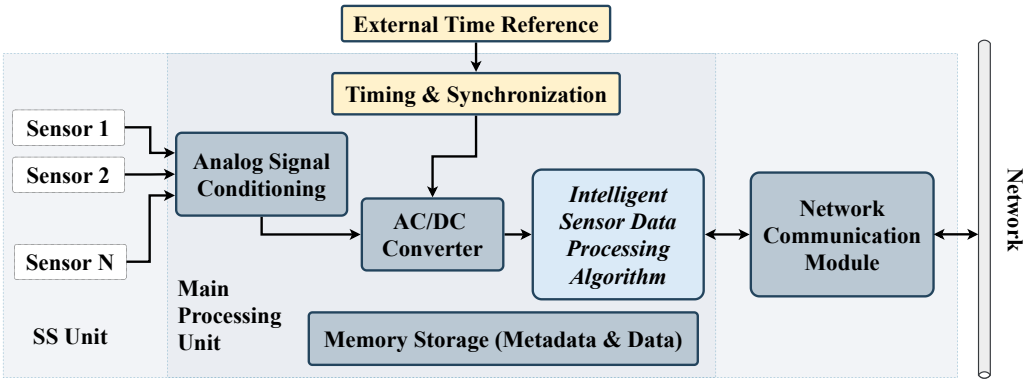

Figure 2.4 – A general SS representation for SG

Sensors provide electrical signals such as voltage and current from power lines in μGs. The internal clock timestamps sensor data and synchronizes with an external time reference, such as Global Positioning System (GPS), One pulse-per-second (1PPS), Inter-Range Instrumentation Group-B (IRIG-B), IEEE 1588 Precision Time Protocol (PTP), or Network Time Protocol (NTP). The analog signal is then calibrated and conditioned in the processing block, and ADC converts the signal to digital form. In contrast, the processing module processes metadata data and simultaneously applies intelligent algorithms under time-synchronized events to improve sensing and measurement accuracy. Finally, the network communication module is wired (serial or Ethernet) or wireless (IEEE 802.11a/b/g/n/ac, WiMAX or 3G/4G/LTE/5G cellular network) communications infrastructure.

2.2.1.1 Smart Meter (SM)

A SM follows a conventional electricity meter, which has only the feature of measuring the consumed electricity. Smart meters are ICT-enabled machines that trace a large number of information, e.g., features of consumption patterns over time. SMs further enable dynamic pricing in the electricity sector, where only one (fixed price per kilowatt-hour) or a maximum of two price levels (day and night supply) have been commercially available so far. Moreover, SMs allow the customer to choose to switch the consumption to off-peak times and save money considering the electricity price will be lower. This is even possible to be automated since devices, *e.g.*, freezers, dishwashers, washing machines, in private households as well as industrial coolers and high-energy-consuming machines,

can be allowed to be directly steered by the energy price or even the energy supplier in order to smoothen the demand curve.

2.2.1.2 Phasor Measurement Unit (PMU)

The PMU measures the phasor of the current and voltage of the connected bus. This device uses the GPS receiver to collect the buses' data at diverse places. The control unit receives collected data through the Phasor Data Concentrator (PDC). The PMU 's provided real-time time-synchronized data and high resolution for advanced applications, such as wide-area situational awareness, state estimation, monitoring system dynamics, and validating system models. ADC takes data samples from the AC waveform and applies the DFT. Concerning the common reference axis, the voltages of different buses are compared and monitored (YANG et al., 2018).

A PMU is a microprocessor-based device that uses the capabilities of Digital Signal Processor (DSP) to measure 50/60 Hz AC waveforms (ANANDAN et al., 2019) at a typical rate of 16-64 samples per cycle. These PMU are optimally placed at different substations and can provide time-sampled positive sequence voltages and currents for all monitored buses. Transformers provide analog input signals for voltage and current. To take full advantage of Synchro-Phasor Measurement (SPM), the architecture involves PMU, communication links, PDC. It is worth noticing that the recent commercialization of the GPS with the accuracy of timing pulses in the order of 1 microsecond (1μs) is made possible by many industries (GHARAVI; HU, 2018; ANDRESEN et al., 2018). By using 1μs-PMUs, a high degree of accuracy in monitoring and faults detection is achieved.

2.2.1.3 Merging Unit (MU)

MU is a method capable of converting analog signals from legacy CTs and VTs to sampled/digital values. Those devices merge (align) multiple phases based on time synchronization and transmitting Sampled Values (SV). The relay is protected by a network based on the International Electrotechnical Commission (IEC) 61850-9-2 standard protocol. MU provides the real-time status of the grid.

A key challenge facing the grid is the communication interoperability of these smart sensors. A set of existing standard communication protocols for SS and generic SS based on SM-, PMU- and MU are listed in the table 2.3.

2.2.2 Supervisory Control and Data Acquisition (SCADA)

The SCADA is an automation and control system based on computers and directly applicable to supervise SG systems. The supervisory control emerged to operate and control from a remote location. The control system is combined with data acquisition systems (WISCHKAEMPER et al., 2015; GHARAVI; HU, 2018). The main functions of

Table 2.3 – Common interface standards for SS

Smart Sensors	Interface Standards	Network Connections	
		Wired	*Wireless*
PMU	IEEE 1344 IEEE C37.l18.2 IEC 61850-90-5	TCP/IP UDP/IP RS232 Optical	3G/4G/LTE Cellular WiFi WiMAX
MU	IEC 60044-8 IEC 61869-9 IEC 61850-9-2	TCP/IP UDP/IP Optical	3G/4G/LTE Cellular WiFi
SM	IEC 62053-23 IEC 62056-21	TCP/IP UDP/IP RS232 Optical	3G/4G/LTE Cellular WiFi ZigBee
general purpose SSs (Current, Voltage, Temperature, etc.)	IEEE 1815 IEEE 1815.1 IEEE 1451 ISO/IEC/IEEE 21451 ISO/IEC 30101	TCP/IP UDP/IP RS232 Optical	3G/4G/LTE Cellular WiFi WiMAX ZigBee 6LowPAN

the SCADA are monitoring, data presentation, data acquisition, supervisory control, alarm display. It consists of hardware and software monitoring levels. The main components of SCADA are Remote Terminal Units (RTU), Programmable Logic Controller (PLC), telemetry system, data acquisition server, Human Machine Interface (HMI). The computer collects the data and sends signals to the control unit. Sensors can be analog or digital and interfaced with the system. These cannot provide the dynamic state of the power system. The received data is also not time-synchronized. SCADA provides stable information, low sampling density, and asynchronous (FERREIRA; BARROS, 2018; RAWAT et al., 2016). The dynamic state of the system is not provided, so immediate action cannot be taken in the event of a failure. Master Terminal Unit (MTU) is the main part of the SCADA system, the server; all communications, data from RTU are managed and stored, while commands and interfaces to operators are controlled by MTU manage.

Consider the diagram of the SCADA system depicted in Figure 2.5 which consists of several blocks, specifically, substation sensors (PLC, CTs, VTs, Temperature, Oil indicators, others) to RTU forward through a communication infrastructure, routed to the SCADA network to a specific application. Those applications include Open Platform Communications (OPC) Server, HMI Station, Supervisory system, SCADA Programming, Database, and Application Server.

2.2.3 Synchronized Phasor Measurement System (SMPS)

The Synchronized Phasor Measurement System (SMPS) was firstly developed in mid-1980's (PHADKE, 1993). It measures the phasor of voltage, current, and the local

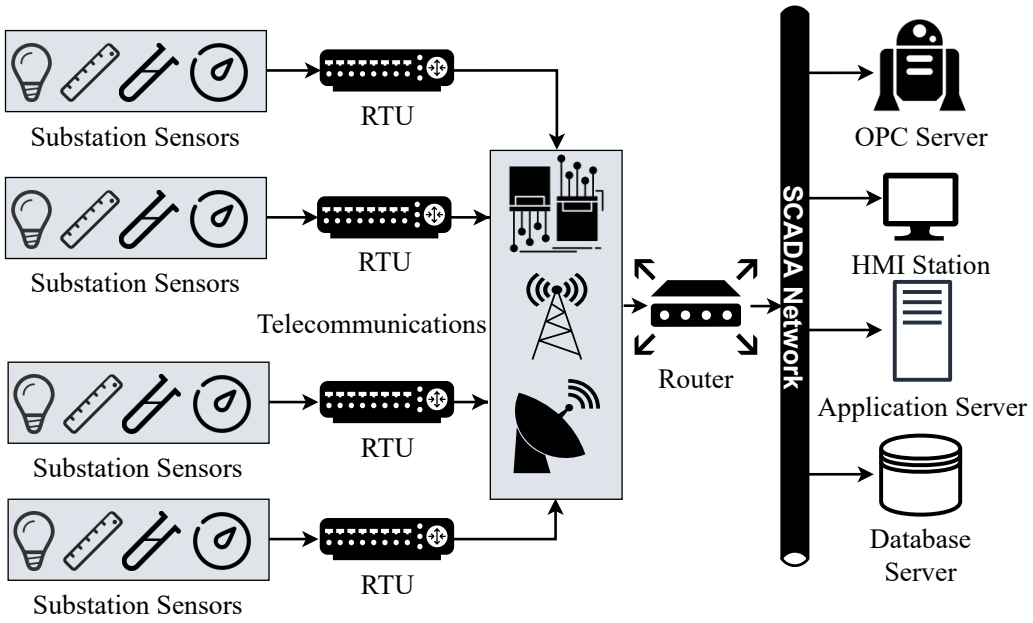

Figure 2.5 – SCADA network architecture for SG systems.

frequency and its rate of changes. This SMPS consists of three main parts namely PMU, PDC, and Communication system. The PDC gathers the data from several PMU and rejects the bad data, and aligns the timestamps (ZHANG et al., 2013b).

Figure 2.6 illustrates the structure of a WAMS system including the PMU unit-specific components. PMU record measurements and timestamps each measurement using the GPS. Data from a single PMU is routed to PDC, which aggregates and time-aligns the data before passing it to downstream application consumers. PDC has been extended to provide additional data processing, and storage capabilities (WALLACE et al., 2016). The equivalent part of the power system is modeled based on the PMU measurements. It is called System Identification and is an integral part of Wide Area Monitoring, and Control (PERTL et al., 2018).

2.2.4 Advanced Metering Infrastructure (AMI)

AMI is a critical component that requires an understanding of the vision of SG. In general, AMI consists of the SMs and the Meter Data Management System (MDMS) (DEPURU et al., 2011). Figure 2.7 represents AMI elements from an SM with a meter board and data tables transmitting data via a serial port through a communication board to a concentrator. Followed by the MDMS to the application layer (*e.g.* DMS or/and Consumer Information System (CIS)) Sensing or perception acts as an essential process of interacting with the outer environment throughout the current status of the system is denoted with quantified characteristics (JIANG et al., 2018a). Each intelligent device takes up some computing power and has self-sufficient capacities, distributing data and information that other devices cannot perceive.

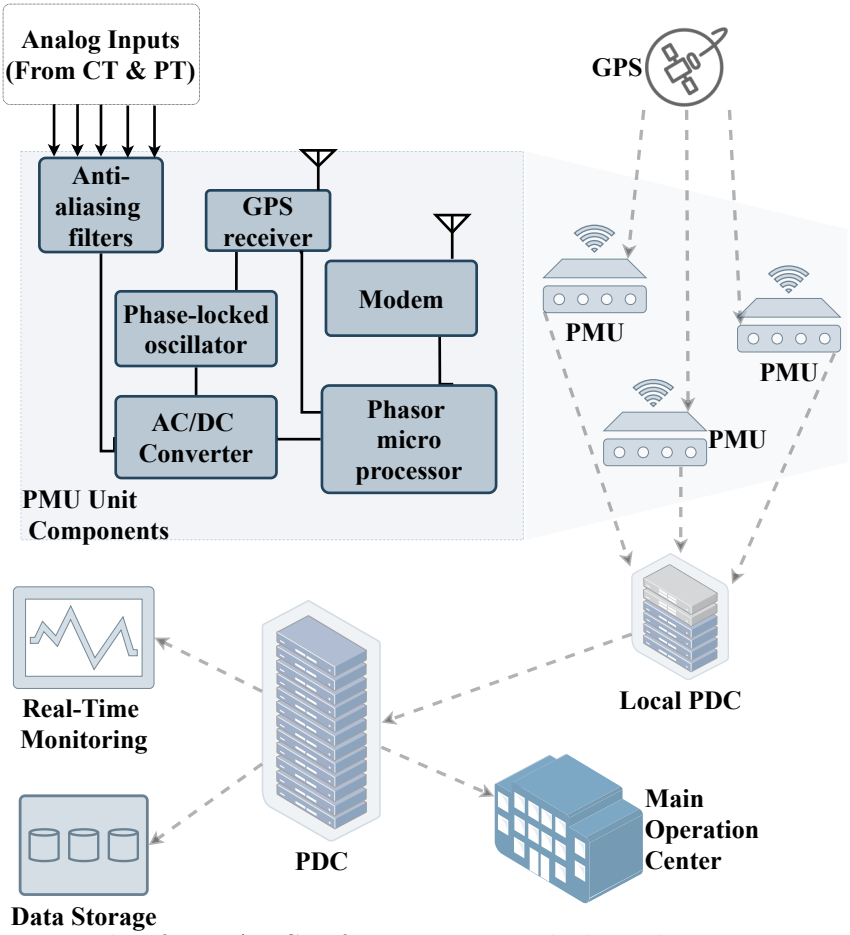

Figure 2.6 – Example of a WAMS infrastructure including the PMU Unit components.

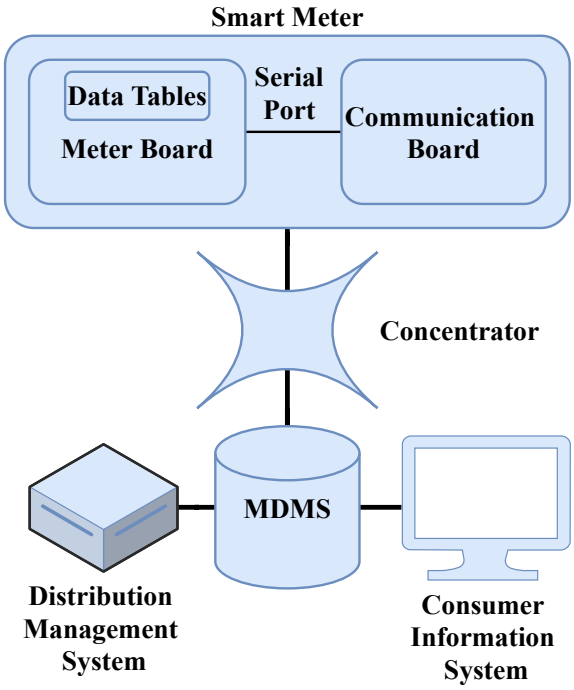

Figure 2.7 – Advanced Metering Infrastructure (AMI).

The SMs consist of the communication board and the meter board that is connected typically using a serial port. The communication board handles the job of communicating with external nodes such as collectors or home devices to accomplish the required computations. A set of tables in the main-board store critical information in the form of keys and passwords to establish secured communication. The meter board also performs the power consumption measurements. The communication board uses an interrupt-based mechanism to obtain data or other needed information from the meter board. The data is then finally sent to the utility by the communication board (EMMANUEL; RAYUDU, 2016). The MDMS is an essential component in AMI and serves as a database for long term data storage and management of events and data usage (WISCHKAEMPER et al., 2015; ANDRESEN et al., 2018; MAHMOUD; XIA, 2019).

AMI also facilitates two-way communication between meter and distribution system operators. The two-way communication facilitates operations of many services for the distribution system operator that have been very hard to implement without smart metering attributes (EMMANUEL; RAYUDU, 2016; BAHMANYAR et al., 2017). For instance, a system operator detects a power outage faster without the customer's interaction. Also, reporting the power quality delivered is another service provided by smart metering. SM also allows detailed monitoring of power flows within the distribution system that was previously available only at the substation/transmission level (TARHUNI et al., 2015). This careful monitoring enables utilities to respond promptly to fluctuations in consumption levels. The power flow monitoring information is also helpful for real-time pricing, which is handled by one technology known as Demand Side Management (DSM). Recent advancements in SM technologies for systems have made several utilities and states induce different time-based pricing initiatives(PHAN; CHEN, 2017; DHEND; CHILE, 2018).

The presence of the SM throughout the world should double from 2017 to 2024, starting up new possibilities for customer-side control and analytics. Consequently, the combined global investment on AMI will roughly multiply over the same time, growing from $73 billion in 2017 to $145.8 billion in 2024 (all values USD) (KELLY; ELBERG, 2020). Table 2.4 summarizes the new AMI deployments announced on the world markets between April 2019 and September 2019. This counts a more significant expansion over the Asian Pacific Region with over 13 million SM units.

According to (COMMISSION, 2019) SM penetration in the United States (US) by 2020 will be over 90%, with an estimation of more than 85 million SMs installed. Table 2.5 shows the number of SM by city SG projects in the US published in OpenEI.org. Besides, Asia will be the largest market for smart meters over the next five years, considering almost two-thirds of the global AMI installed base through 2024. China is the key market driver in the region. The country now ranks for more than half of all smart meters installed worldwide. The State Grid Corporation of China — the country's main power distribution

Table 2.4 – New AMI Deployments Announced, World Markets: April 2019 to September 2019 (KELLY; ELBERG, 2020)

Region	Country	Stakeholder	Meters
Asia Pacific	Taiwan	Taipower	12,000,000
Asia Pacific	Pakistan	Lahore Electric Supply Company	1,200,000
Western Europe	Sweden	E.ON	1,000,000
Latin America	Uruguay	UTE	750,000
North America	US	City of Colorado Springs, Colorado	590,000
North America	US	Ohio Power	475,000
Middle East	Kuwait	Kuwait Ministry of Electricity and Water	300,000

and transmission utility — stationed 476 million smart meters between 2011 and 2017. India will emerge as an increasingly important player in the Asian market, thanks to the new installation of a centralized AMI procurement and financing process. As a result, India is forecasted to surpass Japan as the second-largest AMI market in Asia by as early as 2023.

2.2.4.1 AMI Technical Requirements

The capabilities of an AMI to support the simultaneous operation of major functions, including SM price-induced controls, Distribution Automation (DA), Demand Response (DR) and EV charging/discharging applications in terms of throughput and latency, have been analyzed in (BIAN et al., 2019). Numerical performance results for selected communication technologies and protocols are summarized in Table 2.6, showing that SG applications can run concurrently by piggybacking on existing AMI infrastructure and still achieve their Delay request. Table 2.6 provides a comparison of AMI communication technology implementations across regions and countries. The main technology relies on different elements such as existing metering infrastructure, previous communication protocols for utilities, communication costs, RF spectrum availability and environmental conditions, *e.g.* high-density buildings or to The distance behind - the transport network. Since different SG applications have different characteristics, including data size, data sampling frequency, latency, and reliability requirements, it is critical to ensure the proper functioning of all SG applications, especially those sharing the same bandwidth with an AMI network.

2.2.4.2 AMI Communication Network Security

The use of wireless communication in AMI leads to security issues in such systems. There are several security issues concerning AMI that need attention, ranging from the consumer level to the generation as well as the producer level (MOGHADDASS; WANG, 2018). The adversary can launch an attack by sending false signals to meters that may lead to a power outage in a particular area and disturb the demand generation model.

Table 2.5 – US Smart Grid Projects including AMI according to OpenEI.org

Project	City	State	Smart Meters
ALLETE Inc., d/b/a Minnesota Power	Duluth	Minnesota	8,000
Baltimore Gas and Electric Company	Baltimore	Maryland	2,000,000
Black Hills Power, Inc.	Rapid City	South Dakota	69,000
Black Hills/Colorado Electric Utility Co.	Pueblo	Colorado	42,000
CenterPoint Energy	Houston	Texas	2,200,000
Central Maine Power Company	Augusta	Maine	600,000
Cheyenne Light, Fuel and Power Company	Cheyenne	Wyoming	39,102
City of Fulton, Missouri	Fulton	Missouri	5,000
City of Glendale Water and Power	Glendale	California	86,526
City of Quincy, FL	Quincy	Florida	56,000
City of Westerville, OH	Westerville	Ohio	13,000
Cleco Power LLC	Pineville	Louisiana	279,000
Cobb Electric Membership Corporation	Marietta	Georgia	190,000
Connecticut Municipal Electric Energy Cooperative	Norwich	Connecticut	22,000
Denton County Electric Cooperative d/b/a CoServ Electric	Corinth	Texas	140,000
Entergy New Orleans, Inc.	New Orleans	Louisiana	4,700
Lakeland Electric	Lakeland	Florida	124,000
Marblehead Municipal Light Department	Marblehead	Massachusetts	10,000
Navajo Tribal Utility Association	Ft. Defiance	Arizona	28,000
Pacific Northwest Generating Cooperative	Portland	Oregon	97,666
Reliant Energy Retail Services, LLC	Houston	Texas	140,000
Salt River Project	Tempe	Arizona	580,893
San Diego Gas and Electric Company	San Diego	California	1,400,000
Sioux Valley Southwestern Electric Cooperative, Inc.	Colman	South Dakota	29,000
South Kentucky Rural Electric Cooperative Corporation	Somerset	Kentucky	68,000
South Mississippi Electric Power Association (SMEPA)	Hattiesburg	Mississippi	225,757
Stanton County Public Power District	Stanton	Nebraska	2,315
Talquin Electric Cooperative, Inc.	Quincy	Florida	56,000
Tri State Electric Membership Corporation	McCaysville	Georgia	15,000
Wellsboro Electric Company	Wellsboro	Pennsylvania	4,589
Woodruff Electric	Forrest City	Arkansas	14,450

OpenEI.org is developed and maintained by the National Renewable Energy Laboratory with funding and support from the U.S. Department of Energy and a network of International Partners & Sponsors. Information updated on 28 January 2020.

Table 2.6 – Predominant SM network Communication Technologies by Region

Region	**Country**	**Technology**		
		Mostly	$\Longleftrightarrow$	*Hardly*
Asia	China	PLC	RF Mesh	NB-IoT
	India	RF Mesh	-	-
Europe	Italy	PLC	-	-
	UK	Cellular	RF Point-to-Point	-
Latin America	Costa Rica	RF Mesh	-	-
	Uruguay	Cellular	WiMAX	-
North America	Canada	RF Mesh	PLC	WiMAX
	US	RF Mesh	PLC	WiMAX
Oceania	Australia	WiMAX	RF Mesh	RF Point-to-Point
	New Zealand	RF Mesh	RF Point-to-Point	-

The adversary can also make use of the study of the utilization pattern of the consumers for devising new forms of attacks. Similar to other existing systems, AMI needs to adhere to the requirements of the security primitives of confidentiality, integrity, availability, and non-repudiation (MAHMOUD; XIA, 2019).

AMI maintains confidentiality by preventing any unauthorized access to consumer energy consumption patterns and maintaining system integrity by detecting illegal data changes. Availability requires authorized users to access data on demand (PHAN; CHEN, 2017; GAO et al., 2012). If the necessary data is not found when needed, the system violates the usability aspect of the system security requirements. Any natural or intentional event, such as a hacking attack, must not prevent the system from functioning correctly. For example, if a hacker wants to clog the network, the system must respect availability. Accountability (Non-repudiation) refers to the act of non-repudiation, *i.e.* an entity cannot deny the receipt or transmission of data. In the AMI network, prompt responses to command and control ensure accountability (MAHMOUD; XIA, 2019).

SG initiative brings the integration of intelligence information exchange among users, operators, and control devices. It demands a detailed examination and more systematic quantification of the human dynamics correlated with multiple cyber-attacks against many critical power system components (XIANG et al., 2018). Vulnerable cyber networks and growing cyber intrusion activities achieve many levels of consequences on power systems differing from the disclosure of confidential information to harmful large-scale outages (MANANDHAR et al., 2014; HUANG et al., 2016; ZHANG et al., 2013a). Even before SG, multiple significant outages have been caused primarily by events and failures associated with the processing and communication infrastructure (TOKEL et al., 2018).

2.2.5 Cyber-security in SG Monitoring

Since controlling and monitoring rely on the Internet Protocols (IPs) and general public solutions, the SG may be tempting to attackers as critical infrastructure. SG 's critical interconnected nature delivers it as a target of cyber-terrorism. Therefore, it is imperative to examine the components and broadly identify the vulnerabilities and all possible cybersecurity threats that exist in the SG infrastructure (GUNDUZ; DAS, 2020). All parts of the SG system must secure the main security objectives must be met. The primary security objectives are confidentiality, integrity, and availability (CIA triple). In SG, the exact association of vulnerabilities and cybersecurity threat categories enables the specification of appropriate countermeasures and responses to cyberattacks.

SG security concerns include data acquisition, and control devices such as PLC, SMs, IEDs, RTU, and PMUs. Further network security difficulties include firewalls, countermeasures, attack scenarios, encryption, intrusion analysis, routers, and forensic analysis. Due to security risks in common Information Technologys (ITs) background, we can assume that almost all aspects associated with ITs technology in SG applications have potential vulnerabilities.

Attacks on the electric grid resulting in infrastructural failures include cybersecurity breaches, cascade failures, blackouts, etc. AMI is more vulnerable as it is central to the SG operation. The energy demand is ever-increasing worldwide, and to effectively cater for the increased demands, existing generation, transmission, and distribution capacity require improved expansive integration and coordination for a secure and efficient supply. As a result, there is a need for adequately analyzing security issues in critical SG systems.

AMI architecture is more susceptible to cyber-attacks given the fact that it consists of a network of sensors, meters, devices, and computers for data recording and analysis. As a result, the SG security will have to cater but not limited to the AMI, Wide-Area Situational Awarenesss (WASAs), ITs Network integration, interoperability, DER, customer privacy, and efficiency. The attacks have majorly been targeted at AMI, especially the SM component, for electricity theft. AMI security requirements as it relates to the entire system, as well as its personnel and third parties' privacies, were developed by Advanced Security Acceleration Project – Smart Grid (ASAP – SG) and NIST led Cyber Security Coordination Task Group (CSCTG) (OTUOZE et al., 2018). SG commonly uses standard frameworks that provide comprehensive security measures considering different architectures.

Cyber-attacks are arguably the most discussed attacks over SG systems due to the vulnerabilities of the infrastructure to digital attacks. It can lead the system to total collapse if not properly guarded. Any significant attack can mislead the utilities in making wrong decisions about usage and capacity and possibly blind them from impending problems or ongoing attacks. Confidentiality, authentication, and critical data privacy for grid reliability and efficiency must be guaranteed to prevent unauthorized modifications through the infrastructure. Therefore, Distributed cyber-security systems are designed to

monitor the architecture in maintaining data integrity. (SHRESTHA et al., 2020) proposes a methodology called Smart Grid Security Classification (SGSC) developed for complex systems such as SG, centering on the specific aspects of the AMI metering infrastructure.

Cyber-attacks can hit the utility of a physical system, render them inoperable, hand over control of those systems to an outside entity, or endanger the privacy of employees and customer data. Most attacks regularly take one or a combination of four principal ***types of attacks*** (KIMANI et al., 2019):

- A device attacks are designed for compromising and controlling mesh network devices.
- A data attack attempts to illegally insert, alter or delete data or control commands in communication network traffic to trick SG into making wrong decisions/actions.
- A privacy attacks aim to learn private or personal information about users by analyzing data from SG web resources.
- A network availability attacks occur primarily in the form of Denial of Services (DoSs). It intends to exhaust or overwhelm the network's communication and computing resources, causing communications to fail or delay.

Among the cyber menaces on SG and SCADA systems, the false data injection attacks have attracted a significant amount of research from the security and energy industries (FERRAG et al., 2020). Based on cyber-physical channels, *e.g.*, eavesdropping, the attackers insert false data into smart meters to falsify the state of the power system, *e.g.* electricity theft. Although security protocols have been developed for SCADA systems, some critical issues concerning false data injections attacks remain primarily unresolved, such as intrusion into the control center at the cloud computing layer. The most common attack type at the physical layer concerning availability is jamming (GUNDUZ; DAS, 2020). Jamming attacks occur mainly in wireless networks at the physical layer. Attackers only need to connect to the communication channel to perform a jamming attack. Table 2.7 depicts the type of attacks according to the level of the network layer.

2.3 SG Communications Infrastructure

The integration and interoperability of the conventional electricity grid with communication technologies present critical constraints for the evolution. The reformation of the power grid system was defined as part of the "Third Industrial Revolution" for energy (EMMANUEL; RAYUDU, 2016; BUSH, 2014). Traditional power systems typically operate in a centralized fashion, using a radial topology where a single power source powers a group of consumers. The reliability of this topology is very low because any power failure or trip along the path interrupts power delivery on the network (NTALAMPIRAS, 2016; FADUL et al., 2014; WU et al., 2017). As a result, many utilities employ loop or hybrid network

Table 2.7 – Classification of SG Cyber-Attack types according to Network Layer (GUNDUZ; DAS, 2020)

Network Layer	Attack Type
Application Layer	CPU Exhausting, LDoS, HTTP Flooding, Protocol, Stack Buffer Overflow, Data Injection Attacks
Transport Layer	IP Spoofing, Packet Sniffing, Wormhole, Data Injection, Traffic Flooding, Buffer Flooding, Buffer Overflow, DoS/DDoS, MITM, Covert Attack, Replay Attack
MAC Layer	Traffic Analysis, Masquerading, ARP Spoofing, MITM, TSA, MAC DoS Attack, Flooding Attacks, Jamming Attack
Physical Layer	Eavesdropping, Smart Meter Tampering Attacks, TSA, Jamming Attacks

topologies to provide alternate paths in a failure. However, other prevailing factors such as an increasing global appetite for energy, frequent power outages, security issues, global demand to build an expansive structure, electricity theft, current evolution in information and communication technologies, serve as drivers for the modernization of the power grid (GUARRACINO et al., 2012). Integration of IoTs technology together with the power grid points to enhance the reliability of grids through continuous monitoring of component status, as well as environmental behaviors and consumer activities monitoring (JARADAT et al., 2015). A considerable amount of data related to monitoring and control transmitters across SG wireless communication infrastructures suffer from intensive interference and increasing competition over the limited and crowded radio spectrum considering the existing wireless networking standards (WANG et al., 2013).

The standard SG communication network architecture comprises a three-layer hierarchical network, i.e., a Home Area Network (HAN), a Neighborhood Area Network (NAN), and a WAN. In the HAN layer, PLC and Zigbee technologies have been proven to be the best choices (HAN et al., 2014). This network plays an essential role in the SG data communication bridge between the HAN and WAN. This data network sustains connections between the demand and supplies sides to trade the electricity data from customers to suppliers to run many SG applications. Furthermore, NAN, sometimes called the Field Area Network (FAN), connects many electric devices in the transmission and distribution lines to monitor, control, and protect the power network. From this perspective, NAN is the most significant network layer in SG communication and demands more research efforts to build up a mature and reliable communication system for the smart cities context.

NAN/FAN applications require data transmission from many terminal devices to a data concentrator/hub/substation or vice-versa. Consequently, these applications require communication technologies that support a higher data rate (100 kbps-10 Mbps) and a more extensive coverage distance (up to 10 km). ZigBee mesh networks, WiFi

mesh networks, PLC, as well as long-distance wired and wireless technologies, such as WiMAX, Cellular networks, Digital Subscriber Line (DSL) and Coaxial Cable are standard technologies for NAN/FAN applications (KUZLU et al., 2014).

Networking Requirements for the SG network differ in various critical aspects from those Network Service Providers (NSP). NSPs are originally designed to support their customers' multimedia applications (including Voice over IP (VoIP)). At the same time, SG networks must support mission-critical applications such as SCADA, teleprotection, and synchrophasors that have significantly more stringent requirements on reliability, security, and performance. Consequently, the network design paradigm for the SG network differs substantially from the data network design practices used by NSPs.

With the emergence of the IoT and Machine-to-Machine (M2M) communications, it is expected massive growth in the sensor-node deployment. In general, IoT applications require EE and low-complexity nodes for a variety of uses in scalable wireless highly EE networks. Currently, sensing applications in short-range environments use wireless technologies such as IEEE 802.11 Wireless Local Area Network (WLAN), IEEE 802.15.1 Bluetooth, IEEE 802.15.3 ZigBee, Low-Rate Wireless Personal Area Network (LR-WPAN), and others (HABIBZADEH et al., 2019). In contrast, long-range SG applications include wireless cellular standards, including 2G, 3G, 4G, and 5G technologies. Primarily, WLAN and Bluetooth were designed for high-speed data communication.

In contrast, ZigBee and LR-WPAN are designed for wireless sensing applications in local environments. This includes low data rate applications with communication distances from a few meters to hundreds of meters, depending on Line-of-Sight (LoS), obstacles in the path, interference, maximum transmit power, etc. Wireless cellular networks such as 2G, 3G, and 4G are designed for voice and data communications, not primarily for wireless Machine-Type Communication (MTC) applications, including sensing tasks. Although these techniques are used in some applications for sensing in one way or another, their performance metrics in terms of reliability-performance-complexity trade-offs in wireless sensor networks may be unacceptable.

Figure 2.8 represents an integrated SG architectural view. A graphical overview of the grid includes clusters that form the general SG pattern. The mesh components are located in topological communities grouped by the system. The two dimensions of the SG plane are areas that represent the level of power system management: process, field, station, operations, and domains that cover the entire power conversion chain: generation, transmission, distribution, distributed energy, and customer sites. Communication characteristics belong to another dimension of five interoperability layers: business layer, functional layer, information layer, communication layer, and component layer. The communication layer interacts directly with each component in the grid. Inside the communication, direct infrastructure links (A, B, C, F, L, H) bring specific applications into the component layer.

The WAN or FAN are often referred to as the backhaul. Backhaul networks

(represented by the circles labeled L, C in Figure (2.8) can use wired or wireless technologies, enabling the aggregation and transportation of customer-related SG telemetry data, substations automation critical operations data, relevant DER, and μG field data, and mobile workforce information. NANs represented by circle B in the figure, integrates SMs and sensors nodes. The inter-substation network (F) carries revenue-generating data and critical protective relaying data. The backbone (H) is the network that interconnects all grid networks, providing a path for exchanging information.

Many of the communication applications are susceptible to single-point failures. Impacts of those communication failures degenerate system behavior, *e.g.* protection misoperation. Many proposals for a communication framework use existing architecture within the application of pair-to-pair, also relaying, among devices (CALDERARO et al., 2011; RAHMAN et al., 2018), where all messages received by devices are acknowledged with a reply. There is no correlation between communication links and fault indicator components, a measurement of total reliability (TARHUNI et al., 2015). A framework that provides continuous, reliable, secure, and sustainable diversified SG communication represents a challenge for actual implementations. Deployment of SG components needs proper determination, and implementation of a communication network satisfying the security standards of SG communication (DEPURU et al., 2011; YANG et al., 2018). The concept of using device-to-device communication or distributed solutions to compose and deliver services has been a favored trend for SG (RIDHAWI et al., 2020). Assuredly, SG applications would benefit from next-generation device-to-device networks for service delivery, composition, enhancement, and analysis.

2.3.1 SG Communication Protocols

SG communications comprehend most modern communication technologies such as RF mesh, PLC, and/or ZigBee (PASDAR et al., 2013; CHEN et al., 2015; GAO et al., 2012). Nevertheless, each of these has its drawbacks. The RF mesh has low network capacity, high interference, and less coverage area. PLC suffers from low bandwidth, and the noise on the transmission line network affects the quality of the signal (MADETI; SINGH, 2017a; MILIOUDIS et al., 2015). Following, LoRaWAN and SigFox with high reliability and scalability but suitable only for short and periodical communications (LALLE et al., 2019). Finally, ZigBee suffers from low processing capabilities, small memory size, and noise interference with WiFi, Bluetooth, and microwave. Due to relatively low latency, large bandwidth, and high coverage throughout residential areas, the cellular networks have become a promising technology for the SG data network. Cellular networks primarily designed for Human-to-Human (H2H) communications may have an undergoing with the size and the type of data from SG devices. SG communication mainly considers M2M data communication without any human intervention (DHEND; CHILE, 2018).

A detailed list of the most relevant technologies used for the intercommunication

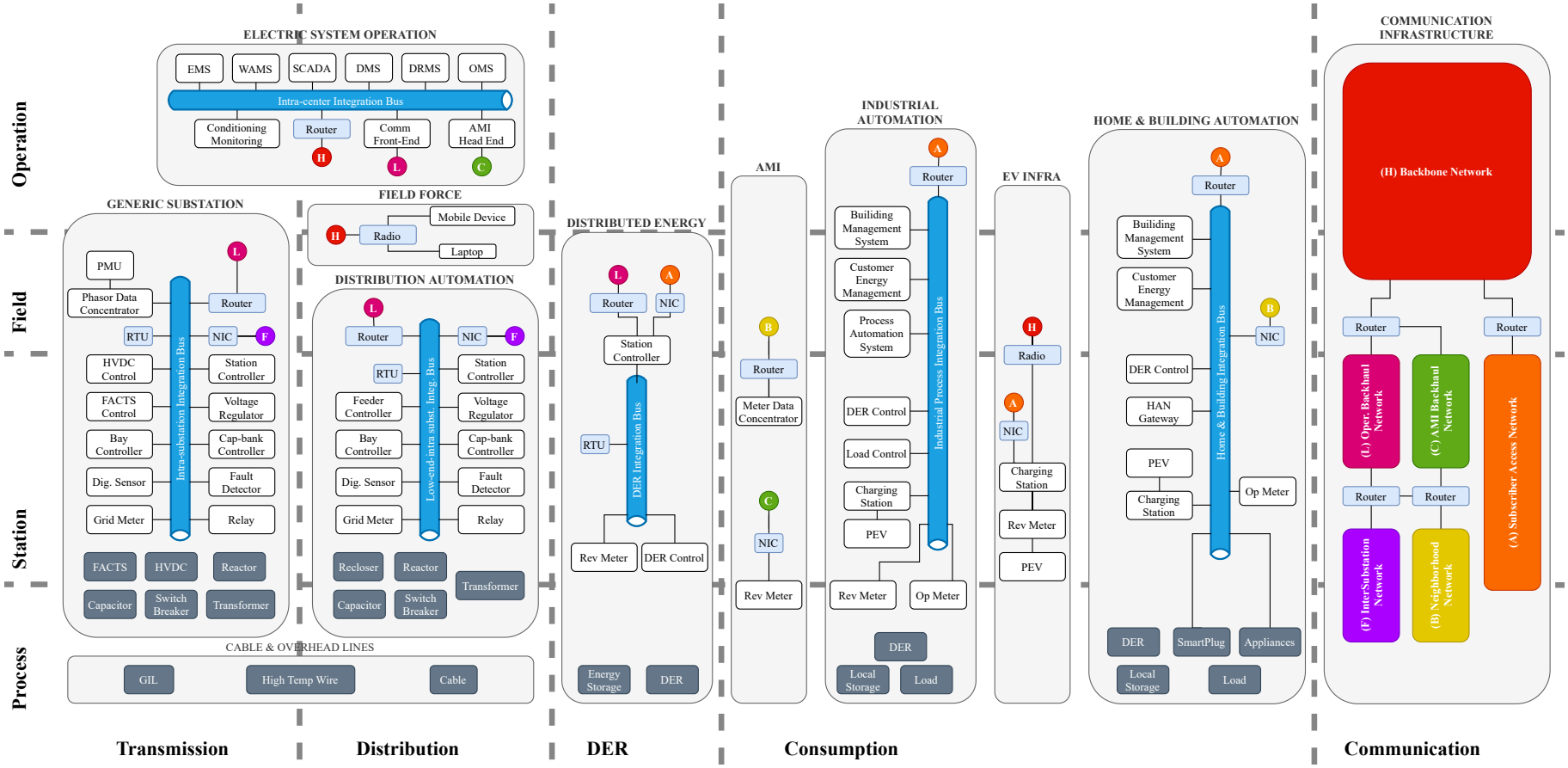

Figure 2.8 – Smart Grid Architecture overview (Adapted from (SMART..., 2013))

within and between these domains can be found in Table 2.8 based on (MATTIOLI; MOULINOS, 2016). Various protocols exist for substation automation, including proprietary protocols with custom communication links. Substation automation devices require interoperation from different vendors. As a notable mention, the IEC 61850 protocol family is specially adapted to integrate grid sections.

Despite the research above, analyses of the importance of improving the security of the interdependencies in SG are crucial factors to reduce cascade failures. Although more complex networks have been intensively studied for over a decade, the researchers still focus on the case of an isolated network without external interaction. Nevertheless, it is known that smart systems are building and working coordinate way; consequently, these systems must be designed as interdependent networks. The research on the interdependency problems will guide the development and application of new system ideas and design proposals to mitigate the hazards posed by these interdependencies.

The communication in SG systems should be distributed in a way that a failure of one device will not create a communications outage in a segment of the network. This can be accomplished with redundant communication devices that ensure that no device is connected only through one path.

An important application of IoT is the SG. The perception layer includes smart meters, network devices, and communication protocols. This layer collects information and sends it through a network layer comprising different wired and wireless industry-specific or public communication networks. Within this topic, it is important to evaluate the performance of available access protocols for specific SG applications next to propose new protocols to achieve the next generations' network requirements.

The addition of modern protection functions is a difficulty in the emerging context of SG and may be achieved through the application of a compound of both existing and evolving technologies (HUANG et al., 2016). The latter must be designed for real-time signal analysis and should be as computationally efficient as possible as a protective device function.

2.3.2 5G Technology Enabling for SG

The 5Gs is offering a significant advance in the combination of latency reduction and reliability enhancement. Following the beginning of 5G, electricity distribution has been one of the major use cases for URLLC (HOVILA et al., 2019). 5G replacing optical communication links to achieve improved flexibility, reliability, and cost savings. Furthermore, 5G floors the way for broader integration of renewable energy sources to the electric power network. The mixture of low latency and high reliability makes 5G an option for replacing fixed connections. SG communication often has special performance requirements, especially very low latency ($\leq$ 1ms). The IEC 61850 standard defined the

Table 2.8 – SG Communication Protocols

SG Domain	Communication Media and Low Level Protocols
Last mile networks (FAN, NAN, AMI)	Wired: BPL (PLC), DLC (PLC), fibre, twisted pair, PDH, SONET/SDH, xDSL, POTS, PRIME (PLC), Meters&More (PLC), ANSI C12.18, ANSI C12.21. Wireless: radio frequency, microwave, cellular, GPRS, UMTS, LTE, IEEE 802.16 (WiMAX). Medium independent: TCP/IP suite, ANSI C12.22.
Backhaul Network	Wired: twisted pair, cable, fibre optic, POTS, SDH/SONET, PPP. Wireless: cellular, microwave, radio frequency, 3G, WIMAX, LTE. Medium independent: Frame Relay, ATM, MPLS, TCP/IP suite.
AMI networks	Wired: BPL (PLC), DLC (PLC), fibre, twisted pair, PDH, SONET/SDH, xDSL, POTS, PRIME (PLC), Meters&More (PLC), ANSI C12.18, ANSI C12.21. Wireless: radio frequency, microwave, cellular, GPRS, UMTS, LTE, IEEE 802.16 (WiMAX). Medium independent: TCP/IP suite, ANSI C12.22.
DER networks	Wired: serial, Ethernet, PPP. Wireless: radio, IEEE 802.15.4 ZigBee. Medium independent: TCP/IP suite.
Transmission grid networks	Wired: Serial Line, Ethernet, Frame Relay, PPP, ATM/TDM, BPL, DLC/PLC. Wireless: radio frequency, microwave, cellular, IEEE 802.16 (WiMAX). Medium independent: TCP/IP suite. IEC 61850 protocol family.
Link Layer/MPLS	Wired: Serial Line, xDSL, Ethernet, Frame Relay, PPP, ATM, TDM. Wireless: GPRS, Wi-Max, 2G, 3G, 4G, VSat, Wi-Fi, ZigBee. PLC: (Broadband Power Line, such as IEEE P1901 standard), DLC (Distribution Line Communications, such as PRIME), nb PLC (Narrowband PLC, such as Meters&More). MPLS: Multiprotocol Label Switching, it is "protocol agnostic" and commonly referred as layer 2.5.
Network Layer	Medium independent: IPv4, IPv6, IPsec.
Transport Layer	Medium independent: TCP, UDP, TLS/SSL.
Windmills	IEC 61850 protocol.
Hydro Power Plants	IEC 61850-7-410 protocol.
Other Systems	IEC 61850-7-420 protocol.

GOOSE protocol for transferring time-critical information, such as control commands and alarms, between IEDs with millisecond transfer delays (NGUYEN et al., 2020).

URLLCs is one of the three prominent use cases for 5G. In 3GPP, the first official release of 5G was Release 15, completed in June 2018. The primary use cases considered

in the 15th edition are from industrial automation and power distribution. The 3GPP Service and System Aspects (SA) working group has been working on various use cases, their requirements, and network architecture support for the URLLC service. Additionally, the 3GPP Radio Access Network (RAN) working group has specified radio-level standards in our area of interest. In Rel-15, the system design goal is set to achieve communication reliability corresponding to Block Error Rate (BLER), which is 10^{-5} for 32 bytes, and a user plane delay of 1ms (HOVILA et al., 2019).

Currently, 3GPP is working on Rel-17 stage 3 (March 2022) and Rel-8 (early stages available in Q1 2022). It also extends the supported services to cover Time-Sensitive Communications (TSC), *e.g.* vertical industries' widely deployed Time-Sensitive Network (TSN). The coveted target is to reach communication reliability corresponding to the BLER of 10^{-6} with sub-millisecond latency. Besides, further communication requirements must be considered, such as:

- Enhanced uplink configured grant transmission;
- Improved control channel reliability;
- Mini-slot repetition to achieve high reliability;
- Enhanced PDCP layer duplication;
- Intra/inter-UE multiplexing between different services;
- Enhance scheduling to support time-sensitive communications;
- Accurate time synchronization among involved network nodes within the same synchronization domain.

In this context, 5G technology is desirable for implementing a communication infrastructure that enables data traffic from measurement devices to control centers in WAMS. 5G is expected to meet the requirements of the SG implementation with highly reliable communication, low latency, strong security mechanisms to prevent malicious intrusion, and high scalability (ZERIHUN et al., 2020).

Internet-of-Things-Grid (IoTG) is a 5G communication solution developed based on Narrowband Internet-of-Things (NB-IoT) and Enhanced Machine-Type Communication (eMTC), a dedicated industry spectrum for utilities in the VHF and UHF bands. IoT-G technology supports the aggregation of the fragmented narrowband spectrum to achieve broadband transmission capability (HAO et al., 2019; MATINKHAH; SHAFIK, 2019). In addition, IoTG inherits the fundamental physical layer design parameters, including the frame length and subcarrier spacing from 3GPP NB-IoT and EMTC technology, while incorporating many 5G New Radio (NR) technical features, including grant-free transmission-based protocol, self-contained frame structure, Code Block Group (CBG) transmission-based, and Integrated Access Backhaul (IAB) (HAO et al., 2019).

2.3.3 5G Technology for SG Teleprotection

Teleprotection signals from protective relays are crucial in PS. They support control power grid load and protect network equipment from severe harm. By allowing load-sharing, grid regulations, and fast fault clearance, teleprotection guarantee continuous power supply. Protection requirements, hence, must be guaranteed urgent delivery when problems are detected, allowing faulty equipment disconnection before a systemwide disaster occurs (BUDKA et al., 2014). As utilities move from legacy synchronous digital hierarchy/synchronous optical network (SDH/SONET) communication networks to packet-based networks, the complexity in guaranteeing protection performance intensifies.

Utility communications networks have been SDH- and SONET-based (BUDKA et al., 2014). That is evolving as legacy infrastructure, and substation devices move to Ethernet transport and IP/packet-based networks. The SG evolution is a crucial driver for this transformation because packet transport offers high capacity at a lower operating cost. This helps to handle traffic generated by advanced grid applications. Next-generation SCADA systems, wide-area situation awareness synchrophasor measurements, and IP-based video surveillance are a few applications that demand the use of packet-switched networks (LAVERTY et al., 2010). Also, regulation in substation automation, such as the IEC 61850 standard, requires Ethernet capabilities throughout transmission and distribution.

Latency, or signal delay, requirements for utility networks diversify, but most line equipment can endure shortage or interruption faults of up to five power cycles. After that, the equipment might sustain resolute damage, or the fault might affect other network parts. As a safety precaution, the actual operating time of the protection system is limited to 70-80 milliseconds, including fault identification, command transmission, and line breaker switching times. Some system components, such as large electromechanical switches, are less sensitive and take up most of the time, leaving only a 10-millisecond window for communication elements.

New IEC standards are even more stringent regarding protection messages. The communicating endpoints distinguish the backbone network domain in the high and extra-high voltage areas (i.e., primary substations). The diameter of the area to be reached is usually less than 1000 km. The most critical applications are protection functions (so-called teleprotection, differential protection), which require ultra-stable, reliable, secure, and real-time communication between the main substation and the control center. Therefore, these networks are today dedicated optical wired networks. The specific requirements are:

- Bandwidth: in the Mbps to Gbps range between the main substation and the control center.
- E2E delay (upper limit): <5ms between main substation and control center. IEC, "IEC 61850 Part 5: Communication requirements for functions and equipment types".

- Packet-loss: $< 10^{-9}$ (must meet E2E latency requirements, and unconfirmed status information distribution (*eg* based on GOOSE) must function properly, i.e. for high pressure/ultra high pressure requirements are higher than for medium voltage applications).
- Availability: >99,999% equals 5 minutes of downtime per year
- Failure Convergence Time: Need for seamless failover, i.e. no loss of information in the event of a failure, while maintaining real-time delivery of data (i.e. within milliseconds)
- Handling crises (surviving massive prolonged power outages, ensuring black start capability): Mandatory.

Gathering, SG services are often associated with strict reliability requirements and only tolerate short packet losses. Therefore, 5G must contain a wide variety of use-case characteristics related to a complex set of requirements as described above. New technological elements and some disruptive technologies are required to accommodate these elements under common network topologies. The design of a new radio access network includes seamlessly integrated interactions between various communication interfaces. It ends with a fundamental model shift in connectivity theory in the future 5G vision. 5G Effective integration of access technologies introduces a multi-connection approach, where user equipment connects to multiple access technologies or frequency bands simultaneously, which helps address crisis management requirements.

2.4 Detecting and Locating Faults

Protective devices automatically isolate a faulted area from the rest of the network when a short circuit fault occurs. Nevertheless, it is challenging to recognize the infringed sections of the network and the faulted parts. Existing methods consider algorithms that implement available information (i.e., data, measurements) to estimate faults or affected areas. Fault location studies are categorized into two main groups depending on the results, and objective (BAHMANYAR et al., 2017). One group comprehends *outage area location methods*, which incorporates procedures using many available data sources such as customer outage calls or fault indicator signals to estimate the most probable affected area. The second group handles data and measurements to *locate the fault which caused the outage*. SG considers several fault diagnosis techniques; those techniques should include real-time estimation. In this context, Table 2.9 and 2.1 reviews works dealing with fault detection/location techniques; notice that a few of these researches include SG approach.

In this sense, Table 2.1 summarizes a selection of research surveys on fault detection/location techniques for SG systems. Few research works provide models and

comprehensively characterize faults in SG systems. In general, a systematic review has demonstrated that surveys and tutorials available in the literature report fault detection/locating in specific system applications, *e.g.* transmission, distribution, DG, EV, while several of them present comparisons in terms of requirements, advantages, and limitations. A summary of works dealing with fault detection/location in system-level applications is presented in Table 2.10.

Table 2.9 – Description of related papers for Fault detection or location methods.

Reference	One-phrase description
(SANTIS et al., 2018)	Cluster-based learning approach for localized and classified faults
(MISHRA et al., 2016)	Combined wavelet and data-mining for fault detection and classification
(HE; ZHANG, 2011)	Graph approach for secured fault detection and localization
(ZHANG; MU, 2018)	A fault detection method of microgrids based on the PQ control strategy
(RAHMAN et al., 2015)	Des-centralized protection scheme to improve transient stability using multi agent approach
(TOKEL et al., 2018)	A new approach for machine learning-based fault detection and classification
(JIANG et al., 2018b)	A Petri Net Approach to Fault Diagnosis and Restoration
(MILIOUDIS et al., 2015)	Detection and location of high impedance faults utilizing PLC
(JIANG et al., 2014)	Fault Detection, Identification, and Location with machine learning clustering algorithm
(MESKINA et al., 2014)	A multi-agent architecture to allow fault detections and dynamic recoveries
(BANGALORE; TJERNBERG, 2015)	A maintenance scheduler framework of gearbox bearings from onshore wind turbines
(CHAKRABORTY; DAS, 2018)	Detects high impedance fault depending on the number of even harmonics in the voltage.
(GHARAVI; HU, 2018)	Disturbance Detection and Classification based on K-mean optimization
(ALHELOU et al., 2018)	Fault detection and isolation for systems with unknown inputs

Continued on next page

Table 2.9 – *Continued from previous page*

Reference	One-phrase description
(HE; ZHANG, 2010)	Fault localization using the phasor angles across the buses as a Gaussian Markov random field
(HE; BLUM, 2011)	Faults detection in changes in system matrices of the state space model
(JIANG et al., 2016)	A framework for characterizing and managing the data generated by the synchrophasor
(KATIC; STANISAVLJEVIC, 2018)	Voltage dips detection based on harmonic footprint
(KOZIY et al., 2013)	A wavelet multiresolution analysis technique for event detection and current pattern recognition
(MAHFOUZ; ELSAYED, 2016)	Fault detection and classification algorithm using cross-correlation coefficients
(MANANDHAR et al., 2014)	Detection of faults and attacks including false data injection attack in smart grid
(PARIKH et al., 2013)	Fault Detection, Isolation, and service Restoration algorithm using IEC 61850 based GOOSE tech
(PASDAR et al., 2013)	Injection of high frequency current signal to determine changes in the impedance characteristics
(RAWAT et al., 2016)	Fault diagnosis using the status of an intelligent electronic device and circuit breakers
(SHAO et al., 2017)	Fault detection mechanism for wireless sensor networks based on credibility and cooperation
(DAS et al., 2017)	Fault location using voltage measurements from WAMS and the network bus admittance matrix
(DHAR et al., 2018)	Fault detection and location of PV DC Microgrid Using Differential Protection Strategy
(DOBAKHSHARI; RANJBAR, 2015)	A wide-area fault-location scheme capable of detecting and identifying erroneous measurements
(LI et al., 2018)	Fault detection method for voltage source converter based multi-terminal DC
(SALEH et al., 2017b)	Travelling-wave based method to detect, classify, and locate different dc fault types
(YU et al., 2017)	Fault detection scheme for microgrid based on wavelet transform and deep neural networks

Continued on next page

Table 2.9 – *Continued from previous page*

Reference	One-phrase description
(GOPAKUMAR et al., 2018)	Fault monitoring system for detecting and classifying transmission lines faults
(HARROU et al., 2018)	Fault detection and diagnosis of PV systems based on statistical monitoring approaches
(AFFIJULLA; TRIPATHY, 2018)	A fault detection technique utilizing a phasor estimation to compute fault impedance
(CHAITANYA; YADAV, 2018)	A fuzzy-based intelligent fault detection and classification
(CHEN et al., 2016a)	Fault detection and classification on convolutional sparse autoencoder
(CHEN et al., 2016b)	Fault detection algorithm for PV systems under the sequential change detection framework
(COSTA et al., 2015)	Detection of Transients Induced by High-Impedance Faults
(DARYALAL; SARLAK, 2017)	Travelling wave-based criteria for detecting such faults
(HASHEMI et al., 2017)	Fault detection during power swings using the properties of fundamental frequency phasors
(KUO et al., 2017)	PV fault detection using fractional-order color relation classifier
(MADETI; SINGH, 2017b)	Fault detection technique that analyzes the anomalies of faulty PV strings and arrays
(NAGANANDA et al., 2015)	PMU placement and fault detection algorithm to detect changes in the susceptance
(QI et al., 2017)	Discrete wavelet transform (DWT) to detection of series arc faults in smart homes
(SALEH et al., 2017a)	A real-time discrete wavelet transform to detect the voltage transients generated
(WANG et al., 2018)	High-impedance fault detection based on nonlinear voltage–current characteristic
(WISCHKAEMPER et al., 2015)	Integration of waveform analytics to improved situational awareness
(XI et al., 2017)	Power line fault detection based on self-encoding neural network

Continued on next page

Table 2.9 – *Continued from previous page*

Reference	One-phrase description
(YANG et al., 2016)	Fault detection such as broken-rotor-bar and bearing faults
(YI; ETEMADI, 2017)	Fault detection algorithm based on multiresolution signal decomposition for feature extraction
(ZHANG; MU, 2018)	Fault component characteristics of a microgrid under different impedance faults
(HUANG et al., 2016)	Real-time detection scheme against false data injection attack
(KUMAR; BHOWMIK, 2018)	Islanding detection technique using the ANN classifier
(MARTINEZ-FIGUEROA et al., 2017)	Smart sensor to detect and quantify PQD
(MOGHADDASS; WANG, 2018)	Real-time anomaly detection framework based upon smart meter data collected
(SEYEDI et al., 2017b)	Structure for the centralized detection of disturbances with noisy data and packet delay
(YEN et al., 2019)	Early detection of short-duration voltage anomalies from smart meters
(ACHLERKAR et al., 2018)	Detection and classification of power quality disturbances
(CHEN et al., 2015)	A correlation-based anomaly detection algorithm
(SUN et al., 2016)	A probabilistic framework to analyze large-scale real-time tweets to detect power outages
(MISHRA et al., 2014)	Algorithm for transmission line fault classification by using wavelet
(ZHANG et al., 2013a)	Defensive techniques such as intrusion detection
(DEVI et al., 2018)	Fault occurrence and location using optimal PMUs
(DHEND; CHILE, 2017)	Fault locating factors using a wavelet function
(ROBSON et al., 2014)	Fault-location method for use on highly branched networks

Table 2.10 – Fault detection/location system-level of application

Level	References
Transmission	(FERREIRA et al., 2016; HE; ZHANG, 2011; RAHMAN et al., 2015; JIANG et al., 2018b; JIANG et al., 2014; GHARAVI; HU, 2018; HE; ZHANG, 2010; HE; BLUM, 2011; JIANG et al., 2016; MANANDHAR et al., 2014; RAWAT et al., 2016; SHAO et al., 2017; DAS et al., 2017; DOBAKHSHARI; RANJBAR, 2015; LI et al., 2018; GOPAKUMAR et al., 2018; AFFIJULLA; TRIPATHY, 2018; CHEN et al., 2016a; DARYALAL; SARLAK, 2017; HASHEMI et al., 2017; NAGANANDA et al., 2015; HUANG et al., 2016; MARTINEZ-FIGUEROA et al., 2017; YEN et al., 2019; MISHRA et al., 2014; ZHANG et al., 2013a; DEVI et al., 2018)
Distribution	(SANTIS et al., 2018; MISHRA et al., 2016; ZHANG; MU, 2018; MILIOUDIS et al., 2015; MESKINA et al., 2014; CHAKRABORTY; DAS, 2018; ALHELOU et al., 2018; KATIC; STANISAVLJEVIC, 2018; MAHFOUZ; EL-SAYED, 2016; MANANDHAR et al., 2014; PARIKH et al., 2013; PASDAR et al., 2013; RAWAT et al., 2016; SHAO et al., 2017; LI et al., 2018; SALEH et al., 2017b; YU et al., 2017; CHAITANYA; YADAV, 2018; COSTA et al., 2015; KUO et al., 2017; WANG et al., 2018; WISCHKAEMPER et al., 2015; XI et al., 2017; ZHANG; MU, 2018; HUANG et al., 2016; KUMAR; BHOWMIK, 2018; MARTINEZ-FIGUEROA et al., 2017; MOGHADDASS; WANG, 2018; SEYEDI et al., 2017b; YEN et al., 2019; ACHLERKAR et al., 2018; CHEN et al., 2015; SUN et al., 2016; ZHANG et al., 2013a; DHEND; CHILE, 2017; ROBSON et al., 2014)
Comercial - Residential	(MISHRA et al., 2016; KOZIY et al., 2013; MANANDHAR et al., 2014; DHAR et al., 2018; KUO et al., 2017; QI et al., 2017; SALEH et al., 2017a; HUANG et al., 2016; MARTINEZ-FIGUEROA et al., 2017; SUN et al., 2016; ZHANG et al., 2013a)
DG	(ZHANG; MU, 2018; BANGALORE; TJERNBERG, 2015; ALHELOU et al., 2018; MAHFOUZ; EL-SAYED, 2016; MANANDHAR et al., 2014; DHAR et al., 2018; LI et al., 2018; SALEH et al., 2017b; YU et al., 2017; HARROU et al., 2018; CHAITANYA; YADAV, 2018; CHEN et al., 2016b; KUO et al., 2017; MADETI; SINGH, 2017b; SALEH et al., 2017a; YANG et al., 2016; YI; ETEMADI, 2017; ZHANG; MU, 2018; HUANG et al., 2016; KUMAR; BHOWMIK, 2018; MARTINEZ-FIGUEROA et al., 2017; MOGHADDASS; WANG, 2018; SEYEDI et al., 2017b; YEN et al., 2019; ACHLERKAR et al., 2018; CHEN et al., 2015; ZHANG et al., 2013a; AHMADIPOUR et al., 2018; AHMADIPOUR et al., 2018; AHMADIPOUR et al., 2019; AHMADIPOUR et al., 2019)
EV	(ALHELOU et al., 2018; LI et al., 2018)

2.4.1 Non-Permanent Faults Energy Distribution Networks

The blackout area locating method is used to find the status of the protection equipment and thus determine the blackout area, and the fault localization method aims to locate the permanent fault causing the blackout. The fault location method can also be applied to *non-permanent faults*. About 75–90% of distribution network failures are transient (ANDERSON, 2009). Identifying their location offers the possibility to take remedial action to avoid continued outages in the future, further improving reliability by enhancing the infrastructure. There are several methods currently used to locate transmission network faults. However, compared to the SG arrival, fault localization in the distribution network faces new problems. Most of the transmission lines are equipped with special protection devices, measuring devices and fault locators. In contrast, distribution networks typically have spurs and load taps along their lines, complicating the fault location procedure. According to (BAHMANYAR et al., 2017; MOGHADDASS; WANG, 2018) some of the fault location problems and challenges in distribution networks are listed here:

- Geographic dispersion of distribution networks over a vast area;
- Existence of non-homogeneous lines;
- Presence of laterals, load taps and sometimes single and two-phase loads;
- Limited measurements, typically only available at substations;
- Dynamic topology of distribution networks;
- The effect of fault resistance which is usually non-negligible;
- Multiple fault location in distribution networks due to the presence of several branches.

The small-scale DER, such as microturbines, photovoltaics, wind turbines, fuel cells, and storage devices, are generally interfaced employing a Voltage-Sourced Converter (VSC) due to their compliance in rendering controlled and high-quality power to loads and the grid. A challenging task in protecting the inverter-interfaced islanded μG is to limit the current fault level; this degenerates the performance of traditional over-current protection schemes. Many fault detection strategies consider monitoring the VSC to establish fault characteristics (SADEGHKHANI et al., 2016).

2.4.2 Methods and Algorithms for Fault Detection-Location

To date, a plethora of research studies analyzed fault detection/location via either *impedance-based methods* or *computer simulations*, or even *numerical optimization* algorithms using an *analytical* or *learning*-based approach. In the following, different main

literature algorithms are detailed and discussed. The discussions begin with the impedance-based methods, the most advanced class. Next, analytical methods have different requirements and algorithms. Finally, more recent learning-based fault detection/localization algorithms are discussed.

2.4.2.1 Impedance-based Methods

Methods for FD/L-SG based on impedance use steady-state measurements of currents and voltages during the fault to estimate an apparent impedance (or reactance) correlated with a distance to the fault. The main shortcoming of impedance-based methods is the miss-estimation due to many potential faulty points at the same distance. While all impedance-based fault location methods rely on the same fundamental concepts and assumptions, some features and differences influence their performance and range of application. Impedance-based fault methods have been used extensively in the legacy power system; however, SG changing topology represents a challenge for the accuracy of such methods. (WANG et al., 2018; CHAKRABORTY; DAS, 2018) are relevant works related to impedance-based methods. Both works applied a high impedance fault detection in distribution systems considering data from SMs. Waveforms measurements bring a trending topic to detect SG disturbances. Besides, those methods proved to be robust within non-linearities of the system for a wider number of system disturbances.

2.4.2.2 Analytical Methods

Analytical methods for FD/L-SG are generic processes combining the power of the scientific method with the use of a formal process to solve electrical fault problems, among others. In fault detection, those methods are based on the system model by using knowledge of the system to create an analytical mathematical model. Many analytical methods implement a general-purpose estimation method for the particular detection process. The quality of fault detection depends mainly on two factors: the algorithm's sophistication and the system's sampling rate. Signal processing techniques represent an extended applied principle. Techniques as correlation, wavelet transform, and Fourier transform are effective techniques for fault detection. (WANG et al., 2018; DHEND; CHILE, 2017; YEN et al., 2019) show that those techniques achieve great accuracy with low-complexity techniques.

2.4.2.3 Learning-based Methods

Learning-based methods for FD/L-SG comprise computer algorithms based on Machine Learning (ML) principle that improves fault detection automatically through experience. Mainly described as ML processes, those algorithms formulate a mathematical model based on sample data, *i.e.* training data, to make forecasts or decisions without

being explicitly programmed to do so. In this fault scenario, mathematical classification models that belong to supervised learning methods are trained on the training set of a labeled dataset to identify the redundancies, faults, and anomalous samples accurately. Artificial Neural Networkss (ANNs) are amongst the most mature and widely deployed mathematical classification algorithms in fault detection, and diagnosis (BANGALORE; TJERNBERG, 2015; KATIC; STANISAVLJEVIC, 2018; YU et al., 2017; XI et al., 2017; KUMAR; BHOWMIK, 2018; MARTINEZ-FIGUEROA et al., 2017; AHMADIPOUR et al., 2018; AHMADIPOUR et al., 2018; AHMADIPOUR et al., 2019; AHMADIPOUR et al., 2019). ANNs are easy to implement and well-known for their efficient self-learning capabilities of the complex associations, which inherently exist in fault detection and diagnosis problems. Another advantage of ANNs is that they perform automatic feature extraction by designating negligible weights to the irrelevant features, helping the system to avoid dealing with another feature extractor. Notwithstanding, ANNs tend to over-fit the training set, which raise consequences of having poor validation accuracy on the validation set. Henceforth, often, some regularization terms and prior knowledge are added to the ANNs model to avoid over-fitting and reach higher performance. Furthermore, properly determining the hidden layer's size requires an exhaustive tuning parameterization to circumvent poor approximation and generalization capabilities.

Diverse authors highlights the importance of computational intelligence to detect islanding phenomenon in smart distributed grids (AHMADIPOUR et al., 2018; AHMADIPOUR et al., 2018; AHMADIPOUR et al., 2019; AHMADIPOUR et al., 2019). Those works present a probabilistic Neural Network (NN) and Support Vector Machine (SVM) as powerful self-adapted machine learning techniques for fault detection. The authors analyze many islanding conditions with different active DG, load, capacitor or motor switching, external faults under several loading conditions, and DG participation.

Table 2.11 – Comparison of fault detection/location methods available in the literature.

Impedance-based	Analytical		Learning-based	
(MILIOUDIS et al., 2015; CHAKRABORTY; DAS, 2018)	*CORR*	(YEN et al., 2019; CHEN et al., 2015; MAHFOUZ; EL-SAYED, 2016; SEYEDI et al., 2017b)	*AI*	(RAWAT et al., 2016)
(AFFIJULLA; TRIPATHY, 2018; PASDAR et al., 2013)	*DFT*	(HASHEMI et al., 2017)	*CLUSTER*	(SANTIS et al., 2018; GHARAVI; HU, 2018; SHAO et al., 2017)
(NAGANANDA et al., 2015; SALEH et al., 2017a)	*DWT*	(QI et al., 2017; SALEH et al., 2017a)	*FUZZY*	(CHAITANYA; YADAV, 2018; YI; ETEMADI, 2017)
(WANG et al., 2018)	*FFT*	(WANG et al., 2018; YANG et al., 2016; GOPAKUMAR et al., 2018)	*LEARNING*	(SUN et al., 2016)
(ZHANG; MU, 2018; DEVI et al., 2018)	*GRAPH*	(HE; ZHANG, 2011)	*ML*	(SUN et al., 2016; TOKEL et al., 2018; JIANG et al., 2014)
	LL	(CHEN et al., 2016b; DARYALAL; SARLAK, 2017)	*MULTI-AGENT*	(RAHMAN et al., 2015; MESKINA et al., 2014)
	MA	(HARROU et al., 2018)	*ANN*	(BANGALORE; TJERNBERG, 2015; KATIC; STANISAVLJEVIC, 2018)
	MARKOV	(GHARAVI; HU, 2018; HE; ZHANG, 2010; JIANG et al., 2016; HUANG et al., 2016)		(YU et al., 2017; XI et al., 2017; KUMAR; BHOWMIK, 2018; MARTINEZ-FIGUEROA et al., 2017; AHMADIPOUR et al., 2018)
	MLE	(MOGHADDASS; WANG, 2018)		(AHMADIPOUR et al., 2018; AHMADIPOUR et al., 2019; AHMADIPOUR et al., 2019)
	TRAVELING-WAVE	(ROBSON et al., 2014; SALEH et al., 2017b)	*PETRI-NET*	(JIANG et al., 2018b)
	UIO	(ALHELOU et al., 2018)	*SPARSE AUTOENCODER*	(CHEN et al., 2016a)
	VMD	(ACHLERKAR et al., 2018)		
	WA	(WISCHKAEMPER et al., 2015)		
	WT	(MISHRA et al., 2016; KOZIY et al., 2013; MISHRA et al., 2014; DHEND; CHILE, 2017; COSTA et al., 2015)		

Table 2.11 suggests the preference for Analytical or Learning-based algorithms over impedance-based methods for fault detection or location problems. Furthermore, the more recent the previous research works show that they are largely focused on the application of ANNs and MLs algorithms. Better results appear using mixed-schemes Analytical and learning-based; (HUANG et al., 2016) successfully implement a Markov-chain-based analytical model and clustering classification technique. Also, according to Table 2.10, the system-level application marks a tendency on methods reliability. Therefore, legacy transmission and distribution systems still prefer impedance-based methods. Nevertheless, whether DG penetrations and other smart elements integrated into the network, learning-based became a powerful tool. Table 2.10 presents a summary of the system-level of application.

2.5 Future Research and Challenges in SG systems

The key elements to improve SG faults monitoring, detection, and location infrastructure are highlighted in this section. Notwithstanding the high number of proposals, the consolidation into one integrated tool that includes fault detection, classification, and location modules can be very challenging due to SG complex topologies. Furthermore, the emerging new sensing technologies and embedded computing present an opportunity to achieve QoS application requirements. Herein, we focus on the challenges related to adapting legacy monitoring infrastructure, scalable communication architecture, cyber-security intrusion detection, real-time estimation, and handling a massive number of metering devices. The new panorama in future SG systems for intelligent city context may lie in the exploitation of ML techniques where heterogeneous energy systems interact with many other systems architecture at different application levels (IBRAHIM et al., 2020). In the following, the main challenges that need to be addressed in SG faults monitoring, detection, and location infrastructure are pointed out.

2.5.1 Legacy Monitoring Infrastructure

The worldwide electricity and energy sectors are looking to transform its century-old patchwork of electricity infrastructure into the SG of the 21st century. The transition requires a phased restructuring of the entire power system structure. Future FD/L-SG in the context of smart cities involves the use of new tools, techniques, and technologies (such as distributedArtificial Intelligence (AI) and energy resources) to build on existing infrastructure to improve the quality, efficiency, and security while enabling the development of a robust architecture for the grid.

To date, there is a large number of legacy data sources in the grid. Limitations to update those devices for AMI or PMU type have required backtrack compatibility to

achieve SGs requirements. Servitization[1] and Industry 4.0 are considered two of the most recent trends transforming industrial companies. Servitization focuses on adding value to the customer (demand-pull), while Industry 4.0 is frequently related to adding value to the manufacturing process (technology-push). In the SGs context, solutions result in the development of low-cost retrofit or upgrade kits that allow integrating legacy equipment into the smart environment and thus enable digital servitization (FRANK et al., 2019). Smart sensors or edge gateways are aggregated to the SGs systems in the context of flexible and low-cost solutions from IoT sensors and smart-gateway to gather data, a package of sensors, and connectivity.

2.5.2 Scalable Communication

SGs system implies the deployment of a large number of sensors over a large area to perform monitoring and control functions. Therefore, one of the challenges in SGs is to build a scalable communication architecture to handle a large amount of data/information generated by a large number of sensors. An SGs communication infrastructure requires to provide extensibility in terms of joining new devices and services into it, also improving the real-time monitoring of SM. SGs requirements should be constantly evaluated in terms of scalability and efficiency.

The lack of scalability and high installation cost concerns wired communication technologies. Moreover, wireless technologies would be preferred due to their high flexibility and scalability for wide-area communications. Though, to avoid adding more wireless access points and routers, the mMTC section offers the scalability in wireless technologies without increasing the total installation costs of the network. Hence, appearing and effective big data technologies, such as deep data mining, stream data processing, data clustering, cloud computing, envelope analysis, and machine learning methods, are crucial to pursuing the goal of scalability in SGs (FAHEEM et al., 2018).

Ultimate SGs relies on the standardization of smart metering techniques to enable their continuous operation. Within 5G arrival, far-reaching activities are being performed in standardizing components and communication. Standardization forms an integral part of ensuring interworking, and this factor needs more attention to make interoperability achievable for communication and information in SGs.

2.5.3 Cyber-security Intrusion Detection

SGs Security concerns address data acquisition, control devices, network security challenges, including firewalls, attack scenarios, countermeasures, encryption, intrusion analysis, forensic analysis, and routers. Analyzing cyberattacks to consider essential

[1] In the emerging servitization-centered economy, companies are shifting from selling products to selling access to and the outcome those products deliver, redefining the way the manufacturers do business.

elements of information security can provide practical solutions to current and future attacks in SGs applications in a well-organized and helpful manner. Similarly, due to the characteristics of smart grid applications, specific solutions need to be created for their personal needs.

ML approaches are used to determine, discover, and identify unauthorized use and injection of false data in networks, including SGs systems. Choosing the most efficient ML method(s) is related to their performance in cybersecurity datasets. Hence, we conclude that further research is required to provide a comparative study of ML methods for cybersecurity intrusion detection in SGs systems. Furthermore, the best-suited ML method may be different for different types of scenarios. Thus, the comparative study must comprise a rich collection of systems, types of attacks, and scenarios. Future research should evaluate auditing performance to detect any compromised device where a high number of devices in an IoT based SGs. How strict access control and authentication methods affect multiple access performance in a massive device scenario.

Furthermore, the main issues in detecting cyber threats are computational efficiency and minimizing false-positive rates. Therefore, future applications should increase the computational speed of security algorithms while maintaining high detection accuracy and low false-positive rate. Another research hole is mitigating cyber threats that have infected intelligent grids. In the existing context, detection and prevention of cyber threats can reduce these threats. Therefore, future trends in this research area are expected to be cyber threat mitigation and powerful deep learning algorithms to detect cyber threats effectively.

2.5.4 Real-time Estimation

Fundamental aspects of future smart cities are SM and AMI. Its comprehensive enactment leads to a significant impact on the efficient functioning of smart cities. Impact related to total savings or greater ease of use for consumers at all income levels and suppliers of utilities by providing real-time data collection and user consumption patterns. The development of smart cities depends on the wireless network standards, which must assure attending utility demands at lower costs, more bandwidth, and quality of service. Moreover, infra-structure legacy related to the wireless network and existing IoT concepts and implementation is fundamental to achieving a fully interconnected city. Future works focus on the role of real-time monitoring in smart cities.

Real-time estimation should consider forecasting schemes into distribution networks, taking into account dynamically changing environments and corresponding time dependencies (LIANG et al., 2020). The SGs scenarios imply a bunch of data processing that requires efficient low-complexity and high-performance signal processing algorithms. A real-time estimator should be both flexible and practical, providing an accurate evaluation of the

SGs state under a wide variety of operation conditions, from fault to typical operation scenarios (RIVAS et al., 2020).

2.5.5 Massive-congested AMI Deployments

Beyond the quality and computational requirement of handling data, the overarching concerns of handling data emanating from numerous IoT devices will likewise have to be investigated profundity. RA protocols for massive SGs communication devices and system performance stand for trending research. The influence of RA protocols in achieving QoS SGs requirements encourages future research works brought out in this area. It is paramount to establish the role of RA in accomplishing the QoS requirements and point out the contrasts between traditional electrical systems and SGs QoS requirements.

RA congestion occurs when a massive number of devices transmit data at the same time with the exact clock synchronization. This issue causes a collision that drives a negative impact on a cellular network's performance in terms of packet losses, energy consumption, and longer delay (KARUPONGSIRI et al., 2017). Moreover, the trend of M2M device connections is more prominent than mobile phone users. One of the critical roles of SGs devices is to broadcast data in a periodic time. Due to the limited number of preamble signatures, a considerable number of M2M devices accessing the network will result in the recycling of the identical preambles causing a preamble conflict issue (BOCKELMANN et al., 2018). For instance, in LTE networks with the Random Access Channel (RACH), all devices can establish connections with an eNode-B without centralized control (MADUENO et al., 2016). Although devices (e.g., SMs) communication handles the regular time to access a network. This is the worst-case scenario concerning preamble signatures, even if some are kept for specific devices.

2.6 Conclusions

The fundamental notion of a more efficient, data-dependent, and consumer-centered counterpart of the conventional power grid constitutes the Smart Grid concept. Smart devices with processing, storage, and communication capabilities integrate the power grid to become the IoE or IoTG. IoE has the potential to transform various aspects of the legacy power system and our lives as an interconnected innovative society. Unlike the traditional power grid with limited information for fault diagnosis, the SGs can derive actions from many sources of information and improve many aspects of the system.

In this work, in total, more than 150 papers published in high-impact journals from 2015 to 2020 have been extensively reported observing the evolution of FD/L-SG techniques, methods, and systems. More specifically, 60% of cited journal papers have been published in high JCR impact factor journals (IF$>$ 3.0), while 12% of citations come from relevant conference papers. Over 76% of cited papers from 2015 or newer and 40%

published in 2018 or newer. This extensive literature review revealed a tendency of the application of machine learning-based tools in undertaking several FD/L-SG problems and offered the scope of future development of promising subjects with the appliance of the monitoring network. Notwithstanding, the quick expansion in the use of learning-based (ML tools) prevails and is worth further research effort. Moreover, high-performance data processing and analysis for intelligent decision-making of large-scale complex multi-energy systems, lightweight machine learning-based solutions in IoE. This work also highlighted the lack of efficient underlying computing and communication technologies,*e.g.*, edge computing and future 5G wireless networks, for advanced applications in SGs systems.

Furthermore, this chapter discussed the current trends and new perspectives in SGs faults scenarios through the understanding of the monitoring infrastructure, the communication infrastructure, and the advanced detection and location techniques, with a particular focus on the identification of the trending research topics. In addition, the chapter offers a comprehensive point-of-view to researchers, academicians, and professionals interested in exploring relations between SGs monitoring and the FD/L-SG techniques. Finally, it provided a framework for the additional exploration and expansion of knowledge and insights of SGs monitoring and the FD/L-SG techniques.

3 Harmonics in Power System

This chapter presents an adaptive harmonic disturbances detection under fault conditions in a SG system. Monitoring and controlling SG networks require real-time measuring. This measuring demands high-speed, fully integrated, and two-way communication technologies. On a fault condition, the online accurate monitoring becomes difficult due to the transient current occurrences requiring adaptive methods to achieve SG requirements. In this chapter an adaptive technique to reliable monitoring harmonic distortion in the power network has been proposed. Harmonic estimation is implemented by utilizing the LS, Kalman filter (KF), Maximum Likelihood estimation (MLE), and Goertzel Algorithm to obtain the amplitude of the harmonics in the network and its variation under dynamic fault conditions. The tested μSG includes wind turbine (WindT) and PV panels with time-variable loads at a medium voltage level. Consequently, the total demand distortion (TDD) estimations using the filtering estimators are also compared with the predictions obtained by the Tenti conservative power theory (TENTI et al., 2007; TENTI et al., 2011) accordingly. Finally, a performance-complexity trade-off analysis demonstrated the (dis)advantages of each filtering method.

3.1 Harmonics Presence

The traditional power quality analysis focused on voltage quality (voltage dips, interruptions, and voltage distortions, etc). The conventional view of power quality with power electronics features the current quality, which considers the nonlinear load current impacts into the network and how such current disturbance affects the grid.

Harmonic analysis comprises the harmonics estimation from nonlinear loads. Harmonics are one of the major power quality concerns. Actual power quality subjects cover many matters such as voltage sags and swell, transients, under and overvoltages, frequency variations, outright interruptions, power quality for sensitive electronic equipment. Harmonics have injurious effects on electrical equipment, which can be summarized in Fig. 3.1 (SEUBERLICH et al., 1985; IEEE, 2014; DAS, 2015a): A number of power theories exist to explain the active, reactive, and instantaneous power relations in presence of harmonics (Fryze theory in the time domain, Shepherd and Zakikhani theory in the frequency domain, Czarnecki power theory in the frequency domain, and Nabe and Akagi instantaneous power theory) (DAS, 2015c).

The conservative power theory (CPT) offers a structure to approach SG characterization and control problems, including the definition of power and current terms related to active, reactive, and harmonic phenomena (TENTI et al., 2011). Thus, for a general

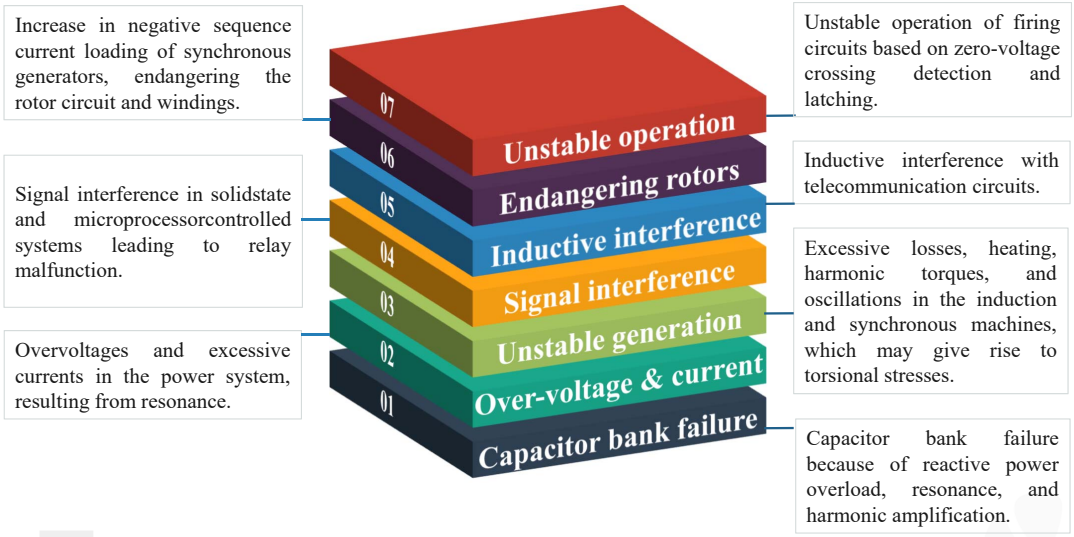

Figure 3.1 – Harmonics harmful effects (SEUBERLICH et al., 1985; IEEE, 2014; DAS, 2015a)

condition (See (3.1)), the total current (i) can be decomposed into:

$$i = i_a + i_r + i_v \tag{3.1}$$

Active current (i_a): constant conversion of useful energy.

Reactive current (i_r): related to the phase shift between voltage and current, whether caused by the presence of energy storage elements (inductors and capacitors) or by the presence of current-deflecting electronic circuits;

Void current (i_v): scattered and load-generated harmonic current, which do not contain fundamental components, active power, nor reactive power (TENTI et al., 2011; TENTI et al., 2007).

$$i_v = i_{sa} + i_{sr} + i_g \tag{3.2}$$

- Scattered current terms (i_{sa}, i_{sr}): Account for different values of equivalent admittance at different harmonics.
- Load-generated current harmonics (i_g): Harmonic terms that exist in currents only, not in voltages.

SG monitoring function requires the installation of AMI with power quality (PQ) capability. The utility wants to bill customers for actual costs of producing total power (Active, reactive, and void power).

The TDD (see (3.5)), THD_{v} (see (3.3)), and THD_{i} (see (3.4)) are terms defined by the standards (IEC, 1992-2016; IEEE, 2014) to measure this distortion at the point of common coupling (PCC). The PCC is established as the point where the user connects to the supply. Normally, High-voltage DC (HVDC) systems and Static var compensators

(SVCs) owned and operated by the utility are dismissed from the definition of the PCC (DAS, 2015b).

$$THD_v = \frac{\sqrt{\sum_{k=2}^{\infty} v_k^2}}{v_f} \cdot 100 \qquad [\%] \tag{3.3}$$

where v_k and v_f are amplitude values of the kth and fundamental harmonics of the measured voltage, correspondingly.

$$THD_i = \frac{\sqrt{\sum_{k=2}^{\infty} i_k^2}}{i_f} \cdot 100 \qquad [\%] \tag{3.4}$$

where i_k and i_f are amplitude values of the kth and fundamental harmonics of the measured current, accordingly.

The TDD is the critical base which determines how the harmonics are limited. Defined as the total root sum square harmonic current distortion as a percentage of maximum fundamental load current I_L.

$$TDD = \frac{\sqrt{\sum_{k=2}^{\infty} i_k^2}}{I_L} \cdot 100 \qquad [\%] \tag{3.5}$$

The limits specified in Institute of Electrical and Electronics Engineers (IEEE) 519 standard allows higher current distortion limits from large consumers, as the short-circuit levels in their systems will, generally, be higher. Table 3.1 shows part of the current distortion limits specified in (IEEE, 2014). The maximum harmonic current distortion for individual harmonics or TDD depends on the ratio of the short circuit current (I_{SC}) available at the PCC to the maximum fundamental load current (I_L). It is worth mentioning that I_L is different from i_f, the actual fundamental amplitude of the measured signal.

Table 3.1 – Maximum Harmonic Current Distortion in % of I_L (Odd Harmonics) [a] from (IEEE, 2014).

I_{sc}/I_L	**Ind. harmonics** ($h < 11$)	**TDD** [%]
General Distribution Systems (120 V - 69 kV)		
< 20 [c]	4.0	5.0
$20 - 50$	7.0	8.0
$50 - 100$	10.0	12.0
$100 - 1000$	12.0	15.0
> 1000	15.0	20.0
General Transmission Systems (161 kV)		
< 50	2.0	2.5
> 50	3.0	3.8

[a] Even harmonics are limited to 25% of the odd harmonic limits above.

3.2 Harmonics Estimation Methods for Power Systems

Signal processing includes the measurement, monitoring, and processing sequences from the acquisition, analysis, detection, extraction, and classification of the waveforms which might carry useful information for identification of system events, phenomena, and load characteristics. The literature in technical protection mentions that new protection methods and algorithms require high sampling rates, i.e., higher than 64 samples per cycle. The use of high sampling rates on the voltage and current signals are common in power-quality and data-logger applications (RIBEIRO et al., 2013). Against this background, it is worth to note that PMUs native sampling rate are 24, 32, 40 up to 64 samples per cycle (KITZIG et al., 2019).

Power system state estimation is an important module in the SCADA system for power grid operation(GIANNAKIS et al., 2013). QoS and reliability requirements for SG demand actual electrical parameters estimation to perform an accurate power systems analysis. Estimation of power systems harmonics in SG is an important subject to achieve QoS requirements.

3.2.1 Sinusoidal Model

To identify harmonic and interharmonic disturbances, sinusoidal models are the most proper choice. In the sinusoidal models, the discrete-time vector measured signal $\vec{z}$ of finite length N is represented by a signal vector $\vec{s}$, which is a sinusoidal waveform with K sinusoidal components, plus the additive white Gaussian noise (AWGN) $\vec{\eta}$ with zero mean and known variance σ^2, *i.e.* each element of the vector has following distribution $\vec{\eta} \sim \mathcal{N}(0, \sigma^2)$:

$$z(n) = s(n) + \eta(n) \tag{3.6}$$

$$s(n) = \sum_{k=1}^{K} a_k \cos(n\omega_k + \phi_k) \tag{3.7}$$

$$\vec{z}_{1xN} = \vec{s}_{1xN} + \vec{\eta}_{1xN} \tag{3.8}$$

where n is the discrete-time index, a_k is the magnitude, ϕ_k is the initial phase angle, $\omega_k = 2\pi f_k$ is the harmonic (or interharmonic) frequency in radius, and K is the total number of sinusoids.

3.2.2 Noise in Power Systems

The Gaussian noise assumption is commonly made in power system state estimation. This assumption is an approximation to reality. Several studies in power systems have demonstrated that outliers with uniform or Gaussian distribution may corrupt Gaussian noises. Lately, PMU measurements reveal sudden changes or even unavailability due to

communication malfunction, producing outliers and then generating non-Gaussian measurement errors (ZHAO et al., 2019; CHEN et al., 2019; NWANKPA; SHAHIDEHPOUR, 1990).

Accordingly, among noise occurrences, in power system estimation, commonly one can assume Gaussian noise, non-Gaussian noise, derivated from changing operating status of the communication channels, the GPS synchronization process, or the actual power systems variations, and finally, the outliers measured points can be justified to the impulsive noise, loss of communication channels, as well as the saturation of the potential transformer (PT) or the CT devices, or even due to the bad PMU measurements deviation.

3.2.3 Windowing Process for Adaptive Estimation

The analyzed harmonic estimation algorithms use a temporal windowing process to obtain an updating, sometimes adaptive estimation, resulting in improved estimation and timely execution. Fig. 3.2 illustrates the moving temporal window process as implemented in this work. In such a moving time window specified by length L, the window is moved sample-by-sample over the data, and estimates of harmonic parameters are computed over the data in the current window. The output n for each input sample is an estimate over the window, taking into account the current sample and the previous $L-1$ samples. In the first step, the algorithm fills the window with zeros in order to compute the first $L-n$ output when the window does not have enough data yet. In subsequent time steps, the algorithm is completed with zeros until $n \geq L$ in order to fill the current processing window.

Normally, PMUs with low native sampling rates deteriorate estimation precision. A signal acquired via N samples will require a minimum window length, $L_{\min}$, equal to the PMUs native sampling rates for a cycle. For reference, this work considers $N = 64$ [samples per cycles] with a $cycle = 1/f_u = (60\,Hz)^{-1} = 16.66\,ms$. Even though smaller subsets (window length $< L_{\min}$) despite improving the processing performance, they also affect the precision of the estimation parameters of the electrical system.

3.2.4 Harmonics Estimation using LS

Equation (3.7) using the sum-to-product identities can be re-written by

$$s(n) = \sum_{k=1}^{K} \left(a_k \cos(n\omega_k)\cos(\phi_k) - a_k \sin(n\omega_k)\sin(\phi_k)\right) \tag{3.9}$$

converting into following expression

$$s(n) = \sum_{k=1}^{K} \begin{bmatrix}\cos(n\omega_k) & \sin(n\omega_k)\end{bmatrix}\begin{bmatrix}\alpha_k & \beta_k\end{bmatrix}^T \tag{3.10}$$

where $\alpha_k = a_k \cos\phi_k$ and $\beta_k = -a_k \sin\phi_k$ are the parameters to estimate or the vector $\vec{\theta}(n)$.

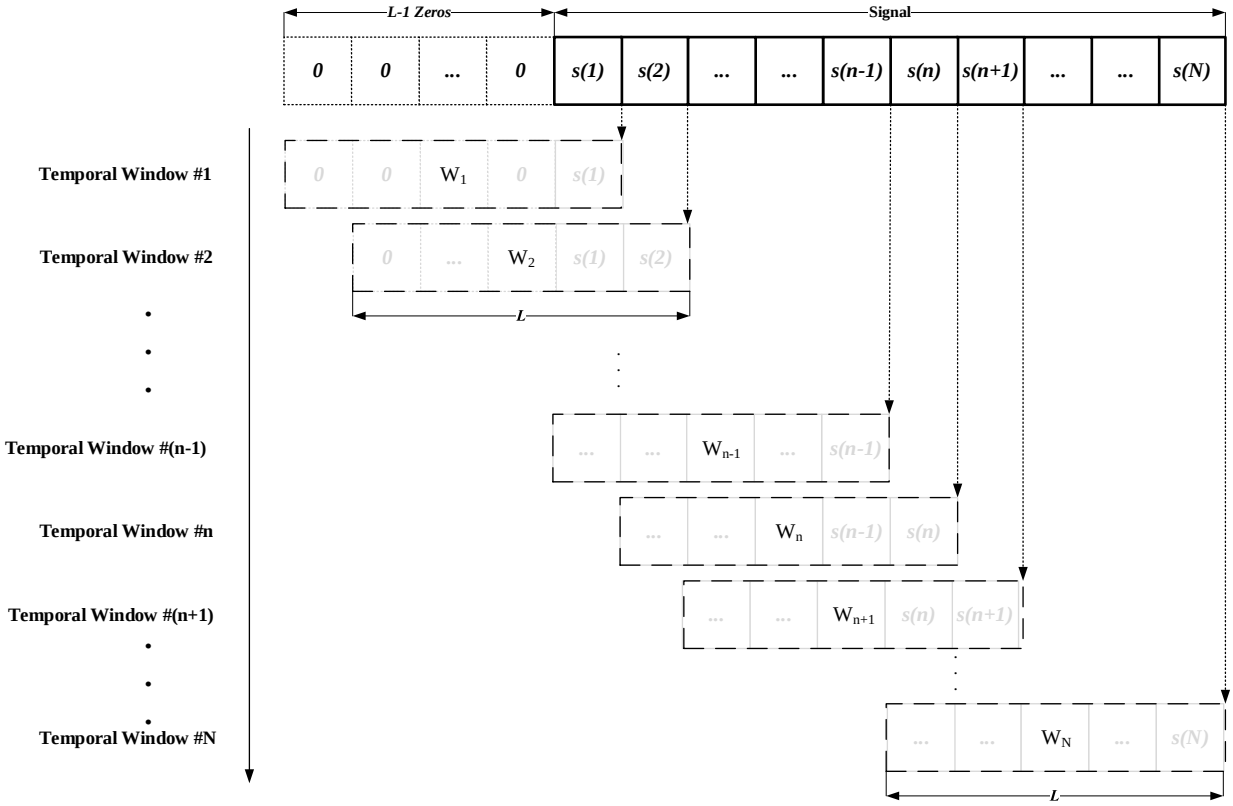

Figure 3.2 – Moving Rectangular Window Processing

The resulting sampled linear model of the system with additive noise from (3.7) evaluated in a Window of size L with LS is given by

$$\vec{s}(n) = \vec{H}(n)\vec{\theta}(n) \tag{3.11}$$

where $\vec{s}(n)$ is a vector of size L from the signal measurements at a window n; $\vec{H}(n)$ is the system structure matrix of dimension $(L+1)$x$2K$; $\vec{\theta}(n)$ vector for the amplitudes to estimate of dimension K.

The estimation model for the system is

$$\hat{\vec{s}}(n) = \vec{H}(n)\hat{\vec{\theta}}(n) \tag{3.12}$$

The estimate $\hat{\vec{\theta}}(n)$ for the required parameter vector $\vec{\theta}(n)$ can be obtained by minimizing the objective function

$$J[\hat{\vec{\theta}}(n)] = \tilde{\vec{s}}^T(n)\tilde{\vec{s}}(n) \tag{3.13}$$

where $\tilde{\vec{s}}$ represents the error in the estimated and the measured values. Differentiating with respect to $\vec{\theta}(n)$ and then setting it to zero gives the required LS estimation algorithm

$$\hat{\vec{\theta}}_{LS}(n) = [\vec{H}^T(n)\vec{H}(n)]^{-1}\vec{H}^T(n)\vec{s}(n) \tag{3.14}$$

The system structure matrix $\vec{H}(n)$ is given by

$$\vec{H}(n) = \begin{bmatrix} \cos(\omega_1 t_{n-L}) & \cos(\omega_1 t_{n-(L+1))}) & \dots & \cos(\omega_1 t_n) \\ \sin(\omega_1 t_{n-L}) & \sin(\omega_1 t_{n-(L+1)}) & \dots & \sin(\omega_1 t_n) \\ \vdots & \vdots & \ddots & \vdots \\ \cos(\omega_K t_{n-L}) & \cos(\omega_K t_{n-(L+1)}) & \dots & \cos(\omega_K t_n) \\ \sin(\omega_K t_{n-L}) & \sin(\omega_K t_{n-(L+1)}) & \dots & \sin(\omega_K t_n) \end{bmatrix} \tag{3.15}$$

3.2.5 Harmonics Estimation using Kalman Filter (KF)

Kalman filters are a specific type of filter. Their solution is based on a set of state-space equations. KF is an invaluable tool for many power system applications, such as tracking harmonics in real-time, estimating voltage and current parameters in power system protection, and estimating transient parameters. Given observation data $\vec{z}(n)$, KF is described by a set of state equations and a set of observation equations as follows:

$$\text{State:} \quad \vec{x}(n) = \vec{A}(n-1)\vec{x}(n-1) + \vec{w}(n) \tag{3.16}$$

$$\text{Observation:} \quad \vec{z}(n) = \vec{C}(n)\vec{x}(n) + \vec{\eta}(n) \tag{3.17}$$

where $\vec{x}(n)$ is a vector of state variables, $\vec{A}(n-1)$ is the state transition matrix; $\vec{w}(n)$ and $\vec{\eta}(n)$ are zero-mean white noise processes, uncorrelated to each other and to the state and output vectors. Their correlation matrices are $\vec{Q}_w = \mathbb{E}\{\vec{w}(n)\vec{w}^T(n)\}$ and $\vec{Q}_\eta = \mathbb{E}\{\vec{\eta}(n)\vec{\eta}^T(n)\}$, respectively. In (3.17), the matrix $\vec{C}(n)$ represents the relation between the state vector $\vec{x}(n)$ and the measurement $\vec{z}(n)$. Individual harmonic may be considered as stationary data, leading to an approximation to expedite estimation, **i.e.,** $\vec{A}(n)$ and $\vec{C}(n)$ are time independent: $\vec{A}(n) = \vec{A}$ and $\vec{C}(n) = \vec{C}$. To apply a KF , one of the most essential concerns is to define the state variables $\vec{x}(n)$ according to the given problem. The statistical independence characteristics of the noise parameters constitute a serious constraint when power signals are KF estimated. The presence of harmonics usually correlates errors (modeled by the noise sources) with themselves and to the state and output vectors.

Nowadays SG systems are no longer considered stationary. In general, existing systems reveal a short time-varying behavior caused by complex non-linear systems integration, seasonal load changes, the presence of unmeasured disturbances, operator interventions. Nonstationary process monitoring is complex, generally addressed with adaptive estimation strategies. Kalman filters addressed to estimate the state vector in a linear system model, including noisy or incomplete measurements, and more importantly, consider the nonstationary problem nature.

Once the state variables are defined, the exact expressions of the state equations and the observation equations are determined with fixed matrices $\vec{A}$ and $\vec{C}$. Moreover, it requires a careful examination of whether the white-noise assumption holds for $\vec{w}(n)$ and $\vec{\eta}(n)$ under the given state and observation equations. If the assumption does not hold, the

performance of a KF could be undesired. This KF only considers a practical power system data analysis example where the sinusoidal models in Equation (3.6) are used (BOLLEN; GU, 2006). Hence, the observations can be expressed as:

$$z(n) = \sum_{k=1}^{K} s_k(n) + \eta(n) \tag{3.18}$$

where the kth harmonic component is $s_k(n) = a_k \exp jn\omega_k$, $k = 1, ..., K$. The purpose of using a KF is to estimate harmonic-related power system distortions and to estimate the parameters associated with these harmonics (*e.g.*, the magnitudes and phase angles). For a total of K harmonics, defining the state vector $\vec{x}(n)$ that contains $2K$ elements:

$$\vec{x}(n) = [s_{1,r}(n)s_{1,i}(n) \dots s_{K,r}(n)s_{K,i}(n)]^T \tag{3.19}$$

where each real and imaginary component of $s_k(n)$ is written as

$$s_{k,r}(n) = \Re[s_k(n)] = a_k \cos(n\omega_k + \phi_k) \tag{3.20}$$

$$s_{k,i}(n) = \Im[s_k(n)] = a_k \sin(n\omega_k + \phi_k) \tag{3.21}$$

Consider the state variables $s_{k,r}(n+1)$ and $s_{k,i}(n+1)$ at time $n+1$. It follows that

$$s_{k,r}(n+1) = a_k \cos((n+1)\omega_k + \phi_k) \equiv s_{k,r}(n)\cos(\omega_k) - s_{k,i}(n)\sin(\omega_k) \tag{3.22}$$

$$s_{k,i}(n+1) = a_k \sin((n+1)\omega_k + \phi_k) \equiv s_{k,r}(n)\sin(\omega_k) + s_{k,i}(n)\cos(\omega_k) \tag{3.23}$$

Combining eq. (3.19), eq. (3.22) and (3.23), the state transition matrix $\vec{A}$ in eq. (3.16) can be written as:

$$\vec{A} = \begin{bmatrix} \cos(\omega_1) & -\sin(\omega_1) & 0 \dots 0 & 0 & 0 \\ \sin(\omega_1) & \cos(\omega_1) & 0 \dots 0 & 0 & 0 \\ \vdots & \vdots & \vdots \ddots \vdots & \vdots & \vdots \\ 0 & 0 & 0 \dots 0 & \cos(\omega_k) & -\sin(\omega_k) \\ 0 & 0 & 0 \dots 0 & \sin(\omega_k) & \cos(\omega_k) \end{bmatrix} \tag{3.24}$$

where ω_k can be chosen as the true power system harmonics or interharmonics. Choosing power system harmonics implies that $\omega_k = k\omega_0$, $k = 1, ..., K$, $\omega_0 = 2\pi f_0/f_s$ is the fundamental frequency of the power system (in radian per second), and f_s is the sampling frequency (in hertz). It is worth mentioning that to implement the KF algorithm for harmonics estimation, the matrix $\vec{A}$ should be fully specified. This also means that the frequencies $\omega_k = k\omega_0$, $k = 1, ..., K$, are fixed and pre-specified, rather than parameters to be estimated. Moreover, in our harmonic estimation problem via Kalman filtering approach, the observation equation (3.17) is treated as a scalar, $z(n) \in \Re$; as a consequence, matrix $\vec{C}$ becomes a vector of zeros and ones:

$$\vec{c} = [1 \quad 0 \quad 1 \quad 0 \quad \dots \quad 1 \quad 0] \tag{3.25}$$

where "1" holds for real harmonic component, while "0" for imaginary harmonic component. Besides, the observation noise vector $\vec{\eta}(n) = [\eta(n) \quad 0 \quad \dots \quad 0 \quad 0]^T$ and the model noise

vector $\vec{w}(n) = [w(n) \quad 0 \quad \dots \quad 0 \quad 0]^T$ are both of dimension $\Re^{2K\times 1}$. In our simulation results, the power of measurement noise is set to $\sigma_\eta^2 = 0.25$, and a low power value for the process noise $\sigma_w^2 = 0.01$ is chosen in order to emulate a typical relatively small variances in the estimated state variables (BOLLEN; GU, 2006).

With prior definitions in this section for both the state and observation equations, the harmonic model is fully specified in the state space. In our KF -based parameter estimation approach, the time-dependent harmonic-related parameters come with the magnitudes $A_k(n)$ and the initial phase angles ϕ_k of the harmonics $s_k(n)$, $k = 1, 2, ..., K$; such magnitude and phase for the kth harmonic can be computed at each time instant n as:

$$A_k(n) = \sqrt{[s_{k,r}(n)]^2 + [s_{k,i}(n)]^2} \tag{3.26}$$

$$\phi_k(n) = \tan^{-1}\left[\frac{s_{k,i}(n)}{s_{k,r}(n)}\right] \tag{3.27}$$

KF is an adaptive estimator which in the harmonic estimation problem processes samples one-by-one, using estimated state from the previous time step and the current measurement to compute the estimate for the current state. The notation $\hat{\vec{x}}(n)$ represents the estimate of $\vec{x}(n)$, as defined in Eq. (3.19), at time n given observations up to prior time observation. Accordingly, this KF is conceptualized as two distinct steps: "Predict" and "Correction". The predict step uses the state estimate from the previous timestep, $\vec{x}(n-1)$, and previous covariance, $\vec{P}(n-1)$, to provide an estimation to the current state and the current covariance. Using estimate values, one can obtain:

$$\hat{\vec{x}}(n) = \vec{A}\hat{\vec{x}}(n-1) \qquad \text{State Prediction} \tag{3.28}$$

$$\hat{\vec{P}}(n) = \vec{A}\hat{\vec{P}}(n-1)\vec{A}^T + \hat{\vec{Q}}_w \qquad \text{Covariance Prediction} \tag{3.29}$$

Besides, to expeditiously compute the predicted state and covariance, the Kalman gain matrix is deployed:

$$\vec{K}(n) = \left[\hat{\vec{P}}(n)\vec{c}^T\right]\left[\vec{c}\hat{\vec{P}}(n)\vec{c}^T + \hat{\vec{Q}}_\eta\right]^{-1} \qquad \text{Kalman Gain} \tag{3.30}$$

Hence, in the correction step, the current *a priori* predictions, obtained in (3.28) and (3.29) , are combined with current observation $z(n)$ to improve the state estimation:

$$\hat{\vec{x}}(n) = \hat{\vec{x}}(n) + \vec{K}(n)[z(n) - \vec{c}\hat{\vec{x}}(n-1)] \qquad \text{State Correction} \tag{3.31}$$

$$\hat{\vec{P}}(n) = \left[\vec{I} - \vec{K}(n)\vec{c}\right]\hat{\vec{P}}(n) \qquad \text{Covariance Correction} \tag{3.32}$$

where $\hat{\vec{x}}(n)$ in (3.31), and $\hat{\vec{P}}(n)$ from (3.32) representing the updated and improved estimations, termed *a posteriori* state estimate and *a posteriori* covariance matrix estimate, respectively.

3.2.6 Harmonics Estimation Using Maximum Likelihood Estimation (MLE)

The probability density function (PDF) for a sinusoidal parameter estimation problem is proportional to the likelihood function (LF) of the unknown frequencies as described by (KAY, 1993):

$$\mathcal{L}(\vec{x};\vec{\theta}) \propto p(\vec{x};\vec{\theta}) = \frac{1}{[2\pi\sigma^2]^{\frac{N}{2}}} \exp\left\{-\frac{1}{2\sigma^2}\sum_{n=1}^{N}\left[x(n) - \sum_{k=1}^{K} A_k \cos[2\pi f_k n + \phi_k]\right]^2\right\} \tag{3.33}$$

where $\vec{\theta} = \{\vec{A}, \vec{f}, \vec{\phi}\}$, with amplitude $A_k > 0$, f_k is the harmonic frequency, and ϕ_k the phase for each k harmonic (or inter-harmonic) to be estimate.

Log-likelihood function (LLF) is a logarithmic transformation of the LF . Since exponential functions introduce unnecessary computation steps to find the maximum cost function, it is more suited to work with the log-likelihood version of the cost function. Note that logarithm is rigidly increasing functions; hence, maximizing the likelihood function in (3.33) is equivalent to maximizing the log-likelihood version of the original cost function. Then the LLF is

$$\ell(\vec{x};\vec{\theta}) = -N\log[\pi\sigma^2] - \left\{-\frac{1}{2\sigma^2}\sum_{n=1}^{N}\left[x(n) - \sum_{k=1}^{K} A_k \cos(2\pi f_k n + \phi_k)\right]^2\right\} \tag{3.34}$$

Maximizing (3.34) is equivalent to minimizing the negative of a scaled and normalized version of $\ell(\cdot)$, resulting:

$$J(\vec{A}, \vec{f}, \vec{\phi}) = \sum_{n=1}^{N}\left[x(n) - \sum_{k=1}^{K} A_k \cos(2\pi f_k n + \phi_k)\right]^2 \tag{3.35}$$

The MLE would require a multidimensional minimization of equation (3.35). Considering independent data sets, the multidimensional MLE of amplitude A_k, frequency f_k, and phase ϕ_k for the kth harmonic over N samples can be found minimizing

$$J(A_k, f_k, \phi_k) = \sum_{n=1}^{N}\left[x(n) - A_k \cos(2\pi f_k n + \phi_k)\right]^2 \tag{3.36}$$

We first expand the cosine to yield

$$J(A_k, f_k, \phi_k) = \sum_{n=0}^{N-1}\left[x(n) - A_k \cos\phi_k \cos(2\pi f_k n) + A_k \sin\phi_k \sin(2\pi f_k n)\right]^2 \tag{3.37}$$

Although J is nonquadratic in A and ϕ_k, we may transform it to a quadratic function by letting

$$\alpha_1(k) = A_k \cos\phi_k \tag{3.38}$$

$$\alpha_2(k) = -A_k \sin\phi_k \tag{3.39}$$

which is a one-to-one transformation. The inverse transformation is given by

$$A_k = \sqrt{\alpha_1^2 + \alpha_2^2} \tag{3.40}$$

$$\phi_k = \arctan\left(\frac{-\alpha_2}{\alpha_1}\right) \tag{3.41}$$

Also, let

$$\vec{c}(k) = [1 \cos 2\pi f_k \ldots \cos 2\pi f_k(N-1)]^T \tag{3.42}$$

$$\vec{s}(k) = [0 \sin 2\pi f_k \ldots \sin 2\pi f_k(N-1)]^T \tag{3.43}$$

Then, we have

$$J'(\alpha_1, \alpha_2, f_k) = (\vec{x} - \alpha_1\vec{c} - \alpha_2\vec{s})^T(\vec{x} - \alpha_1\vec{c} - \alpha_2\vec{s}) = (\vec{x} - \vec{H}\vec{\alpha})^T(\vec{x} - \vec{H}\vec{\alpha}) \tag{3.44}$$

where $\vec{\alpha} = [\alpha_1\alpha_2]^T$ and $\vec{H} = [\vec{c} \quad \vec{s}]$. the minimizing solution is

$$\hat{\vec{\alpha}} = (\vec{H}^T\vec{H})^{-1}\vec{H}^T\vec{x} \tag{3.45}$$

Equation (3.45) is equivalent to Equation (3.14). We may affirm that the solution from LS and MLE are equal and should treat as one estimating technique.

3.2.7 Harmonics Estimation Using Goertzel Algorithm

The Goertzel algorithm is a technique for efficient evaluation of the individual terms of the DFT, used in dual-tone multifrequency decoding and phase/frequency-shift keying modem implementations. The algorithm is performed in the form of a second-order Infinite Impulse Response (IIR) filter. The Goertzel algorithm implements the DFT as a recursive difference equation. To establish this difference equation, express the DFT as the convolution of an N-point input, $x(n)$, with the impulse response:

$$h(n) = W_N^{-kn}u(n) \tag{3.46}$$

$$W_N^{-kn} = \exp(-j\omega_0) \tag{3.47}$$

where $u(n)$ is the unit step sequence and $\omega_0 = 2\pi k/N$ is the frequencies chosen for the Goertzel analysis. Besides, the index number k indicating the frequency index of the DFT , which is selected from the set of index numbers $k \in \{0, 1, 2, ..., N-1\}$.

The Z-transform of the impulse response is

$$H(z) = \frac{1 - W_N^k z^{-1}}{1 - 2\cos(2\pi k/N)z^{-1} + z^{-2}} \tag{3.48}$$

Obtaining the following form:

$$y_N = \sum_{n=0}^{N} x(n)e^{-j2\pi\frac{nk}{N}} \tag{3.49}$$

In general, Goertzel is slower than DFT when computing all the possible DFT indices, but is most useful when $\vec{x}$ is a long vector, and the DFT computation is required for only a subset.

3.3 Micro Smart Grid Implementation

A μSG, consisting of distributed generators, load, energy storage, and protection control devices, is an independently controllable system comprising complete power generation, transmission, distribution, and energy utilization systems (LIU et al., 2018). Fig. 3.3 illustrates a schematic diagram of the studied μSG system.

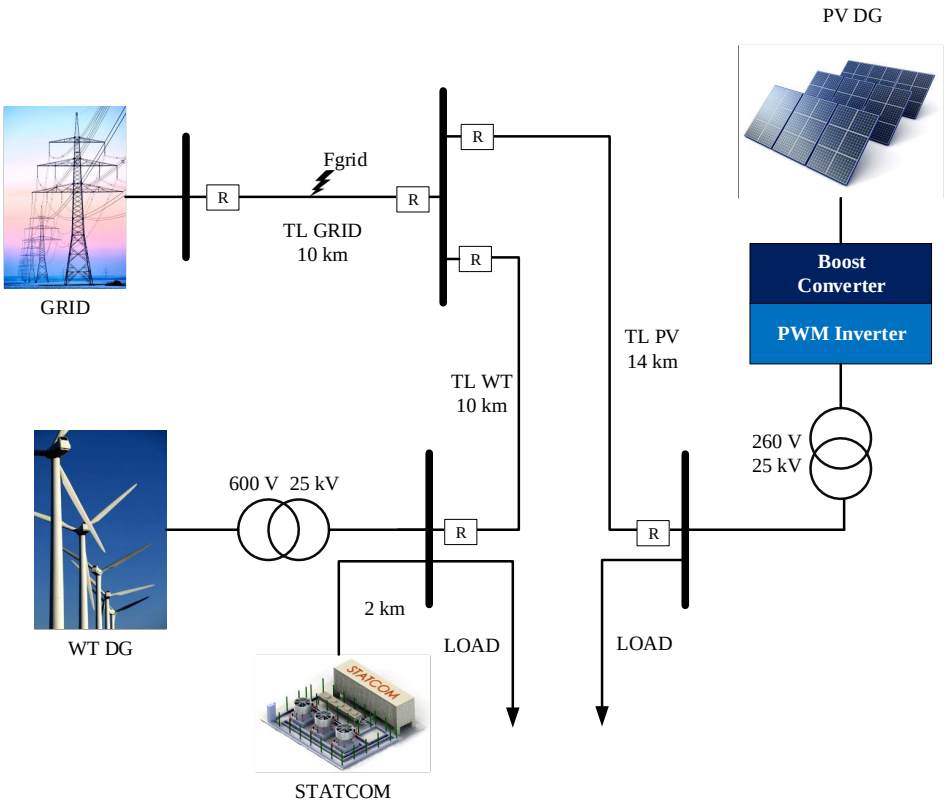

Figure 3.3 – Schematic for SG including DG

The studied μSG consists of 6 wind turbines (1.5 MW each) with a wind speed up to 15m/s at 0 m above ground level. The WindT connected to WT-Bus through a 10 MVA 600 V 25 kV transformer. The turbines are coupled to induction generators with fixed capacitors for excitation and a rated speed of 15 m/s. Local variable loads are included in the system with total active and reactive power of 2.5 MW and 300 kVAR, respectively. Wind energy conversion system connected to the common bus through 25 kV medium voltage feeder (Transmission Line (TL) WT) of 10 km length. The second DG unit is 100 kW PV panel and connected to the grid through a DC/DC boost converter (5 kHz - 500V) and a DC/ AC three-phase two-level inverter. After inversion, the arrays are interfaced to the PV-Bus through 260 V 25 kV transformer. PV-Bus connected to Grid-Bus through medium voltage feeder (TL PV) of 14 km length. The equivalent generator of the public grid is connected to Grid-Bus through a medium voltage line (TL Grid) of 10 km length. In order to enhance the performance of the wind DG unit under time-varying wind speed, as well as fault conditions, the STATCOM was installed at WT-Bus. The fault to be evaluated was located in the middle of the TL Grid medium voltage line, named

FGRID under the bolt symbol. The communication interfaces between the indicated relays (R) in Fig. 3.3 and central storage and processing location must follow the requirements according to SG application. Table 3.2 depicts the system parameter values deployed in the numerical simulations discussed in section 3.3.

This μSG system presents a dynamic operation including non-static loads. Values in Table 3.2 represent maximum load values. PV generation has variations derived from environmental conditions. Wind speed presents a linear increasing behavior, important considerations to prompt harmonic presence on this system. In general, this system will display an escalating load demand response.

Table 3.2 – System Parameters

Component	Quantities	Values	Component	Quantities	Values
WT Generator	6	575 V 1.5 MW	TL GRID	1	10 km
PV Generator	1	500 V 100 kW	PV Transformer	1	260 V 25 kV 100 kVA
Public Grid	1	25 kV 2500 MVA	WT Transformer	1	600 V 25 kV 10.5 MVA
TL WT	1	10 km	STATCOM	1	3 MVAR
TL PV	1	14 km	Loads	2	2.5 MW 300kVAR

3.4 Numerical Results and Simulation

In this section, we describe the simulation parameters and procedure. Next, we offer and discuss numerical results to corroborate the effectiveness of the estimation filters for μSG power system applications. After obtaining numerical simulation results, we determine the amplitude for individual harmonics, the TDD calculation, and normalized mean squared error (NMSE) representation including an evaluation for non-gaussian noise introduction. Next, a Time-delay comparison for this specific μSG scenario is developed. After that, we provide a complexity-performance trade-off analysis deploying such estimation tools. Finally, we offer a synthesis of the above-discussed results and information needed to conclude on the best estimation filtering choice.

3.4.1 Simulation Setup

μSG model is simulated using MATLAB/Simulink under normal and faulted conditions to validate the proposed algorithm. Table 3.3 resumes simulation parameters. This simulation required prior knowledge of the amplitude of the individual harmonics, a signal reference, to evaluate estimation accuracy. To obtain those reference signals, this work employs a decomposition utilizing the Simulink data, i.e., the signal emulated

Table 3.3 – Matlab-Simulink Simulation Parameters

Parameter	**Value**
Samples per cycle	64
Nominal Frequency	$60\,Hz$
Sampling Frequency	$f_s = 3840\,sps$
Sampling Time	$T_s = 2.604210^{-4} s$
Total Simulation Time	$5\,s$
Fault incident Time	$1.5\,s$
Fault Time Duration	$0.1\,s$
Sampled Signals	Voltage and Current
	Emulation parameters, Fig. 3.4
Harmonic frequency	$f_k = k \cdot 60\,Hz, \quad k = 1, 3, \ldots, 11$
Bandwidth of the PBF	$B_k = 10\,Hz, \ \forall k$

in the Simulink-MatLab platform is individually filtered to separate required harmonic components and next to rebuild those signals for estimation. Fig. 3.4 shows the Matlab-Simulink Signal Emulation. Current Signal from Matlab-Simulink, $\vec{i}_{MS}$, is filtered for K bandpass filters, with center frequency $f_k = \frac{f_{H,k}+f_{L,k}}{2}$ for each k harmonic, and constant bandwidth $B = B_k = f_{H,k} - f_{L,k}$, $\forall k$. This filtered signals, $(i_1, i_2, \ldots, i_k, \ldots, i_K)$, are the reference current signals. After a reconstruction process, signal obtain, $\vec{i}_r$, is the input for the estimation algorithm to obtain the individual harmonic current estimation, $(\hat{i}_1, \hat{i}_2, \ldots, \hat{i}_k, \ldots, \hat{i}_K)$. Then, $TDD[\%]$ and $\hat{TDD}[\%]$ are obtained using reference and estimated signals, accordingly. NMSE is finally calculated to validate estimation results using those data.

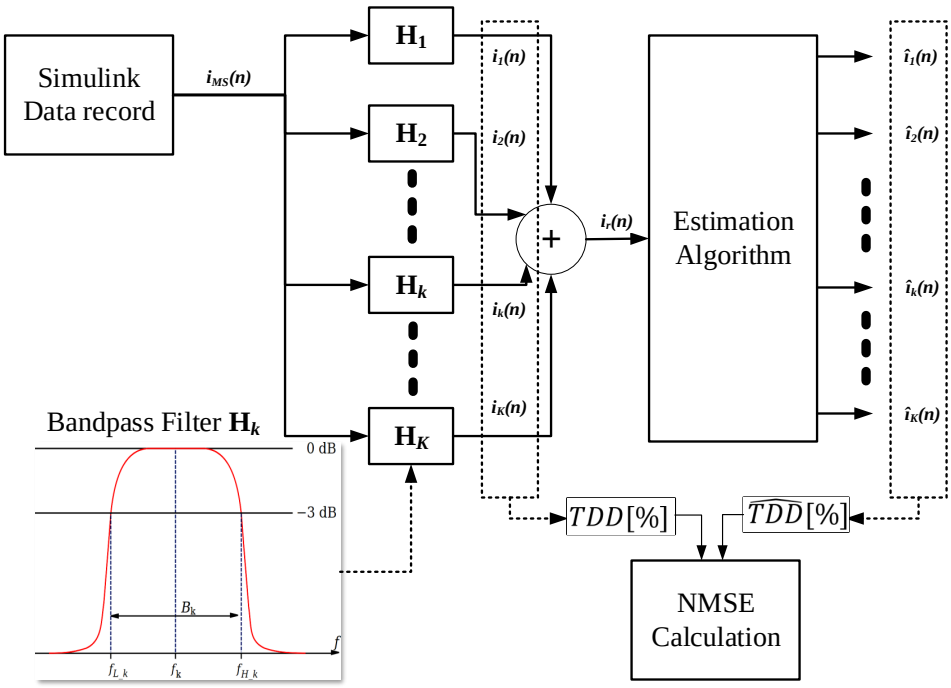

Figure 3.4 – Matlab-simulink Signal Emulation

Power system fault is classified into two types: symmetrical fault and asymmetrical fault. A symmetrical or balanced fault affects each of the three phases equally. An asymmetric or unbalanced fault does not equally affect each of the three phases. A rough occurrence of symmetrical faults is 2 to 5% of the total system faults. However, if these faults occur, they cause very severe damage to equipment even though the system remains in a balanced condition. The studied SG subjected to symmetrical three-phase fault located at midpoints of Fgrid feeder for TL_{grid} as illustrated in Fig. 3.3 and measured at sending-end. The next section presents results for the three-phase-ground symmetrical fault.

3.4.2 Amplitude Estimation

To illustrate the effectiveness of the applied techniques Fig. 3.5 and Fig. 3.6 depict individual harmonic amplitude for the first six odd harmonics order, i.e., $K = 1, 3, 5, 7, 9, 11$ accordingly, considering a time window of 2.5 seconds and a fault occurrence. Fig. 3.5.a) pictures the fundamental amplitude estimation. It is observed that the proposed algorithms estimate the system states accurately after starting. Indeed, Fig. 3.5 to 3.6.(e) explicitly show the difficulty in precisely tracking actual state for transient conditions, at system start, and under fault conditions. During this period, all filtering algorithms suffer to keep the filtered signal tracked with the true signal (marked as "Real"), besides the presence of a time delay. This time delay has been calculated using the correlation between real signal and estimated signal. It is impossible to define the best estimation only to evaluate such results. Moreover, the LS, MLE, and Goertzel Algorithms present a similar behavior in all states.

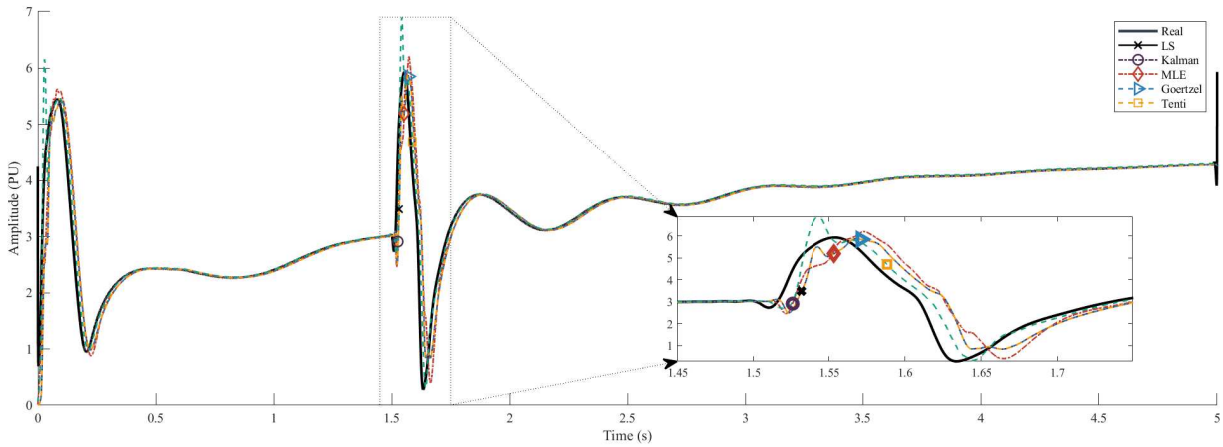

Figure 3.5 – Filtering estimation for the Fundamental amplitude component for each filtering algorithm analyzed.

When referring to harmonic amplitude estimation, Fig. 3.6.(a) to 3.6.(e) the outcome with a good representation of the stationary state estimation but with a noticed error for the transient or stationary conditions. Indeed, the behavior of the filtering-based

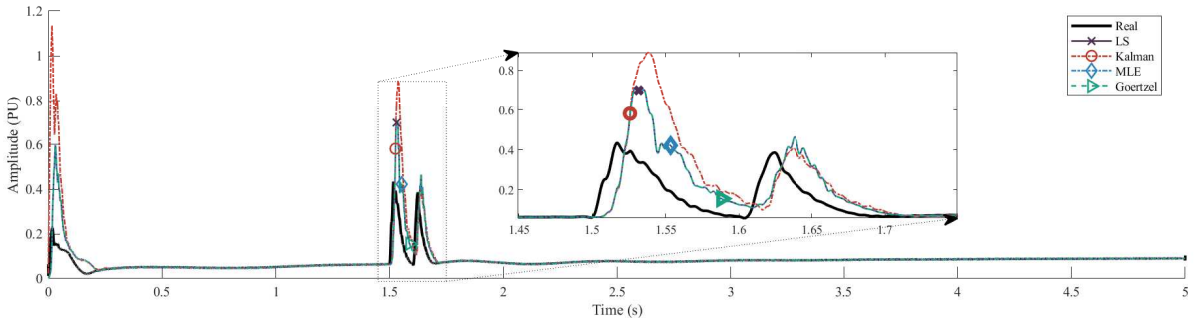

a) Filtering for the 3th harmonic component.

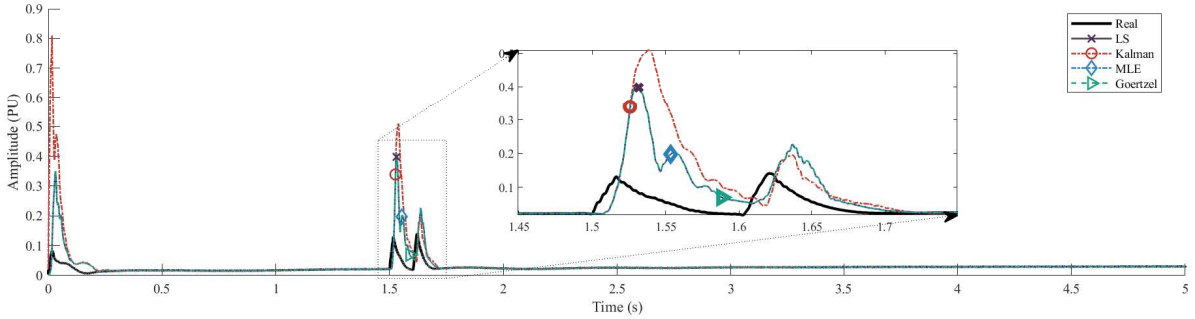

b) Estimations for the 5th harmonic component.

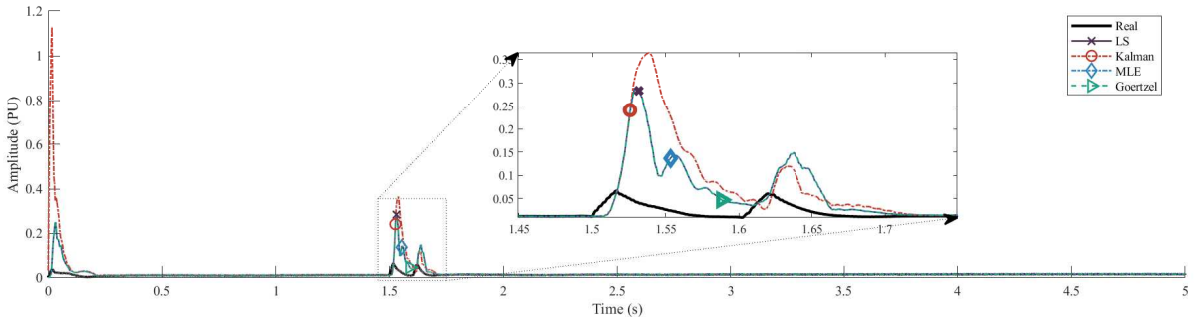

c) Estimations for the 7th harmonic component.

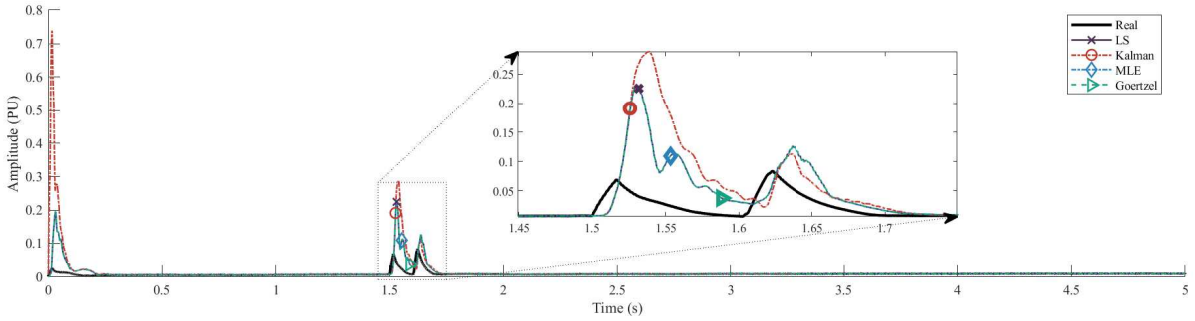

d) Estimations for the 9th harmonic component.

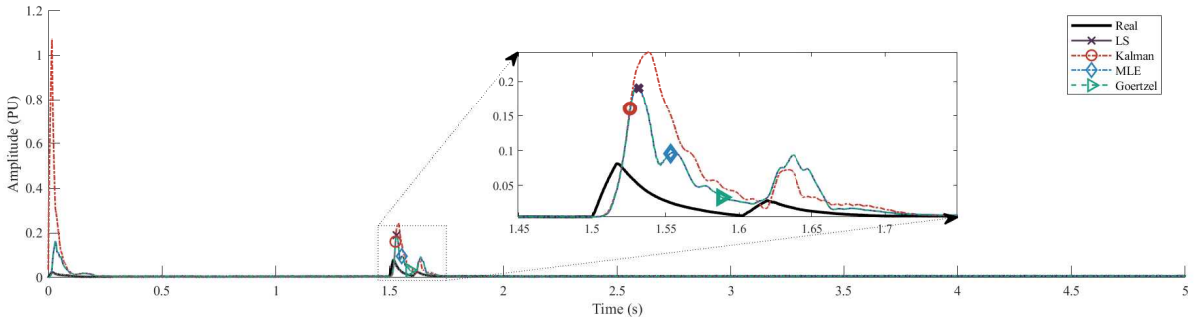

e) Estimations for the 11th harmonic component.

Figure 3.6 – Filtering estimation for the odd harmonic amplitude components for each filtering algorithm analyzed.

estimation algorithms demonstrates a high sensitivity to changes of the signal; hence, whenever substantive changes exist, all the analyzed estimation algorithms exceed, at a certain level, the expected values. Particularly, KF presents a higher TDD error estimation levels for all harmonics considered.

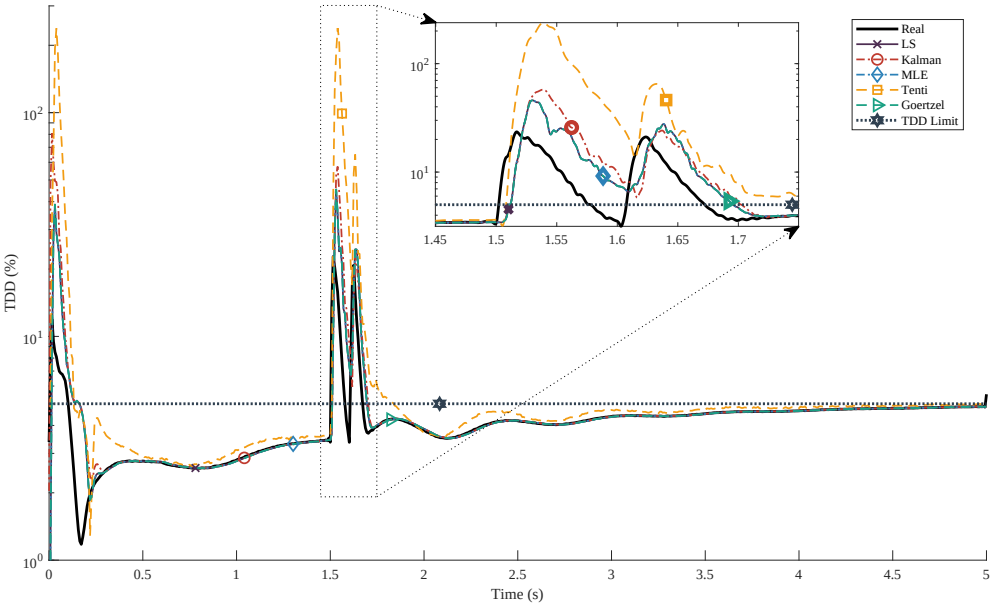

Figure 3.7 – Percentage for the Total Demand Distortion (TDD %).

3.4.3 TDD Calculation

The TDD is an important figure of merit to evaluate the quality of harmonic estimation of the different methods. Fig. 3.7 compares TDD from estimation algorithms with the "TDD Limit" threshold obtained from Table 3.1. It is noteworthy mentioning that the TDD Limit depends on the relation between maximum short-circuit current and maximum load current at the fundamental frequency, $\frac{I_{sc}}{I_l}$, as indicated in Table 3.1.

One can observe from Fig. 3.7 that, for all filtering estimation methods, the estimated TDD is close to the actual value, remaining under TDD limit. An exception appears during and right-after the system fault when TDD estimation is also affected by a time-delay. Besides, Fig. 3.7 shows the TDD results for the Tenti algorithm dismissing the behavior presented by other estimation algorithms. This relates to the fact that the current component containing harmonics (I_v) through the Tenti algorithm contains current harmonic components that do not have a pair in the voltage component. In other words, distorted voltage components will generate harmonic components not included in the void current. Notice that through this chapter Tenti algorithm is not considered an estimator due to not being capable of estimating individual harmonic components. Remembering, harmonic estimation is not the purpose of the Tenti algorithm but the active and reactive

current components estimation. This active and reactive current may have components beyond fundamental (60 Hz) frequency.

3.4.4 NMSE Analysis

Fig. 3.8 compares NMSE between normal (Fig. 3.8.(a),(e),(f)) and fault (Fig. 3.8.(b),(c),(d)) power grid conditions; in such context, the figure of merit NMSE at instant τ can be defined as:

$$\text{NMSE}[\tau] = \frac{\frac{1}{n}\sum_{i=1}^{n}(\text{TDD}[\tau] - \widehat{\text{TDD}}_i[\tau])^2}{(\text{TDD}[\tau])^2} \tag{3.50}$$

where $\widehat{\text{TDD}}_i[\tau]$ is an estimation performed by Kalman, MLE, LS, Goertzel filtering estimation algorithms for the ith TDD at the time τ, the total number of predictions is n, and $\text{TDD}[\tau]$ is the true TDD at instant τ. These values are important to validate prior discussion where estimation error increases under non-stationary conditions. Even though, Fig. 3.8 illustrates a minor error for LS, MLE, and Goertzel algorithm in both scenarios.

As complement, Fig. 3.9 illustrates NMSE analysis at $SNR = 40dB$ to remark differences among estimation algorithms. Notice that the effect of wideband additive Gaussian noise is negligible for estimators provided that the Signal-to-noise ratio (SNR) is larger than 40 dB (PHADKE; THORP, 2008). Hence, as expected, under low SNR regime of 20dB, estimation error level is higher for all filtering harmonic estimation methods.

3.4.5 Poisson Impulsive Noise Impact on the Harmonic Estimators Performance

To evaluate the impulsive noise impact on the performance of each harmonic estimation algorithm, this work deploys a Poisson distribution to model data corruption occurrence. This impulsive noise is represented by randomly distributed events where signal amplitude is corrupted beyond normal/expected values. In this subsection, four scenarios have been considered:

Case 1: In average, over a time interval t_{iN}, the PMU received signal contains 0.1% of corrupted samples.

Case 2: In average, over a time interval t_{iN}, the PMU received signal contains 1% of corrupted samples.

Case 3: In average, over a time interval t_{iN}, the PMU received signal contains 5% of corrupted samples.

Case 4: In average, over a time interval t_{iN}, the PMU received signal contains 30% of corrupted samples.

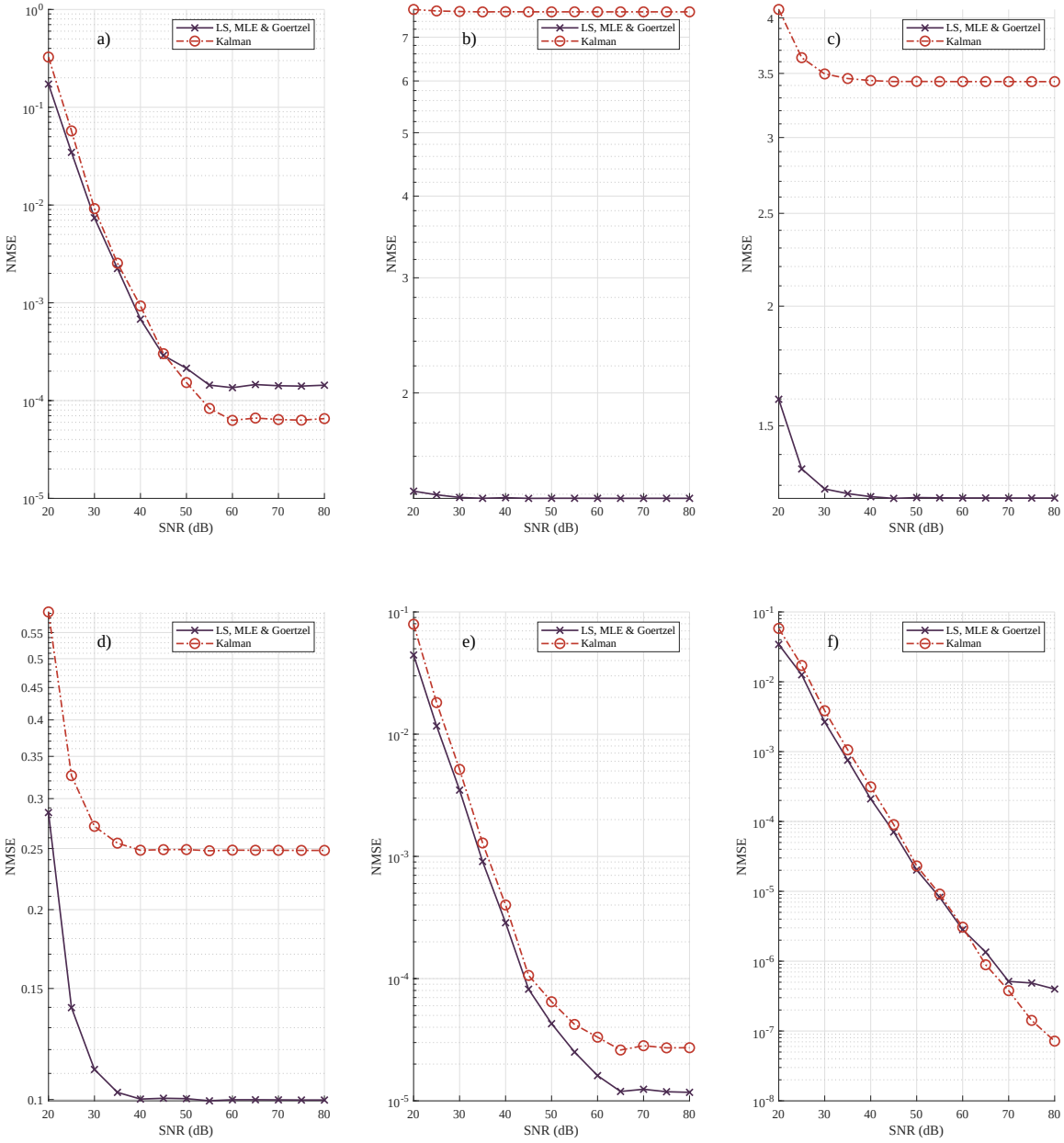

Figure 3.8 – NMSE harmonic estimation comparison under normal and fault power grid operation conditions. $T = (a)1.00;\ (b)1.55;\ (c)1.60;\ (d)1.70;\ (e)2.50;\ (f)4.00$ secs.

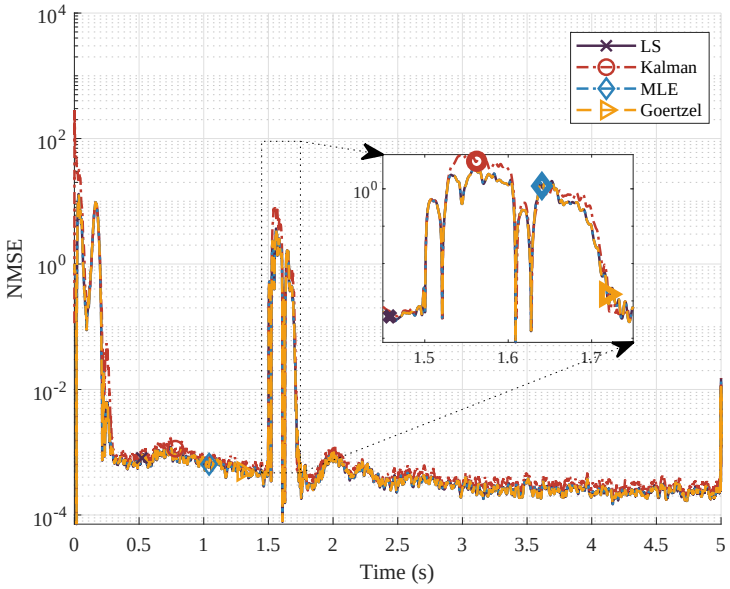

Figure 3.9 – NMSE vs Time (s) at SNR = 40 dB.

A corrupted sample with a no-valid value may assume a suitable average value to improve estimation. As a result, we have assumed two possible valid values in the analyzed scenarios in this work.

Assumption I: when a corrupted sample is interpreted as a null-zero amplitude.

Assumption II: when a corrupted sample takes the value from the last cycle mean amplitude.

3.4.5.1 Poisson Impulsive Noise

The missing/corrupted data measurements described previously in Case 1 to 4 is modeled as a Poisson impulsive process. A Poisson random process is a model for a series of discrete events where the average time between events is known, but the actual temporal occurrence of each event is random. Besides, the amplitude of such impulsive noise can be modelled as the negative amplitude of the signal, or as a high amplitude into the interval $[a_{\min}, a_{\max}]$, while the probability of occurrence of several p impulses into a time interval t_{iN} is given by

$$PS_N(p, t_{iN}) = \frac{[\lambda t_{iN}]^p}{p!} e^{-\lambda t_{iN}} \tag{3.51}$$

where λ is the average number of impulses per time unit. Hence, for the cases 1, 2, 3, and 4, the density $\lambda = \left[\frac{1}{768}, \frac{8}{768}, \frac{38}{768}, \frac{230}{768}\right]$ $\left[\frac{\text{impulse}}{\text{sample}}\right]$.

A Poisson impulsive noise can be obtained taking the derivative of the Poisson random process. Indeed, let n be the instant of time in the Poisson PS_N process. If the discrete-time random variable $PT_{iN}(n)$ describes a train of pulses occurring at random

and independent times, $PT_{iN}(n)$ can be constructed from the derivative of the Poisson random process PT_N as:

$$P_{iN}(n) = \frac{dP_N(n)}{dn} \tag{3.52}$$

The test results adopting *Assumption I* and *II* are depicted in Table 3.4. It is observed that NMSE for all cases is greater than the AWGN case when the first assumption for no-valid values is implemented. However, considering *Assumption II*, where a mean amplitude replaces the corrupted sample, the NMSE difference among AWGN and the four cases discussed is dramatically reduced. For the time interval between $1.5s$ and $1.7s$ such difference is notable for a higher number of distorted samples. This is expected because it assumes that the electrical power system only suffers from additive white noise in the previous evaluations. In the literature, there exist estimation algorithm adaptations to deal with non-Gaussian noise sources (ZHAO et al., 2019; CHEN et al., 2019; NWANKPA; SHAHIDEHPOUR, 1990); those algorithms present a better response under such scenarios but compromise processing performance while increasing substantially the computational complexity.

Table 3.4 – Average NMSE values for the Harmonic Estimators under Poisson impulsive noise

Algorithms	$1s \leq t_{iN} \leq 1.2s$					$1.5s \leq t_{iN} \leq 1.7s$				
	AWGN	Case 1	Case 2	Case 3	Case 4	AWGN	Case 1	Case 2	Case 3	Case 4
Assumption I – Corrupted sample replaced by null amplitude										
LS, MLE & Gtz.	0.0027	0.8641	14.5091	73.6173	404.8783	4.6091	4.6190	15.1908	81.5194	268.5128
Kalman	0.0040	1.5350	22.7900	132.0113	660.9734	10.0873	10.1070	27.3063	138.7219	423.3353
Assumption II – Corrupted sample replaced by an average amplitude value										
LS, MLE & Gtz.	0.0027	0.0353	0.6518	25.5618	29.2463	4.6091	4.6190	5.5078	6.0187	6.4647
Kalman	0.0040	0.0546	1.0465	53.688	62.3469	10.0873	10.1070	11.0872	12.0857	17.2456

3.4.6 Time-Delay using Correlation

In general, time delay in the estimation arises for all filtering harmonic estimation processes. Also, the time differences between the real (actual) current curve and the estimated curves are more noticeable when harmonic order increases; specifically, this power grid system application presents a decreasing amplitude for an increasing harmonic order; such a situation affects estimation under non-stationary conditions.

Variations in time delay cause signal distortion, which affects obtaining reliable measurements to achieve QoS requirements of the Smart μG. Table 3.5 brings the minimum requirements for Measurement Transfer Time (MTT). MTT refers to "end-to-end" delay, from occurrence to the PMU acquisition/processing, through communication, to final decoding of the frame/packet. As pointed out in the table, data frames must reach and be decoded in the central application within 16 ms of the power system event for the most critical scenario.

Table 3.5 – Delay/Quality Parameters (NASPI) (NASPI, 2017; NASPI, 2018).

Application	MTT(ms)	TW(sec)	MR (Reports/sec)
Voltage Stability	500	300	30
Frequency Stability	50	5	60
Long-term Stability	1000	600	30
State Estimation	1000	300	5
Small-Signal Stability	50	600	60
Disturbance Analysis	1000	N/A	60
Event Detection	**20**	300	60
FACTS Feedback	**16**	300	60
Out of step protection	**16**	5	60

MTT: measurement transfer time: maximum time from the event occurring on the power system for data reaches its final destination
TW: time window – Specific data ranges an application requires for proper operation.
MR: message rate – Specific reporting rates required by the application.

This work obtains the estimated delay by using the cross-correlation between each algorithm's input and output signal at a specified window. Then, it calculates the normalized cross-correlation between each pair of signals and obtains the negative of the lag for which the normalized cross-correlation has the most significant absolute value. Pairs of signals need not be exact delayed copies of each other. As a result, Table 3.6 presents the average time-delay for all algorithms, considering different estimation steps in the filtering harmonic estimation process. It is worth mentioning that this average value considers the overall algorithm iterations and the overall harmonic estimations of individuals' time delays. In this case, all values are above the minimum requirement, with Kalman filtering estimation as the minimum attained time-delay result. Furthermore, this time comprehends only the signal processing step; a more accurate statement must include communication latency from PMU unit to the data center.

Table 3.6 – Average Time-Delay (ms).

Parameter	LS	Kalman	MLE	Goertzel
Avg. Delay [ms]	12.5434	5.2517	12.5434	12.5434

3.4.7 Complexity-Performance Tradeoff

The computational complexity for those harmonics estimation (HE) methods based on the *number of floating point operations (FLOPs)* complexity is synthesized on Table 3.7 which describes the number of operations needed to execute an algorithm by sample. This does not consider any additional cost per operation but flops minimum counting, also equal weight operations; for all calculations, K is the total number of harmonic frequencies, and L is the windows sample size.

Table 3.7 – Computational Complexity for the HE Methods.

HE	**Complexity** (FLOPS)	
Method	**Domination**	**Total**
LS	$\mathcal{O}(LK^2)$	$\frac{8}{3}LK^2 + 2K(L+1) + 2L$
Kalman	$\mathcal{O}(K^3)$	$11K^3 + 3K^2 + 6K$
MLE	$\mathcal{O}(LK^2)$	$\frac{8}{3}LK^2 + 2K(L+1) + 2L$
Goertzel	$\mathcal{O}(LK)$	$K(3L+4)$
Tenti	$\mathcal{O}(L)$	$27L$

For an LS estimation with L samples and $2K$ variables to estimate, operations include a matrix multiplication of one $2K$xL matrix and one Lx$2K$ matrix, and two matrix multiplications of one Lx$2K$ matrix and one 1xL vector, considering also a matrix inversion regards a complexity $\mathcal{O}(LK^2)$ or $\mathcal{O}(K^3)$ whether $K > L$. Due to the final result on MLE algorithm complexity remains equal to LS.

KF with the advantage of sample-by-sample estimation stands on a complexity depending only in the $2K$ dimension and containing matrix multiplication only with order $2K$ with multiple $2K$ multiplications and 3 $2K$ additions, achieving a complexity $\mathcal{O}(K^3)$.

Tenti algorithm, or CPT, does not achieve the harmonic estimation status because it is not possible to obtain individual harmonics amplitude. In order to obtain the fundamental amplitude, it will include 14 multiplications/division and 13 additions/subtractions each of L size, a complexity $\mathcal{O}(L)$.

Goertzel estimation algorithm requires computing a set of K DFT terms using K applications of the Goertzel algorithm on a data set with L values has complexity $\mathcal{O}(LK)$. To compute a single DFT bin $X(f)$ for an input sequence of length L, the Goertzel algorithm requires L multiplications and $2L$ additions/subtractions within the loop, as well as 2 multiplications and 2 final additions/subtractions, for a total of $L+2$ multiplications and $2L+2$ additions/subtractions. This is repeated for each of the K frequencies.

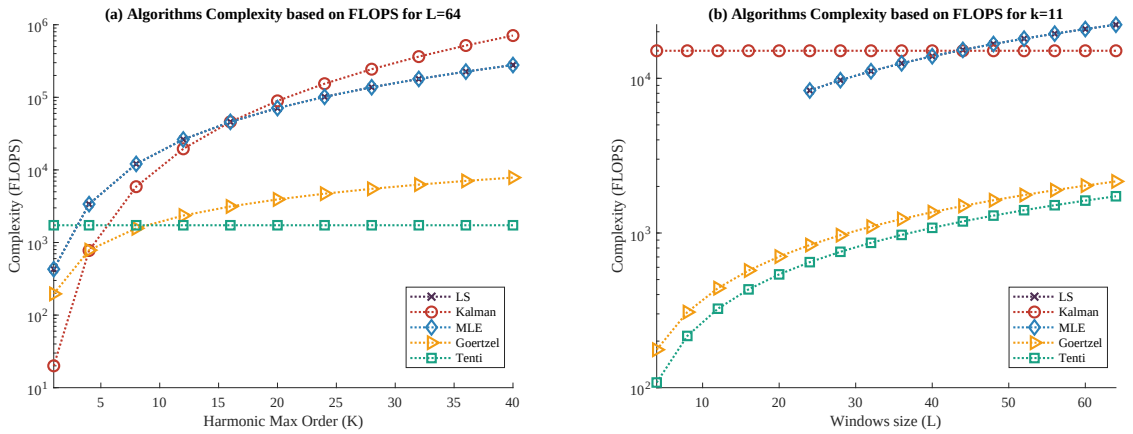

Figure 3.10 – Flops Complexity for the HE methods with respect to: a) harmonic order estimation and fixed window size $L = 64$; b) increasing window size $L \in 4;\ 64$ and fixed harmonic order $K = 11$.

Fig. 3.10.a) depicts the algorithm complexity (FLOPS) as a function of the number of harmonics estimation $K \in [2;\ 30]$, and considering a fixed $L = 64$ window size; while Fig. 3.10.b) exhibits algorithm complexity for a fixed number of harmonic order $K = 11$ and increasing window size $L \in [4;\ 64]$.

When $L \leq 2K$ LS and MLE methods expend more time to converge with no possible solution found. This represents a limitation for legacy sensors with a low sampling rate. On the other hand, KF without windows size dependency delivers a better harmonic estimation performance-complexity tradeoff. Goertzel filter brings lower complexity than other implemented algorithms, achieving the best performance for this section benchmark. In the considered filtering application, KF represents an advantage over the other methods with a good estimation and better performance-complexity tradeoff. Indeed, due to the much lower effort in different K and L arrangements, such tradeoff indicates that the Kalman filtering method constitutes the great harmonic estimation technique for SG and μSG power quality applications. Notice that Tenti appears only as a reference; this method does not estimate individual harmonic amplitudes.

3.5 Conclusions

Estimation filters introduce a delay that may affect minimum requirements for SG monitoring and control systems. In this work, a more comprehensive numerical comparison framework has been carried out to determine the best harmonic estimation algorithm. Hence, the effectiveness and efficiency of the applied estimation algorithms have been investigated considering three different aspects: amplitude error estimation, time-delay introduction, and computational complexity. The five harmonic estimation strategies analyzed have presented a significant performance in single and multiple amplitude harmonic estimations under stationary conditions and Gaussian noise. However, figures of merit, such as NMSE, have been degraded under non-gaussian noise. Moreover, all estimators considered have presented a significant error on the amplitude estimation under fault conditions, leaving the algorithm choice to a performance-complexity tradeoff.

On the other hand, the SG scenarios imply a bunch of data processing which requires efficient signal processing algorithms implying low complexity and improved performance. Under such conditions and scenarios, KF demonstrated to be slightly superior. Thus, the Kalman harmonic estimator has been demonstrated to be both flexible and practical, providing an accurate evaluation of the intelligent μG under a wide variety of operation conditions, from fault to normal, from Gaussian and non-Gaussian noise operation.

4 Quality of Services and Random Access Protocols

This chapter deals with the reliability of random access (RA) protocols for wireless m-SGC. We propose and analyze an improved grant-free RA (GF-RA) protocol for critical SG applications under strict QoS m-SGC requirements. At first, we discuss the main features of the SG NAN architecture. We explore the main features of low-rate machine-type wireless networks, and also we describe a technology characterization of Wireless Neighborhood Area Networks (WNANs) in medium-range coverage applications. We propose a new-improved irregular repetition slotted ALOHA, combing Raptor codes and irregular ALOHA, namely RapIRSA random access protocol, to better respond to critical high-reliability QoS requirements under a 5G network perspective. Then, we compare and comprehensively analyze the proposed RapIRSA protocol with two existing RA protocols, the IRSA protocol, and the classical Slotted ALOHA. Finally, We summarize the potential challenges in implementing the proposed RA protocol for SG critical applications considering a massive number of SS.

4.1 Quality of Services, Smart Grid, and Communication

Most of the modern SG QoS models arrange a mapping method with an electrical-telecommunication design. The industry application experience and electrical engineering decisions rarely foresaw SG service requirements.

Wireless communications represent a challenge to SG implementation as many mission-critical applications require real-time data transfer. Maintaining delay and reliability SG requirements over wireless shared network disputes with the possibility to extend the number of sensor devices in a wireless network (KHALID; SHOBOLE, 2021). Also, Wireless communications bring several security concerns for SG; (KHALID; SHOBOLE, 2021) explores techniques to improve the robustness of wireless mesh networks for mission-critical applications. As SG states as a cyber-physical grid with IoT and 5G data acquisition integration multiple access emerges as trending research (SHAHINZADEH et al., 2020).

A *grant-based* (GB) scheduling operation guarantees that a user has restricted resources to the wireless channel, consequently circumventing unspecified collisions increasing latency and communication overhead (LIU et al., 2021). On the other hand, *grant-free* (GF) based RA protocols represent a solution to decrease the access latency (BERARDINELLI et al., 2018). GF-based protocols use transmission over shared resources if

multiple neighboring users transmit simultaneously. Oversharing creates potential collisions that jeopardize transmission reliability. Currently, academic research and standardization commissions have proposed approaches to enhance the backed traffic loading with GF RA schemes while guaranteeing high reliability and low latency (RECAYTE et al., 2020).

Several ALOHA-like schemes use Successive interference cancellation (SIC) techniques to resolve multiple collided packets (LIVA, 2011; OINAGA et al., 2020; HUANG et al., 2021). A certain number of time-slots compose the slotted-ALOHA (S-ALOHA) temporal frame where the user transmits a predefined number of times. IRSA optimizes the probability mass function to maximize the peak throughput performance. IRSA performance proves better than S-ALOHA and contention resolution diversity slotted ALOHA (CRDSA) (LIVA, 2011; MUNARI; FROLOV, 2020; MOROGLU et al., 2020; SAHA et al., 2021). Furthermore, the adjustment of the number of time-slots relies on the BS since transmission reaching nominal throughput. Thus, the proper time-frame length avoids decay in the throughput performance.

Contributions. The focus of this chapter is to analyze the influence of GF-RA protocols in achieving QoS m-SGC requirements and propose a RA protocol for critical SG applications considering a massive number of SS. The main *contributions* are threefold: *i*) propose an improved Raptor Code IRSA-based RA grant-free protocol to better adapt to critical high-reliability QoS requirements under a 5G networks perspective; *ii*) propose and comprehensively characterize modifications to suit RA protocols, depending on existing applications and number of devices in SG applications; *iii*) explore the main SG critical application while characterizing the QoS requirements in SGC systems.

The remainder of the chapter is divided into following sections: The m-SGC schemes and applications are revisited in Section 4.2 . Section 4.3 introduces metrics for QoS for smart grid systems. Random Access protocols suitable for m-SGC systems are considered in Section 4.4. Section 4.5 introduces the proposed RA protocol. Extensive numerical results are explored in Section 4.6. Section 4.7 draw the main conclusions and future trends.

4.2 m-SGC Architecture and Applications

SS and SG applications rely on IoT and low-power wide-area network (LPWAN) (SALEEM et al., 2019; CHAUDHARI; ZENNARO, 2020; KAVEH; MOSAVI, 2020). It performs a significant part in accomplishing the active and changing requirements of applications and services while implementing a framework for allowing powerful and dynamic solutions. Smart Utility Network (SUN) targets multiple applications within shared networks (Jinho Choi et al., 2016). For a utility, this implies performing monitoring and control over the same resources. SUN devices provide wide-long-range point-to-point connections including a large number of outdoor devices. SUN aims low-power wireless

applications that usually demand the maximum transmit power available under proper administration.

SUN application requirements demand a peer-to-peer topology (SOCIETY, 2020). In a star topology, devices establish communications with a single central controller, named the NAN coordinator. Each device with an identified application performs full-duplex communications. The NAN coordinator controls the entire NAN. Also, every device has a single address notwithstanding the network topology. On the contrary, a *peer-to-peer* network considers routing messages among and through any device.

Most of the delay allowances discussed in this work are a compilation of the requirements specified in previous works (IEEE, 2005; CHAN et al., 2006; ITU, 2003; ITU, 2014; HU et al., 2010). In (DESHPANDE et al., 2011), there is a quantitative characterization of priorities for SG applications based on these standard and recommendation documents, and pragmatic needs for utility. Note that Table 4.1 includes the priority of an application relative to others.

Table 4.1 – Latency & Priority by SG application type.

Application type	**Latency (ms)**	**Priority 0-max 100-min**
Teleprotection (60 Hz, 50 Hz)	8,10	10
SCADA Transmission	10	20
Teleprotection	16	15
Synchrophasors	20	12
SCADA Distribution	100	25
Distribution automation	100	26
Distributed generation - distributed storage	100	27
MWF	100	30
Business voice	200	60
Dynamic Line Rating	200	28
CCTV	200	55
SCADA, DA, DG/DS, DLR	200	45
Business data	250	70
AMI	250	40
Protection	500	80
Many/others	2000	100

This table shows only higher priority application by application type (non-exhaustive)

Delay allowances listed in Table 4.1 are end-to-end Uplink delays.

4.3 Metrics and Definitions in SG QoS

From the power system perspective, the latency requirement depends on the cycle of the electrical utility cycle ($T = 1/f$) to keep the stable stage of a wave. Data latency

is the time between a specific state occurrence and acts upon an application (KANSAL; BOSE, 2012). The total delay on the communication network comprises propagation delays, transmission delays, queuing delays, and processing delays. Primarily, *latency* (L) represented by:

$$L = \tau \frac{1}{f} \tag{4.1}$$

where τ is the delay factor (in cycles). Real-time scale SG network consider short/small values of τ.

We define in the following the QoS metrics RA-related to SG applications: throughput, the latency of message, Packet Delivery Rate (PDR) reliability, and critical latency response.

4.3.1 Latency in SG Message

This work focuses on applications with communication latency performance as a priority and do not accept outdated data. Thus, we define the hard delay metric in the subsequent outlines.

Definition 1. ***(Hard delay, HD)*** *Application with a hard delay requirement turns useless if its delay passes the QoS requirement even in successful message delivery.*

Next, the delay requirement τ_{req} includes the required network bandwidth as:

$$BW_{\text{req}} = S \left(8 \frac{\text{bits}}{\text{byte}}\right) \frac{1}{\tau_{\text{req}}} M \qquad [bits \cdot Hz] \tag{4.2}$$

where S and M are the service's data size in bytes, and the number of users, respectively.

4.3.2 Packet Delivery Rate (PDR) and Packet Loss Rate (PLR)

Definition 2. ***(Packet delivery rate, PDR)*** *represents the proportion of the total number of packets received by the Data Collector Unit (DCU) successfully, P_R, to the total number of packets generated by the SG source nodes, P_G:*

$$PDR = \frac{\sum_{i=1}^{M} P_{R_i}}{\sum_{i=1}^{M} P_{G_i}} = \frac{P_R}{P_G} \tag{4.3}$$

Definition 3. ***Packet Loss Rate (PLR)*** *is a matched metric to the PDR defined as the probability for a user incorrectly decoded at the receiver after accessed the channel. Using eq. (4.3) one can obtain an approximate expression for PLR:*

$$PLR = 1 - PDR = 1 - \frac{P_R}{P_G} \tag{4.4}$$

4.3.3 Reliability

A conventional reliability definition in computer systems delivers SG network reliability metric (SAHNER et al., 1996). Network reliability counts the probability of a system achieving its services accordingly in specified time duration. Accordingly, we define the *reliability factor* in the SG network context as:

Definition 4. ***(Reliability, $\mathcal{R}$)*** *The network reliability stands as the probability of succeeding in delivering a message to the destinations node (related to the PDR metric) within the delay requirement. The reliability decreases when the message arrives after the delay requirement.*

SG network reliability under HD definition, $\tau_{\mathrm{HD_{req}}}$ can be defined as follows.

$$\mathcal{R}(\tau) = \begin{cases} PDR & \tau \leq \tau_{\mathrm{HD_{req}}} \\ 0 & \tau > \tau_{\mathrm{HD_{req}}} \end{cases} \tag{4.5}$$

We introduce a new concept named application complying rate (ACR) that represents the number of users to comply successfully with the UL connection within delay requirements $\tau_{\mathrm{HD_{req}}}$. In the context of SG applications, the ACR reliability can be defined as:

$$\mathcal{R}_{\mathrm{ACR}} = \frac{1}{N} \sum_{k=1}^{N} \frac{m_{\tau_k}}{m_k} \tag{4.6}$$

Such reliability metric quantifies the proportion of active users who succeed in sending a packet m_{τ_k} in each slot k within the latency requirement time τ_{req_i} during N slots; m_k is the number of total active users in each slot.

In eq. (4.6), the QoS metric divert from the communication perspective as allows to track specific application problems. In this sense, this network reliability metric quantifies, under the specified protocol, trusted data delivery.

4.4 RA Protocols for Required QoS in m-SGC Networks

For RA protocol applied to m-SGC networks, in this section, we define suitable network scenarios in the following. We consider a cellular-based single-cell system with M total users connected to the BS, where m users are active at any time occurrence t. Furthermore, a Beta or a Poisson distribution determined the distribution of the active users m (see Section 4.4.2).

4.4.1 ALOHA-based Classical RA Protocol for SG systems

ALOHA-based protocols are among the RA protocols group of high-reliability and high-throughput applications (BERIOLI et al., 2016). This work concentrates on extensions of the ALOHA model, holding terminals send a slotted packet over the channel as quickly as it is produced and without performing distributed coordination strategies.

In the sequence, we define the premises for evaluating the performance of the implemented/developed RA protocols in terms of two metrics. The first metric, *throughput* (S), summarizes the average amount of data blocks accomplished at the receiver over a reference period. The second one operates as a complementary metric, namely the *packet loss rate* (PLR), eq. (4.4).

Slotted ALOHA. Fig. 4.1 depicts a sketch of the slotted ALOHA and the IRSA RA protocols. n slots lasting T_F seconds build a frame F. The total active users is m. Each MAC frames of a duration of T_F, composed of n slots of duration $t_s = T_F/n$. Let's consider that in every MAC frame a measurable number (m) of users try a packet transmission. In each MAC frame, an m user performs a unique transmission associated with a new packet or the retransmission of a previous collided.

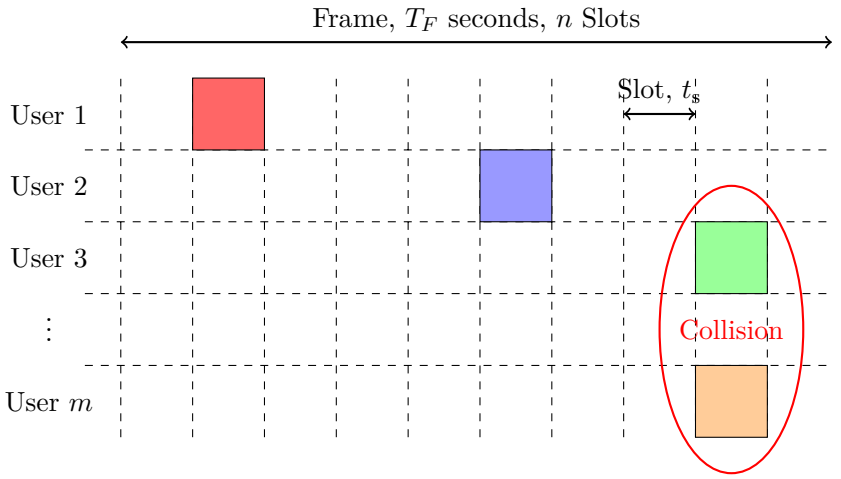

a) S-ALOHA protocol

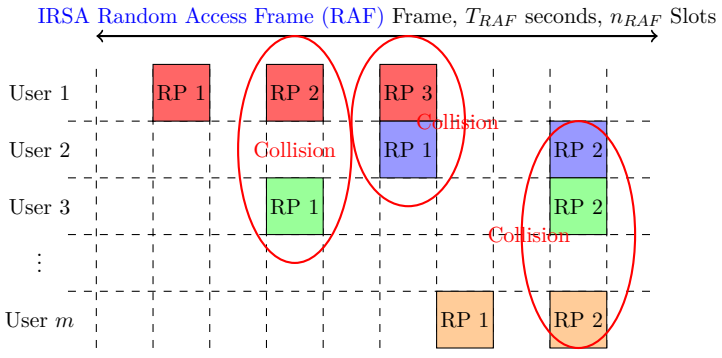

b) IRSA protocol

Figure 4.1 – Sketch of a) S-ALOHA; b) IRSA protocols as presented by (LIVA, 2011)

The *normalized offered traffic* (or channel load) follows by:

$$G = \frac{m}{n} \qquad \left[\frac{\text{packet}}{\text{slot}}\right] \tag{4.7}$$

Therefore, the normalized throughput (or channel output) S is characterized as the probability of successful packet transmission per slot, where n is the number of slots transmitted in T_F seconds. Fig. 4.1 (a) presents an S-ALOHA frame with individual packet transmission by MAC frame. Collisions drive retransmissions in the subsequent frame. Hence, the throughput for the S-ALOHA protocol can be defined as a function of normalized offered traffic (LIVA, 2011):

$$S(G) = G \cdot e^{-G} \tag{4.8}$$

where the peak throughput is attained at $S(1) = e^{-1} \approx 0.37$.

IRSA Protocol in Fig. 4.1.b) relies on the repetition of each packet access strategy by MAC frame. Each packet is transmitted d times in a MAC frame. The repetition rate d ranges from packet-to-packet based on a statistical distribution. Hence, we define the *user sampling degree distribution* by:

$$\Lambda(x) = \sum_{d=1}^{d_{\text{m}}} \Lambda_{\text{d}} x^d, \quad \text{with} \quad \sum_{d=1}^{d_{\text{m}}} \Lambda_{\text{d}} = 1 \tag{4.9}$$

where $0 \leq \Lambda \leq 1$ and each transmitter independently sends the replicas within the n time slots composing the MAC frame. Random transmission slots contain a maximum of d_{m} replicas sent.

Each packet contains a header with an index with the location of its copy. After receiving a packet successfully, the BS extracts the index identifying the replica positions. When packet replicas collide, they are extracted from the signal received in the corresponding slot removing the interference contribution. This procedure allows decoding packets transmitted in the same slot.

4.4.2 Traffic Model, Time Arrival, and Time Instance

MTC traffic patterns differ from those for H2H traffic. Better traffic models prompt better management of shared network resources and guarantee QoS for many types of devices. 3GPP proposes a simple Poisson process to model different kinds of network access coordinated or uncoordinated machine-to-machine (M2M) traffic (SUNITA; Bharathi Malakreddy, 2019). Consequently, different arrival rate λ dynamically depends on the channel and system scenarios. 5G system scenarios are compiled in (NAVARRO-ORTIZ et al., 2020).

3GPP Specification number 37.868 define M2M traffic types, including a load analysis for SM, fleet management, and earthquake monitoring applications. The document

embraces a SM service with metering data reports, in fixed time intervals, and the load control and alarm events occurring randomly, being modeled by Poisson processes. Table 4.2 compiles the two traffic models.

Table 4.2 – 3GPP traffic models for MTC proposed in the 3GPP TR 37.868 document.

Parameter	**Statistical Characterization**
	Traffic model 1
Number of MTC devices	$M \in \{1000, 3000, 5000, 10000, 30000\}$
Arrival distribution	Uniform distribution over $T_{\mathrm{A}} = 60$s
pk_s	200 bytes
	Traffic model 2
Number of MTC devices	$M \in \{1000, 3000, 5000, 10000, 30000\}$
Arrival distribution	Beta distribution over $T_{\mathrm{A}} = 10$s
pk_s	200 bytes

Then IRSA protocol design in (LIVA, 2011) considers Poisson traffic, *i.e.*, constant mean arrival even in SS applications with a disrupted appearance. On the other hand, the traffic model in (GURSU et al., 2019b) considers the Beta distribution that implicitly requires a time-varying mean parameter. Hence, the arrival distribution of the M_v active users in SG applications can be modelled by a Poisson or a Beta distributions (GURSU et al., 2019b; GURSU et al., 2019a).

Typical but different behaviour in terms of number of user activation is found considering Poisson and Beta distribution, Fig. 4.2.

After star, an IRSA-frame does not permit seeking users. Each late-activated user must wait for a full-frame duration T_F. Existence of a waiting time T_W within two IRSA-frames relies on latency limitations. Indeed the worst-case scenario implies a user decoded following the expiration of the IRSA frame.

Hereafter, the maximum latency Δ_{x_i} of the user i can be separated as

$$\Delta_{x_i} = T_W + 2T_F = T_{\mathrm{Ac}} + T_F \leq \Delta_{\mathrm{X}} \tag{4.10}$$

A user's maximum latency should not exceed the latency constraint Δ_{X}. This scheme implies the accumulation of all users activated between IRSA frames.

4.4.3 Successive Interference Cancellation (SIC)

The scenarios involving M2M communications with smart sensors call for new ideas of RA schemes. The adoption of simple SIC techniques makes it feasible to deliver throughput enhancements in RA-based communication systems (MENGALI et al., 2018). Following a MAC frame receiving and buffering, the receiver looks for *Singleton slots*; slots with interference-free packets.

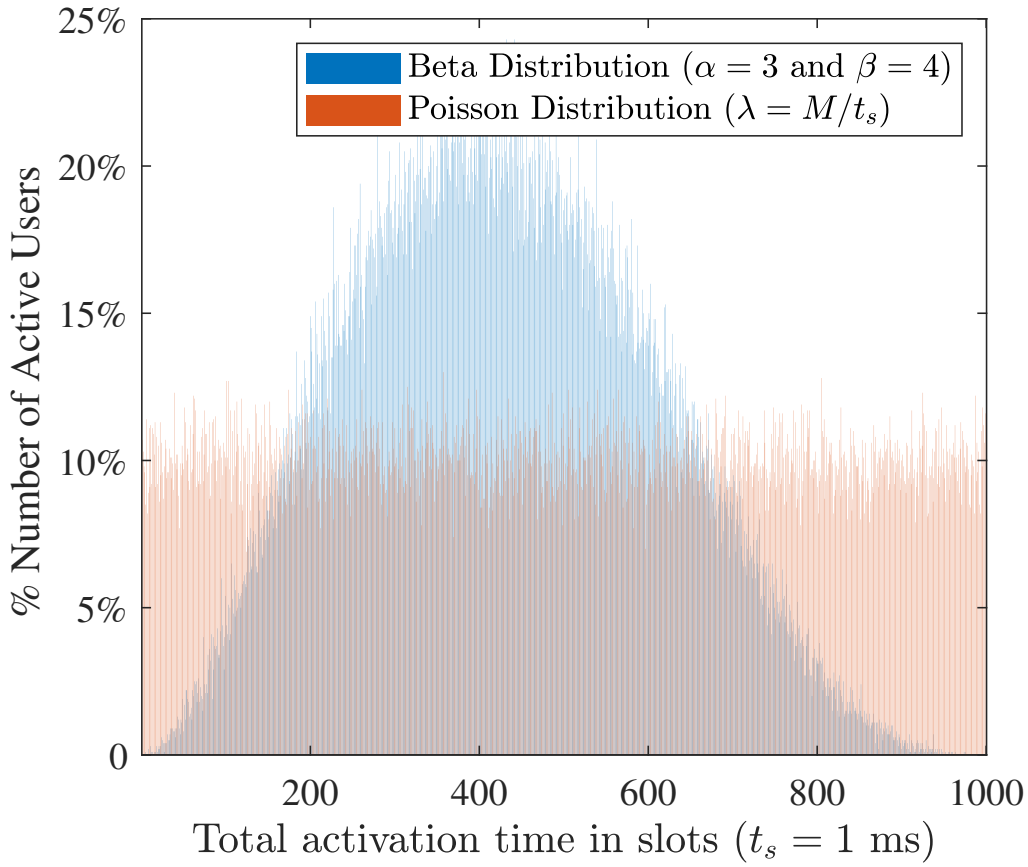

Figure 4.2 – Users arrival in a Frame F with n time-slots considering Poisson $\times$ Beta distribution and $M = 100$ devices.

A graphical model describes the iterative SIC process (BERIOLI et al., 2016), depicting the MAC frame standing through a bipartite graph $\mathcal{G} = (\mathcal{U}, \mathcal{S}, \mathcal{E})$ composed by three sets:

$\mathcal{U}$ $= \{U_1, U_2, \ldots, U_m\}$ of m *user nodes* (UNs);

$\mathcal{S}$ $= \{S_1, S_2, \ldots, S_n\}$ of n *slot nodes* (SNs);

$\mathcal{E}$ $=$ *set of edges.*

The UN U_i connects to the slot number (SN) S_j by an edge conditioned to the copy of the ith packet of the ith user is transmitted in the jth slot. Fig. 4.3 depicts the graph illustration of a MAC frame with $n = 5$ slots and $m = 4$ users attempting a transmission. Notice that there is a 2-gather for users 1, 2, and 4, while user 3 packets repeates three times. One *singleton slot* for received frame. A particular slot node has degree d if it is adjacent to d edges; for instance, in the example of Fig. 4.3, S_1 has degree $d = 2$, and that S_2 has degree $d = 1$.

To model the SIC process through a graph, some simple rules are applied. Iteratively, we search for SNs with degree $d = 1$. Estimate S_i to have degree 1, and indicate by U_j its

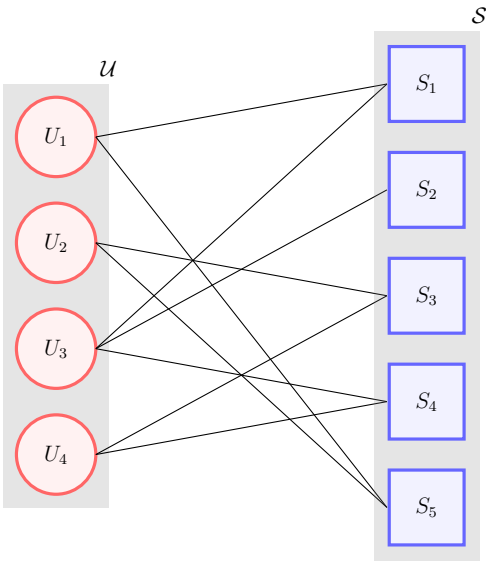

Figure 4.3 – Bipartite graph for a MAC frame with $n = 5$ slots and $m = 4$ users attempting a transmission

only neighbor. Hence, we exclude the edges connected to S_i and U_j; equal to exclude the interference addition on the packet of user j in each transmitted slot. The SIC process repeats on the up-to-date graph. Following these rules, the SIC process to improve IRSA protocol of example of Fig. 4.3 is sketched in steps of graph model in Fig. 4.4.

The fundamental concept of SIC is decoding users' signal (devices) successively. After decoding one user, its signal is pushed away from the total received signal before decoding the subsequent user's signal. In this work, we use the advantage of a singleton where at least one device is free of interference.SIC implementation represents an advantage compared to conventional decoding process, which treats other interfering users' signal as noise.

4.4.4 Time-domain Structure

The parameters of SG system considered herein are based on the 5G NR standard (DAHLMAN et al., 2018). Time-domain NR transmissions enter into 10 ms length frames. Each frame contains 10 equally sized subframes of duratio n 1 ms. Subcarrier-Spacing (ScS) establish the bandwidth of each frame (BW_{F}) and the number of slots in a subframe. With slot-based scheduling, a slot is a minimum measure with a duration of t_{s} seconds. This work does not use a symbol level scheduling.

4.5 Proposed RA Protocol for m-SGC Networks

In this section we propose a new RA protocol aiming to achieve higher throughput under overloaded networks using additional nodes working as precoding of Raptor codes.

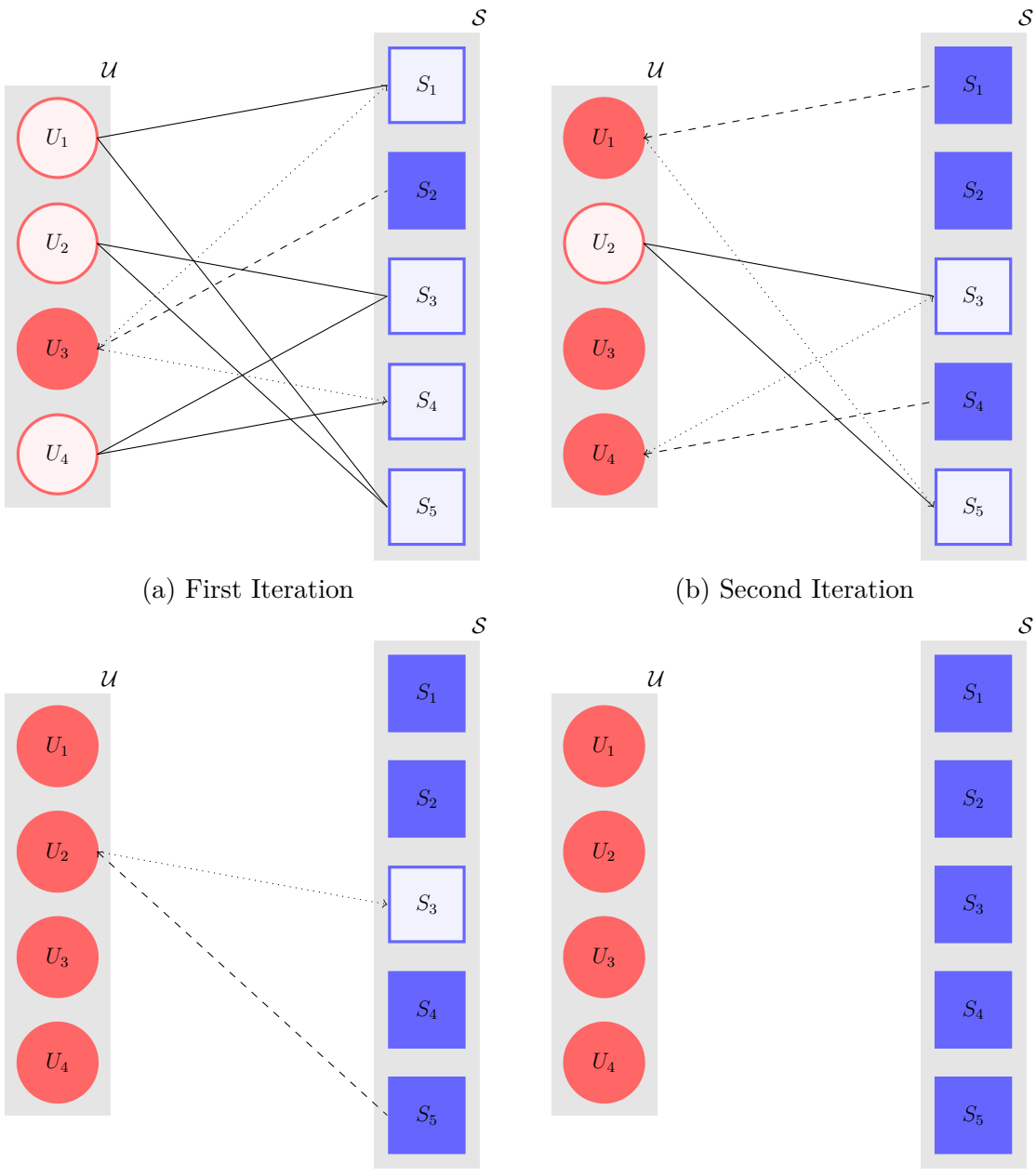

(a) First Iteration

(b) Second Iteration

(c) Third Iteration

(d) Last Iteration

Figure 4.4 – SIC decoding for the collision pattern of Fig. 4.3, tracked over the corresponding graph.

This Raptor code implementation uses a subclass of the bipartite graph described in (RAMATRYANA; ANWAR, 2017; SHOKROLLAHI, 2006).

Considering SG scenarios, we propose a modification in the traditional IRSA protocol, mainly in the values of the operational parameters and in the substructure of the protocol, depending on the application requirements, and aiming at enhancing the ALOHA for URLLC and MTC services. We label QoS information into active users preamble. This information adjusts the IRSA protocol to achieve QoS requirements.

4.5.1 Combining Raptor Codes and IRSA (RapIRSA)

We consider m active users sending packets to BS or DCU. Some users will send packets via *connecting nodes* ($c\mathcal{N}$). All $c\mathcal{N}$ are placed equitably reaching many possible directly visible users. Each $c\mathcal{N}$ uses the Decode-and-Forward (DF) protocol to deliver the information to the BS. $c\mathcal{N}$ has less probability of packet collisions compared to BS because $c\mathcal{N}$ only received packets of data from connected users.

Fig. 4.5 illustrates the Raptor codes-structured (RapC) wireless networks. This follows a bipartite graph model illustrated in Fig. 4.3. Besides, $c\mathcal{N}$ represented by dark circles in a separated time slot; m represents the number of active users, n_{RapC} is the SN in the frame, and $q = \lfloor \eta \cdot n_{\text{RAF}} \rfloor$ is the number of $c\mathcal{N}$. Besides, n_{RapC} contain two elements, as n_{RAF} for SN of RAF, and n_q for SN of $c\mathcal{N}$s. Hence, the total SN is defined as:

$$n_{\text{RapC}} = n_{\text{RAF}} + n_q \tag{4.11}$$

The normalized offered traffic G follows Eq. (4.7).

In the example of Fig. 4.5, five users $\mathcal{U} = \{U_1, U_2, \ldots, U_5\}$ and two $c\mathcal{N} = \{c\mathcal{N}_1, c\mathcal{N}_2\}$ have been considered. Connecting nodes $c\mathcal{N}$ do not have prior information about users' messages. After receiving data from neighboring devices they decode-and-forward (DF) the messages to the BS for final processing. $c\mathcal{N}_1$ decodes one packet from U_1 and U_5, and then forward the first decoded packet to the BS. Likewise, $c\mathcal{N}_2$ receives packets from U_2 and U_3, it decodes one packet, and then forward the decoded packets to BS. Fig. 4.5 represents RapC with $\eta = \frac{1}{7}$ and $q = 2$.

The pseudo-code for the adopted graph-based decoding algorithm is described in the Algorithm 1. Moreover, Fig. 4.6 depicts an additional graph from BS $\mathcal{G}_{\text{BS}}$ and two $c\mathcal{N}$s ($\mathcal{G}_{c\mathcal{N}_1}$ and $\mathcal{G}_{c\mathcal{N}_2}$) seen by DCU.

Fig. 4.7 depicts the time-slot structure including the RAF implemented in the IRSA protocol and the slots with information from the $c\mathcal{N}$s. BS will use pre-coding through $c\mathcal{N}$s to detect failing nodes during the contention period. As discussed in the numerical results, Section 4.6, the RapIRSA protocol is able to improve throughput performance substantially although the overloaded network configurations.

SP-IRSA & SP-RapIRSA. Service Priority-based Irregular Repetition Slotted ALOHA (SP-IRSA) and Service Priority-based Raptor Code Irregular Repetition Slotted ALOHA

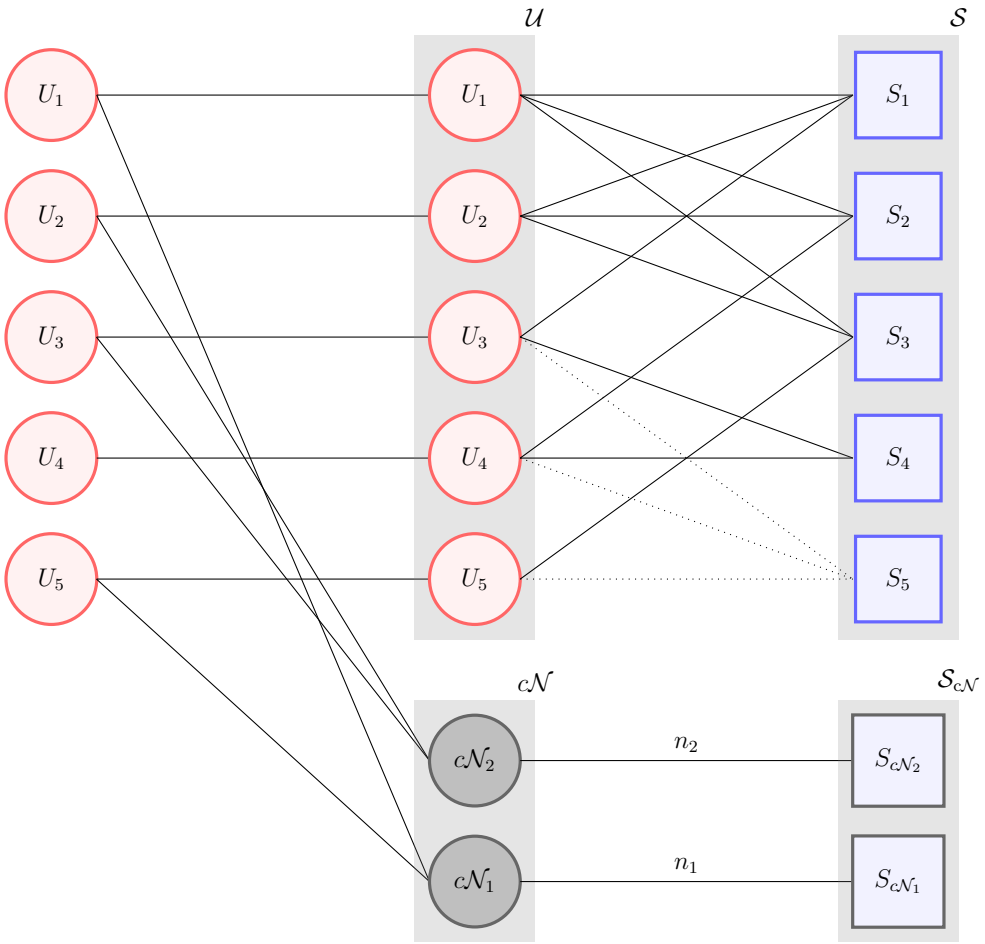

Figure 4.5 – Raptor codes-structured wireless networks

Algorithm 1: Network Decoding with RapC

Data: Connected bipartite graphs $\mathcal{G}_{\text{BS}}$ and $\mathcal{G}_{c\mathcal{N}_j}$.
Result: Information from each m decoded.
for $j = 1$ *until* q **do**
  Loop Passive Nodes $\mathcal{G}_{c\mathcal{N}_j}$**:** Analyze $\mathcal{G}_{c\mathcal{N}_j}$ and access user U_i connected to a slot node having degree $d = 1$; **if** *degree* $d = 1$ **then**
    Obtain information of U_i ;
    Deduct the collected signals in all slot nodes correlated to user U_i with user U_i's information at graph $\mathcal{G}_{c\mathcal{N}_j}$;
    Send information of U_i via $S_{c\mathcal{N}_j}$ and deduct all slot nodes correlated to user U_i at graph $\mathcal{G}_{\text{BS}}$;
  end
end
Loop BS $\mathcal{G}_{\text{BS}}$**:** Implement SIC decoding algorithm as describe in Section 4.4.3;

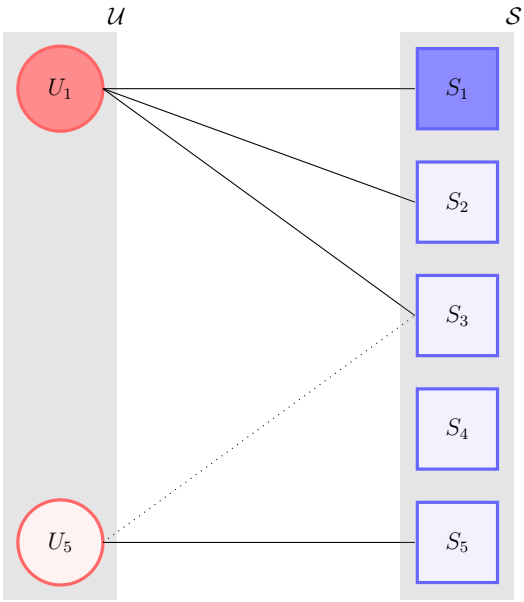

(a) Graph view from $c\mathcal{N}_1$

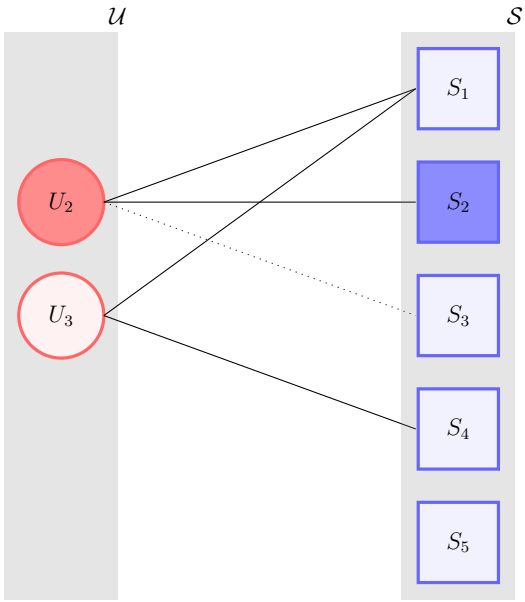

(b) Graph view from $c\mathcal{N}_2$

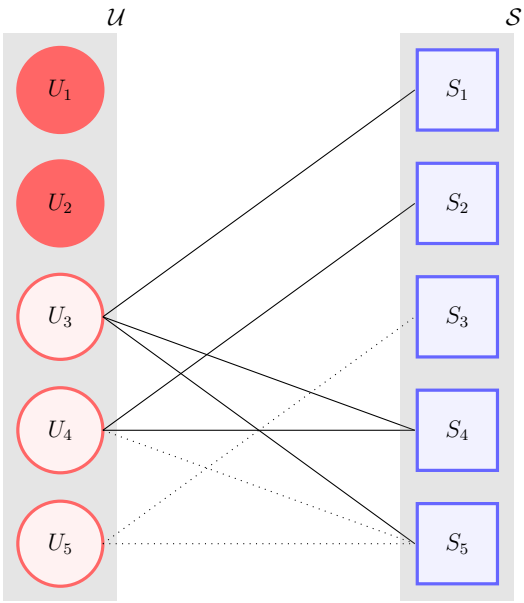

(c) Graph view from BS

Figure 4.6 – Bipartite graphs-based message decoding received from the main links $\mathcal{G}_M$, connecting node $c\mathcal{N}_1$, and $c\mathcal{N}_2$.

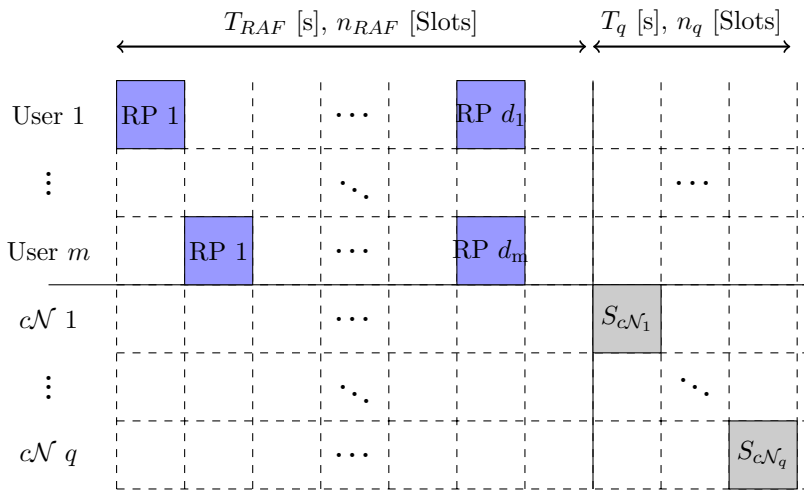

Figure 4.7 – Overview of RapIRSA time-slots structure

(SP-RapIRSA) protocols employ additional preamble information to denote the number of packets in the channel, thus the high priority services have higher repetition probability. Such approach based on service priority does not consider the access probabilities adjusted according to the traffic load as Irregular Repetition Slotted ALOHA with Priority (P-IRSA) (SUN et al., 2016), which requires a further access controller. SP-IRSA protocol arranges m users into P_L different priority levels based on service-defined priority. Each user carrier services ID to determine whether repetition rate changes according to priority. The categorical priority level vector $\vec{p}_L$ increases (or decreases) the repetition probability of Λ_{d}. With a finite number of SG applications, the level P_L of each service modifies the maximum of d_{m} replicas a user m could send. Consequently, a user with a higher-level priority sends more replicas of its packet.

SP-S-ALOHA. Following the SP-IRSA description, we have implemented the same Service Priority-based on the S-ALOHA algorithm, namely SP-S-ALOHA. In this case, the service priority modifies the backoff maximum value in the user connection. Whether if the backlogged active users no comply in the attempt, the QoS system counts as an error, *i.e.*, in the worst-case scenario where backoff value is close to the maximum service priority, the user only will have an attempt to complete the uplink connection.

4.6 Numerical Results

In this section, we present the simulation results of the proposed service priority RA algorithms based on S-ALOHA, IRSA, and RapIRSA protocols. The simulation process directly follows the SG RA protocols revisited in Section 4.4, as well as the proposed RA algorithms for m-SGC networks described in Section 4.5. All the simulations uses the MATLAB and JULIA programming languages over a Intel Xeon Gold 5118 with 64 GB of Memory RAM. The main parameters values adopted in numerical simulations are

summarized in Table 4.3.

We consider a future AMI scenario of SG networks, considering an urban area with up to 10^6 SM uniformly distributed in a 1×1 km service area. The coordinator node is center-located, and the $c\mathcal{N}$s, corresponding to the RapIRSA protocols, are located to access as many as possible different devices.

Table 4.3 – Simulation Parameters

Parameter	**Value**
Service Area	$A = 1\text{km}^2$
# m Users	Up to $M = 10^6$ devices
Active Users distribution	Poisson & Beta
Time-slot duration	1 ms
IRSA RAF Length	$n_{\text{RAF}} = 50$ *slots*
# Replicas (Max.)	$d_{\text{m}} = 8$
Degree distribution	$\Lambda_8(x) = 0.5x^2 + 0.28x^3 + 0.22x^8$
# SIC iterations (Max.)	$\mathcal{I} = 20$
S-ALOHA Back-off limit	$B_{\text{off}} = 50$ *slots*
number of $c\mathcal{N}$	$q = [2 \quad 3 \quad 8]$
fraction of n_{RapC}	$\eta = 0.25$
# SP m Users	Up to $M = 10^4$ devices
Priority Level	$\vec{p}_L = [0(\text{max}) \quad 100(\text{min})]$
# Realizations	100
Simulation time	10 s

Fig. 4.8 depicts the throughput for S-ALOHA (SA), IRSA, RapIRSA$(0.25, 8)$, and RapIRSA$(0.25, 2)$ implementations for two different users' arrival distributions. This simulation includes the theoretical throughput for S-ALOHA algorithm considering the Poisson distribution and an asymptotic ($n_{\text{RAF}} \to \infty$) representation of the IRSA protocol. Note that RapIRSA improved throughput not only for $G > 1$ but its performance is also comparable with the asymptotic IRSA with the Poisson distribution. It's worth mentioning, RapIRSA for $G > 1.4$ present a better throughput under traffic governed by a Beta distribution. In our specific scenario, this finding represents a breakthrough to determine that the RapIRSA protocol attains better performance.

Accordingly, Fig. 4.9 depicts the packet loss rate versus the network load. Under low and moderate-to-high network loading condition, *i.e.*, $0 < G < 1.2$ (Poisson distribution) and $0 < G < 0.6$ (Beta distribution), those values indicate a considerable advantage from IRSA and RapIRSA over S-ALOHA protocol, considering both arrival distributions.

4.6.1 Latency

When we first introduced Fig. 4.7 the extra slots n_q for each frame in the RapIRSA protocol, it creates concern about increasing latency. As delay constraints are fundamental to achieve QoS requirements, an additional evaluation of these parameters is presented in

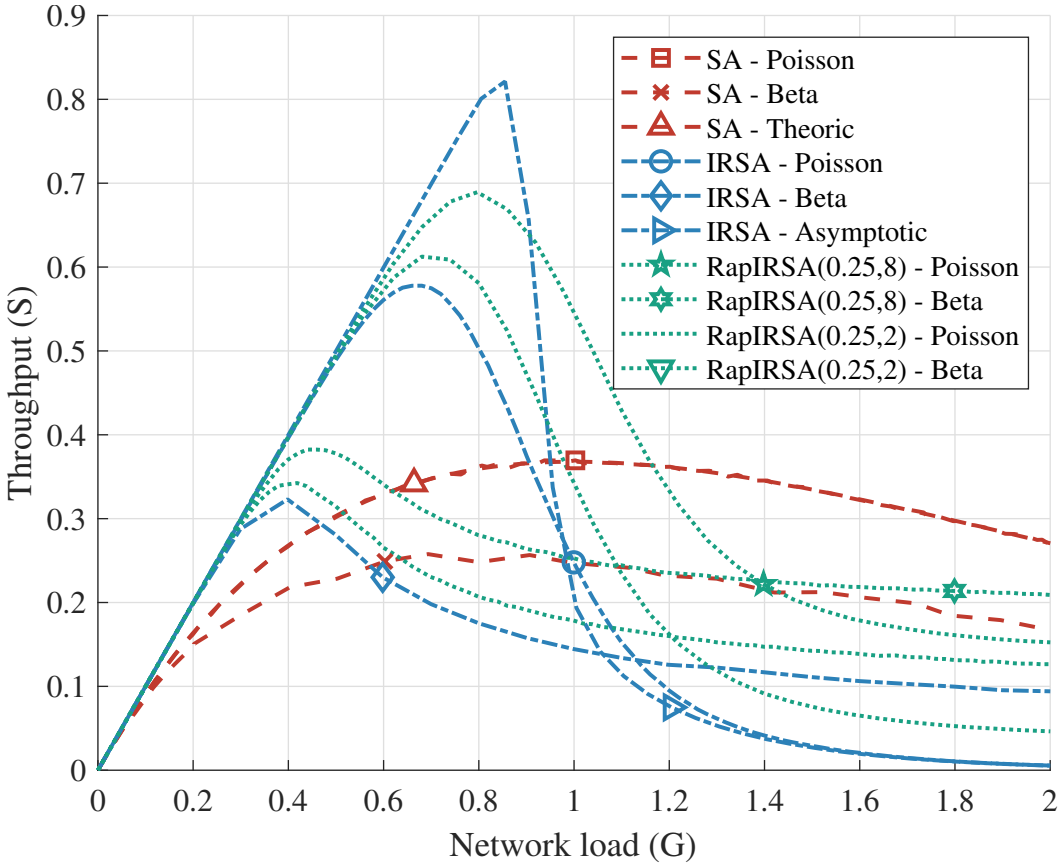

Figure 4.8 – Simulated throughput for SA, and for IRSA and RapIRSA with $\Lambda_8(x)$.

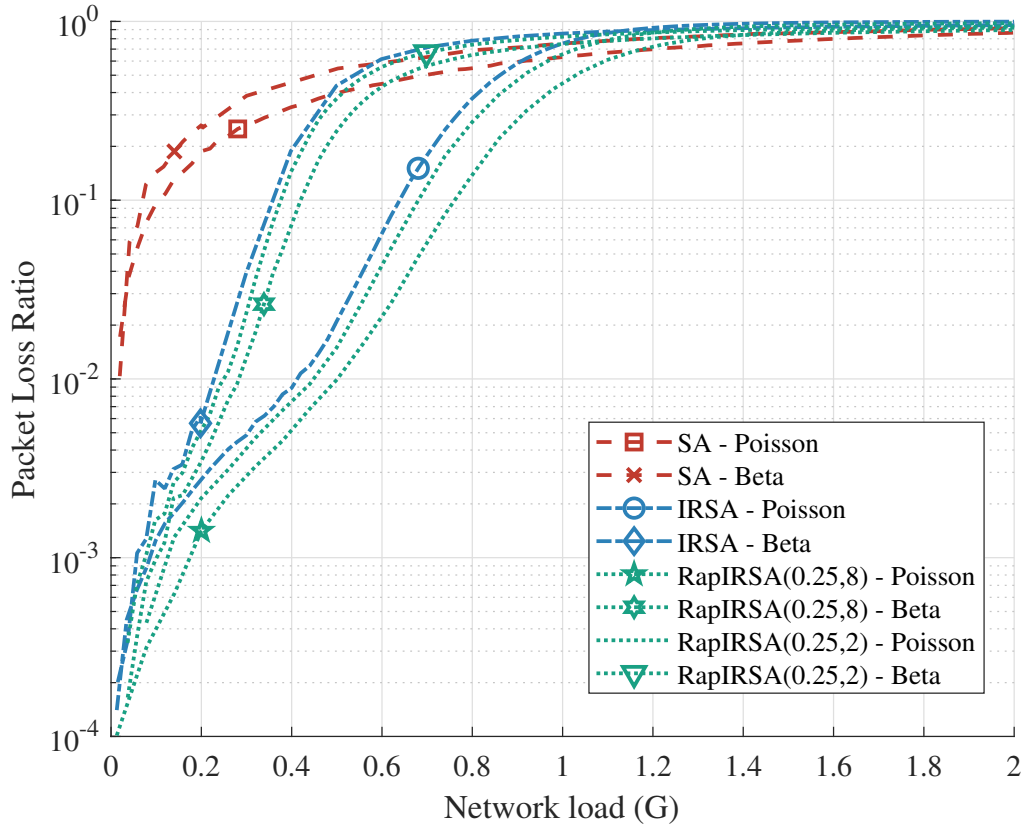

Figure 4.9 – Packet loss ratio for SA, and for IRSA with $\Lambda_8 = 0.5x^2 + 0.28x^3 + 0.22x^8$.

Fig. 4.10 to chart those values within IRSA and SA protocols. Fig. 4.10 shows that the average delay for all algorithms presents different behaviors. S-ALOHA maintains a steady increasing behavior as network loading increases, resulting in high delays (over 10^5 slots) in the high network loading ranging $1 < G < 2$. Moreover, the IRSA protocol presents a remarkable performance without delay for low-medium network loading ($G < 0.5$). Furthermore, RapIRSA keeps an almost constant operation point for all network loading. Even for measurement of average delay (slots) per active users in Fig. 4.10 (right y-axis), the delays of the S-ALOHA protocol appear unfeasible under requirements described in Table 4.1 for many of the SG applications. Table 4.1 scales priority in SG application type based on maximum tolerable latency.

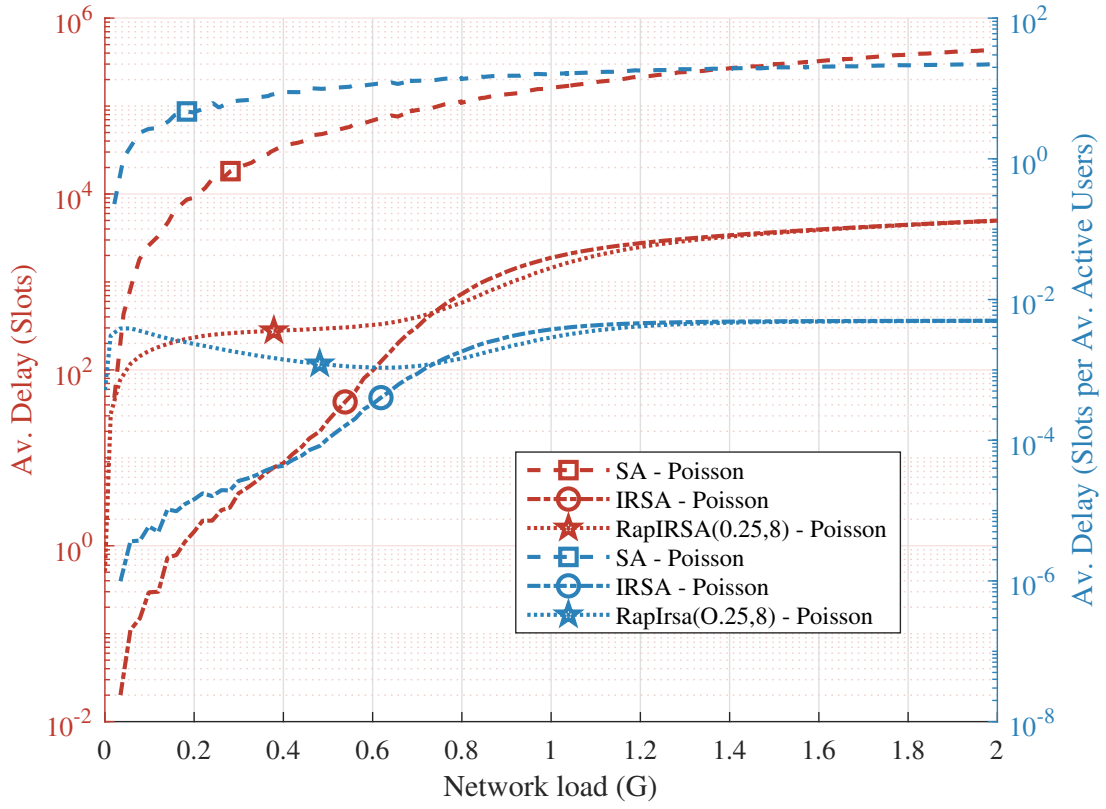

Figure 4.10 – Average delay in terms of # slots (left y-axis) and # slots per average # active users (right y-axis) *vs* Network loading

4.6.2 Application Complying Rate (ACR) Reliability

Fig. 4.11 compares the percentage of ACR reliability to evaluate the RA algorithm capability in achieving a certain QoS requirement. Under such specific reliability metric, and the modifications in the IRSA protocol introduced in Sec. 4.5, which are based on Raptor codes deployment and service priority, the QoS information was labelled into the active users preamble. The ACR reliability metric is evaluated with up to 10^4 devices; all SP RA protocols discussed in this work use the $\vec{p}_L$ values described in Table 4.1. The

ACR reliability curves in Fig. 4.11 corroborate the viability of the proposed RapIRSA and SP-RapIRSA algorithms to improve RA protocols performance, as well as, reach QoS requirements, described as one of the main objectives of the proposed work. Both RapIRSA variants, SP-RapIRSA and RapIRSA, provides the best ACR values across the entire networking loading range. Moreover, Fig. 4.11 reveals that the critical scenario of 90% ACR reliability ($\mathcal{R}_{\text{ACR}} = 0.9$), is attained for different network loading, depending of which RA protocol is adopted; the best performance is achieved by the SP-RapIRSA for a network loading of $G = 0.2$, followed by the RapIRSA protocol. The ACR reliability metric reveals the crucial trade-off between a delivered packet within the latency constraints. Notice that promising RA protocols for m-SGC applications require considering carefully the ACR reliability constraint.

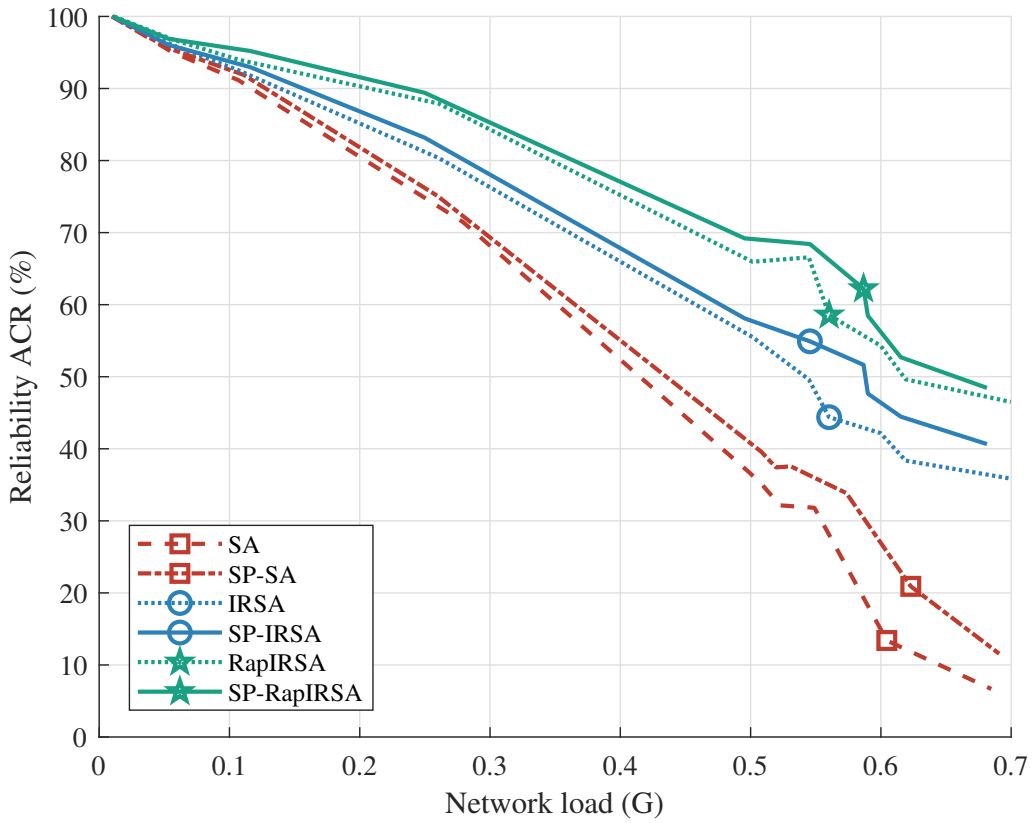

Figure 4.11 – Application complying rate (%) to measure algorithm capability to achieve QoS requirement

After this breakthrough and in contrast with the outstanding throughput present by the RapIRSA protocol, one can infer that among the three GF RA protocols analyzed, the RapIRSA is the most feasible protocol for SG applications. Even with the addition of extra slots for the $c\mathcal{N}$ delays, RapIRSA can comply with tied throughput, PLR, and latency performance requirements in the current SG networks.

4.7 Conclusions

We propose a service priority RA protocol for SG communication network applications. The proposed algorithm is based on the S-ALOHA and IRSA RA protocols with adapting parameters considering the QoS requirements as priority, latency, and data rates metrics. The proposed protocol aims to enhance the probability of success of various SG applications.

The RapIRSA protocol is proposed in this chapter to guarantee better throughput of active users with the help of connecting nodes ($c\mathcal{N}$). We have shown that relative to SA and IRSA in particular for multipacket messages, the RapIRSA can increase the reliability and keep the throughput above all-others. The RapIRSA is better than SA and IRSA, indicating this protocol is suitable for SG applications.

Future protocols for smart sensors applications: The inquire of adapting IRSA & RapIRSA for smart sensors is defined by: a) they reach their peak performance without latency constraints; b) they rely on reliability constraints rather than latency constraints. Latency constraints on IRSA & RapIRSA depend on the limit of the frame size. Nevertheless, a decreasing frame size support fewer users, rejecting some users from the system; However, IRSA & RapIRSA represents acceptable solutions for many critical cases.

5 Energy Efficiency in RIS-Aided UL MU-MIMO With User-side Precoding

This Chapter investigates a user-side precoding design for EE maximization in a RIS-aided MU MIMO UL network with a set of multi-antenna BS and multi-antenna UT. Beneath this design, we jointly optimize a UT's signal power covariance matrix, the RIS phase shift matrix, and the UT's beamforming vector, aiming to improve the overall system EE. We deploy a Manifold particle swarm optimization (PSO)-based optimization technique to solve the non-convex EE maximization problem in the RIS-aided UL MU-MIMO system. Via numerical results, we show that the proposed framework achieves significantly increased system EE values compared with non-optimized precoding schemes such as random schemes. Both the user-side precoding design and UTs equipped with multiple antennas simultaneously bring benefits to the RIS-aided UL MU-MIMO system.

5.1 RIS-Aided Uplink Multi-User MIMO

Beyond 5G technology includes reflecting intelligence surfaces (RIS), which are likely to be used (e.g., in buildings and vehicles) to maintain reliability in scenarios where physical obstacles exist between the transmitter and the receiver (IMOIZE et al., 2021). The author in (ZHOU et al., 2020a) presents a structure for RIS-aided transmission in multiple-input multiple-output (MIMO) systems; topology with a precoding design for massive MIMO reduces CSI exchange among the UT and the BS (GOUDA et al., 2020). Authors (WU; ZHANG, 2019b) and (XIE et al., 2020b) consider active and passive beamforming subject to users' average transmit power limitations. Besides, (XIE et al., 2020b) focuses on optimizing UL beamforming at the BS and passive beamforming at the RIS, employing a low-complexity max-min strategy. The author in (WU et al., 2021) uses the direct link to support RIS-aided channel as an advantage for energy detection for spectrum sensing. A joint beamforming optimization design for a multi-cell system aiming to maximize spectral efficiency (SE) and minimize the mean squared error (MSE) of the users' received symbols is developed in (REHMAN et al., 2021b). The above works do not consider UT side beamforming for multi-antenna devices. We consider a scenario where mobile wireless users maintain quasi-stationary positions to benefit from user-side precoding, and they establish connections to the BS aided by an outdoor or indoor RIS.

We focus on the UL of a multiple access multi-user (MU) MIMO system, where M UTs each equipped with N_m antennas transmit simultaneously to a base station (BS)

equipped with B antennas, representing a classical MIMO scenario (Fig. 5.1). The addition of a RIS facilitates the communication link between users and the BS. The RIS contains N_R reconfigurable reflecting elements. The RIS delivers a phase-shifted version of the transmitted signal, allowing to maximize the composite UT-RIS-BS channel gain.

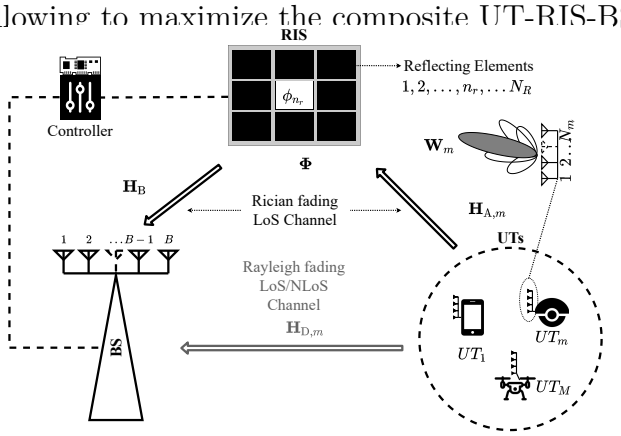

Figure 5.1 – RIS-aided MU-MIMO system model with LoS/NLoS BS-UT links.

The primary *contribution* of this chapter is the formulation of an energy efficiency (EE) optimization problem in a RIS-aided MU-MIMO uplink network, and a solution methodology based on the Manifold-PSO. We solve the problem of maximizing the system EE by sequentially optimizing a UT's power consumption per the transmit power covariance matrix, the RIS phase shift matrix, and the UT's beamforming vector. We formulate the joint optimization problem under a Riemannian manifold joint-optimization method to solve a two-variable problem (BORCKMANS et al., 2010; GROHS et al., 2020; HU et al., 2020). To the best of our knowledge, this is the first work dealing simultaneously with the user-side precoding and multi-antenna user transmission design in a RIS-aided UL MU-MIMO setup.

The remainder of this chapter is organized as follows. The RIS-assisted MU-MIMO system, problem formulation, and methods are described in Section 5.2, including meta-heuristic optimization method on manifolds and particle swarm optimization (PSO). Section 5.3 describes our proposed solutions. Section 5.4 provides numerical results corroborating our findings. Section 5.5 draws concluding remarks.

5.2 System Model and Problem Formulation

The received signal $\vec{r} \in \mathbb{C}^B$ at the BS is given by:

$$\vec{r} = \sum_{m=1}^{M} (\vec{H}_{\mathrm{D},m} + \vec{H}_{\mathrm{B}} \vec{\Phi} \vec{H}_{\mathrm{A},m}) \vec{s}_m + \vec{n}, \tag{5.1}$$

where $\vec{H}_{\mathrm{D},m} \in \mathbb{C}^{B \times N_{\mathbf{m}}}$ represents the channel matrix from the M UT-to-BS, $\vec{H}_{\mathrm{B}} \in \mathbb{C}^{B \times N_{\mathbf{R}}}$ represents the channel matrix between RIS-to-BS and $\vec{H}_{\mathrm{A},m} \in \mathbb{C}^{N_R \times N_{\mathbf{m}}}$ represents the channel matrix from the M UT-to-RIS, $\vec{n} \sim \mathcal{CN}(0, \sigma^2 \vec{I}_B)$ represents the thermal noise with $\vec{I}_B$ representing a $B \times B$ identity matrix. The RIS phase shift matrix is defined as:

$$\vec{\Phi} = \mathrm{diag}\{\phi_1, \ldots, \phi_{n_r}, \ldots, \phi_{N_R}\}, \text{ where } \phi_{n_r} = \exp(j\theta_{n_r}).$$

$\vec{s}_m \in \mathbb{C}^{N_m \times 1}$ denotes the m-th transmitted signal from the UT, with mean $\vec{0}$ and covariance matrix $\vec{Q}_m = \mathbb{E}\{\vec{s}_m \vec{s}_m^{\mathrm{H}}\} \in \mathbb{R}$. In $\vec{\Phi}$, element ϕ_m represents the reflection coefficient of the n-th RIS element which only affects the phase shifts. We assume a continuous phase (CP) shift. The channel from the UT to the RIS and the RIS to the BS are based on a *line-of-sight* (LoS) Rician fading model.

5.2.1 Spectral Efficiency and Energy Efficiency

Considering expectation with respect to the UT-RIS $\vec{H}_{\mathrm{A},m} \forall m$, we synthesize the ergodic spectral efficiency (SE) expression for the RIS-aided UL MU-MIMO system as (YOU et al., 2021):

$$\begin{aligned} \mathrm{SE}(\vec{Q}, \vec{\Phi}) = \mathbb{E}\Big\{ & \log_2 \det \Big(\vec{I}_B + \\ & \frac{1}{\sigma^2} \sum_m (\vec{H}_{\mathrm{D},m} + \vec{H}_{\mathrm{B}} \vec{\Phi} \vec{H}_{\mathrm{A},m}) \vec{Q}_m \\ & (\vec{H}_{\mathrm{D},m}^{\mathrm{H}} + \vec{H}_{\mathrm{A},m}^{\mathrm{H}} \vec{\Phi}^{\mathrm{H}} \vec{H}_{\mathrm{B}}^{\mathrm{H}}) \Big) \Big\} \text{ [bits/s/Hz]}. \end{aligned} \tag{5.2}$$

The total power consumption includes the circuit/hardware power required for regular operation. Besides, it considers end-to-end RIS-aided transmission from the m-th UT to the BS for the m-th link:

$$P_m = \xi_m \operatorname{Tr}\{\vec{Q}_m\} + P_{c,m} + P_{\mathrm{BS}} + N_R P_{\mathrm{RIS}}. \tag{5.3}$$

Extending for all UT's, and considering RIS-aided MU-MIMO in the UL,

$$P_{\mathrm{tot}} = \sum_m (\xi_m \operatorname{Tr}\{\vec{Q}_m\} + P_{c,m}) + P_{\mathrm{BS}} + N_R P_{\mathrm{RIS}}, \tag{5.4}$$

where $\xi_m = \rho_m^{-1}$ with $0 < \rho_m < 1$ reflects the inefficiency of the transmit power amplifiers selected at m-th UT; $P_{c,m}$ and P_{BS} represent the circuit power consumption at UT m and the BS. $N_R P_{\mathrm{RIS}}$ expresses that the RIS power consumption proportional to the number of RIS elements.

Next, following the definition of the system ergodic SE in Eq. (5.2) and the power consumption model in Eq. (5.4), we characterize RIS-aided system EE as:

$$\mathrm{EE}(\vec{Q}, \vec{\Phi}) = \mathrm{BW} \frac{\mathrm{SE}(\vec{Q}, \vec{\Phi})}{P_{\mathrm{tot}}} \quad \text{[bits/Joule]}, \tag{5.5}$$

where BW represents the system bandwidth.

5.2.2 Precoding - SVD and ZF Precoders

All channels from UT to BS, as illustrated in Fig. 5.1, are represented by $\vec{H}_m = \vec{H}_{\mathrm{D},m} + \vec{H}_{\mathrm{B}} \vec{\Phi} \vec{H}_{\mathrm{A},m}$. Assuming the availability of $\vec{H}_m$ at each UT, the precoding matrix $\vec{W}_m \in \mathbb{C}^{B \times N_m}$ for the m-th user is as follows:

$$\vec{\tilde{s}}_m = \vec{W}_m \vec{s}_m. \tag{5.6}$$

The precoding modifies Eq. (5.1) as given below:

$$\vec{\tilde{r}} = \sum_{m=1}^{M} \vec{H}_m \vec{W}_m \vec{s}_m + \vec{n} \;=\; \sum_{m=1}^{M} \vec{H}_m \vec{\tilde{s}}_m + \vec{n}. \tag{5.7}$$

Using *singular value decomposition* (SVD), if $\vec{H}_m$ has rank r, there exist two unitary matrices ($\vec{U}_m$ and $\vec{V}_m$), and a diagonal matrix $\vec{D}_m = \text{diag}\{\vartheta_1, \vartheta_2, \ldots, \vartheta_r\}$ such that

$$\vec{H}_m = \vec{U}_m \vec{D}_m \vec{V}_m^{\text{H}}. \tag{5.8}$$

Note that the highest modes of the SVD decomposition contained in the eigenvalues in $\mathbf{D}_m$ are associated with the best decomposed parallel channels. The parallel channels are assigned powers in an orderly way and each eigenvector associated with a specific channel receives the respective power contained in the individual eigenvalue.

Zero-forcing (ZF) precoding implements a pseudo-inverse matrix as:

$$\vec{W}_{\text{ZF}_m} = \vec{H}_m^{+}. \tag{5.9}$$

The precoding matrix $\vec{W}_m$ may refer to the optimized precoding matrix $\hat{\vec{W}}_m$, the SVD precoding matrix $\vec{V}_m$, or the $\vec{W}_{\text{ZF}_m}$ precoding.

5.2.3 SE and EE Under Precoding

With precoding $\vec{W}_m$ at the m-th UT, the SE and EE expressions in (5.2) and (5.5) are modified, including the term for a normalized covariance matrix $\hat{\vec{Q}}_m$. The new expression for SE becomes:

$$\begin{aligned} \text{SE}_{\forall}(\vec{W}, \vec{\Phi}) = \mathbb{E}\Big\{ \log_2 \det \Big(\vec{I}_B + \\ \frac{1}{\sigma^2} \sum_m (\vec{H}_{\text{D},m} + \vec{H}_{\text{B}} \vec{\Phi} \vec{H}_{\text{A},m}) \vec{W}_m \hat{\vec{Q}}_m \vec{W}_m^{\text{H}} \\ (\vec{H}_{\text{D},m}^{\text{H}} + \vec{H}_{\text{A},m}^{\text{H}} \vec{\Phi}^{\text{H}} \vec{H}_{\text{B}}^{\text{H}}) \Big) \Big\} \text{ [bits/s/Hz]}, \end{aligned} \tag{5.10}$$

while the new expressions for EE and power consumption are

$$\text{EE}_{\forall}(\vec{\Phi}, \vec{W}) = \text{BW} \frac{\text{SE}_{\forall}(\vec{\Phi}, \vec{W})}{P_{\text{tot}}^{W}} \quad \text{[bits/Joule]}, \tag{5.11}$$

$$P_{\text{tot}}^{W} = \sum_m (\xi_m ||\vec{W}_m|| + P_{c,m}) + P_{\text{BS}} + N_R P_{\text{RIS}}. \tag{5.12}$$

The denominator in (5.11) is denoted by the term P_{tot}^{W}, equal to the trace of the diagonal eigenvalues matrix.

5.2.4 Problem Formulation

The objective is to maximize the system EE in the RIS-aided UL MU-MIMO system under a minimum signal-to-interference-plus-noise ratio (SINR) constraint for the mth user, denoted by $\bar{\gamma}_m > 0$, $m \in \mathcal{M} = \{1, \ldots, M\}$. Based on the assumed system model,

we jointly consider the design of the RIS phase shift matrix $\vec{\Phi}$, and the UT's beamforming vector $\vec{W}_m$, by solving the following problem:

$$\underset{\vec{\Phi},\vec{W}}{\text{maximize}} \quad \text{EE}_{\forall}(\vec{\Phi},\vec{W}) \tag{5.13a}$$

$$\text{s.t.} \quad \text{SINR}_m(\vec{\Phi},\vec{W}) \geq \bar{\gamma}_m \tag{5.13b}$$

$$||\vec{W}_m|| \leq P_{\max,m} \quad \forall m \in \mathcal{M} \tag{5.13c}$$

$$|\phi_{n_r}| = 1 \quad \forall\, n_r \in \{1,\ldots,N_R\}, \tag{5.13d}$$

where

$$\text{SINR}_m(\vec{\Phi},\vec{W}) = \frac{|(\vec{H}_{\text{D},m} + \vec{H}_{\text{B}}\vec{\Phi}\vec{H}_{\text{A},m})\vec{W}_m|^2}{\sum_{j\neq m}^{M}|(\vec{H}_{\text{D},m} + \vec{H}_{\text{B}}\vec{\Phi}\vec{H}_{\text{A},m})\vec{W}_j|^2 + \sigma^2}. \tag{5.14}$$

Due to $\vec{W}$ and $\vec{\Phi}$ coupling in the users' SINR expression, constraints in (5.13b) are non-convex, hence, obtaining its globally optimal solution is challenging. For this reason, we propose a joint optimization algorithm based on manifold constrained optimization to solve this non-convex optimization problem.

It is well known that expectation operation preserves convexity (BOYD; VANDENBERGHE, 2004). Indeed, if $f(x)$ is convex and $\vec{Y}$ is a random variable, then $\mathbb{E}\{f(x-\vec{Y})\}$ is convex. The logarithm-determinant function is a concave function. The constraints (5.13c) and (5.13d) are convex. However, since constraint (5.13b) in non-convex, the quasi-concavity of the objective function in Eq. (5.11), as a result of a concave function (numerator) over an affine function (denominator) in Eq. (5.12), results in a non-convex fractional optimization problem.

5.3 Manifold PSO-Based Solution Method

We use a Riemannian manifold joint-optimization method (TRENDAFILOV; GALLO, 2021). MANOPT toolbox for optimization on manifolds and matrices is suitable for non-convex problems (BOUMAL et al., 2014). We develop **Algorithm 2** to solve a modified version of the original optimization problem in Eq. (5.13) as follows:

$$\underset{\vec{\Phi},\vec{W}}{\text{minimize}} \quad -\text{EE}_{\forall}(\vec{\Phi},\vec{W}) \tag{5.15a}$$

$$+\frac{\alpha}{2}\sum_{m=1}^{M}(\max\{0,\bar{\gamma}_m - \text{SINR}_m(\vec{\Phi},\vec{W})\})^2$$

$$\text{s.t.} \quad ||\vec{W}_m|| \leq P_{\max,m} \quad \forall m \in \mathcal{M} \tag{5.15b}$$

$$|\phi_{n_r}| = 1 \quad \forall\, n_r \in \{1,\ldots,N_R\}, \tag{5.15c}$$

where $\text{SINR}_m(\vec{\Phi},\vec{W})$ is given in (5.14). The algorithm sequentially solves the jointly coupled $[\vec{\Phi},\vec{W}]$ optimization problem for maximum system EE. It runs L channel realizations to obtain the expected SE value in Eq. (5.10). A constraint manifold approach formulates each optimization variable as: $\mathscr{P}$: *Complex circle factory manifold*, and $\mathscr{W}$: *Sphere complex*

factory manifold. Each realization includes the following steps: i) generate randomly a phase shift matrix $\vec{\Phi}$, for RIS within CP restrictions, i.e. random/initial parameters $(\vec{\Phi}^0, \vec{W}^0)$; ii) define the RIS-BS and UT-RIS channels; iii) joint sequently optimize $\vec{\Phi}_m$ and $\vec{W}_m$ until convergence as described in Algorithm 2.

We consider three system configurations or initial conditions to analyze the effect of UT precoding $\vec{W}^0$: a) without initial precoding (*w/o prec*), i.e. $\vec{W}^0 = \vec{1}$. Therefore, the power is equally distributed across the N_m antennas and equal to $\frac{P_{\max}}{N_m}$. In this case, the covariance matrix $\vec{Q}_m$ represents UT's transmit power for the first iteration of the algorithm. b) SVD precoding (*prec-SVD*), the received signal takes the form of Eq. (5.7) and (5.8) then $\vec{W}^0 = \vec{V}_m$. c) ZF precoding (*prec-ZF*), with received signal as in Eq. (5.7) and (5.9) then $\vec{W}^0 = \vec{H}_m^+$. When stated as *w/o prec*, the $\text{EE}_{\vec{W}} = \text{EE}$ is given by Eq. (5.5).

The algorithm runs for different values of UT maximum power to compute EE. The algorithm assigns maximum transmit power to all users for each budget power configuration. Next, it defines the objective of EE optimization as in Eq. (5.13).

An iterative joint optimization process is executed with the following stopping condition: let $\sigma^{\text{EE}_\forall(\vec{W})}$ and $\sigma^{\text{SE}_\forall(\vec{W})}$ denote the standard deviation of the $\text{EE}_\forall(\vec{\Phi}^\iota, \vec{W}^\iota)$ and the $\text{SE}_\forall(\vec{\Phi}^\iota, \vec{W}^\iota)$'s five last iterations $(\iota, \iota-1, \ldots, \iota-5)$, respectively. The algorithm will attain convergence when both of them fall below a predefined threshold value, e.g. $\varepsilon < 10^{-2}$. This algorithm sequentially optimizes each of the two optimization variables: $\vec{\Phi}_m$, and $\vec{W}_m$. Indeed, for each optimization variable, the following procedure is executed: i) define the corresponding manifold; ii) define the cost function with updated variables; iii) update the variable using the MANOPT-PSO algorithm, accordingly. Manopt-PSO algorithm relies on an iterative optimization process.

After obtaining the corresponding optimized variable, it re-calculates SE from Eq. (5.10), the total consumed system power P_{tot} as predicted in Eq. (5.12), and the corresponding EE, Eq. (5.11), for each step. At this point, i.e. at ιth iteration, we have obtained optimized $\vec{\Phi}_m^\iota$, and $\vec{W}_m^\iota$. Hence, in the last stage, we get the Frobenius norm for all $\vec{W}$ to verify maximum power constraints. Finally, the algorithm calculates the average EE and SE and retrieves the *normalized maximum precoding norm* (NMPN) for all L realizations:

$$\text{NMPN} = P_{\max,m}^{-1} \max\{||\vec{W}_1||, \ldots, ||\vec{W}_m||, \ldots, ||\vec{W}_M||\}. \tag{5.16}$$

Computational complexity: Optimizing on a manifold $(\mathscr{P}, \mathscr{W})$ is not essentially different from optimizing in $\mathbb{R}^n$ (BOUMAL et al., 2018). The computation time offers us an idea of the computational complexity of the different design approaches. The average computation time per iteration for running Algorithm 2 is summarized in Table 5.1. This time includes average iteration time until convergence or iteration limit. Note that, for the max-SE design, the algorithm using SVD or ZF initial precoding requires 15.9% and 35.6% more time w.r.t. *w/o prec*. For max-EE design, this reduces to 11.2% and 30.3%, respectively.

Algorithm 2: Iterative $[\vec{\Phi}, \vec{W}]$ for Max-EE

Data: Scenario, System, and PSO input parameters
Result: Obtain $\text{EE}(\vec{\Phi}, \vec{W})$
for $l = 1$ *until* L **do**
  Generate transmitted signal;
  Randomly generate phase shift matrix Φ for RIS;
  Define $\vec{H}_B$ RIS-BS channel;
  Define $\vec{H}_{A,m}$ UT-RIS channel;
  for $p = 1$ *until* $P_{\max,m}$ **do**
    Assign maximum transmit power for all users;
    Define optimization objectives SE or EE;
    for *each precoding criterion* **do**
      $\iota = 0$;
      Calculate $\text{EE}(\vec{\Phi}^0, \vec{W}^0)$ and $\text{SE}(\vec{\Phi}^0, \vec{W}^0)$. ;
      while $\sigma^{EE_\forall(\vec{W})} > \varepsilon$ *and* $\sigma^{SE_\forall(\vec{W})} > \varepsilon$ **do**
        $\iota = \iota + 1$;
        Step 1 - Init. $\vec{\Phi}_m$ Optimization;
        Define manifold $\rightarrow \mathscr{P}^\iota$;
        Define cost function $\text{EE}^\iota_{\vec{W}}(\vec{\Phi}, \vec{W}^{\iota-1})$;
        Update $\vec{\Phi}^\iota$ using PSO algorithm;
        Calculate $\text{EE}^\iota_{\vec{W}}(\vec{\Phi}^\iota, \vec{W}^{\iota-1})$ and $\text{SE}^\iota_{\vec{W}}(\vec{\Phi}^\iota, \vec{W}^{\iota-1})$;
        Step 2 - Init. $\vec{W}_m$ Optimization;
        Define manifold $\rightarrow \mathscr{W}^\iota$;
        Define cost function $\text{EE}^\iota_\forall(\vec{\Phi}^\iota, \vec{W})$;
        Update $\vec{W}^\iota$ using PSO algorithm;
        Calculate $\text{EE}^\iota_\forall(\vec{\Phi}^\iota, \vec{W}^\iota)$ and $\text{SE}^\iota_\forall(\vec{\Phi}^\iota, \vec{W}^\iota)$;
        Obtain Frobenius Norm for all $\vec{W}^\iota$;
      end
    end
  end
end
Calculate EE^ι and SE^ι averaged for L realizations;
Retrieve maximum Norm $\vec{W}^\iota$;

Table 5.1 – Average time per algorithm iteration (EE and SE)

Criterion	Avg. time	Criterion	Avg. time
$t^{\text{SE}^0}_{\text{avg-iter}}$	0.3346 s	$t^{\text{EE}^0}_{\text{avg-iter}}$	0.4374 s
$t^{\text{SE}^{\text{SVD}}}_{\text{avg-iter}}$	0.3881 s	$t^{\text{EE}^{\text{SVD}}}_{\text{avg-iter}}$	0.4886 s
$t^{\text{SE}^{\text{ZF}}}_{\text{avg-iter}}$	0.4537 s	$t^{\text{EE}^{\text{ZF}}}_{\text{avg-iter}}$	0.5701 s

5.4 Numerical Results

The effectiveness of RIS-aided MU-MIMO with user precoding is corroborated by the following numerical results. Table 5.2 outlines the system and channel parameter values. The values are based on those in (YOU et al., 2021; ZENG et al., 2021).

Table 5.2 – Simulation parameters

Parameter	**Value**
Rician κ factor	$\kappa_{\text{dB}} = 3$ [dB]
SNR	SNR= 20 [dB]
Number of antennas per UT	$N_m = 16$
Number of antennas at BS	$B = 8$
Number of RIS elements	$N_R = 32$
Number of UT's	$M = 4$
Modulation order	$\mathbb{M} = 2$
Number of channel realization	$L = 1000$
Transmission bandwidth	BW = 100 [MHz]
Inefficiency of UT power amplif.	$\xi_m = 1/0.3 = 3.33$
Power circuitry per UT	$P_{c,m}$ = 10 [dBm]
Power at BS	P_{BS} = 39 [dBm]
Power of each RIS element	P_{RIS} = 5 [dBm]
Max power per UT	$P_{\max}$ = 20 [dBm]
Minimum (SINR) per user	$\bar{\gamma}_m$ = 0 [dBm], $\forall m$
Algorithm stop factor	$\varepsilon = 0.01$
Number of maximum iterations	$\iota_{\max} = 200$

To assess the effectiveness of the introduced optimization methodology, we first consider the SE maximization problem. Fig. 5.2a shows SE vs. $P_{\max}$ performance when $\xi \to \infty$, under different criteria. According to this figure, optimized precoding, i.e. with $\text{SE}_{\forall}^{0}(\vec{\Phi}^{\iota}, \vec{W}^{\iota})$ and $\text{SE}_{\forall}^{\text{SVD}}(\vec{\Phi}^{\iota}, \vec{W}^{\iota})$, SE improves for all available power values, while for $\text{SE}_{\forall}^{\text{ZF}}(\vec{\Phi}^{\iota}, \vec{W}^{\iota})$ no benefits in SE are observed. The SVD-based precoding slightly increases spectral efficiency while reducing the energy consumption only for $P_{\max} = 25$ [dBm] (in Fig. 5.2a, $\text{SE}_{\forall}^{\text{SVD}}(\vec{\Phi}^{\iota}, \vec{W}^{\iota}) > \text{SE}_{\forall}^{0}(\vec{\Phi}^{\iota}, \vec{W}^{\iota})$). Similarly, in Fig. 5.2b, $\text{EE}_{\forall}^{\text{SVD}}(\vec{\Phi}^{\iota}, \vec{W}^{\iota}) > \text{EE}_{\forall}^{0}(\vec{\Phi}^{\iota}, \vec{W}^{\iota})$.

Fig. 5.2b reveals the overall benefit of optimized precoding (except for $\text{SE}_{\forall}^{\text{ZF}}(\vec{\Phi}^{\iota}, \vec{W}^{\iota})$) for EE optimization for all available power scenarios considered. For the EE vs. $P_{\max}$, the EE first increases and then decreases with increasing $P_{\max}$, resulting in a quasi-concave curve. Hence, there is an optimal power consumption that maximizes the system EE. For $P_{\max} \geq 5$ dBm, optimized precoding design (i.e. when using $\text{EE}_{\forall}^{0}(\vec{\Phi}^{\iota}, \vec{W}^{\iota})$ and $\text{EE}_{\forall}^{\text{SVD}}(\vec{\Phi}^{\iota}, \vec{W}^{\iota})$

achieves better EE. Moreover, for $N_m = 16$ antennas per UT, the maximum EE (attainable at $P_{\max,m} \approx 25$ dBm) gain w.r.t. no precoding optimization and no RIS phase optimization ($-\star-$ $\text{EE}^0_\forall(m, \vec{\Phi}^0, \vec{W}^0)$), compared to precoding optimization and RIS phase optimization ($-\triangleright-$ $\text{EE}^0_\forall(m, \vec{\Phi}^\iota, \vec{W}^0)$) is observed to be consistently moderate.

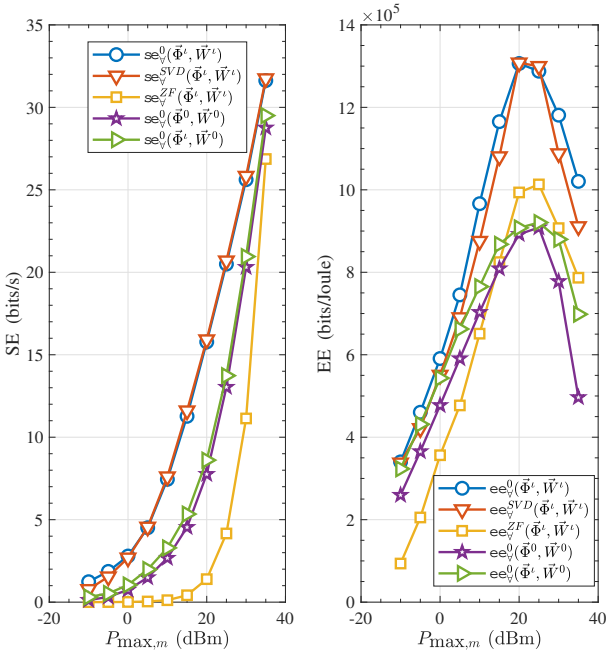

a) max-SE **b**) max-EE

Figure 5.2 – SE and EE optimization vs. available power per UT under distinct optimization variables $\vec{\Phi}$ and $\vec{W}$. Index ι is for last iteration of the optimization algorithm; superscript ^{0} represents absence of precoding in initial solution of the algorithm; in contrast, ZF or SVD is for initial precoding solutions.

In Fig. 5.3, the NMPN in Eq. (5.16), is calculated to both the optimization methodologies, $\text{SE}^0_\forall(\vec{\Phi}^\iota, \vec{W}^\iota)$ and $\text{EE}^0_\forall(\vec{\Phi}^\iota, \vec{W}^\iota)$. Notice that for the SE optimization criterion, as expected, the amount of power consumed by a UT is closer to the total power available, especially for the first-range of available power $P_{\max,m} \in [-10; 5]$ dBm. Moreover, the NMPN is not precisely under the max-SE methodology since the proposed algorithm is quasi-optimal.

Fig. 5.4 shows $\text{EE}^0_\forall(\vec{\Phi}^\iota, \vec{W}^\iota)$ improvement for an iterative optimization process ($\iota_{\max} = 200$ iterations). Notice that there is a more significant improvement in EE across the iterations for those lower power values, i.e. $P_{\max,m} \in \{-10, -5, 0\}$ [dBm]. Also, Fig. 5.4 confirms that the optimum EE under the iterative criterion $\text{EE}^0_\forall(\vec{\Phi}^\iota, \vec{W}^\iota)$ in **Algorithm 1** is attained with $P_{\max,m} \approx 25$ [dBm] and $\iota \geq 160$ iterations.

Fig. 5.5 shows how EE improves with the number of transmit antennas. The selection of an optimized precoding matrix $\vec{W}$ results in more substantial EE gains for an increasing number of transmit antennas at each UT. The overall energy consumption at a UT however will depend on the number of RF chains used, which is not considered herein.

To summarize the main results: i) Optimized precoding brings SE and EE benefits to all available power values, ii) *w/o prec* precoding increases SE while reducing the energy

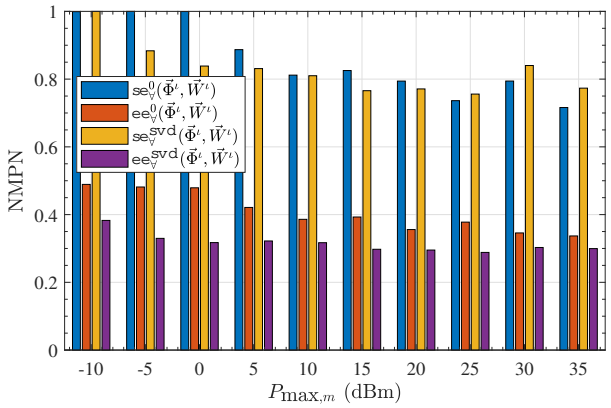

Figure 5.3 – Normalized maximum precoding norm vs. $P_{\max,m}$ for both designs $\text{EE}_{\forall}^{0}$–$\text{SE}_{\forall}^{0}$ and $\text{EE}_{\forall}^{\text{SVD}}$–$\text{SE}_{\forall}^{\text{SVD}}$

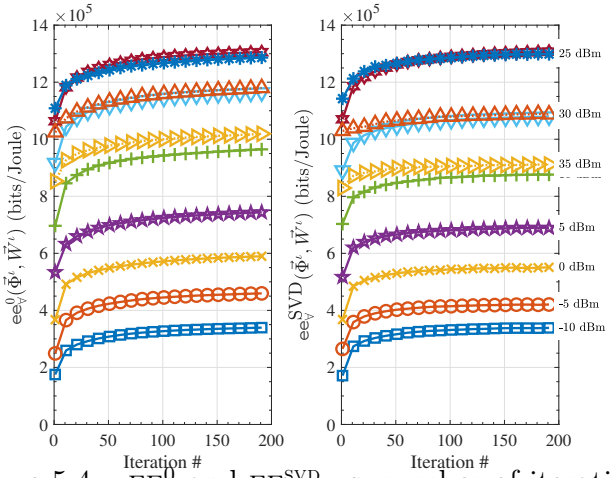

Figure 5.4 – $\text{EE}_{\forall}^{0}$ and $\text{EE}_{\forall}^{\text{SVD}}$ vs. number of iterations.

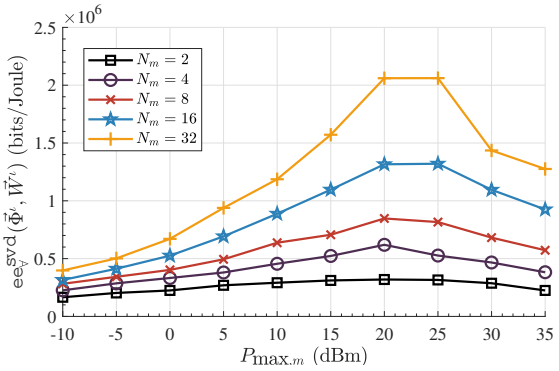

Figure 5.5 – EE for a different number of transmit antennas under $\iota_{\max} = 200$ and $\iota_{\text{avg}} = 187.9$.

consumption at multi-antenna UTs, and iii) EE increases with the number of transmitting antennas when power consumption in the RF chains is not considered.

5.5 Conclusion

We have proposed a method for optimizing user-side transmit precoding with multiple antennas and passive beamforming at RIS that maximizes the system EE. We have shown the benefits of increasing the number of antennas at the UTs to improve the EE of RIS-aided uplink MU-MIMO systems. The proposed manifold PSO-based optimization methodology has shown to be capable of significantly enhancing the system EE performance with an increasing number of transmitting antennas ($N_m \geq 4$).

6 Conclusions

This chapter summarizes the main findings of this thesis by highlighting the most important problems addressed. Moreover, we outline some potential lines of research that may result from the work developed.

6.1 Generalizations

The large-scale integration of small and medium-sized system generators of various technologies, such as renewable energy generators, energy storage systems, and demand response, into the grid is a fundamental challenge for a successful energy evolution. Due to the deep integration of communication systems at multiple levels, communication systems will play a central role in future intelligent power systems. Their integration into the power system will require the active participation of multidisciplinary professionals with knowledge of electricity markets and grid operations in a coherent communications experience.

The SG situation into the subsequent B5G/6G communication generation represents the driving force behind the motivation of this thesis to conceptualize, develop, and implement new protocols and strategies for future SG.

The distinct pillars of innovation, findings, and conclusions of this thesis revolve around the following four key points:

1. Characterize the SG faults scenarios is critical in achieving a better response.
2. The conceptualization and the development of proper estimation techniques for the SG fault detection scenario.
3. A case study analysis considers SG requirements and behavior in several massive devices' existing communication network access.
4. Establish communication technologies to improve coverage and reliability, maximizing energy efficiency.

The conceptualization and the development of a Smart Grid Fault detection infrastructure started this research to showcase how wireless communication systems are crucial to the next-generation grid. This research framework looks to expand the SG universe considering and highlighting the importance of the communications infrastructure. All aspects are discussed and considered small and medium-sized SS through a B5G/6G communication network.

6.2 Summary of Contributions

This section summarizes the contributions of this thesis and the conclusions from the results obtained.

Chapter 2 presented an SG fault detection and classification infrastructure survey, including SG communication support. Including relevant state-of-the-art papers from the most significant research databases. Chapter 3 proposed an adaptive technique to reliable monitoring harmonic distortion in the power network. Conclusively, a performance-complexity tradeoff analysis demonstrated each filtering method's (dis)advantages. Chapter 4 highlighted the significance of existing and future random access (RA) protocols for massive smart grid communication (m-SGC) devices and system performance. We presented a new, improved irregular repetition slotted ALOHA (RapIRSA) RA protocol to better respond to critical high-reliability QoS requirements under a 5G communications perspective, summarizing the potential challenges in implementing the proposed RA protocol. Chapter 5 investigated a distributed precoding design for energy efficiency maximization in a RIS-aided MU MIMO UL network with a set of multi-antenna BSs and multi-antenna UTs. We deployed a Manifold PSO-based optimization technique to solve the non-convex EE maximization, showing that the proposed framework significantly increases system EE values compared with non-optimized precoding schemes such as random schemes.

6.3 Listing Thesis's Contributions.

1. We created a comprehensive structure for classifying the relevant SG requirements and future developments to bridge the gap between legacy and future fault detection techniques, discussing the classification of different fault scenarios in a comprehensive framework.

2. We demonstrated (dis)advantages of adaptive technique to reliable monitoring harmonic distortion in the power network, including a performance-complexity tradeoff analysis to conclude the best estimation filtering choice.

3. We proposed an improved Raptor Code IRSA-based RA grant-free protocol to better adapt to critical high-reliability QoS requirements, depending on existing applications and the number of devices in SG applications. For this to be possible, we explored the main SG critical application while characterizing the QoS requirements in SGC systems.

4. We formulated an EE optimization problem and the solution methodology based on the Manifold-PSO, taking advantage of derivative-free heuristic optimization algorithms to find optimal solutions. We showed that user-side precoding along with

multi-antenna user transmission benefit simultaneously from RIS-aided communication, bringing advantages for the system EE in the UL MU-MIMO setup.

6.4 Outlook on future research

The developments and results presented in this thesis point to new questions, technical products, and research that may further strengthen the work presented here. First, this thesis focuses on the SG interoperability and reliability of their systems, including fault detection, evaluation of existing estimation techniques, QoS requirements, and energy-efficient communications. However, the key to these estimation techniques is to understand the SG fault architecture from the bottom to the top. Each innovative group has a specific importance. Hence, faults detection should evaluate only critical applications, indicating communication infrastructure dependency. Similarly, state estimation and forecast algorithms will require original data from a future utility partner to obtain real-network data. In particular, this will create a reliable and accurate algorithm able to estimate faults in the network.

On the other hand, the SG concept is still in the development stage. It will go through several technological and policy change programs. Currently, SG face many challenges, such as transmission capacity, ability to integrate renewable energy to high penetration levels, vast communication infrastructure, data security, cyber attacks, data management, active customer engagement, advanced monitoring, and control technologies, and competitive prices. SG must address these challenges to evolve.

At the same time, low-cost hardware can take advantage of the spread of network diversification and penetration into crowded areas. Although broad in scope, it also prevents damage to minimum bend radius, maximum practical tension, vibration damping, and more. This will help us optimize costs and provide a contingency-free network. Such an implementation would significantly enhance grid data center interoperability and Extensibility for interactive SG applications.

Cost is one of the most significant constraints to innovative grid development and implementation, especially in developing countries. Many financial resources are associated with transmission and distribution systems, metering, and other related technologies. A complete financial feasibility report is essential before implementation. This economic viability must include the nation's ability to pay for smart grid infrastructure development costs.

Bibliography

ABU-SIADA, A.; MIR, S. A new on-line technique to identify fault location within long transmission lines. *Engineering Failure Analysis*, Elsevier, v. 105, n. June, p. 52–64, nov 2019. ISSN 13506307. Cited on page 37.

ACHLERKAR, P. D.; SAMANTARAY, S. R.; Sabarimalai Manikandan, M. Variational Mode Decomposition and Decision Tree Based Detection and Classification of Power Quality Disturbances in Grid-Connected Distributed Generation System. *IEEE Transactions on Smart Grid*, IEEE, v. 9, n. 4, p. 3122–3132, jul 2018. ISSN 1949-3053. Available on: <https://ieeexplore.ieee.org/document/7740071/>. Cited 5 times on page(s) 53, 78, 79, 83, and 184.

AFFIJULLA, S.; TRIPATHY, P. A Robust Fault Detection and Discrimination Technique for Transmission Lines. *IEEE Transactions on Smart Grid*, IEEE, v. 9, n. 6, p. 6348–6358, nov 2018. ISSN 1949-3053. Available on: <https://ieeexplore.ieee.org/document/7935455/>. Cited 5 times on page(s) 53, 77, 79, 83, and 181.

AFTAB, M. A.; HUSSAIN, S. S.; ALI, I.; USTUN, T. S. Dynamic protection of power systems with high penetration of renewables: A review of the traveling wave based fault location techniques. *International Journal of Electrical Power & Energy Systems*, Elsevier, v. 114, n. May 2019, p. 105410, jan 2020. ISSN 01420615. Cited on page 37.

AHMADIPOUR, M.; HIZAM, H.; Lutfi Othman, M.; Mohd Radzi, M. A. An anti-islanding protection technique using a wavelet packet transform and a probabilistic neural network. *Energies*, v. 11, n. 10, 2018. ISSN 19961073. Cited 4 times on page(s) 79, 82, 83, and 185.

AHMADIPOUR, M.; HIZAM, H.; Lutfi Othman, M.; RADZI, M. A. M.; CHIREH, N. A novel islanding detection technique using modified Slantlet transform in multi-distributed generation. *International Journal of Electrical Power and Energy Systems*, Elsevier, v. 112, n. January, p. 460–475, 2019. ISSN 01420615. Cited 4 times on page(s) 79, 82, 83, and 183.

AHMADIPOUR, M.; HIZAM, H.; OTHMAN, M. L.; RADZI, M. A. M.; MURTHY, A. S. Islanding detection technique using Slantlet Transform and Ridgelet Probabilistic Neural Network in grid-connected photovoltaic system. *Applied Energy*, v. 231, n. August, p. 645–659, 2018. ISSN 03062619. Cited 4 times on page(s) 79, 82, 83, and 185.

AHMADIPOUR, M.; HIZAM, H.; OTHMAN, M. L.; Mohd Radzi, M. A.; CHIREH, N. A fast fault identification in a grid-connected photovoltaic system using wavelet multi-resolution singular spectrum entropy and support vector machine. *Energies*, v. 12, n. 13, 2019. ISSN 19961073. Cited 4 times on page(s) 79, 82, 83, and 185.

ALHELOU, H. H.; GOLSHAN, M. H.; ASKARI-MARNANI, J. Robust sensor fault detection and isolation scheme for interconnected smart power systems in presence of RER and EVs using unknown input observer. *International Journal of Electrical Power & Energy Systems*, Elsevier, v. 99, n. February, p. 682–694, jul 2018. ISSN 01420615. Available on: <https://doi.org/10.1016/j.ijepes.2018.02.013https://linkinghub.elsevier.com/retrieve/pii/S0142061517314382>. Cited 5 times on page(s) 53, 75, 79, 83, and 179.

ANANDAN, N.; E, S. P.; S, S.; S, R.; BHUVANESWARI, T. Wide area monitoring system for an electrical grid. *Energy Procedia*, Elsevier B.V., v. 160, n. 2018, p. 381–388, feb 2019. ISSN 18766102. Available on: <https://linkinghub.elsevier.com/retrieve/pii/S1876610219312615>. Cited 2 times on page(s) 56 and 183.

ANDERSON, P. Protective Schemes for Stability Enhancement. In: *Power System Protection*. IEEE, 2009. Available on: <http://ieeexplore.ieee.org/search/srchabstract.jsp?arnumber=5264147>. Cited on page 80.

ANDRESEN, C. A.; TORSAETER, B. N.; HAUGDAL, H.; UHLEN, K. Fault Detection and Prediction in Smart Grids. In: *2018 IEEE 9th International Workshop on Applied Measurements for Power Systems (AMPS)*. IEEE, 2018. p. 1–6. ISBN 978-1-5386-5375-3. Available on: <https://ieeexplore.ieee.org/document/8494849/>. Cited 5 times on page(s) 43, 51, 56, 60, and 179.

ARTALE, G.; CATALIOTTI, A.; COSENTINO, V.; Di Cara, D.; GUAIANA, S.; NUCCIO, S.; PANZAVECCHIA, N.; TINE, G. Smart Interface Devices for Distributed Generation in Smart Grids: The Case of Islanding. *IEEE Sensors Journal*, v. 17, n. 23, p. 7803–7811, dec 2017. ISSN 1530-437X. Available on: <http://ieeexplore.ieee.org/document/7976285/>. Cited 2 times on page(s) 52 and 184.

BABAEI, M.; SHI, J.; ABDELWAHED, S. A Survey on Fault Detection, Isolation, and Reconfiguration Methods in Electric Ship Power Systems. *IEEE Access*, IEEE, v. 6, p. 9430–9441, 2018. ISSN 2169-3536. Available on: <http://ieeexplore.ieee.org/document/8275481/>. Cited 2 times on page(s) 43 and 181.

BAECKELAND, N.; HERTELEER, B.; KLEEMANN, M. Modelling fault behaviour of power electronic converters. *International Journal of Electrical Power & Energy Systems*, Elsevier, v. 123, n. March, p. 106230, dec 2020. ISSN 01420615. Cited on page 50.

BAHMANYAR, A.; JAMALI, S.; ESTEBSARI, A.; BOMPARD, E. A comparison framework for distribution system outage and fault location methods. *Electric Power Systems Research*, Elsevier B.V., v. 145, p. 19–34, apr 2017. ISSN 03787796. Available on: <http://dx.doi.org/10.1016/j.epsr.2016.12.018https://linkinghub.elsevier.com/retrieve/pii/S0378779616305302>. Cited 5 times on page(s) 43, 60, 74, 80, and 182.

BANGALORE, P.; TJERNBERG, L. B. An Artificial Neural Network Approach for Early Fault Detection of Gearbox Bearings. *IEEE Transactions on Smart Grid*, IEEE, v. 6, n. 2, p. 980–987, mar 2015. ISSN 1949-3053. Available on: <http://ieeexplore.ieee.org/document/7012091/>. Cited 6 times on page(s) 53, 75, 79, 82, 83, and 179.

BELTRAN-CARBAJAL, F.; TAPIA-OLVERA, R.; VALDERRABANO-GONZALEZ, A.; YANEZ-BADILLO, H. An asymptotic and algebraic estimation method of harmonics. *Electric Power Systems Research*, v. 206, p. 107771, 2022. ISSN 0378-7796. Available on: <https://www.sciencedirect.com/science/article/pii/S0378779622000013>. Cited on page 37.

BERARDINELLI, G.; Huda Mahmood, N.; ABREU, R.; JACOBSEN, T.; PEDERSEN, K.; KOVACS, I. Z.; MOGENSEN, P. Reliability Analysis of Uplink Grant-Free Transmission Over Shared Resources. *IEEE Access*, v. 6, p. 23602–23611, 2018. ISSN 2169-3536. Available on: <https://ieeexplore.ieee.org/document/8340053/>. Cited on page 113.

BERIOLI, M.; COCCO, G.; LIVA, G.; MUNARI, A. Modern Random Access Protocols. *Foundations and Trends® in Networking*, v. 10, n. 4, p. 317–446, 2016. ISSN 1554-057X. Available on: <http://www.nowpublishers.com/article/Details/NET-047>. Cited 2 times on page(s) 118 and 121.

BETTAYEB, M.; QIDWAI, U. Recursive estimation of power system harmonics. *Electric Power Systems Research*, v. 47, n. 2, p. 143–152, oct 1998. ISSN 03787796. Cited on page 37.

BIAN, D.; KUZLU, M.; PIPATTANASOMPORN, M.; RAHMAN, S.; SHI, D. Performance evaluation of communication technologies and network structure for smart grid applications. *IET Communications*, v. 13, n. 8, p. 1025–1033, may 2019. ISSN 1751-8628. Available on: <https://digital-library.theiet.org/content/journals/10.1049/iet-com.2018.5408>. Cited on page 61.

BOCKELMANN, C.; PRATAS, N. K.; WUNDER, G.; SAUR, S.; NAVARRO, M.; GREGORATTI, D.; VIVIER, G.; De Carvalho, E.; JI, Y.; STEFANOVIC, C.; POPOVSKI, P.; WANG, Q.; SCHELLMANN, M.; KOSMATOS, E.; DEMESTICHAS, P.; RACEALA-MOTOC, M.; JUNG, P.; STANCZAK, S.; DEKORSY, A. Towards Massive Connectivity Support for Scalable mMTC Communications in 5G Networks. *IEEE Access*, v. 6, n. ii, p. 28969–28992, 2018. ISSN 21693536. Cited 3 times on page(s) 35, 87, and 184.

BOLLEN, M. H. J.; GU, I. Y.-H. Processing of Stationary Signals. In: *Signal Processing of Power Quality Disturbances*. Hoboken, NJ, USA: John Wiley Sons, Inc., 2006. p. 163–276. Available on: <http://doi.wiley.com/10.1002/9780471931317.ch3https://onlinelibrary.wiley.com/doi/10.1002/9780471931317.ch3>. Cited 2 times on page(s) 96 and 97.

BORCKMANS, P. B.; ISHTEVA, M.; ABSIL, P.-A. A Modified Particle Swarm Optimization Algorithm for the Best Low Multilinear Rank Approximation of Higher-Order Tensors. In: *Lecture Notes in Computer Science (including subseries Lecture Notes in Artificial Intelligence and Lecture Notes in Bioinformatics)*. [s.n.], 2010. v. 6234 LNCS, p. 13–23. ISBN 3642154603. Available on: <http://link.springer.com/10.1007/978-3-642-15461-4_2>. Cited on page 134.

BOUMAL, N.; ABSIL, P.-A.; CARTIS, C. Global rates of convergence for nonconvex optimization on manifolds. *IMA Jour. of Num. Anal.*, v. 39, n. 1, p. 1–33, 02 2018. ISSN 0272-4979. Available on: <https://doi.org/10.1093/imanum/drx080>. Cited on page 138.

BOUMAL, N.; MISHRA, B.; ABSIL, P.-A.; SEPULCHRE, R. Manopt, a Matlab toolbox for optimization on manifolds. *Journal of Machine Learning Research*, v. 15, n. 42, p. 1455–1459, 2014. Available on: <https://www.manopt.org>. Cited on page 137.

BOYD, S.; VANDENBERGHE, L. *Convex Optimization*. Cambridge University Press, 2004. Hardcover. ISBN 0521833787. Available on: <http://www.amazon.com/exec/obidos/redirect?tag=citeulike-20&path=ASIN/0521833787>. Cited on page 137.

BUDKA, K.; DESHPANDE, J.; THOTTAN, M. *Communication Networks for Smart Grids: Making Smart Grid Real*. [S.l.: s.n.], 2014. ISBN 9781447163015. Cited on page 73.

BUSH, S. F. Network Theory and Smart Grid Distribution Automation. *IEEE Journal on Selected Areas in Communications*, IEEE, v. 32, n. 7, p. 1451–1459, jul 2014. ISSN 0733-8716. Available on: <http://ieeexplore.ieee.org/lpdocs/epic03/wrapper.htm?arnumber=6840974>. Cited 2 times on page(s) 65 and 179.

CALDERARO, V.; HADJICOSTIS, C. N.; PICCOLO, A.; SIANO, P. Failure Identification in Smart Grids Based on Petri Net Modeling. *IEEE Transactions on Industrial Electronics*, IEEE, v. 58, n. 10, p. 4613–4623, oct 2011. ISSN 0278-0046. Available on: <http://ieeexplore.ieee.org/document/5704195/>. Cited 2 times on page(s) 68 and 183.

CARTA, D.; MUSCAS, C.; PEGORARO, P. A.; SULIS, S. Identification and Estimation of Harmonic Sources Based on Compressive Sensing. *IEEE Transactions on Instrumentation and Measurement*, IEEE, v. 68, n. 1, p. 95–104, jan 2019. ISSN 0018-9456. Cited on page 38.

CHAITANYA, B.; YADAV, A. An intelligent fault detection and classification scheme for distribution lines integrated with distributed generators. *Computers & Electrical Engineering*, Elsevier, v. 69, n. May, p. 28–40, jul 2018. ISSN 00457906. Available on: <https://doi.org/10.1016/j.compeleceng.2018.05.025https://linkinghub.elsevier.com/retrieve/pii/S0045790617331002>. Cited 5 times on page(s) 53, 77, 79, 83, and 181.

CHAKRABORTY, S.; DAS, S. Application of Smart Meters in High Impedance Fault Detection on Distribution Systems. *IEEE Transactions on Smart Grid*, v. 3053, n. c, p. 1–1, 2018. ISSN 1949-3053. Available on: <http://ieeexplore.ieee.org/document/8341819/>. Cited 6 times on page(s) 53, 75, 79, 81, 83, and 179.

CHAN, K.; BABIARZ, J.; BAKER, F. *Configuration Guidelines for DiffServ Service Classes*. [S.l.], 2006. 1–58 p. Available on: <https://tools.ietf.org/html/rfc4594https://www.rfc-editor.org/info/rfc4594http://tools.ietf.org/pdf/rfc4594.pdf>. Cited on page 115.

CHAUDHARI, B. S.; ZENNARO, M. *Introduction to low-power wide-area networks*. INC, 2020. 1–13 p. ISBN 9780128188804. Available on: <http://dx.doi.org/10.1016/B978-0-12-818880-4.00001-6>. Cited on page 114.

CHEN, K.; HU, J.; HE, J. Detection and Classification of Transmission Line Faults Based on Unsupervised Feature Learning and Convolutional Sparse Autoencoder. *IEEE Transactions on Smart Grid*, IEEE, v. 9, n. 3, p. 1–1, 2016. ISSN 1949-3053. Available on: <http://ieeexplore.ieee.org/document/7539352/>. Cited 5 times on page(s) 53, 77, 79, 83, and 181.

CHEN, L.; LI, S.; WANG, X. Quickest Fault Detection in Photovoltaic Systems. *IEEE Transactions on Smart Grid*, IEEE, v. 9, n. 3, p. 1–1, 2016. ISSN 1949-3053. Available on: <http://ieeexplore.ieee.org/document/7546863/>. Cited 5 times on page(s) 53, 77, 79, 83, and 181.

CHEN, M.; MIAO, Y.; HUMAR, I. *OPNET IoT Simulation*. [S.l.: s.n.], 2019. ISBN 9789813291690. Cited 2 times on page(s) 93 and 109.

CHEN, P.-Y.; YANG, S.; MCCANN, J. A. Distributed Real-Time Anomaly Detection in Networked Industrial Sensing Systems. *IEEE Transactions on Industrial Electronics*, IEEE, v. 62, n. 6, p. 3832–3842, jun 2015. ISSN 0278-0046. Available on: <http://ieeexplore.ieee.org/lpdocs/epic03/wrapper.htm?arnumber=6882174>. Cited 6 times on page(s) 53, 68, 78, 79, 83, and 184.

COMMISSION, F. E. R. *2019 Assessment of Demand Response and Advanced Metering*. [S.l.], 2019. Cited on page 60.

COSOVIC, M.; TSITSIMELIS, A.; VUKOBRATOVIC, D.; MATAMOROS, J.; ANTON-HARO, C. 5G Mobile Cellular Networks: Enabling Distributed State Estimation for Smart Grids. *IEEE Communications Magazine*, v. 55, n. 10, p. 62–69, 2017. ISSN 01636804. Cited 2 times on page(s) 35 and 184.

COSTA, F. B.; SOUZA, B. A.; BRITO, N. S. D.; SILVA, J. A. C. B.; SANTOS, W. C. Real-Time Detection of Transients Induced by High-Impedance Faults Based on the Boundary Wavelet Transform. *IEEE Transactions on Industry Applications*, IEEE, v. 51, n. 6, p. 5312–5323, nov 2015. ISSN 0093-9994. Available on: <http://ieeexplore.ieee.org/document/7110357/>. Cited 4 times on page(s) 77, 79, 83, and 181.

COUTO, M.; LOPES, J. P.; MOREIRA, C. Control strategies for Multi-Microgrids islanding operation through Smart Transformers. *Electric Power Systems Research*, Elsevier, v. 174, n. April, p. 105866, sep 2019. ISSN 03787796. Cited on page 49.

DAHLMAN, E.; PARKVALL, S.; SKÖLD, J. *5G NR: the Next Generation Wireless Access Technology*. 1. ed. Elsevier, 2018. 469 p. ISBN 9780128143230. Available on: <https://linkinghub.elsevier.com/retrieve/pii/C20170013472>. Cited on page 122.

DARYALAL, M.; SARLAK, M. Fast fault detection scheme for series-compensated lines during power swing. *International Journal of Electrical Power & Energy Systems*, Elsevier Ltd, v. 92, p. 230–244, nov 2017. ISSN 01420615. Available on: <http://dx.doi.org/10.1016/j.ijepes.2017.05.015https://linkinghub.elsevier.com/retrieve/pii/S014206151631955X>. Cited 5 times on page(s) 53, 77, 79, 83, and 181.

DAS, J. Effects of Harmonics. In: *Power System Harmonics and Passive Filter Designs*. Hoboken, NJ, USA: John Wiley & Sons, Inc, 2015. p. 331–378. ISBN 9781118861622. Cited 3 times on page(s) 27, 89, and 90.

DAS, J. Harmonic Distortion Limits According to Standards. In: *Power System Harmonics and Passive Filter Designs*. Hoboken, NJ, USA: John Wiley & Sons, Inc, 2015. p. 427–451. ISBN 9781118861622. Cited on page 91.

DAS, J. Power System Harmonics. In: *Power System Harmonics and Passive Filter Designs*. Hoboken, NJ, USA: John Wiley & Sons, Inc, 2015. p. 1–29. ISBN 9781118861622. Cited on page 89.

DAS, S.; SINGH, S. P.; PANIGRAHI, B. K. Transmission line fault detection and location using Wide Area Measurements. *Electric Power Systems Research*, Elsevier B.V., v. 151, p. 96–105, oct 2017. ISSN 03787796. Available on: <http://dx.doi.org/10.1016/j.epsr.2017.05.025https://linkinghub.elsevier.com/retrieve/pii/S0378779617302237>. Cited 4 times on page(s) 53, 76, 79, and 181.

DEPURU, S. S. S. R.; WANG, L.; DEVABHAKTUNI, V. Smart meters for power grid: Challenges, issues, advantages and status. *Renewable and Sustainable Energy Reviews*, Elsevier Ltd, v. 15, n. 6, p. 2736–2742, aug 2011. ISSN 13640321. Available on: <http://dx.doi.org/10.1016/j.rser.2011.02.039https://linkinghub.elsevier.com/retrieve/pii/S1364032111000876>. Cited 3 times on page(s) 58, 68, and 183.

DESHPANDE, J. G.; KIM, E.; THOTTAN, M. Differentiated services QoS in smart grid communication networks. *Bell Labs Technical Journal*, v. 16, n. 3, p. 61–81, dec 2011. ISSN 10897089. Available on: <http://ieeexplore.ieee.org/lpdocs/epic03/wrapper.htm?arnumber=6770300>. Cited on page 115.

DEVI, M. M.; GEETHANJALI, M.; DEVI, A. R. Fault localization for transmission lines with optimal Phasor Measurement Units. *Computers & Electrical Engineering*, Elsevier Ltd, v. 70, p. 163–178, aug 2018. ISSN 00457906. Available on: <https://doi.org/10.1016/j.compeleceng.2018.01.043https://linkinghub.elsevier.com/retrieve/pii/S0045790617307516>. Cited 5 times on page(s) 53, 78, 79, 83, and 180.

DHAR, S.; PATNAIK, R. K.; DASH, P. K. Fault Detection and Location of Photovoltaic Based DC Microgrid Using Differential Protection Strategy. *IEEE Transactions on Smart Grid*, IEEE, v. 9, n. 5, p. 4303–4312, sep 2018. ISSN 1949-3053. Available on: <https://ieeexplore.ieee.org/document/7820172/>. Cited 4 times on page(s) 53, 76, 79, and 181.

DHEND, M. H.; CHILE, R. H. Fault Diagnosis of Smart Grid Distribution System by Using Smart Sensors and Symlet Wavelet Function. *Journal of Electronic Testing*, Journal of Electronic Testing, v. 33, n. 3, p. 329–338, jun 2017. ISSN 0923-8174. Available on: <http://link.springer.com/10.1007/s10836-017-5658-9>. Cited 6 times on page(s) 53, 78, 79, 81, 83, and 180.

DHEND, M. H.; CHILE, R. H. Fault Diagnosis in Smart Distribution System Using Smart Sensors and Entropy. In: *Lecture Notes in Electrical Engineering*. [S.l.: s.n.], 2018. v. 435, p. 623–631. ISBN 9789811042850. Cited 3 times on page(s) 60, 68, and 180.

DILEEP, G. A survey on smart grid technologies and applications. *Renewable Energy*, v. 146, p. 2589–2625, feb 2020. ISSN 09601481. Available on: <https://linkinghub.elsevier.com/retrieve/pii/S0960148119312790>. Cited 2 times on page(s) 47 and 184.

DOBAKHSHARI, A. S.; RANJBAR, A. M. A Wide-Area Scheme for Power System Fault Location Incorporating Bad Data Detection. *IEEE Transactions on Power Delivery*, IEEE, v. 30, n. 2, p. 800–808, apr 2015. ISSN 0885-8977. Available on: <http://ieeexplore.ieee.org/document/7010971/>. Cited 4 times on page(s) 53, 76, 79, and 181.

ELKALASHY, N. I.; KAWADY, T. A.; ASHMAWY, M. G.; LEHTONEN, M. Transient selectivity for enhancing autonomous fault management in unearthed distribution networks with DFIG-based distributed generations. *Electric Power Systems Research*, Elsevier B.V., v. 140, p. 568–579, nov 2016. ISSN 03787796. Available on: <http://dx.doi.org/10.1016/j.epsr.2016.05.017https://linkinghub.elsevier.com/retrieve/pii/S0378779616301699>. Cited on page 182.

EMMANUEL, M.; RAYUDU, R. Communication technologies for smart grid applications: A survey. *Journal of Network and Computer Applications*, Elsevier, v. 74, p. 133–148, oct 2016. ISSN 10848045. Available on: <http://dx.doi.org/10.1016/j.jnca.2016.08.012https://linkinghub.elsevier.com/retrieve/pii/S1084804516301734>. Cited 4 times on page(s) 36, 60, 65, and 183.

FADUL, J. E.; HOPKINSON, K. M.; ANDEL, T. R.; SHEFFIELD, C. A. A Trust-Management Toolkit for Smart-Grid Protection Systems. *IEEE Transactions on Power Delivery*, v. 29, n. 4, p. 1768–1779, aug 2014. ISSN 0885-8977. Available on: <http://ieeexplore.ieee.org/document/6678325/>. Cited 2 times on page(s) 65 and 184.

FAHEEM, M.; SHAH, S.; BUTT, R.; RAZA, B.; ANWAR, M.; ASHRAF, M.; NGADI, M.; GUNGOR, V. Smart grid communication and information technologies in the perspective of Industry 4.0: Opportunities and challenges. *Computer Science Review*, Elsevier Inc., v. 30, p. 1–30, nov 2018. ISSN 15740137. Cited on page 85.

FARUGHIAN, A.; KUMPULAINEN, L.; KAUHANIEMI, K. Review of methodologies for earth fault indication and location in compensated and unearthed MV distribution networks. *Electric Power Systems Research*, Elsevier B.V., v. 154, p. 373–380, jan 2018. ISSN 03787796. Available on: <https://doi.org/10.1016/j.epsr.2017.09.006https://linkinghub.elsevier.com/retrieve/pii/S0378779617303735>. Cited 2 times on page(s) 43 and 180.

FERRAG, M. A.; BABAGHAYOU, M.; YAZICI, M. A. Cyber security for fog-based smart grid SCADA systems: Solutions and challenges. *Journal of Information Security and Applications*, Elsevier Ltd, v. 52, p. 102500, jun 2020. ISSN 22142126. Cited on page 65.

FERREIRA, E. F.; BARROS, J. D. Faults Monitoring System in the Electric Power Grid of Medium Voltage. *Procedia Computer Science*, Elsevier B.V., v. 130, p. 696–703, 2018. ISSN 18770509. Available on: <https://doi.org/10.1016/j.procs.2018.04.123https://linkinghub.elsevier.com/retrieve/pii/S187705091830485X>. Cited 2 times on page(s) 57 and 180.

FERREIRA, V.; ZANGHI, R.; FORTES, M.; SOTELO, G.; SILVA, R.; SOUZA, J.; GUIMARÃES, C.; GOMES, S. A survey on intelligent system application to fault diagnosis in electric power system transmission lines. *Electric Power Systems Research*, v. 136, p. 135–153, jul 2016. ISSN 03787796. Available on: <https://linkinghub.elsevier.com/retrieve/pii/S0378779616300086>. Cited 3 times on page(s) 43, 79, and 182.

FRANK, A. G.; MENDES, G. H.; AYALA, N. F.; GHEZZI, A. Servitization and Industry 4.0 convergence in the digital transformation of product firms: A business model innovation perspective. *Technological Forecasting and Social Change*, Elsevier, v. 141, n. January, p. 341–351, apr 2019. ISSN 00401625. Cited on page 85.

GAO, J.; XIAO, Y.; LIU, J.; LIANG, W.; CHEN, C. P. A survey of communication/networking in Smart Grids. *Future Generation Computer Systems*, Elsevier B.V., v. 28, n. 2, p. 391–404, feb 2012. ISSN 0167739X. Available on: <http://dx.doi.org/10.1016/j.future.2011.04.014https://linkinghub.elsevier.com/retrieve/pii/S0167739X11000653>. Cited 3 times on page(s) 63, 68, and 183.

GARANAYAK, P.; PANDA, G.; RAY, P. K. Harmonic estimation using RLS algorithm and elimination with improved current control technique based SAPF in a distribution network. *International Journal of Electrical Power and Energy Systems*, Elsevier Ltd, v. 73, p. 209–217, 2015. ISSN 01420615. Cited on page 37.

GHARAVI, H.; HU, B. Space-Time Approach for Disturbance Detection and Classification. *IEEE Transactions on Smart Grid*, IEEE, v. 9, n. 5, p. 5132–5140, sep 2018. ISSN 1949-3053. Available on: <https://ieeexplore.ieee.org/document/7875093/>. Cited 6 times on page(s) 53, 56, 75, 79, 83, and 179.

GHOSH, P.; EISELE, S.; DUBEY, A.; METELKO, M.; MADARI, I.; VOLGYESI, P.; KARSAI, G. Designing a decentralized fault-tolerant software framework for smart grids and its applications. *Journal of Systems Architecture*, Elsevier B.V., v. 109, n. March, p. 101759, oct 2020. ISSN 13837621. Cited on page 46.

GIANNAKIS, G. B.; KEKATOS, V.; GATSIS, N.; KIM, S.-J.; ZHU, H.; WOLLENBERG, B. F. Monitoring and Optimization for Power Grids: A Signal Processing Perspective. *IEEE Signal Processing Magazine*, v. 30, n. 5, p. 107–128, sep 2013. ISSN 1053-5888. Cited on page 92.

GIRGIS, A. A.; CHANG, W. B.; MAKRAM, E. B. A digital recursive measurement scheme for on-line tracking of power system harmonics. *IEEE Transactions on Power Delivery*, v. 6, n. 3, p. 1153–1160, 1991. ISSN 19374208. Cited on page 37.

GOPAKUMAR, P.; MALLIKAJUNA, B.; REDDY, M. J. B.; MOHANTA, D. K. Remote monitoring system for real time detection and classification of transmission line faults in a power grid using PMU measurements. *Protection and Control of Modern Power Systems*, Protection and Control of Modern Power Systems, v. 3, n. 1, p. 16, dec 2018. ISSN 2367-2617. Available on: <https://pcmp.springeropen.com/articles/10.1186/s41601-018-0089-x>. Cited 5 times on page(s) 53, 77, 79, 83, and 181.

GOPAKUMAR, P.; REDDY, M. J. B.; MOHANTA, D. K. Adaptive fault identification and classification methodology for smart power grids using synchronous phasor angle measurements. *IET Generation, Transmission & Distribution*, v. 9, n. 2, p. 133–145, jan 2015. ISSN 1751-8687. Available on: <http://digital-library.theiet.org/content/journals/10.1049/iet-gtd.2014.0024https://digital-library.theiet.org/content/journals/10.1049/iet-gtd.2014.0024>. Cited on page 180.

GOUDA, B.; ATZENI, I.; TöLLI, A. Distributed precoding design for cell-free massive mimo systems. In: *2020 IEEE 21st International Workshop on Signal Processing Advances in Wireless Communications (SPAWC)*. [S.l.: s.n.], 2020. p. 1–5. Cited 2 times on page(s) 38 and 133.

GRID, S.; DESIGNS, A. Smart Grid Architectural Designs. In: *Smart Grid*. Hoboken, NJ, USA: John Wiley & Sons, Inc., 2012. p. 1–15. ISBN 9781118156117. Cited on page 35.

GROHS, P.; HOLLER, M.; WEINMANN, A. *Handbook of Variational Methods for Nonlinear Geometric Data*. Cham: Springer International Publishing, 2020. 1–701 p. ISBN 978-3-030-31350-0. Available on: <http://link.springer.com/10.1007/978-3-030-31351-7>. Cited on page 134.

GUARRACINO, M. R.; IRPINO, A.; RADZIUKYNIENE, N.; VERDE, R. Supervised classification of distributed data streams for smart grids. *Energy Systems*, v. 3, n. 1, p. 95–108, mar 2012. ISSN 1868-3967. Available on: <http://link.springer.com/10.1007/s12667-012-0049-x>. Cited 2 times on page(s) 66 and 184.

GUNDUZ, M. Z.; DAS, R. Cyber-security on smart grid: Threats and potential solutions. *Computer Networks*, Elsevier B.V., v. 169, p. 107094, mar 2020. ISSN 13891286. Cited 4 times on page(s) 29, 64, 65, and 66.

GURSU, H. M.; KELLERER, W.; STEFANOVIC, C. On Throughput Maximization of Grant-Free Access with Reliability-Latency Constraints. In: *ICC 2019 - 2019 IEEE International Conference on Communications (ICC)*. IEEE, 2019. v. 2019-May, p. 1–7. ISBN 978-1-5386-8088-9. ISSN 15503607. Available on: <https://ieeexplore.ieee.org/document/8761270/>. Cited on page 120.

GURSU, H. M.; MOROGLU, M. C.; VILGELM, M.; CLAZZER, F.; KELLERER, W. System Level Integration of Irregular Repetition Slotted ALOHA for Industrial IoT in 5G New Radio. *IEEE International Symposium on Personal, Indoor and Mobile Radio Communications, PIMRC*, v. 2019-September, p. 2–8, 2019. Cited on page 120.

HABIBZADEH, H.; NUSSBAUM, B. H.; ANJOMSHOA, F.; KANTARCI, B.; SOYATA, T. A survey on cybersecurity, data privacy, and policy issues in cyber-physical system deployments in smart cities. *Sustainable Cities and Society*, Elsevier, v. 50, p. 101660, oct 2019. ISSN 2210-6707. Cited on page 67.

HAN, J.; CHOI, C.-s.; PARK, W.-k.; LEE, I.; KIM, S.-h. Smart home energy management system including renewable energy based on ZigBee and PLC. *IEEE Transactions on Consumer Electronics*, v. 60, n. 2, p. 198–202, may 2014. ISSN 0098-3063. Available on: <http://ieeexplore.ieee.org/document/6851994/>. Cited on page 66.

HAO, H.; WANG, Y.; SHI, Y.; LI, Z.; WU, Y.; LI, C. IoT-G: A Low-Latency and High-Reliability Private Power Wireless Communication Architecture for Smart Grid. In: *2019 IEEE International Conference on Communications, Control, and Computing Technologies for Smart Grids (SmartGridComm)*. [S.l.]: IEEE, 2019. p. 1–6. ISBN 978-1-5386-8099-5. Cited on page 72.

HARE, J.; SHI, X.; GUPTA, S.; BAZZI, A. Fault diagnostics in smart micro-grids: A survey. *Renewable and Sustainable Energy Reviews*, Elsevier, v. 60, p. 1114–1124, jul 2016. ISSN 13640321. Available on: <http://dx.doi.org/10.1016/j.rser.2016.01.122https://linkinghub.elsevier.com/retrieve/pii/S1364032116001775>. Cited 3 times on page(s) 47, 50, and 180.

HARROU, F.; SUN, Y.; TAGHEZOUIT, B.; SAIDI, A.; HAMLATI, M.-E. Reliable fault detection and diagnosis of photovoltaic systems based on statistical monitoring approaches. *Renewable Energy*, Elsevier Ltd, v. 116, p. 22–37, feb 2018. ISSN 09601481. Available on: <https://doi.org/10.1016/j.renene.2017.09.048https://linkinghub.elsevier.com/retrieve/pii/S0960148117309114>. Cited 5 times on page(s) 53, 77, 79, 83, and 181.

HASHEMI, S. M.; SANAYE-PASAND, M.; SHAHIDEHPOUR, M. Fault Detection During Power Swings Using the Properties of Fundamental Frequency Phasors. *IEEE Transactions on Smart Grid*, IEEE, v. 10, n. 2, p. 1–1, 2017. ISSN 1949-3053. Available on: <http://ieeexplore.ieee.org/document/8076915/>. Cited 5 times on page(s) 53, 77, 79, 83, and 181.

HE, M.; ZHANG, J. Fault Detection and Localization in Smart Grid: A Probabilistic Dependence Graph Approach. *2010 First IEEE International Conference on Smart Grid Communications*, IEEE, p. 43–48, 2010. Cited 5 times on page(s) 53, 76, 79, 83, and 179.

HE, M.; ZHANG, J. A Dependency Graph Approach for Fault Detection and Localization Towards Secure Smart Grid. *IEEE Transactions on Smart Grid*, IEEE, v. 2, n. 2, p. 342–351, jun 2011. ISSN 1949-3053. Available on: <http://ieeexplore.ieee.org/document/5767534/>. Cited 5 times on page(s) 53, 75, 79, 83, and 179.

HE, Q.; BLUM, R. S. Smart Grid Fault Detection Using Locally Optimum Unknown or Estimated Direction Hypothesis Test. *Energy Procedia*, v. 12, p. 170–179, 2011. ISSN 18766102. Available on: <http://dx.doi.org/10.1016/j.egypro.2011.10.024http://linkinghub.elsevier.com/retrieve/pii/S1876610211018509https://linkinghub.elsevier.com/retrieve/pii/S1876610211018509>. Cited 4 times on page(s) 53, 76, 79, and 179.

HONARMAND, M. E.; GHAZIZADEH, M. S.; HOSSEINNEZHAD, V.; SIANO, P. Reliability modeling of process-oriented smart monitoring in the distribution systems. *International Journal of Electrical Power & Energy Systems*, Elsevier, v. 109, n. September 2018, p. 20–28,

jul 2019. ISSN 01420615. Available on: <https://doi.org/10.1016/j.ijepes.2019.01.036https://linkinghub.elsevier.com/retrieve/pii/S0142061518330072>. Cited 2 times on page(s) 54 and 183.

HOVILA, P.; SYVÄLUOMA, P.; KOKKONIEMI-TARKKANEN, H.; HORSMANHEIMO, S.; BORENIUS, S.; LI, Z.; UUSITALO, M. 5G networks enabling new smart grid protection solutions. In: *CIRED 2019 Conference*. [S.l.: s.n.], 2019. p. 3–6. ISBN 978-2-9602415-0-1. ISSN 2032-9644. Cited 2 times on page(s) 70 and 72.

HOWELL, S.; REZGUI, Y.; HIPPOLYTE, J.-L.; JAYAN, B.; LI, H. Towards the next generation of smart grids: Semantic and holonic multi-agent management of distributed energy resources. *Renewable and Sustainable Energy Reviews*, Elsevier Ltd, v. 77, n. March, p. 193–214, sep 2017. ISSN 13640321. Available on: <http://dx.doi.org/10.1016/j.rser.2017.03.107https://linkinghub.elsevier.com/retrieve/pii/S1364032117304392>. Cited on page 184.

HU, B.; GHARAVI, H. A Fast Recursive Algorithm for Spectrum Tracking in Power Grid Systems. *IEEE Transactions on Smart Grid*, v. 10, n. 3, p. 2882–2891, may 2019. ISSN 1949-3053. Cited on page 38.

HU, J.; LIU, X.; WEN, Z.-W.; YUAN, Y.-X. A Brief Introduction to Manifold Optimization. *Journal of the Operations Research Society of China*, Operations Research Society of China, v. 8, n. 2, p. 199–248, jun 2020. ISSN 2194-668X. Available on: <https://doi.org/10.1007/s40305-020-00295-9http://link.springer.com/10.1007/s40305-020-00295-9>. Cited on page 134.

HU, Y.; DONNELLY, M.; HELMER, T.; TRAM, H.; MARTIN, K.; GOVINDARASU, M.; ULUSKI, R.; CIONI, M. Naspinet specification - an important step toward its implementation. In: *Proceedings of the 2010 43rd Hawaii International Conference on System Sciences*. Washington, DC, USA: IEEE Computer Society, 2010. (HICSS '10), p. 1–9. ISBN 978-0-7695-3869-3. Available on: <http://dx.doi.org/10.1109/HICSS.2010.284>. Cited on page 115.

HUANG, Y.; TANG, J.; CHENG, Y.; LI, H.; CAMPBELL, K. A.; HAN, Z. Real-Time Detection of False Data Injection in Smart Grid Networks: An Adaptive CUSUM Method and Analysis. *IEEE Systems Journal*, IEEE, v. 10, n. 2, p. 532–543, jun 2016. ISSN 1932-8184. Available on: <http://ieeexplore.ieee.org/lpdocs/epic03/wrapper.htm?arnumber=6949126>. Cited 8 times on page(s) 53, 63, 70, 78, 79, 83, 84, and 183.

HUANG, Y.-C.; SHIEH, S.-L.; HSU, Y.-P.; CHENG, H.-P. Iterative Collision Resolution for Slotted ALOHA with NOMA for Heterogeneous Devices. *IEEE Transactions on Communications*, v. 6778, n. c, p. 1–1, 2021. ISSN 0090-6778. Available on: <https://ieeexplore.ieee.org/document/9354838/>. Cited on page 114.

IBRAHIM, M. S.; DONG, W.; YANG, Q. Machine learning driven smart electric power systems: Current trends and new perspectives. *Applied Energy*, Elsevier, v. 272, n. May, p. 115237, aug 2020. ISSN 03062619. Available on: <https://doi.org/10.1016/j.apenergy.2020.115237https://linkinghub.elsevier.com/retrieve/pii/S0306261920307492>. Cited 2 times on page(s) 52 and 84.

IEC. *Electromagnetic Compatibility*. Geneva, CH, 1992–2016. Cited on page 90.

IEEE. Ieee standard communication delivery time performance requirements for electric power substation automation. *IEEE Std 1646-2004*, p. 1–36, Feb 2005. ISSN null. Cited on page 115.

IEEE. IEEE Recommended Practice and Requirements for Harmonic Control in Electric Power Systems. *IEEE Std 519-2014 (Revision of IEEE Std 519-1992)*, v. 2014, 2014. Cited 5 times on page(s) 27, 29, 89, 90, and 91.

IEEE Standard for A Smart Transducer Interface for Sensors and Actuators–Mixed-Mode Communication Protocols and Transducer Electronic Data Sheet (TEDS) Formats. *IEEE Std 1451.4-2004*, p. 1–454, 2004. Cited on page 54.

IEEE Standard for Electric Power Systems Communications-Distributed Network Protocol (DNP3). *IEEE Std 1815-2012 (Revision of IEEE Std 1815-2010)*, p. 1–821, 2012. Cited on page 54.

IEEE Standard Profile for Use of IEEE 1588 Precision Time Protocol in Power System Applications. *IEEE Std C37.238-2017 (Revision of IEEE Std C37.238-2011)*, p. 1–42, 2017. Cited on page 54.

IMOIZE, A. L.; ADEDEJI, O.; TANDIYA, N.; SHETTY, S. 6G Enabled Smart Infrastructure for Sustainable Society: Opportunities, Challenges, and Research Roadmap. *Sensors*, v. 21, n. 5, p. 1709, mar 2021. ISSN 1424-8220. Available on: <https://www.mdpi.com/1424-8220/21/5/1709>. Cited 2 times on page(s) 38 and 133.

INSTITUTE, E. P. R. Sensor Technologies for a Smart Transmission System. *An EPRI White Paper*, n. December, 2009. Cited on page 36.

IRFAN, M.; IQBAL, J.; IQBAL, A.; IQBAL, Z.; RIAZ, R. A.; MEHMOOD, A. Opportunities and challenges in control of smart grids – Pakistani perspective. *Renewable and Sustainable Energy Reviews*, Elsevier Ltd, v. 71, n. December 2014, p. 652–674, may 2017. ISSN 13640321. Cited on page 37.

ITU, I. T. U. G.114 - One-way transmission time. *ITU-T*, p. 1–20, 2003. Available on: <https://www.itu.int/rec/T-REC-G.114-200305-I/en>. Cited on page 115.

ITU, I. T. U. G.107 : The E-model: a computational model for use in transmission planning. *ITU-T*, 2014. Cited on page 115.

JARADAT, M.; JARRAH, M.; BOUSSELHAM, A.; JARARWEH, Y.; AL-AYYOUB, M. The Internet of Energy: Smart Sensor Networks and Big Data Management for Smart Grid. *Procedia Computer Science*, Elsevier Masson SAS, v. 56, n. 1, p. 592–597, 2015. ISSN 18770509. Cited 2 times on page(s) 66 and 183.

JIANG, H.; DAI, X.; GAO, D. W.; ZHANG, J. J.; ZHANG, Y.; MULJADI, E. Spatial-Temporal Synchrophasor Data Characterization and Analytics in Smart Grid Fault Detection, Identification, and Impact Causal Analysis. *IEEE Transactions on Smart Grid*, IEEE, v. 7, n. 5, p. 2525–2536, sep 2016. ISSN 1949-3053. Available on: <http://ieeexplore.ieee.org/document/7452675/>. Cited 5 times on page(s) 53, 76, 79, 83, and 179.

JIANG, H.; ZHANG, J. J.; GAO, W.; WU, Z. Fault Detection, Identification, and Location in Smart Grid Based on Data-Driven Computational Methods. *IEEE Transactions on Smart Grid*, IEEE, v. 5, n. 6, p. 2947–2956, nov 2014. ISSN 1949-3053. Available on: <http://ieeexplore.ieee.org/lpdocs/epic03/wrapper.htm?arnumber=6850055>. Cited 5 times on page(s) 53, 75, 79, 83, and 179.

JIANG, Y.; YIN, S.; KAYNAK, O. Data-Driven Monitoring and Safety Control of Industrial Cyber-Physical Systems: Basics and Beyond. *IEEE Access*, IEEE, v. 6, p. 47374–47384, 2018. ISSN 2169-3536. Available on: <https://ieeexplore.ieee.org/document/8444966/>. Cited 2 times on page(s) 58 and 180.

JIANG, Z.; LI, Z.; WU, N.; ZHOU, M. A Petri Net Approach to Fault Diagnosis and Restoration for Power Transmission Systems to Avoid the Output Interruption of Substations. *IEEE Systems Journal*, v. 12, n. 3, p. 2566–2576, sep 2018. ISSN 1932-8184. Available on: <https://ieeexplore.ieee.org/document/7891534/>. Cited 5 times on page(s) 53, 75, 79, 83, and 180.

Jinho Choi; LEE, K.; Yonggu Lee; Nam Yul Yu. Secure compressive random access for meter reading in smart grid using multi-antenna access point. In: *2016 IEEE International Conference on Smart Grid Communications (SmartGridComm)*. IEEE, 2016. p. 116–121. ISBN 978-1-5090-4075-9. Available on: <http://ieeexplore.ieee.org/document/7778748/>. Cited on page 114.

KANSAL, P.; BOSE, A. Bandwidth and latency requirements for smart transmission grid applications. *IEEE Transactions on Smart Grid*, IEEE, v. 3, n. 3, p. 1344–1352, 2012. ISSN 19493053. Cited on page 116.

KARUPONGSIRI, C.; MUNASINGHE, K. S.; JAMALIPOUR, A. A Novel Random Access Mechanism for Timely Reliable Communications for Smart Meters. *IEEE Transactions on Industrial Informatics*, v. 13, n. 6, p. 3256–3264, dec 2017. ISSN 1551-3203. Cited 2 times on page(s) 87 and 183.

KATIC, V. A.; STANISAVLJEVIC, A. M. Smart Detection of Voltage Dips Using Voltage Harmonics Footprint. *IEEE Transactions on Industry Applications*, v. 54, n. 5, p. 5331–5342, sep 2018. ISSN 0093-9994. Available on: <https://ieeexplore.ieee.org/document/8325307/>. Cited 7 times on page(s) 37, 53, 76, 79, 82, 83, and 179.

KAVEH, M.; MOSAVI, M. R. A Lightweight Mutual Authentication for Smart Grid Neighborhood Area Network Communications Based on Physically Unclonable Function. *IEEE Systems Journal*, IEEE, v. 14, n. 3, p. 4535–4544, sep 2020. ISSN 1932-8184. Available on: <https://ieeexplore.ieee.org/document/9036056/>. Cited on page 114.

KAY, S. M. *Fundamentals of Statistical Signal Processing: Estimation Theory*. Upper Saddle River, NJ, USA: Prentice-Hall, Inc., 1993. ISBN 0-13-345711-7. Cited on page 98.

KAZEMI, S.; LEHTONEN, M. Impact of smart subtransmission level fault current mitigation solutions on service reliability. *Electric Power Systems Research*, Elsevier B.V., v. 96, p. 9–15, mar 2013. ISSN 03787796. Available on: <http://dx.doi.org/10.1016/j.epsr.2012.09.003https://linkinghub.elsevier.com/retrieve/pii/S0378779612002854>. Cited on page 180.

KELLY, M.; ELBERG, R. *Executive Summary : Global AMI Tracker 4Q19 Smart Meter Projects : Project Tracking , Regional Analysis , and Market Shares*. [S.l.], 2020. Cited 3 times on page(s) 29, 60, and 61.

KENNEDY, K.; LIGHTBODY, G.; YACAMINI, R. An Adaptive Linear Combiner for On-Line tracking of Power System Harmonics. *IEEE Transactions on Power Systems*, IEEE, v. 11, n. 4, p. 752–757, 1996. ISSN 08858950. Cited on page 37.

KHALID, H.; SHOBOLE, A. Existing Developments in Adaptive Smart Grid Protection: A Review. *Electric Power Systems Research*, Elsevier, v. 191, n. September 2020, p. 106901, feb 2021. ISSN 03787796. Available on: <https://doi.org/10.1016/j.epsr.2020.106901https://linkinghub.elsevier.com/retrieve/pii/S0378779620306994>. Cited on page 113.

KHAZAEI, J.; FAN, L.; JIANG, W.; MANJURE, D. Distributed prony analysis for real-world pmu data. *Electric Power Systems Research*, v. 133, p. 113–120, 2016. ISSN 0378-7796. Available on: <https://www.sciencedirect.com/science/article/pii/S0378779615003855>. Cited on page 37.

KIMANI, K.; ODUOL, V.; LANGAT, K. Cyber security challenges for IoT-based smart grid networks. *International Journal of Critical Infrastructure Protection*, Elsevier B.V., v. 25, p. 36–49, 2019. ISSN 18745482. Cited on page 65.

KITZIG, J.; SCHLAGHECKE, S.; BUMILLER, G. Power quality measurement system with pmu functionality based on interpolated sampling. *IEEE Transactions on Instrumentation and Measurement*, v. 68, n. 4, p. 1014–1025, April 2019. Cited on page 92.

KORDESTANI, M.; SAIF, M. Data fusion for fault diagnosis in smart grid power systems. In: *2017 IEEE 30th Canadian Conference on Electrical and Computer Engineering (CCECE)*. IEEE, 2017. p. 1–6. ISBN 978-1-5090-5538-8. ISSN 08407789. Available on: <http://ieeexplore.ieee.org/document/7946717/>. Cited on page 180.

KOSMADAKIS, G.; KARELLAS, S.; KAKARAS, E. Renewable and Conventional Electricity Generation Systems: Technologies and Diversity of Energy Systems. In: MICHALENA, E.; HILLS, J. M. (Ed.). *Lecture Notes in Energy*. London: Springer London, 2013, (Lecture Notes in Energy, v. 23). p. 9–30. ISBN 978-1-4471-5594-2. Cited on page 50.

KOU, L.; LIU, C.; CAI, G.-w.; ZHANG, Z. Fault Diagnosis for Power Electronics Converters based on Deep Feedforward Network and Wavelet Compression. *Electric Power Systems Research*, Elsevier, v. 185, n. May, p. 106370, aug 2020. ISSN 03787796. Cited on page 49.

KOZIY, K.; Bei Gou; ASLAKSON, J. A Low-Cost Power-Quality Meter With Series Arc-Fault Detection Capability for Smart Grid. *IEEE Transactions on Power Delivery*, IEEE, v. 28, n. 3, p. 1584–1591, jul 2013. ISSN 0885-8977. Available on: <http://ieeexplore.ieee.org/document/6502756/>. Cited 6 times on page(s) 37, 53, 76, 79, 83, and 179.

KUMAR, D.; BHOWMIK, P. S. Artificial neural network and phasor data-based islanding detection in smart grid. *IET Generation, Transmission & Distribution*, v. 12, n. 21, p. 5843–5850, nov 2018. ISSN 1751-8687. Available on: <https://digital-library.theiet.org/content/journals/10.1049/iet-gtd.2018.6299>. Cited 6 times on page(s) 53, 78, 79, 82, 83, and 183.

KUO, C.-L.; CHEN, J.-L.; CHEN, S.-J.; KAO, C.-C.; YAU, H.-T.; LIN, C.-H. Photovoltaic Energy Conversion System Fault Detection Using Fractional-Order Color Relation Classifier in Microdistribution Systems. *IEEE Transactions on Smart Grid*, IEEE, v. 8, n. 3, p. 1163–1172, may 2017. ISSN 1949-3053. Available on: <http://ieeexplore.ieee.org/document/7312489/>. Cited 4 times on page(s) 53, 77, 79, and 181.

KUZLU, M.; PIPATTANASOMPORN, M.; RAHMAN, S. Communication network requirements for major smart grid applications in HAN, NAN and WAN. *Computer Networks*, v. 67, p. 74–88, jul 2014. ISSN 13891286. Available on: <https://linkinghub.elsevier.com/retrieve/pii/S1389128614001431>. Cited on page 67.

LALLE, Y.; FOURATI, L. C.; FOURATI, M.; BARRACA, J. P. A comparative study of lorawan, sigfox, and nb-iot for smart water grid. In: *2019 Global Information Infrastructure and Networking Symposium (GIIS)*. [S.l.: s.n.], 2019. p. 1–6. Cited on page 68.

LAVERTY, D. M.; MORROW, D. J.; BEST, R.; CROSSLEY, P. A. Telecommunications for Smart Grid: Backhaul solutions for the distribution network. In: *IEEE PES General Meeting*. IEEE, 2010. p. 1–6. ISBN 978-1-4244-6549-1. Available on: <http://ieeexplore.ieee.org/document/5589563/>. Cited on page 73.

LI, F.; MEMBER, S.; QIAO, W.; SUN, H. Smart Transmission Grid : Vision and Framework. v. 1, n. 2, p. 168–177, 2010. Cited on page 36.

LI, Y.; WU, L.; LI, J.; XIONG, L.; ZHANG, X.; SONG, G.; XU, Z. DC Fault Detection in MTDC Systems Based on Transient High-frequency of Current. *IEEE Transactions on Power Delivery*, IEEE, PP, n. c, p. 1–1, 2018. ISSN 0885-8977. Available on: <https://ieeexplore.ieee.org/document/8550761/>. Cited 4 times on page(s) 53, 76, 79, and 181.

LIANG, G.; LIU, G.; ZHAO, J.; LIU, Y.; GU, J.; SUN, G.; DONG, Z. Super Resolution Perception for Improving Data Completeness in Smart Grid State Estimation. *Engineering*, jun 2020. ISSN 20958099. Cited on page 86.

LIBONI, L. H.; FLAUZINO, R. A.; SILVA, I. N. da; COSTA, E. C. M.; SUETAKE, M. Efficient signal processing technique for information extraction and its applications in power systems. *Electric Power Systems Research*, Elsevier B.V., v. 141, p. 538–548, dec 2016. ISSN 03787796. Available on: <http://dx.doi.org/10.1016/j.epsr.2016.08.019https://linkinghub.elsevier.com/retrieve/pii/S0378779616303200>. Cited on page 184.

LIN, B. R.; HUANG, C. L. Analysis and implementation of zero voltage switching integrated buck-flyback converter. *International Review of Electrical Engineering*, v. 6, n. 7, p. 2846–2852, 2011. ISSN 18276660. Cited on page 37.

LIU, W.; LI, N.; JIANG, Z.; CHEN, Z.; WANG, S.; HAN, J.; ZHANG, X.; LIU, C. Smart Micro-grid System with Wind/PV/Battery. *Energy Procedia*, Elsevier B.V., v. 152, p. 1212–1217, 2018. ISSN 18766102. Cited on page 100.

LIU, Y.; DENG, Y.; ELKASHLAN, M.; NALLANATHAN, A.; KARAGIANNIDIS, G. K. Analyzing Grant-Free Access for URLLC Service. *IEEE Journal on Selected Areas in Communications*, v. 39, n. 3, p. 741–755, mar 2021. ISSN 0733-8716. Available on: <http://arxiv.org/abs/2002.07842https://ieeexplore.ieee.org/document/9174916/>. Cited on page 113.

LIVA, G. Graph-Based Analysis and Optimization of Contention Resolution Diversity Slotted ALOHA. *IEEE Transactions on Communications*, IEEE, v. 59, n. 2, p. 477–487, feb 2011. ISSN 0090-6778. Available on: <http://ieeexplore.ieee.org/document/61034/http://ieeexplore.ieee.org/document/5668922/>. Cited 5 times on page(s) 27, 114, 118, 119, and 120.

MADETI, S. R.; SINGH, S. A comprehensive study on different types of faults and detection techniques for solar photovoltaic system. *Solar Energy*, Elsevier, v. 158, n. August, p. 161–185, dec 2017. ISSN 0038092X. Available on: <https://doi.org/10.1016/j.solener.2017.08.069https://linkinghub.elsevier.com/retrieve/pii/S0038092X17307508>. Cited 3 times on page(s) 43, 68, and 181.

MADETI, S. R.; SINGH, S. Online fault detection and the economic analysis of grid-connected photovoltaic systems. *Energy*, Elsevier Ltd, v. 134, p. 121–135, sep 2017. ISSN 03605442. Available on: <http://dx.doi.org/10.1016/j.energy.2017.06.005https://linkinghub.elsevier.com/retrieve/pii/S0360544217309970>. Cited 4 times on page(s) 53, 77, 79, and 182.

MADUENO, G. C.; NIELSEN, J. J.; KIM, D. M.; PRATAS, N. K.; STEFANOVIC, C.; POPOVSKI, P. Assessment of LTE Wireless Access for Monitoring of Energy Distribution in the Smart Grid. *IEEE Journal on Selected Areas in Communications*, v. 34, n. 3, p. 675–688, mar 2016. ISSN 0733-8716. Cited 2 times on page(s) 87 and 183.

MAHELA, O. P.; SHAIK, A. G. Comprehensive overview of grid interfaced wind energy generation systems. *Renewable and Sustainable Energy Reviews*, Elsevier, v. 57, p. 260–281, may 2016. ISSN 13640321. Available on: <http://dx.doi.org/10.1016/j.rser.2015.12.048https://linkinghub.elsevier.com/retrieve/pii/S1364032115014318>. Cited on page 185.

MAHFOUZ, M. M.; EL-SAYED, M. A. Smart grid fault detection and classification with multi-distributed generation based on current signals approach. *IET Generation, Transmission & Distribution*, v. 10, n. 16, p. 4040–4047, dec 2016. ISSN 1751-8687. Available on: <https://digital-library.theiet.org/content/journals/10.1049/iet-gtd.2016.0364>. Cited 5 times on page(s) 53, 76, 79, 83, and 179.

MAHMOUD, M. S.; XIA, Y. Smart Grid Infrastructures. In: *Networked Control Systems*. Elsevier, 2019. p. 315–349. ISBN 9780128161197. Available on: <https://linkinghub.elsevier.com/retrieve/pii/B9780128161197000150>. Cited 3 times on page(s) 60, 63, and 184.

MANANDHAR, K.; CAO, X.; HU, F.; LIU, Y. Detection of Faults and Attacks Including False Data Injection Attack in Smart Grid Using Kalman Filter. *IEEE Transactions on Control of Network Systems*, IEEE, v. 1, n. 4, p. 370–379, dec 2014. ISSN 2325-5870. Available on: <http://ieeexplore.ieee.org/document/6897944/>. Cited 5 times on page(s) 53, 63, 76, 79, and 179.

MAR, A.; PEREIRA, P.; MARTINS, J. F. A survey on power grid faults and their origins: A contribution to improving power grid resilience. *Energies*, v. 12, n. 24, 2019. ISSN 19961073. Cited on page 182.

MARTINEZ-FIGUEROA, G. D. J.; MORINIGO-SOTELO, D.; ZORITA-LAMADRID, A. L.; MORALES-VELAZQUEZ, L.; ROMERO-TRONCOSO, R. D. J. FPGA-Based Smart Sensor for Detection and Classification of Power Quality Disturbances Using Higher Order Statistics. *IEEE Access*, v. 5, p. 14259–14274, 2017. ISSN 2169-3536. Available on:

<http://ieeexplore.ieee.org/document/7994604/>. Cited 7 times on page(s) 36, 53, 78, 79, 82, 83, and 183.

MATINKHAH, S. M.; SHAFIK, W. Smart Grid Empowered By 5G Technology. In: *2019 Smart Grid Conference (SGC)*. [S.l.]: IEEE, 2019. p. 1–6. ISBN 978-1-7281-5894-5. Cited on page 72.

MATTIOLI, R.; MOULINOS, K. *Communication Network Interdependencies in Smart Grids*. [S.l.], 2016. 1-54 p. Cited 2 times on page(s) 35 and 70.

MELO, I. D.; PEREIRA, J. L.; RIBEIRO, P. F.; VARIZ, A. M.; OLIVEIRA, B. C. Harmonic state estimation for distribution systems based on optimization models considering daily load profiles. *Electric Power Systems Research*, Elsevier, v. 170, n. April 2018, p. 303–316, may 2019. ISSN 03787796. Cited on page 37.

MENGALI, A.; De Gaudenzi, R.; STEFANOVIC, C. On the Modeling and Performance Assessment of Random Access with SIC. *IEEE Journal on Selected Areas in Communications*, v. 36, n. 2, p. 292–303, 2018. ISSN 07338716. Cited on page 120.

MESKINA, S. B.; DOGGAZ, N.; KHALGUI, M. New Solutions for Fault Detections and Dynamic Recoveries of Flexible Power Smart Grids. In: *Proceedings of the 11th International Conference on Informatics in Control, Automation and Robotics*. SCITEPRESS - Science and and Technology Publications, 2014. v. 01, n. i, p. 370–377. ISBN 978-989-758-039-0. Available on: <http://www.scitepress.org/DigitalLibrary/Link.aspx?doi=10.5220/0005091303700377>. Cited 5 times on page(s) 53, 75, 79, 83, and 179.

MILIOUDIS, A. N.; ANDREOU, G. T.; LABRIDIS, D. P. Detection and Location of High Impedance Faults in Multiconductor Overhead Distribution Lines Using Power Line Communication Devices. *IEEE Transactions on Smart Grid*, IEEE, v. 6, n. 2, p. 894–902, mar 2015. ISSN 1949-3053. Available on: <http://ieeexplore.ieee.org/document/6954542/>. Cited 6 times on page(s) 53, 68, 75, 79, 83, and 179.

MISHRA, D. P.; SAMANTARAY, S. R.; JOOS, G. A combined wavelet and data-mining based intelligent protection scheme for microgrid. *IEEE Transactions on Smart Grid*, IEEE, v. 7, n. 5, p. 2295–2304, 2016. ISSN 19493053. Cited 5 times on page(s) 53, 75, 79, 83, and 185.

MISHRA, R. C.; DEOGHARE, P. M.; BHALE, C.; LANJEWAR, S. Wavelet based transmission line fault classification and location. In: *2014 International Conference on Smart Electric Grid (ISEG)*. IEEE, 2014. p. 1–5. ISBN 978-1-4799-4103-2. Available on: <http://ieeexplore.ieee.org/document/7005616/>. Cited 5 times on page(s) 53, 78, 79, 83, and 182.

MOGHADDASS, R.; WANG, J. A Hierarchical Framework for Smart Grid Anomaly Detection Using Large-Scale Smart Meter Data. *IEEE Transactions on Smart Grid*, IEEE, v. 9, n. 6, p. 5820–5830, nov 2018. ISSN 1949-3053. Available on: <https://ieeexplore.ieee.org/document/7908945/>. Cited 7 times on page(s) 53, 61, 78, 79, 80, 83, and 183.

MOHARM, K. State of the art in big data applications in microgrid: A review. *Advanced Engineering Informatics*, v. 42, n. June, p. 100945, oct 2019. ISSN 14740346. Cited on page 36.

MOMOH, J. Smart Grid Communications and Measurement Technology. In: *Smart Grid*. Hoboken, NJ, USA: John Wiley & Sons, Inc., 2012. p. 16–28. ISBN 9781118156117. Cited on page 36.

MONADI, M.; GAVRILUTA, C.; LUNA, A.; CANDELA, J. I.; RODRIGUEZ, P. Centralized Protection Strategy for Medium Voltage DC Microgrids. *IEEE Transactions on Power Delivery*, IEEE, v. 32, n. 1, p. 430–440, feb 2017. ISSN 0885-8977. Available on: <http://ieeexplore.ieee.org/document/7543496/>. Cited on page 185.

MORAIS, A. P. de; BRETAS, A. S.; BRAHMA, S.; CARDOSO, G. High-sensitivity stator fault protection for synchronous generators: A time-domain approach based on mathematical morphology. *International Journal of Electrical Power & Energy Systems*, Elsevier, v. 99, n. January, p. 419–425, jul 2018. ISSN 01420615. Cited on page 50.

MOROGLU, M. C.; GURSU, H. M.; CLAZZER, F.; KELLERER, W. Short Frame Length Approximation for IRSA. *IEEE Wireless Communications Letters*, v. 2337, n. c, p. 10–13, 2020. ISSN 21622345. Cited on page 114.

MUNARI, A.; FROLOV, A. Average Age of Information of Irregular Repetition Slotted ALOHA. In: *GLOBECOM 2020 - 2020 IEEE Global Communications Conference*. IEEE, 2020. p. 1–6. ISBN 978-1-7281-8298-8. Available on: <http://arxiv.org/abs/2004.01998https://ieeexplore.ieee.org/document/9322355/>. Cited on page 114.

MUNSHI, A. A.; MOHAMED, Y. A.-R. I. Big data framework for analytics in smart grids. *Electric Power Systems Research*, Elsevier B.V., v. 151, p. 369–380, oct 2017. ISSN 03787796. Available on: <http://dx.doi.org/10.1016/j.epsr.2017.06.006https://linkinghub.elsevier.com/retrieve/pii/S0378779617302559>. Cited 2 times on page(s) 52 and 184.

NAGANANDA, K. G.; KISHORE, S.; BLUM, R. S. A PMU Scheduling Scheme for Transmission of Synchrophasor Data in Electric Power Systems. *IEEE Transactions on Smart Grid*, IEEE, v. 6, n. 5, p. 2519–2528, sep 2015. ISSN 1949-3053. Available on: <http://ieeexplore.ieee.org/document/7017571/>. Cited 5 times on page(s) 53, 77, 79, 83, and 182.

NASPI. *Time Synchronization in the Electric Power System*. [S.l.], 2017. 59 p. Cited 2 times on page(s) 29 and 110.

NASPI. *Categorizing Phasor Measurement Units by Application Data Requirements*. [S.l.], 2018. 7 p. Cited 2 times on page(s) 29 and 110.

NAVARRO-ORTIZ, J.; ROMERO-DIAZ, P.; SENDRA, S.; AMEIGEIRAS, P.; RAMOS-MUNOZ, J. J.; LOPEZ-SOLER, J. M. A Survey on 5G Usage Scenarios and Traffic Models. *IEEE Communications Surveys & Tutorials*, IEEE, v. 22, n. 2, p. 905–929, 2020. ISSN 1553-877X. Available on: <https://ieeexplore.ieee.org/document/8985528/>. Cited on page 119.

NEGARI, S.; XU, D. Fault calculations in AC-DC hybrid systems. In: *IECON 2017 - 43rd Annual Conference of the IEEE Industrial Electronics Society*. IEEE, 2017. p. 1146–1153. ISBN 978-1-5386-1127-2. Available on: <http://ieeexplore.ieee.org/document/8216196/>. Cited on page 182.

NGUYEN, D. T.; SHEN, Y.; THAI, M. T. Detecting Critical Nodes in Interdependent Power Networks for Vulnerability Assessment. *IEEE Transactions on Smart Grid*, IEEE, v. 4, n. 1, p. 151–159, mar 2013. ISSN 1949-3053. Available on: <http://ieeexplore.ieee.org/document/6407159/>. Cited on page 185.

NGUYEN, V.-G.; GRINNEMO, K.-J.; TAHERI, J.; BRUNSTROM, A. A Deployable Containerized 5G Core Solution for Time Critical Communication in Smart Grid. In: *2020 23rd Conference on Innovation in Clouds, Internet and Networks and Workshops (ICIN)*. [S.l.]: IEEE, 2020. p. 153–155. ISBN 978-1-7281-5127-4. Cited on page 71.

NTALAMPIRAS, S. Fault Diagnosis for Smart Grids in Pragmatic Conditions. *IEEE Transactions on Smart Grid*, IEEE, v. 9, n. 3, p. 1–1, 2016. ISSN 1949-3053. Available on: <http://ieeexplore.ieee.org/document/7556303/>. Cited 2 times on page(s) 65 and 180.

NWANKPA, C.; SHAHIDEHPOUR, S. Colored noise modelling in the reliability evaluation of electric power systems. *Applied Mathematical Modelling*, v. 14, n. 7, p. 338–351, jul 1990. ISSN 0307904X. Available on: <https://linkinghub.elsevier.com/retrieve/pii/0307904X9090087L>. Cited 2 times on page(s) 93 and 109.

OINAGA, M.; OGATA, S.; ISHIBASHI, K. Received-Power-Aware Frameless ALOHA for Grant-Free Non-Orthogonal Multiple Access. In: *2020 International Conference on Information Networking (ICOIN)*. IEEE, 2020. v. 2020-Janua, p. 282–285. ISBN 978-1-7281-4199-2. ISSN 19767684. Available on: <https://ieeexplore.ieee.org/document/9016466/>. Cited on page 114.

OTUOZE, A. O.; MUSTAFA, M. W.; LARIK, R. M. Smart grids security challenges: Classification by sources of threats. *Journal of Electrical Systems and Information Technology*, Electronics Research Institute (ERI), v. 5, n. 3, p. 468–483, dec 2018. ISSN 23147172. Cited on page 64.

P., R.; N.A., S.; B., M.; M., J. B. R.; D.K., M. Robust fault analysis in transmission lines using Synchrophasor measurements. *Protection and Control of Modern Power Systems*, Protection and Control of Modern Power Systems, v. 3, n. 1, p. 14, dec 2018. ISSN 2367-2617. Available on: <https://pcmp.springeropen.com/articles/10.1186/s41601-018-0082-4>. Cited on page 182.

PANDA, G.; KUMAR, P.; PUHAN, P. S.; DASH, S. K. Novel schemes used for estimation of power system harmonics and their elimination in a three-phase distribution system. *International Journal of Electrical Power and Energy Systems*, Elsevier Ltd, v. 53, p. 842–856, 2013. ISSN 01420615. Cited on page 37.

PARIKH, P.; VOLOH, I.; MAHONY, M. Distributed fault detection, isolation, and restoration (FDIR) technique for smart distribution system. In: *2013 66th Annual Conference for Protective Relay Engineers*. IEEE, 2013. p. 172–176. ISBN 978-1-4799-0119-7. Available on: <http://ieeexplore.ieee.org/document/6822035/>. Cited 4 times on page(s) 53, 76, 79, and 180.

PASDAR, A. M.; SOZER, Y.; HUSAIN, I. Detecting and Locating Faulty Nodes in Smart Grids Based on High Frequency Signal Injection. *IEEE Transactions on Smart Grid*, IEEE, v. 4, n. 2, p. 1067–1075, jun 2013. ISSN 1949-3053. Available on: <http://ieeexplore.ieee.org/document/6497543/>. Cited 6 times on page(s) 53, 68, 76, 79, 83, and 180.

PERTL, M.; DOUGLASS, P. J.; HEUSSEN, K.; KOK, K. Validation of a robust neural real-time voltage estimator for active distribution grids on field data. *Electric Power Systems Research*, Elsevier B.V., v. 154, p. 182–192, jan 2018. ISSN 03787796. Available on: <https://doi.org/10.1016/j.epsr.2017.08.016https://linkinghub.elsevier.com/retrieve/pii/S0378779617303346>. Cited 2 times on page(s) 58 and 185.

PHADKE, A. Synchronized phasor measurements in power systems. *IEEE Computer Applications in Power*, v. 6, n. 2, p. 10–15, apr 1993. ISSN 0895-0156. Available on: <http://ieeexplore.ieee.org/document/207465/>. Cited on page 57.

PHADKE, A.; THORP, J. *Synchronized Phasor Measurements and Their Applications*. Boston, MA: Springer US, 2008. v. 2. (Power Electronics and Power Systems, v. 2). ISSN 2196-3185. ISBN 978-0-387-76535-8. Cited on page 106.

PHADKE, A. G.; WALL, P.; DING, L.; TERZIJA, V. Improving the performance of power system protection using wide area monitoring systems. *Journal of Modern Power Systems and Clean Energy*, Springer Berlin Heidelberg, v. 4, n. 3, p. 319–331, 2016. ISSN 21965420. Cited on page 54.

PHAN, S. K.; CHEN, C. Big Data and Monitoring the Grid. In: *The Power Grid*. Elsevier, 2017. p. 253–285. ISBN 9780081009529. Available on: <http://dx.doi.org/10.1016/B978-0-12-805321-8.00009-4https://linkinghub.elsevier.com/retrieve/pii/B9780128053218000094>. Cited 4 times on page(s) 52, 60, 63, and 183.

PISANI; GIANNUZZI. Wide area measurement system: the enabler for smarter transmission grids. In: *Wide area monitoring, protection and control systems: the enabler for smarter grids*. Institution of Engineering and Technology, 2016. p. 1–18. Available on: <https://digital-library.theiet.org/content/books/10.1049/pbpo073e{_}>. Cited on page 54.

PRASAD, A.; Belwin Edward, J.; RAVI, K. A review on fault classification methodologies in power transmission systems: Part—I. *Journal of Electrical Systems and Information Technology*, Electronics Research Institute (ERI), v. 5, n. 1, p. 48–60, may 2018. ISSN 23147172. Available on: <http://dx.doi.org/10.1016/j.jesit.2017.01.004https://linkinghub.elsevier.com/retrieve/pii/S2314717217300065>. Cited on page 182.

QI, P.; JOVANOVIC, S.; LEZAMA, J.; SCHWEITZER, P. Discrete wavelet transform optimal parameters estimation for arc fault detection in low-voltage residential power networks. *Electric Power Systems Research*, Elsevier B.V., v. 143, p. 130–139, feb 2017. ISSN 03787796. Available on: <http://dx.doi.org/10.1016/j.epsr.2016.10.008https://linkinghub.elsevier.com/retrieve/pii/S0378779616304059>. Cited 5 times on page(s) 53, 77, 79, 83, and 182.

RAHMAN, M.; ISHERWOOD, N.; OO, A. Multi-agent based coordinated protection systems for distribution feeder fault diagnosis and reconfiguration. *International Journal of Electrical Power & Energy Systems*, v. 97, n. March 2017, p. 106–119, apr 2018. ISSN 01420615. Available on: <https://linkinghub.elsevier.com/retrieve/pii/S0142061517306968>. Cited 2 times on page(s) 68 and 181.

RAHMAN, M.; MAHMUD, M.; POTA, H.; HOSSAIN, M. A multi-agent approach for enhancing transient stability of smart grids. *International Journal of Electrical Power*

& Energy Systems, Elsevier Ltd, v. 67, p. 488–500, may 2015. ISSN 01420615. Available on: <http://dx.doi.org/10.1016/j.ijepes.2014.12.038https://linkinghub.elsevier.com/retrieve/pii/S0142061514007650>. Cited 5 times on page(s) 53, 75, 79, 83, and 184.

RAMATRYANA, I. N. A.; ANWAR, K. Raptor decoding for high overloaded wireless super-dense networks. *2017 8th International Workshop on Signal Design and Its Applications in Communications, IWSDA 2017*, p. 29–33, 2017. Cited on page 124.

RANA, M. M.; XIANG, W.; WANG, E. Smart grid state estimation and stabilisation. *International Journal of Electrical Power & Energy Systems*, Elsevier, v. 102, n. March, p. 152–159, nov 2018. ISSN 01420615. Cited on page 36.

RAWAT, S.; PATEL, A.; CELESTINO, J.; SANTOS, A. L. M. dos. A dominance based rough set classification system for fault diagnosis in electrical smart grid environments. *Artificial Intelligence Review*, Springer Netherlands, v. 46, n. 3, p. 389–411, oct 2016. ISSN 0269-2821. Available on: <http://link.springer.com/10.1007/s10462-016-9468-8>. Cited 6 times on page(s) 53, 57, 76, 79, 83, and 180.

RECAYTE, E.; MUNARI, A.; CLAZZER, F. Grant-Free Access: Machine Learning for Detection of Short Packets. In: *2020 10th Advanced Satellite Multimedia Systems Conference and the 16th Signal Processing for Space Communications Workshop (ASMS/SPSC)*. IEEE, 2020. p. 1–7. ISBN 978-1-7281-5794-8. Available on: <http://arxiv.org/abs/2008.10956https://ieeexplore.ieee.org/document/9268917/>. Cited on page 114.

REHMAN, H. U.; BELLILI, F.; MEZGHANI, A.; HOSSAIN, E. Joint active and passive beamforming design for irs-assisted multi-user mimo systems: A vamp-based approach. *IEEE Transactions on Communications*, IEEE, v. 69, n. 10, p. 6734–6749, 2021. Cited on page 38.

REHMAN, H. U.; BELLILI, F.; MEZGHANI, A.; HOSSAIN, E. Joint active and passive beamforming design for irs-assisted multi-user mimo systems: A vamp-based approach. *IEEE Transactions on Communications*, IEEE, v. 69, n. 10, p. 6734–6749, 2021. Cited on page 133.

REZKALLAH, M.; CHANDRA, A.; HAMADI, A.; IBRAHIM, H.; GHANDOUR, M. Power Quality in Smart Grids. In: *Pathways to a Smarter Power System*. [S.l.]: Elsevier, 2019. p. 225–245. ISBN 9780081025925. Cited on page 37.

RIBEIRO, P. F.; DUQUE, C. A.; RIBEIRO, P. M.; CERQUEIRA, A. S. *Power Systems Signal Processing For Smart Grids*. Chichester, United Kingdom: John Wiley and Sons Ltd, 2013. 1–442 p. ISBN 9781118639283. Cited on page 92.

RIDHAWI, I. A.; OTOUM, S.; ALOQAILY, M.; JARARWEH, Y.; BAKER, T. Providing secure and reliable communication for next generation networks in smart cities. *Sustainable Cities and Society*, Elsevier, v. 56, n. February, p. 102080, may 2020. ISSN 22106707. Cited 2 times on page(s) 68 and 183.

RIVAS, A. E. L.; SILVA, N. da; ABRÃO, T. Adaptive current harmonic estimation under fault conditions for smart grid systems. *Electric Power Systems Research*, v. 183, n. February, p. 106276, jun 2020. ISSN 03787796. Cited on page 87.

ROBSON, S.; HADDAD, A.; GRIFFITHS, H. Fault Location on Branched Networks Using a Multiended Approach. *IEEE Transactions on Power Delivery*, v. 29, n. 4, p. 1955–1963, aug 2014. ISSN 0885-8977. Available on: <http://ieeexplore.ieee.org/document/6840856/>. Cited 5 times on page(s) 53, 78, 79, 83, and 180.

RODRIGUEZ-CALVO, A.; COSSENT, R.; FRÍAS, P. Scalability and replicability analysis of large-scale smart grid implementations: Approaches and proposals in Europe. *Renewable and Sustainable Energy Reviews*, Elsevier Ltd, v. 93, n. May, p. 1–15, oct 2018. ISSN 13640321. Cited on page 37.

SADEGHKHANI, I.; Hamedani Golshan, M. E.; MEHRIZI-SANI, A.; GUERRERO, J. M.; KETABI, A. Transient Monitoring Function-Based Fault Detection for Inverter-Interfaced Microgrids. *IEEE Transactions on Smart Grid*, IEEE, v. 9, n. 3, p. 1–1, 2016. ISSN 1949-3053. Available on: <http://ieeexplore.ieee.org/document/7562364/>. Cited 2 times on page(s) 80 and 181.

SAHA, S.; SUKUMARAN, V. B.; MURTHY, C. R. On the Minimum Average Age of Information in IRSA for Grant-free mMTC. *IEEE Journal on Selected Areas in Communications*, v. 8716, n. c, p. 1–1, 2021. ISSN 0733-8716. Available on: <https://ieeexplore.ieee.org/document/9376691/>. Cited on page 114.

SAHNER, R.; TRIVEDI, K.; PULIAFITO, A. Reliability and Availability Models. In: *Performance and Reliability Analysis of Computer Systems*. Boston, MA: Springer US, 1996. p. 27–46. Available on: <http://link.springer.com/10.1007/978-1-4615-2367-3_2>. Cited on page 117.

SALEEM, Y.; CRESPI, N.; REHMANI, M. H.; COPELAND, R. Internet of Things-Aided Smart Grid: Technologies, Architectures, Applications, Prototypes, and Future Research Directions. *IEEE Access*, v. 7, p. 62962–63003, 2019. ISSN 2169-3536. Available on: <https://ieeexplore.ieee.org/document/8701687/>. Cited 4 times on page(s) 35, 36, 114, and 184.

SALEH, K. A.; HOOSHYAR, A.; EL-SAADANY, E. F. Hybrid Passive-Overcurrent Relay for Detection of Faults in Low-Voltage DC Grids. *IEEE Transactions on Smart Grid*, IEEE, v. 8, n. 3, p. 1129–1138, may 2017. ISSN 1949-3053. Available on: <http://ieeexplore.ieee.org/document/7283661/>. Cited 5 times on page(s) 53, 77, 79, 83, and 182.

SALEH, K. A.; HOOSHYAR, A.; EL-SAADANY, E. F. Ultra-High-Speed Travelling-Wave-Based Protection Scheme for Medium-Voltage DC Microgrids. *IEEE Transactions on Smart Grid*, IEEE, v. 10, n. 2, p. 1–1, 2017. ISSN 1949-3053. Available on: <http://ieeexplore.ieee.org/document/8086193/>. Cited 5 times on page(s) 53, 76, 79, 83, and 181.

SANTIS, E. D.; LIVI, L.; SADEGHIAN, A.; RIZZI, A. Modeling and recognition of smart grid faults by a combined approach of dissimilarity learning and one-class classification. *Neurocomputing*, Elsevier Inc., v. 170, n. 1, p. 368–383, dec 2015. ISSN 09252312. Available on: <http://dx.doi.org/10.1016/B978-0-12-811968-6.00014-0http://linkinghub.elsevier.com/retrieve/pii/S0925231215008632https://linkinghub.elsevier.com/retrieve/pii/S0925231215008632>. Cited on page 180.

SANTIS, E. D.; RIZZI, A.; SADEGHIAN, A. A cluster-based dissimilarity learning approach for localized fault classification in Smart Grids. *Swarm and Evolutionary Computation*, Elsevier, v. 39, n. January 2017, p. 267–278, apr 2018. ISSN 22106502. Available on: <http://dx.doi.org/10.1016/j.swevo.2017.10.007https://linkinghub.elsevier.com/retrieve/pii/S2210650217300238>. Cited 5 times on page(s) 53, 75, 79, 83, and 180.

SANTO, K. G. D.; KANASHIRO, E.; SANTO, S. G. D.; SAIDEL, M. A. A review on smart grids and experiences in Brazil. *Renewable and Sustainable Energy Reviews*, Elsevier Ltd, v. 52, p. 1072–1082, dec 2015. ISSN 13640321. Available on: <https://linkinghub.elsevier.com/retrieve/pii/S1364032115008291>. Cited on page 184.

SAYED, B. T.; DEKDOUK, A.; ASHRAF, Y. A prototype to detect and efficiently rectify faults in a smart power grid using an Intelligent Knowledge Based Information System. *Journal of Theoretical and Applied Information Technology*, v. 95, n. 1, p. 125–138, 2017. ISSN 18173195. Cited on page 180.

SEUBERLICH, T.; DOHERR, M. G.; BOTTERON, C.; NICOLIER, A.; SCHWERMER, H.; BRÜNISHOLZ, H.; HEIM, D.; ZURBRIGGEN, A. The Effects of Power System Harmonics on Power System Equipment and Loads. *IEEE Transactions on Power Apparatus and Systems*, PAS-104, n. 9, p. 2555–2563, jan 1985. ISSN 0018-9510. Cited 3 times on page(s) 27, 89, and 90.

SEYEDI, Y.; KARIMI, H. Coordinated Protection and Control Based on Synchrophasor Data Processing in Smart Distribution Networks. *IEEE Transactions on Power Systems*, IEEE, v. 33, n. 1, p. 634–645, jan 2018. ISSN 0885-8950. Available on: <http://ieeexplore.ieee.org/document/7934361/>. Cited on page 184.

SEYEDI, Y.; KARIMI, H.; GRIJALVA, S. Distributed Generation Monitoring for Hierarchical Control Applications in Smart Microgrids. *IEEE Transactions on Power Systems*, IEEE, v. 32, n. 3, p. 2305–2314, may 2017. ISSN 0885-8950. Available on: <http://ieeexplore.ieee.org/document/7569006/>. Cited 2 times on page(s) 54 and 184.

SEYEDI, Y.; KARIMI, H.; GUERRERO, J. M. Centralized Disturbance Detection in Smart Microgrids With Noisy and Intermittent Synchrophasor Data. *IEEE Transactions on Smart Grid*, v. 8, n. 6, p. 2775–2783, nov 2017. ISSN 1949-3053. Available on: <http://ieeexplore.ieee.org/document/7438902/>. Cited 5 times on page(s) 53, 78, 79, 83, and 183.

SHAHINZADEH, H.; MIRHEDAYATI, A.-s.; SHANEH, M.; NAFISI, H.; GHAREHPETIAN, G. B.; MORADI, J. Role of joint 5g-iot framework for smart grid interoperability enhancement. In: *2020 15th International Conference on Protection and Automation of Power Systems (IPAPS)*. [S.l.: s.n.], 2020. p. 12–18. Cited on page 113.

SHAO, S.; GUO, S.; QIU, X. Distributed Fault Detection Based on Credibility and Cooperation for WSNs in Smart Grids. *Sensors*, v. 17, n. 5, p. 983, apr 2017. ISSN 1424-8220. Available on: <http://www.mdpi.com/1424-8220/17/5/983>. Cited 5 times on page(s) 53, 76, 79, 83, and 180.

SHOKROLLAHI, A. Raptor codes. *IEEE Transactions on Information Theory*, v. 52, n. 6, p. 2551–2567, jun 2006. ISSN 0018-9448. Available on: <http://www.nowpublishers.com/article/Details/CIT-060http://ieeexplore.ieee.org/document/1638543/>. Cited on page 124.

SHRESTHA, M.; JOHANSEN, C.; NOLL, J.; ROVERSO, D. A Methodology for Security Classification applied to Smart Grid Infrastructures. *International Journal of Critical Infrastructure Protection*, Elsevier B.V., v. 28, p. 100342, mar 2020. ISSN 18745482. Cited on page 65.

SILVEIRA, A. M.; ARAÚJO, R. E. A new approach for the diagnosis of different types of faults in dc–dc power converters based on inversion method. *Electric Power Systems Research*, Elsevier, v. 180, n. February 2019, p. 106103, mar 2020. ISSN 03787796. Cited on page 49.

SMART Grid. 2013. Available on: <http://smartgridstandardsmap.com/>. Cited 2 times on page(s) 27 and 69.

SOCIETY, I. C. *IEEE Standard for Low Rate Wireless Networks*. [S.l.]: IEEE, 2020. v. 2020. ISBN 9781504466899. Cited on page 115.

SONG, E. Y.; FITZPATRICK, G. J.; LEE, K. B. Smart Sensors and Standard-Based Interoperability in Smart Grids. *IEEE Sensors Journal*, v. 17, n. 23, p. 7723–7730, dec 2017. ISSN 1530-437X. Cited on page 51.

SRIDHARAN, K.; BABU, B. C.; KANNAN, P. M.; KRITHIKA, V. Modelling of Sliding Goertzel DFT (SGDFT) Based Phase Detection System for Grid Synchronization under Distorted Grid Conditions. *Procedia Technology*, v. 21, p. 430–437, 2015. ISSN 22120173. Cited on page 37.

STANOJEVIC, V. A.; PRESTON, G.; TERZIJA, V. Synchronised Measurements Based Algorithm for Long Transmission Line Fault Analysis. *IEEE Transactions on Smart Grid*, IEEE, v. 9, n. 5, p. 4448–4457, sep 2018. ISSN 1949-3053. Cited on page 37.

SUN, J.; LIU, R.; WANG, Y.; CHEN, C. W. Irregular Repetition Slotted ALOHA with Priority (P-IRSA). In: *2016 IEEE 83rd Vehicular Technology Conference (VTC Spring)*. IEEE, 2016. v. 2016-July, p. 1–5. ISBN 978-1-5090-1698-3. ISSN 15502252. Available on: <http://ieeexplore.ieee.org/document/7504302/>. Cited 6 times on page(s) 53, 78, 79, 83, 127, and 185.

SUNITA, T. N.; Bharathi Malakreddy, A. A Survey of MTC Traffic Models in Cellular Network. In: SMYS, S.; BESTAK, R.; CHEN, J. I.-Z.; KOTULIAK, I. (Ed.). *International Conference on Computer Networks and Communication Technologies*. Singapore: Springer Singapore, 2019, (Lecture Notes on Data Engineering and Communications Technologies, v. 15). p. 681–693. ISBN 978-981-10-8680-9. Available on: <http://link.springer.com/10.1007/978-981-10-8681-6http://link.springer.com/10.1007/978-981-10-8681-6_62>. Cited on page 119.

TARHUNI, N. G.; ELKALASHY, N. I.; KAWADY, T. A.; LEHTONEN, M. Autonomous control strategy for fault management in distribution networks. *Electric Power Systems Research*, Elsevier B.V., v. 121, p. 252–259, apr 2015. ISSN 03787796. Available on: <http://dx.doi.org/10.1016/j.epsr.2014.11.011https://linkinghub.elsevier.com/retrieve/pii/S0378779614004106>. Cited 3 times on page(s) 60, 68, and 181.

TENTI, P.; MATTAVELLI, P.; TEDESCHI, E. Compensation Techniques Based on Reactive Power Conservation. *Electrical Power Quality and Utilisatio, Journal*, XIII, n. 1, p. 8, 2007. ISSN 00029955. Cited 2 times on page(s) 89 and 90.

TENTI, P.; PAREDES, H. K. M.; MATTAVELLI, P. Conservative Power Theory, a Framework to Approach Control and Accountability Issues in Smart Microgrids. *IEEE Transactions on Power Electronics*, v. 26, n. 3, p. 664–673, mar 2011. ISSN 0885-8993. Cited 2 times on page(s) 89 and 90.

THANOS, A. E.; BASTANI, M.; CELIK, N.; CHEN, C.-H. Dynamic Data Driven Adaptive Simulation Framework for Automated Control in Microgrids. *IEEE Transactions on Smart Grid*, IEEE, v. 8, n. 1, p. 209–218, jan 2017. ISSN 1949-3053. Available on: <http://ieeexplore.ieee.org/document/7210221/>. Cited on page 185.

TLEIS, N. D. 2 - theory of symmetrical components and connection of phase sequence networks during faults. In: TLEIS, N. D. (Ed.). *Power Systems Modelling and Fault Analysis*. Oxford: Newnes, 2008, (Newnes Power Engineering Series). p. 28–73. ISBN 978-0-7506-8074-5. Available on: <https://www.sciencedirect.com/science/article/pii/B9780750680745500060>. Cited on page 47.

TOKEL, H. A.; HALASEH, R. A.; ALIREZAEI, G.; MATHAR, R. A new approach for machine learning-based fault detection and classification in power systems. In: *2018 IEEE Power & Energy Society Innovative Smart Grid Technologies Conference (ISGT)*. IEEE, 2018. p. 1–5. ISBN 978-1-5386-2453-1. Available on: <https://ieeexplore.ieee.org/document/8403343/>. Cited 6 times on page(s) 44, 53, 63, 75, 83, and 182.

TRENDAFILOV, N.; GALLO, M. *Multivariate Data Analysis on Matrix Manifolds (with Manopt)*. 1. ed. Cham: Springer Series, 2021. 450 p. ISBN 9783030769734. Cited on page 137.

TUBALLA, M. L.; ABUNDO, M. L. A review of the development of Smart Grid technologies. *Renewable and Sustainable Energy Reviews*, Elsevier, v. 59, p. 710–725, jun 2016. ISSN 13640321. Available on: <http://dx.doi.org/10.1016/j.rser.2016.01.011https://linkinghub.elsevier.com/retrieve/pii/S1364032116000393>. Cited on page 184.

WALLACE, S.; ZHAO, X.; NGUYEN, D.; LU, K.-T. Big Data Analytics on a Smart Grid. In: *Big Data*. Elsevier, 2016. p. 417–429. ISBN 9780128053942. Available on: <https://linkinghub.elsevier.com/retrieve/pii/B9780128053942000179>. Cited 2 times on page(s) 58 and 184.

WANG, B.; GENG, J.; DONG, X. High-Impedance Fault Detection Based on Nonlinear Voltage–Current Characteristic Profile Identification. *IEEE Transactions on Smart Grid*, IEEE, v. 9, n. 4, p. 3783–3791, jul 2018. ISSN 1949-3053. Available on: <https://ieeexplore.ieee.org/document/7792702/>. Cited 6 times on page(s) 53, 77, 79, 81, 83, and 182.

WANG, H.; QIAN, Y.; SHARIF, H. Multimedia communications over cognitive radio networks for smart grid applications. *IEEE Wireless Communications*, v. 20, n. 4, p. 125–132, aug 2013. ISSN 1536-1284. Available on: <http://ieeexplore.ieee.org/document/6590059/>. Cited 2 times on page(s) 66 and 183.

WASEKAR, A.; SARKAR, S.; PATIL, A.; HARTALKAR, A. Design and implementation of a microgrid-fault response system. In: *2017 International Conference on Smart grids, Power and Advanced Control Engineering (ICSPACE)*. IEEE, 2017. v. 2018-Janua, p. 344–351. ISBN 978-1-5090-6348-2. Available on: <http://ieeexplore.ieee.org/document/8343455/>. Cited on page 182.

WISCHKAEMPER, J. A.; BENNER, C. L.; RUSSELL, B. D.; MANIVANNAN, K. Application of Waveform Analytics for Improved Situational Awareness of Electric Distribution Feeders. *IEEE Transactions on Smart Grid*, IEEE, v. 6, n. 4, p. 2041–2049, jul 2015. ISSN 1949-3053. Available on: <http://ieeexplore.ieee.org/document/7095588/>. Cited 7 times on page(s) 53, 56, 60, 77, 79, 83, and 182.

WU, H.; LIU, J.; LIU, Y.; QIU, G.; TAYLOR, G. A. Power system transmission line fault diagnosis based on combined data analytics. In: *2017 IEEE Power & Energy Society General Meeting*. IEEE, 2017. v. 2018-Janua, n. 51437003, p. 1–5. ISBN 978-1-5386-2212-4. ISSN 19449933. Available on: <http://ieeexplore.ieee.org/document/8274635/>. Cited 2 times on page(s) 65 and 182.

WU, Q.; ZHANG, R. Beamforming optimization for intelligent reflecting surface with discrete phase shifts. In: IEEE. *ICASSP 2019-2019 IEEE International Conference on Acoustics, Speech and Signal Processing (ICASSP)*. [S.l.], 2019. p. 7830–7833. Cited on page 38.

WU, Q.; ZHANG, R. Beamforming optimization for intelligent reflecting surface with discrete phase shifts. In: IEEE. *ICASSP 2019-2019 IEEE International Conference on Acoustics, Speech and Signal Processing (ICASSP)*. [S.l.], 2019. p. 7830–7833. Cited on page 133.

WU, W.; WANG, Z.; YUAN, L.; ZHOU, F.; LANG, F.; WANG, B.; WU, Q. Irs-enhanced energy detection for spectrum sensing in cognitive radio networks. *IEEE Wireless Communications Letters*, v. 10, n. 10, p. 2254–2258, 2021. Cited on page 133.

XI, P.; FEILAI, P.; YONGCHAO, L.; ZHIPING, L.; LONG, L. Fault Detection Algorithm for Power Distribution Network Based on Sparse Self-Encoding Neural Network. In: *2017 International Conference on Smart Grid and Electrical Automation (ICSGEA)*. IEEE, 2017. v. 2017-Janua, p. 9–12. ISBN 978-1-5386-2813-3. Available on: <http://ieeexplore.ieee.org/document/8104322/>. Cited 6 times on page(s) 53, 77, 79, 82, 83, and 182.

XIANG, Y.; WANG, L.; ZHANG, Y. Adequacy evaluation of electric power grids considering substation cyber vulnerabilities. *International Journal of Electrical Power & Energy Systems*, Elsevier, v. 96, n. July 2017, p. 368–379, mar 2018. ISSN 01420615. Available on: <https://doi.org/10.1016/j.ijepes.2017.10.004https://linkinghub.elsevier.com/retrieve/pii/S0142061517317428>. Cited 2 times on page(s) 63 and 185.

XIE, H.; XU, J.; LIU, Y.-F. Max-min fairness in irs-aided multi-cell miso systems with joint transmit and reflective beamforming. *IEEE Transactions on Wireless Communications*, IEEE, v. 20, n. 2, p. 1379–1393, 2020. Cited on page 38.

XIE, H.; XU, J.; LIU, Y.-F. Max-min fairness in irs-aided multi-cell miso systems with joint transmit and reflective beamforming. *IEEE Transactions on Wireless Communications*, IEEE, v. 20, n. 2, p. 1379–1393, 2020. Cited on page 133.

XU, Z.; LIU, Y.; ZHAO, D.; CHENG, X.; ZHANG, N. Fault Diagnosis Based on Process Matching in Smart Distribution Grid. In: *2012 Asia-Pacific Power and Energy Engineering Conference*. IEEE, 2012. p. 1–4. ISBN 978-1-4577-0547-2. ISSN 21574839. Available on: <http://ieeexplore.ieee.org/document/6307670/>. Cited on page 180.

YANG, B.; KATSAROS, K. V.; CHAI, W. K.; PAVLOU, G. Cost-Efficient Low Latency Communication Infrastructure for Synchrophasor Applications in Smart Grids. *IEEE Systems Journal*, IEEE, v. 12, n. 1, p. 948–958, mar 2018. ISSN 1932-8184. Available on: <http://ieeexplore.ieee.org/document/7475895/>. Cited 3 times on page(s) 56, 68, and 183.

YANG, T.; PEN, H.; WANG, Z.; CHANG, C. S. Feature Knowledge Based Fault Detection of Induction Motors Through the Analysis of Stator Current Data. *IEEE Transactions on Instrumentation and Measurement*, IEEE, v. 65, n. 3, p. 549–558, mar 2016. ISSN 0018-9456. Available on: <http://ieeexplore.ieee.org/document/7372442/>. Cited 5 times on page(s) 53, 78, 79, 83, and 182.

YE, F. Smart Grid Communication Infrastructures. In: *Smart Grid Communication Infrastructures*. Chichester, UK: John Wiley & Sons Ltd, 2018. p. 15–33. Cited on page 35.

YE, F.; LIANG, Y.; ZHANG, H.; ZHANG, X.; QIAN, Y. Design and Analysis of a Wireless Monitoring Network for Transmission Lines in the Smart Grid. In: *Smart Grid Communication Infrastructures*. Chichester, UK: John Wiley & Sons Ltd, 2018. v. 16, n. 10, p. 91–114. Cited on page 36.

YEN, S. W.; MORRIS, S.; EZRA, M. A.; Jun Huat, T. Effect of smart meter data collection frequency in an early detection of shorter-duration voltage anomalies in smart grids. *International Journal of Electrical Power & Energy Systems*, Elsevier, v. 109, n. January, p. 1–8, jul 2019. ISSN 01420615. Available on: <https://doi.org/10.1016/j.ijepes.2019.01.039https://linkinghub.elsevier.com/retrieve/pii/S0142061518321434>. Cited 6 times on page(s) 53, 78, 79, 81, 83, and 183.

YI, Z.; ETEMADI, A. H. Fault Detection for Photovoltaic Systems Based on Multi-Resolution Signal Decomposition and Fuzzy Inference Systems. *IEEE Transactions on Smart Grid*, IEEE, v. 8, n. 3, p. 1274–1283, may 2017. ISSN 1949-3053. Available on: <http://ieeexplore.ieee.org/document/7505960/>. Cited 5 times on page(s) 53, 78, 79, 83, and 182.

YOU, L.; XIONG, J.; NG, D. W. K.; YUEN, C.; WANG, W.; GAO, X. Energy Efficiency and Spectral Efficiency Tradeoff in RIS-Aided Multiuser MIMO Uplink Transmission. *IEEE Trans. on Signal Proc.*, v. 69, p. 1407–1421, 2021. ISSN 1053-587X. Available on: <https://ieeexplore.ieee.org/document/9309152/>. Cited 2 times on page(s) 135 and 139.

YU, J. J.; HOU, Y.; LAM, A. Y.; LI, V. O. Intelligent Fault Detection Scheme for Microgrids with Wavelet-based Deep Neural Networks. *IEEE Transactions on Smart Grid*, IEEE, v. 10, n. 2, p. 1–1, 2017. ISSN 1949-3053. Available on: <http://ieeexplore.ieee.org/document/8118194/>. Cited 6 times on page(s) 53, 76, 79, 82, 83, and 181.

ZENG, M.; BEDEER, E.; DOBRE, O. A.; FORTIER, P.; PHAM, Q.-V.; HAO, W. Energy-Efficient Resource Allocation for IRS-Assisted Multi-Antenna Uplink Systems. *IEEE Wireless Communications Letters*, v. 2337, n. 1, p. 1–1, 2021. ISSN 2162-2337. Available on: <https://ieeexplore.ieee.org/document/9369326/>. Cited on page 139.

ZERIHUN, T. A.; GARAU, M.; HELVIK, B. E. Effect of Communication Failures on State Estimation of 5G-Enabled Smart Grid. *IEEE Access*, v. 8, p. 112642–112658, 2020. ISSN 2169-3536. Cited on page 72.

ZHANG, F.; MU, L. A Fault Detection Method of Microgrids with Grid-Connected Inverter Interfaced Distributed Generators Based on the PQ Control Strategy. *IEEE Transactions on Smart Grid*, IEEE, PP, n. c, p. 1–1, 2018. ISSN 1949-3053. Available on: <https://ieeexplore.ieee.org/document/8464289/>. Cited 6 times on page(s) 53, 75, 78, 79, 83, and 182.

ZHANG, Y.; WANG, L.; SUN, W. Trust System Design Optimization in Smart Grid Network Infrastructure. *IEEE Transactions on Smart Grid*, IEEE, v. 4, n. 1, p. 184–195, mar 2013. ISSN 1949-3053. Available on: <http://ieeexplore.ieee.org/document/6451183/>. Cited 5 times on page(s) 53, 63, 78, 79, and 183.

ZHANG, Z.; GONG, S.; DIMITROVSKI, A. D.; LI, H. Time Synchronization Attack in Smart Grid: Impact and Analysis. *IEEE Transactions on Smart Grid*, IEEE, v. 4, n. 1, p. 87–98, mar 2013. ISSN 1949-3053. Available on: <http://ieeexplore.ieee.org/document/6400273/>. Cited 2 times on page(s) 58 and 184.

ZHAO, B.; YANG, M.; DIAO, H.; AN, B.; ZHAO, Y.; ZHANG, Y. A novel approach to transformer fault diagnosis using IDM and naive credal classifier. *International Journal of Electrical Power & Energy Systems*, v. 105, n. September 2018, p. 846–855, feb 2019. ISSN 01420615. Cited 3 times on page(s) 49, 93, and 109.

ZHOU, G.; PAN, C.; REN, H.; WANG, K.; NALLANATHAN, A. A framework of robust transmission design for irs-aided miso communications with imperfect cascaded channels. *IEEE Transactions on Signal Processing*, IEEE, v. 68, p. 5092–5106, 2020. Cited on page 133.

ZHOU, X.; WANG, P.; YANG, Z.; TONG, L.; WANG, Y.; YANG, C.; XIONG, N.; GAO, H. A Manifold Learning Two-Tier Beamforming Scheme Optimizes Resource Management in Massive MIMO Networks. *IEEE Access*, v. 8, p. 22976–22987, 2020. ISSN 2169-3536. Available on: <https://ieeexplore.ieee.org/document/8951080/>. Cited on page 38.

ZÚÑIGA, A.; BALEIA, A.; FERNANDES, J.; BRANCO, P. Classical Failure Modes and Effects Analysis in the Context of Smart Grid Cyber-Physical Systems. *Preprints*, n. February, p. 1–25, 2020. Cited on page 184.

Appendix

APPENDIX A – SG Research Classification

Table A.1 – Relevant Publications inside the scope of SG systems

Publication	Scope							
	Fault	*Det.*	*Loc.*	*Monitor.*	***SG***	*μ-grid*	*DG*	***Comm***
MILIOUDIS et al. (2015) (MILIOUDIS et al., 2015)	✓	✓	✓		✓			✓
BUSH (2014) (BUSH, 2014)	✓				✓			✓
JIANG et al. (2014) (JIANG et al., 2014)	✓	✓	✓		✓			
ANDRESEN et al. (2018) (ANDRESEN et al., 2018)	✓	✓		✓	✓			
MESKINA et al. (2014) (MESKINA et al., 2014)	✓	✓		✓	✓		✓	
BANGALORE; TJERNBERG (2015) (BANGALORE; TJERNBERG, 2015)	✓	✓			✓		✓	
CHAKRABORTY; DAS (2018) (CHAKRABORTY; DAS, 2018)	✓	✓			✓			
GHARAVI; HU (2018) (GHARAVI; HU, 2018)	✓	✓			✓			
ALHELOU et al. (2018) (ALHELOU et al., 2018)	✓	✓			✓			
HE; ZHANG (2011) (HE; ZHANG, 2011)	✓	✓			✓			
HE; ZHANG (2010) (HE; ZHANG, 2010)	✓	✓			✓			
HE; BLUM (2011) (HE; BLUM, 2011)	✓	✓			✓			
JIANG et al. (2016) (JIANG et al., 2016)	✓	✓			✓			
KATIC; STANISAVLJEVIC (2018) (KATIC; STANISAVLJEVIC, 2018)	✓	✓			✓			
KOZIY et al. (2013) (KOZIY et al., 2013)	✓	✓			✓	✓		
MAHFOUZ; EL-SAYED (2016) (MAHFOUZ; EL-SAYED, 2016)	✓	✓			✓		✓	
MANANDHAR et al. (2014) (MANANDHAR et al., 2014)	✓	✓			✓			

Continued on next page

Table A.1 – *Continued from previous page*

Publication	Scope							
	Fault	*Det.*	*Loc.*	*Monitor.*	***SG***	*μ-SG*	*DG*	***Comm***
PARIKH et al. (2013) (PARIKH et al., 2013)	✓	✓			✓		✓	
PASDAR et al. (2013) (PASDAR et al., 2013)	✓	✓			✓			
RAWAT et al. (2016) (RAWAT et al., 2016)	✓	✓			✓			
SHAO et al. (2017) (SHAO et al., 2017)	✓	✓			✓		✓	
DEVI et al. (2018) (DEVI et al., 2018)	✓		✓		✓			
DHEND; CHILE (2017) (DHEND; CHILE, 2017)	✓		✓		✓			
FARUGHIAN et al. (2018) (FARUGHIAN et al., 2018)	✓		✓		✓			
ROBSON et al. (2014) (ROBSON et al., 2014)	✓		✓		✓			
FERREIRA; BARROS (2018) (FERREIRA; BARROS, 2018)	✓			✓	✓	✓		
JIANG et al. (2018a) (JIANG et al., 2018a)	✓			✓	✓			
SANTIS et al. (2015) (SANTIS et al., 2015)	✓				✓			
SANTIS et al. (2018) (SANTIS et al., 2018)	✓				✓			
DHEND; CHILE (2018) (DHEND; CHILE, 2018)	✓				✓			
GOPAKUMAR et al. (2015) (GOPAKUMAR et al., 2015)	✓				✓			
HARE et al. (2016) (HARE et al., 2016)	✓				✓	✓		
JIANG et al. (2018b) (JIANG et al., 2018b)	✓				✓		✓	
KAZEMI; LEHTONEN (2013) (KAZEMI; LEHTONEN, 2013)	✓				✓			
KORDESTANI; SAIF (2017) (KORDESTANI; SAIF, 2017)	✓				✓			
NTALAMPIRAS (2016) (NTALAMPIRAS, 2016)	✓				✓			
SAYED et al. (2017) (SAYED et al., 2017)	✓				✓			
XU et al. (2012) (XU et al., 2012)	✓				✓			

Continued on next page

Table A.1 – *Continued from previous page*

Publication	Scope							
	Fault	*Det.*	*Loc.*	*Monitor.*	***SG***	*μ-SG*	*DG*	***Comm***
RAHMAN et al. (2018) (RAHMAN et al., 2018)	✓							✓
TARHUNI et al. (2015) (TARHUNI et al., 2015)	✓							✓
DAS et al. (2017) (DAS et al., 2017)	✓	✓	✓					
DHAR et al. (2018) (DHAR et al., 2018)	✓	✓	✓			✓		
DOBAKHSHARI; RANJBAR (2015) (DOBAKHSHARI; RANJBAR, 2015)	✓	✓	✓					
LI et al. (2018) (LI et al., 2018)	✓	✓	✓					
SALEH et al. (2017b) (SALEH et al., 2017b)	✓	✓	✓			✓		
YU et al. (2017) (YU et al., 2017)	✓	✓	✓			✓		
GOPAKUMAR et al. (2018) (GOPAKUMAR et al., 2018)	✓	✓		✓				
HARROU et al. (2018) (HARROU et al., 2018)	✓	✓		✓				
SADEGHKHANI et al. (2016) (SADEGHKHANI et al., 2016)	✓	✓		✓		✓	✓	
AFFIJULLA; TRIPATHY (2018) (AFFIJULLA; TRIPATHY, 2018)	✓	✓					✓	
BABAEI et al. (2018) (BABAEI et al., 2018)	✓	✓						
CHAITANYA; YADAV (2018) (CHAITANYA; YADAV, 2018)	✓	✓					✓	
CHEN et al. (2016a) (CHEN et al., 2016a)	✓	✓						
CHEN et al. (2016b) (CHEN et al., 2016b)	✓	✓					✓	
COSTA et al. (2015) (COSTA et al., 2015)	✓	✓						
DARYALAL; SARLAK (2017) (DARYALAL; SARLAK, 2017)	✓	✓						
HASHEMI et al. (2017) (HASHEMI et al., 2017)	✓	✓						
KUO et al. (2017) (KUO et al., 2017)	✓	✓				✓		
MADETI; SINGH (2017a) (MADETI; SINGH, 2017a)	✓	✓						

Continued on next page

Table A.1 – *Continued from previous page*

Publication	Scope							
	Fault	*Det.*	*Loc.*	*Monitor.*	***SG***	*μ-SG*	*DG*	***Comm***
MADETI; SINGH (2017b) (MADETI; SINGH, 2017b)	✓	✓						
NAGANANDA et al. (2015) (NAGANANDA et al., 2015)	✓	✓						
QI et al. (2017) (QI et al., 2017)	✓	✓						
SALEH et al. (2017a) (SALEH et al., 2017a)	✓	✓						
TOKEL et al. (2018) (TOKEL et al., 2018)	✓	✓						
WANG et al. (2018) (WANG et al., 2018)	✓	✓						
WISCHKAEMPER et al. (2015) (WISCHKAEMPER et al., 2015)	✓	✓						
XI et al. (2017) (XI et al., 2017)	✓	✓						
YANG et al. (2016) (YANG et al., 2016)	✓	✓						
YI; ETEMADI (2017) (YI; ETEMADI, 2017)	✓	✓					✓	
ZHANG; MU (2018) (ZHANG; MU, 2018)	✓	✓				✓	✓	
BAHMANYAR et al. (2017) (BAHMANYAR et al., 2017)	✓		✓				✓	
MISHRA et al. (2014) (MISHRA et al., 2014)	✓		✓					
ELKALASHY et al. (2016) (ELKALASHY et al., 2016)	✓						✓	
FERREIRA et al. (2016) (FERREIRA et al., 2016)	✓							
MAR et al. (2019) (MAR et al., 2019)	✓							
NEGARI; XU (2017) (NEGARI; XU, 2017)	✓							
PRASAD et al. (2018) (PRASAD et al., 2018)	✓							
P. et al. (2018) (P. et al., 2018)	✓							
WASEKAR et al. (2017) (WASEKAR et al., 2017)	✓					✓		
WU et al. (2017) (WU et al., 2017)	✓							

Continued on next page

Table A.1 – *Continued from previous page*

Publication	Scope							
	Fault	*Det.*	*Loc.*	*Monitor.*	***SG***	*μ-SG*	*DG*	***Comm***
RIDHAWI et al. (2020) (RIDHAWI et al., 2020)					✓			✓
CALDERARO et al. (2011) (CALDERARO et al., 2011)					✓			✓
DEPURU et al. (2011) (DEPURU et al., 2011)					✓			✓
EMMANUEL; RAYUDU (2016) (EMMANUEL; RAYUDU, 2016)					✓			✓
GAO et al. (2012) (GAO et al., 2012)					✓			✓
JARADAT et al. (2015) (JARADAT et al., 2015)					✓			✓
KARUPONGSIRI et al. (2017) (KARUPONGSIRI et al., 2017)					✓			✓
WANG et al. (2013) (WANG et al., 2013)					✓			✓
YANG et al. (2018) (YANG et al., 2018)					✓			✓
PHAN; CHEN (2017) (PHAN; CHEN, 2017)		✓		✓	✓			
HUANG et al. (2016) (HUANG et al., 2016)		✓			✓			
KUMAR; BHOWMIK (2018) (KUMAR; BHOWMIK, 2018)		✓			✓			
MARTINEZ-FIGUEROA et al. (2017) (MARTINEZ-FIGUEROA et al., 2017)		✓			✓			
MOGHADDASS; WANG (2018) (MOGHADDASS; WANG, 2018)		✓			✓			
AHMADIPOUR et al. (2019) (AHMADIPOUR et al., 2019)		✓			✓	✓	✓	
SEYEDI et al. (2017b) (SEYEDI et al., 2017b)		✓			✓	✓	✓	
YEN et al. (2019) (YEN et al., 2019)		✓			✓			
ZHANG et al. (2013a) (ZHANG et al., 2013a)			✓		✓			
ANANDAN et al. (2019) (ANANDAN et al., 2019)				✓	✓			
HONARMAND et al. (2019) (HONARMAND et al., 2019)				✓	✓			
MADUENO et al. (2016) (MADUENO et al., 2016)				✓	✓			

Continued on next page

Table A.1 – *Continued from previous page*

Publication	Scope							
	Fault	*Det.*	*Loc.*	*Monitor.*	***SG***	*μ-SG*	*DG*	***Comm***
MUNSHI; MOHAMED (2017) (MUNSHI; MOHAMED, 2017)				✓	✓			
SEYEDI et al. (2017a) (SEYEDI et al., 2017a)				✓	✓	✓	✓	
ARTALE et al. (2017) (ARTALE et al., 2017)					✓		✓	
COSOVIC et al. (2017) (COSOVIC et al., 2017)					✓		✓	
SANTO et al. (2015) (SANTO et al., 2015)					✓			
DILEEP (2020) (DILEEP, 2020)					✓			
FADUL et al. (2014) (FADUL et al., 2014)					✓			
GUARRACINO et al. (2012) (GUARRACINO et al., 2012)					✓		✓	
HOWELL et al. (2017) (HOWELL et al., 2017)					✓		✓	
LIBONI et al. (2016) (LIBONI et al., 2016)					✓			
MAHMOUD; XIA (2019) (MAHMOUD; XIA, 2019)					✓			
RAHMAN et al. (2015) (RAHMAN et al., 2015)					✓			
SALEEM et al. (2019) (SALEEM et al., 2019)					✓			
SEYEDI; KARIMI (2018) (SEYEDI; KARIMI, 2018)					✓		✓	
TUBALLA; ABUNDO (2016) (TUBALLA; ABUNDO, 2016)					✓			
WALLACE et al. (2016) (WALLACE et al., 2016)					✓			
ZHANG et al. (2013b) (ZHANG et al., 2013b)					✓			
ZÚÑIGA et al. (2020) (ZÚÑIGA et al., 2020)					✓			
BOCKELMANN et al. (2018) (BOCKELMANN et al., 2018)								✓
ACHLERKAR et al. (2018) (ACHLERKAR et al., 2018)		✓					✓	
CHEN et al. (2015) (CHEN et al., 2015)		✓					✓	

Continued on next page

Table A.1 – *Continued from previous page*

Publication	Scope							
	Fault	*Det.*	*Loc.*	*Monitor.*	***SG***	*μ-SG*	*DG*	***Comm***
AHMADIPOUR et al. (2018) (AHMADIPOUR et al., 2018)		✓					✓	
AHMADIPOUR et al. (2018) (AHMADIPOUR et al., 2018)		✓					✓	
AHMADIPOUR et al. (2019) (AHMADIPOUR et al., 2019)		✓					✓	
SUN et al. (2016) (SUN et al., 2016)		✓						
THANOS et al. (2017) (THANOS et al., 2017)				✓		✓		
XIANG et al. (2018) (XIANG et al., 2018)				✓				
MAHELA; SHAIK (2016) (MAHELA; SHAIK, 2016)							✓	
MISHRA et al. (2016) (MISHRA et al., 2016)						✓		
MONADI et al. (2017) (MONADI et al., 2017)						✓		
NGUYEN et al. (2013) (NGUYEN et al., 2013)								
PERTL et al. (2018) (PERTL et al., 2018)							✓	

APPENDIX B – SG Applications based on Tolerable Delay

Table B.1 scales priority in SG application type based on maximum tolerable latency.

Table B.1 – Latency & Priority by SG application

Application type	Application	Latency (ms)	Priority 0-max 100-min
Teleprotection (for 60 Hz, 50 Hz)	(High-speed) protection information	8,10	
SCADA	Load shedding for underfrequency	10	20
Teleprotection	Breaker reclosures	16	15
Teleprotection	Lockout functions	16	12
Teleprotection	Many transformer protection and control applications	16	12
Synchrophasors	PMU measurements + status (class A) If used for protection function	20	12
Synchrophasors	PMU measurements + status (class A) for other than protection	60	12
SCADA	SCADA periodic measurement + status, events, control	100	25
Distribution automation	DA periodic measurement+status, events, control	100	26
Distributed generation - distributed storage	DG/DS measurement+status, events, control	100	27
MWF	PTT signaling - critical	100	30
Synchrophasors	PMU clock synchronization	100	20
MWF, business voice	VoIP bearer (including for PTT)	175	50
Business voice	VoIP signaling (person-to-person)	200	60
Dynamic Line Rating	DLR measurements, status, events, control	200	28
MWF, CCTV	Real-time video (MWF)	200	55
CCTV	On demand CCTV video	200	55
SCADA, DA, DG/DS, DLR, etc.	Critical grid operation data (e.g., DMS, TMS)	200	45
Business data	Critical business data	250	70
SCADA	DMS and TMS applications (other than included above)	250	65
AMI	AMI - critical (e.g., VVWC)	250	40
AMI	AMI - Priority (e.g., ADR, Black Start)	300	70
CCTV	CCTV stream - normal	400	75
Synchrophasors	PMU (other than class A)	500	80
Protection	Some transformer protection and control applications	500	80
SCADA, DA, DG/DS, DLR, etc.	Noncritical operations data	500	80
Business data	Noncritical business data	500	80
SCADA	Image files	1000	90
SCADA	Fault recorders	1000	90
SCADA	(Medium-speed) Monitoring and control information	1000	90
SCADA	(Low-speed) O and M information	1000	90
Protection	Fault isolation and service restoration	1000	90
Some distribution automation, some demand response	Distribution applications	1000	90
AMI	AMI - normal measurements+status, events, control	1000	85
SCADA	Text strings	1000	90
SCADA	Audio and video data streams	1000	78
Many	Best effort, default	2000	100

APPENDIX C – Data Rate requirements in Smart Grid Applications

Table C.1 summarizes the type of application from the minimum required data rate considering different kind of wireless channels.

Table C.1 – Summary of the data rate requirements.

Application	Minimum required data rates (worst case) in kbps									
	Dense urban with AMI data concentrators		Dense urban without AMI data concentrators		Urban with AMI data concentrators		Suburban with AMI data concentrators		Rural without AMI data concentrators	
	Normal	*Critical*	*Normal*	*Critical*	*Normal*	*Critical*	*Normal*	*Critical*	*Normal*	*Critical*
SCADA and DA	165	138	165	138	95	79	140	116	236	197
DG, DS	80	67	80	67	97	80	129	107	161	134
Synchrophasors	213	178	213	178	213	178	213	178	426	355
AMI	165	165	210	279	83	83	83	83	120	160
CCTV	826	1,238	826	1,238	826	1,238	826	1,238	1,651	2,064
Mobile workforce - push-to-talk voice	16	161	16	161	16	129	16	81	16	81
Mobile workforce - live video	0	550	0	550	0	550	0	550	0	550
Person-to-person voice (MWF and substation personnel)	113	435	113	435	113	371	97	274	97	274
Business data (MWF and substation personnel)	124	554	124	554	124	459	96	287	105	296
Dynamic line rating	0	0	0	0	0	0	3	3	8	7
Total data rate	1703	3487	1,747	3,601	1,566	3,167	1,601	2,917	2,820	4,118
Total data only	748	1102	793	1,216	612	879	663	773	1,056	1,149
Total video only	826	1789	826	1,789	826	1,789	826	1,789	1,651	2,614
Total voice only	129	597	129	597	129	500	113	355	113	355

APPENDIX D – Communication Technologies for Smart Grid

Table D.1 comprehends wide communication technologies for the SG, classified by coverage range from some hundred meters up to a hundred km, as well as data rate up to 40Gbps for wired technologies and up to 600Mbps for wireless communication technologies.

Table D.1 – Communication technologies for the SG.

Technology	Standard/protocol	Max. theoretical data rate	Coverage range	Network		
				HAN	***NAN***	***WAN***
Wired communication technologies						
Fiber optic	PON	155 Mbps-2.5 Gbps	Up to 60 km			■
	WDM	40 Gbps	Up to 100 km			■
	SONET/SDH	10 Gbps	Up to 100 km			■
DSL	ADSL	1-8 Mbps	Up to 5 km		■	
	HDSL	2 Mbps	Up to 3.6 km		■	
	VDSL	15-100 Mbps	Up to 1.5 km		■	
Coaxial Cable	DOCSIS	172 Mbps	Up to 28 km		■	
PLC	HomePlug	14-200 Mbps	Up to 200 m	■		
	Narrowband	10-500 kbps	Up to 3 km		■	■
Ethernet	802.3x	10 Mbps-10 Gbps	Up to 100 m	■	■	
Wireless communication technologies						
Z-Wave	Z-Wave	40 kbps	Up to 30 m	■		
Bluetooth	802.15.1	721 kbps	Up to 100 m	■		
ZigBee	ZigBee	250 kbps	Up to 100 m	■	■	
	ZigBee Pro	250 kbps	Up to 1600 m	■	■	
WiFi	802.11x	2-600 Mbps	Up to 100 m	■	■	
WiMAX	802.16	75 Mbps	Up to 50 km		■	■
Wireless Mesh	Various (e.g., RF mesh, 802.11, 802.15, 802.16)	Depending on selected protocols	Depending on deployment	■	■	
Cellular	2G	14.4 kbps	Up to 50 km		■	■
	2.5G	144 kbps			■	■
	3G	2 Mbps			■	■
	3.5G	14 Mbps			■	■
	4G	100 Mbps			■	■
Satellite	Satellite Internet	1 Mbps	100-6000 km			■

APPENDIX E – Particle Swarm Optimization (PSO)

PSO is inspired by the social behavior of birds or schools of fish. Particles P initialize randomly in the manifold constraint. Each particle moves with a certain velocity V, allowing them to update their position iteratively (iteration i) to find the global minimum. During the space search, the speed of each particle accelerates stochastically towards its prior best position (personal best, P_{PB}) and apropos the best solution of the group (global best, P_{GB}). It iteration considers weighting the acceleration randomly.

$$P_i^{t+1} = P_i^t + V_i^{t+1} \tag{E.1a}$$

$$V_i^{t+1} = \omega V_i^t + c_1 r_1 (P_{\text{PB},i}^t - P_i^t) + c_2 r_2 (P_{\text{GB},i}^t - P_i^t) \tag{E.1b}$$

$$\omega \in \mathcal{R}^+ \qquad \textbf{Inertia} \tag{E.1c}$$

$$r_1 \in [0,2]; \qquad c_1 \in \mathcal{R}^+ \qquad \textbf{Cognitive} \tag{E.1d}$$

$$r_2 \in [0,2]; \qquad c_2 \in \mathcal{R}^+ \qquad \textbf{Social} \tag{E.1e}$$

Weights r_1 and r_2 adjust cognitive acceleration, and social acceleration are stochastically. The parameter ω allows defining the ability of the swarm to adjust its direction. The particles have inertia proportional to this coefficient ω. The c_1 parameter concedes establishing the group's capacity to be affected by the best personal solutions over the iterations. The parameter c_2 concedes establishing the group's capacity to be affected by the best global solution obtained over the iterations.